



Mansoura University
Faculty of Engineering
Structural Engineering Department



COMPARISON BETWEEN DIFFERENT CODES IN DESIGN OF STEEL COLD-FORMED SECTIONS UNDER EFFECT OF STATIC LOADS

A thesis

Submitted in Partial Fulfillment for the Requirements
Of the Degree of Master of Science in Structural Engineering

By

Samar El-sayed Ibrahim Abd El-kawy Atya

B.Sc. Civil Engineering – Mansoura University, 2018
Demonstrator in Dept. of Structural Engineering – Mansoura University

Under supervision of

Prof. Dr. Nabil Sayed Mahmoud

Structural Engineering Department
Faculty of Engineering
Mansoura University

Assoc. Prof. Dr. Fikry Abdo Salem

Structural Engineering Department
Faculty of Engineering
Mansoura University

Assoc. Prof. Dr. Mohamed Ghannam

Structural Engineering Department
Faculty of Engineering
Mansoura University

2023



Mansoura University
Faculty of Engineering
Structural Engineering Department



Supervisors Committee

Thesis Title : Comparison Between Different Codes in Design of Steel Cold-Formed Sections under Effect of Static Loads.
Researcher Name : **Samar El-sayed Ibrahim Abd El-kawy Atya.**
Scientific Degree : Master of Science in Engineering (Structural Engineering)

Supervisor Committee

Name	Position	Signature
Prof. Dr. Nabil Sayed Mahmoud	Professor, Structural Engineering Dept., Faculty of Engineering, Mansoura University	
Prof. Dr. Fikry Abdo Salem	Assistant Professor, Structural Engineering Dept., Faculty of Engineering, Mansoura University	
Assoc. Prof. Dr. Mohamed Mohamed Ghannam	Assistant Professor, Structural Engineering Dept., Faculty of Engineering, Mansoura University	

Department Head

Prof. Dr. Mohammed El-Zoghby

Vice Dean
Postgraduate Studies
Affairs and Research

Prof. Dr. Sherif El_badawy

Acting Dean

Prof. Dr. Sherif El_badawy



Mansoura University
Faculty of Engineering
Structural Engineering Department



Supervisors Committee

Thesis Title : Comparison Between Different Codes in Design of Steel Cold-Formed Sections under Effect of Static Loads.
 Researcher Name : Samar El-sayed Ebrahim Atya.
 Scientific Degree : Master of Science in Engineering (Structural Engineering)

Supervisor Committee

Name	Position	Signature
Prof. Dr. Nabil Sayed Mahmoud	Professor, Structural Engineering Dept., Faculty of Engineering, Mansoura University	
Assoc. Prof. Dr. Fikry Abdo Salem	Assistant Professor, Structural Engineering Dept., Faculty of Engineering, Mansoura University	
Assoc. Prof. Dr. Mohamed Mohamed Ghannam	Assistant Professor, Structural Engineering Dept., Faculty of Engineering, Mansoura University	

Department Head

Prof. Dr. Mohammed El-Zoghby

Vice Dean for
Postgraduate Studies
Affairs and Research

Prof. Dr. Sherif El-badawy

Acting Dean

Prof. Dr. Sherif El-badawy



٢٠٢٢



Mansoura University
Faculty of Engineering
Structural Engineering Department



Approval Sheet

Thesis Title : Comparison Between Different Codes in Design of Steel Cold-Formed Sections under Effect of Static Loads.
Researcher Name : **Samar El-sayed Ibrahim Abd El-kawy Atya.**
Scientific Degree : Master of Science in Engineering (Structural Engineering)

Supervisors Committee

Name	Position	Signature
Prof. Dr. Nabil Sayed Mahmoud	Professor, Structural Engineering Dept., Faculty of Engineering, Mansoura University	
Assoc. Prof. Dr. Fikry Abdo Salem	Assistant Professor, Structural Engineering Dept., Faculty of Engineering, Mansoura University	
Assoc. Prof. Dr. Mohamed Mohamed Ghannam	Assistant Professor, Structural Engineering Dept., Faculty of Engineering, Mansoura University	

Examination Committee

Name	Position	Signature
Prof. Dr. Sherif Ahmed Mourad	Professor of steel structures and bridges, Structural Engineering Dept., Faculty of Engineering, Cairo University	
Prof. Dr. Nabil Sayed Mahmoud	Professor, Structural Engineering Dept., Faculty of Engineering, Mansoura University	
Prof. Dr. Saad Eldeen M. Abdrabou	Professor, Structural Engineering Dept., Faculty of Engineering, Mansoura University	
Assoc. Prof. Dr. Fikry Abdo Salem	Assistant Professor, Structural Engineering Dept., Faculty of Engineering, Mansoura University	

	Vice Dean	
Department Head	Postgraduate Studies Affairs and Research	Acting Dean
Prof. Dr. Ahmed Mahmoud Yousef	Prof. Dr. Sherif El_badawy	Prof. Dr. Sherif El_badawy



Mansoura University
Faculty of Engineering
Structural Engineering Department



Approval Sheet

Thesis Title : Comparison Between Different Codes in Design of Steel Cold-Formed Sections under Effect of Static Loads.
 Researcher Name : Samar El-sayed Ebrahim Atya.
 Scientific Degree : Master of Science in Engineering (Structural Engineering)

Supervisors Committee

Name	Position	Signature
Prof. Dr. Nabil Sayed Mahmoud	Professor, Structural Engineering Dept., Faculty of Engineering, Mansoura University	
Assoc. Prof. Dr. Fikry Abdo Salem	Assistant Professor, Structural Engineering Dept., Faculty of Engineering, Mansoura University	
Assoc. Prof. Dr. Mohamed Mohamed Ghannam	Assistant Professor, Structural Engineering Dept., Faculty of Engineering, Mansoura University	

Examination Committee

Name	Position	Signature
Prof. Dr. Sherif Ahmed Mourad	Professor of steel structures and bridges, Structural Engineering Dept., Faculty of Engineering, Cairo University	
Prof. Dr. Nabil Sayed Mahmoud	Professor, Structural Engineering Dept., Faculty of Engineering, Mansoura University	
Prof. Dr. Saad Eldeen M. Abdrabou	Professor, Structural Engineering Dept., Faculty of Engineering, Mansoura University	
Assoc. Prof. Dr. Fikry Abdo Salem	Assistant Professor, Structural Engineering Dept., Faculty of Engineering, Mansoura University	

Department Head

Prof. Dr. Mohammed El-Zoghby

Vice Dean for Postgraduate Studies, Affairs and Research
Acting Dean

Prof. Dr. Sherif El_badawy

Prof. Dr. Sherif El_badawy





Mansoura University
 Faculty of Engineering
 Structural Engineering Department



Thesis Summary () in Library

General Administration of Library

Faculty :	Engineering	Department :	Structural Engineering	No :
Name :	Samar El-sayed Ibrahim Abd El-kawy Atya.	Degree:	Master of Science in Engineering	Date :
Thesis Title :	Comparison Between Different Codes in Design of Steel Cold-Formed Sections under Effect of Static Loads.			

Thesis summary

This research investigated compressive and flexural strengths exhibited by cold-formed steel (CFS) members with channel and Z-profiles. The study encompassed a comprehensive investigation of 500 CFS members. Numerical analysis utilizing finite-element (FE) models based on ABAQUS is conducted. Existing experimental test results were used to validate the accuracy of the FE models, which were then utilized to assess the influence of various parameters on the capacities of these CFS members. Parameters such as the member length-to-depth ratio, the section depth-to-width ratio, the plate slenderness ratio, the lip-to-flange width ratio, and material yield stress were analyzed in detail. The results obtained from FE models were comparatively analyzed against those derived from the codified Effective Width Method (EWM), as specified in current design standards, and the newly progressed Direct Strength Method (DSM). The North American Specification, Eurocode-3_part1.3, and the Egyptian Code of Practice have been used as an example of the EWM. Appendix 1 in the North American Specification is utilized as an example of the DSM. To improve the computational and calculation process, a graphical user interface (GUI) is developed to program the EWM and DSM calculation procedures. This advancement streamlined the analysis, enabling more efficient and accurate evaluations of the innovative CFS profiles' capacities. This research offers valuable insights into the performance of innovative CFS channels and Z-profiles, facilitating a deeper understanding



Mansoura University
Faculty of Engineering



Structural Engineering Department
of their structural capacities and providing a foundation for potential applications in modern engineering design and construction practices.

This thesis tracks in the following order: -

Chapter (1):

This chapter includes the introduction, research objective, and arrangement of the thesis.

Chapter (2):

This chapter includes CFS steel design standards and provisions, an overview of CFS and a detailed review of the previous research worked in the field of CFS.

Chapter (3):

This chapter includes several code equations and formulas for comparison purposes based on Egyptian, American, and European codes.

Chapter (4):

This chapter has a guidebook that covers the whole software manual and gives the user tips on how to use the software more successfully. In addition to verifying the validity and accuracy of the program results, it also contains parametric study based on different codes.

Chapter (5):

This chapter describes the numerical models using a finite element (FE) package and the verification of the results.

Chapter (6):

This chapter generates further data by conducting parametric studies on ultimate CFS capacities using the verified FE model. Additionally, it presents a comparative analysis between different codes and the FE model.

Chapter (7):

This chapter includes summary, conclusions, and recommendations for future work.

Keywords

Cold-formed steel; Axial load capacity; Flexural strength; Finite element model; Effective Width Method; Direct Strength Method; and Codes.

General Administration of Library – Mansoura – 60 Gomhoria street – Mansoura – Egypt

Box: 35516

URL: <http://www.mans.edu.eg>

Email: muecentrlib@mans.edu.eg

Master of Science Thesis

**Comparison Between Different Codes in Design of Steel Cold-Formed Sections
under Effect of Static Loads.**

Samar El-sayed Ibrahim Abd El-kawy Atya.

Demonstrator

Department of Structural Engineering

Faculty of Engineering

Mansoura University

Egypt

بِسْمِ اللَّهِ الرَّحْمَنِ الرَّحِيمِ

مَدِينَةُ الْمَدِينَةِ

[طه : ١١٤]

CONTENTS

	Page
CONTENTS	i
ACKNOWLEDGMENT	vi
ABSTRACT	vii
LIST OF FIGURES	viii
LIST OF TABLES	xii
LIST OF ABBREVIATIONS	xiv
CHAPTER (1): INTRODUCTION	
1.1. BACKGROUND	1
1.2. RESEARCH OBJECTIVE	4
1.3. RESEARCH METHODOLOGY	5
1.4. ARRANGEMENT OF THE THESIS	5
CHAPTER (2): LITERATURE REVIEW	
2.1. INTRODUCTION	7
2.2. COLD FORMED STEEL SECTIONS OVERVIEW	7
2.2.1 Manufacturing of Cold Formed Steel Sections	8
2.2.2 Types of Cold Formed Steel Sections	10
2.2.2.1 Individual Structural Members	10
2.2.2.2 Panels and Decks	11
2.2.3 Advantages of Cold-Formed Steel Sections	12

CONTENTS

2.2.4 Disadvantages of Cold-Formed Steel Sections	16
2.3 DESIG METHODS OF COLD-FORMED SECTIONS	17
2.3.1 Effective Width Method	17
2.3.2 Direct Strength Method	18
2.4 SOFTWARE PROGRAMS	19
2.4.1 Finite Element Analysis (FEA) Software Programs	19
2.4.2 Finite Strip Analysis (FSA) Software Programs	19
2.5 COLD-FORMED STEEL BUCKLING STRENGTH	20
2.6 COLD FORMED SECTION RESEACHES	22
2.6.3 Research on CFS Member Behavior	22
2.6.4 Research on CFS Buckling Behavior	24
2.6.1 Research on CFS Strengthening	24
2.6.2 Research on CFS Simulation	25
2.6.5 Other Investigations	26
CHAPTER (3): STUDY ON DIFFERENT CODES	
3.1. INTRODUCTION	28
3.2 STUDY ON DIFFERENT CODES	28
3.2.1 Comparison Between Dimensional Limits and Considerations	29
3.2.2 Resistance Factors	31
3.2.3 Comparison Between CFS Different Methods	32
3.2.3.1 Design Resistance of Cross Section	32
3.2.3.1.1 Effective Width Method	32
3.2.3.1.2 Direct Strength Method	36

CONTENTS

3.2.3.2 Design of Different Buckling Resistances.	37
3.2.3.3 Beam Column Members	45
CHAPTER (4): THE DEVELOPED PROGRAM	
4.1. INTRODUCTION	47
4.2. PROGRAM INTERFACE	47
4.2.1 Shape & General info.	50
4.2.2 Geometry	52
4.2.3 Material Properties	53
4.2.4 Length and Bracing Conditions	54
4.2.5 Ultimate Loads	55
4.3 EXTRACT RESULTS	55
4.4 PROGRAM RESULTS VERIFICATION	57
4.5 DIFFERENT CODES PARAMETRIC STUDY	58
4.5.1 Effect of Member Slenderness Ratio (λ) Parameter	59
4.5.2 Effect of Web Slenderness Ratio (h/t) Parameter	61
4.5.3 Effect of Flange Slenderness Ratio (b/t) Parameter	62
4.5.4 Effect of Lip-to-Flange Length Ratio (d/b) Parameter	64
4.5.5 Effect of Steel Yielding Stress (Fy) Parameter	65
CHAPTER (5): FINITE ELEMENT MODEL	
5.1. INTRODUCTION	66
5.2 SUMMARY OF EXPERIMENTAL STUDIES	66
5.3 NUMERICAL INVESTIGATION	70
5.3.1 Description	70

CONTENTS

5.3.2 Element Type and Mesh	70
5.3.3 Boundary Condition	72
5.3.4 Method of Loading	73
5.3.5 Residual Stresses and Corner Enhancement	73
5.3.6 Material Properties	73
5.3.7 Geometric Imperfections and Sensitivity Analysis	73
5.4 ELASTIC BUCKLING OF FINITE ELEMENT MODEL	79
5.5 VERIFICATION OF THE FEM	80
CHAPTER (6): PARAMETRIC STUDY	
6.1. INTRODUCTION	116
6.2. PARAMETRIC STUDIES OF DIFFERENT CFS ELEMENTS	117
6.2.1 Effect of Length-to-Web Plate Depth Ratio Parameter	119
6.2.2 Effect of Plate Slenderness Ratio	120
6.2.3 Effect of Lip-to-Flange Plates Length Ratio (d/b) Parameter	121
6.2.4 Effect of Web-to-Flange Plate Length Ratio (h/b) Parameter	122
6.2.5 Yielding Stress (F_y) Parameter	123
6.3 COMPARISON BETWEEN EFFECTIVE WIDTH AND DIRECT STRENGTH	124
METHODS	
6.4 MEMBER UNDER COMBINED BENDING AND AXIAL FORCES	129
6.4.1. Effect of Length-to-Web Plate Depth Ratio (L/h) Parameter	131
6.4.2 Effect of Web Plate Slenderness Ratio (h/t) Parameter	132
6.4.3 Effect of Lip-to-Flange Plates Length Ratio (d/b) Parameter	133
2.4.4 Effect of Web-to-Flange Plate Length Ratio (h/b) Parameter	134

CONTENTS

6.4.5 Effect of Yielding Stress (F_y) Parameter	135
6.4.6 Comparison Between Effective Width and Direct Strength Methods	136
CHAPTER (7): SUMMARY AND CONCLUSIONS	
7.1. SUMMARY	138
7.2 CONCLUSIONS:	138
7.3 FUTURE RECOMMENDATIONS	140
REFERENCES	141

ACKNOWLEDGMENT

Gratitude and thanks to **Allah**, who guides me to the straight path and paves the way for all my works.

First and foremost, I would like to express my sincere gratitude to my advisors, **Prof. Dr. Nabil Said Mahmoud**, and **Asso. Prof. Dr. Fikry A. Salem** for their continuous support of my master study and research, their motivation, immense, and knowledge, supervision, continuous encouragement, deep interest, and helpful advice throughout the preparation of this thesis.

I am also indebted to my co-supervisors, **Asso. Prof. Mohammed Gannam**, **Dr. Ahmed Hussein Ali** for their invaluable advice, guidance, encouragement, constructive criticism offered in various phases of this research, their critical review of the manuscript, their patience, motivation, enthusiasm, valuable advice, and immense knowledge. Their guidance helped me continuously during my research and writing of this thesis. I will never forget their help.

The words stand helpless and cannot express my appreciation to my mother, **Mrs. Fayka El-Shamy**, for her encouragement, sacrifice, unconditional support, and encouragement to pursue my interests, and fruitful care for me throughout my life.

Finally, I wish to express my deepest gratitude to my brother, **Yahia**, and my sisters, **Shorouk** and **Tasnim**, for their unfailing support, patience, love, and encouragement.

Samar Atya

ABSTRACT

This research investigated compressive and flexural strengths exhibited by cold-formed steel (CFS) members with channel and Z-profiles. The study encompassed a comprehensive investigation of 500 CFS members. Numerical analysis utilizing finite-element (FE) models based on ABAQUS is conducted. Existing experimental test results were used to validate the accuracy of the FE models, which were then utilized to assess the influence of various parameters on the capacities of these CFS members. Parameters such as the member length-to-depth ratio, the section depth-to-width ratio, the plate slenderness ratio, the lip-to-flange width ratio, and material yield stress were analyzed in detail. The results obtained from FE models were comparatively analyzed against those derived from the codified Effective Width Method (EWM), as specified in current design standards, and the newly progressed Direct Strength Method (DSM). The North American Specification, Eurocode-3_part1.3, and the Egyptian Code of Practice have been used as an example of the EWM. Appendix 1 in the North American Specification is utilized as an example of the DSM. To improve the computational and calculation process, a graphical user interface (GUI) is developed to program the EWM and DSM calculation procedures. This advancement streamlined the analysis, enabling more efficient and accurate evaluations of the innovative CFS profiles' capacities. This research offers valuable insights into the performance of innovative CFS channels and Z-profiles, facilitating a deeper understanding of their structural capacities and providing a foundation for potential applications in modern engineering design and construction practices.

Keywords

Cold-formed steel; Axial load capacity; Flexural strength; Finite element model; Effective Width Method; Direct Strength Method; and Codes.

LIST OF FIGURES

Figure	Title	Page
2.1	Various shapes of cold-formed sections.	8
2.2	Roll forming	9
2.3	folding and press braking	10
2.4	Typical forms of sections for cold-formed structural members.	11
2.5	Profiled sheets and linear trays.	12
2.6	Typical forms of stiffeners for cold-formed members and sheeting.	12
2.7	Relative differences between CFS building and other building types.	14
2.8	Relative differences between CFS building and other building types regarding both total costs and the construction duration.	14
2.9	Relative differences between cost and weight of CFS and HRS.	15
2.10	Fundamental step for the Effective Width Method (EWM).	18
2.11	Fundamental step for the Direct Strength Method (DSM).	19
2.12	Compression single buckling modes.	20
2.13	Compression interactive (coupled) buckling modes.	22
3.1	Sections with unstiffened compression elements	29
3.2	Sections with stiffened or partially stiffened compression elements.	30
3.3	Sections used in this study.	31
3.4	Assumed model for edge and intermediate stiffeners.	35
3.5	Edge stiffener.	35
3.6	European design buckling curves.	39
4.1	The present program interfaces.	48
4.2	Form of Effective Width Method.	48
4.3	Form of Direct Strength Method.	49
4.4	Form sections of CFS design in the program.	49
4.5	Shape & General info section.	50
4.6	Different codes in Button 4.	50
4.7	Different frame elements in button 5.	51
4.8	Different sectional shapes in button 6.	51

LIST OF FIGURES

4.9	Different units in button 7.	51
4.10	Geometry section.	52
4.11	Choose section from the table of the steel tables.	52
4.12	Entering the dimensions manually.	53
4.13	Material properties section.	53
4.14	Length and bracing Conditions section.	54
4.15	Ultimate loads section in different frame elements.	55
4.16	Extract the check results.	55
4.17	Calculation sheet report.	56
4.18	Effect of member slenderness ratio (λ) parameter on CFS channel.	61
4.19	Effect of Web Slenderness Ratio (h/t) Parameter on CFS channel.	62
4.20	Effect of flange slenderness ratio (b/t) parameter on CFS channel.	64
4.21	Effect of lip to flange length ratio (d/b) parameter on CFS channel.	65
4.22	Effect of steel yielding stress parameter on CFS channel.	65
5.1	Tensile test results.	67
5.2	The cross-section Profile for test specimens used.	68
5.3	Meshing of Zee CFS sections.	71
5.4	Meshing of channel CFS sections.	71
5.5	Interaction and boundary conditions.	72
5.6	Illustration of the member axes and orientations in the FE model.	73
5.7	Five mode shapes used in the Traditional Modal Approach.	75
5.8	Typical finite element mesh and buckling (eigenmode 1) of 2 nd case of loading on short columns as a simulation of that in the experimental study.	76
5.9	Typical finite element mesh and buckling (eigenmode 1) of 4 th case of loading on intermediate columns as a simulation of that in the experimental study	76
5.10	Typical finite element mesh and buckling (eigenmode 1) of Z1T1.5 sample as a simulation of that in the experimental study	77
5.11	Typical finite element mesh and buckling (eigenmode 1) of Z2T1.9 sample as a simulation of that in the experimental study.	77

LIST OF FIGURES

5.12	Load displacement curves from the FEM together with the corresponding tested specimens for short length beam column specimens ($L = 305$ mm) from sample 1 to 6.	111
5.13	Load displacement curves from the FEM together with the corresponding tested specimens for short length beam column specimens ($L = 305$ mm) from sample 7 to 12.	112
5.14	Load displacement curves from the FEM together with the corresponding tested specimens for intermediate length beam column specimens ($L = 610$ mm) for sample 1 to 6.	113
5.15	Load displacement curves from the FEM together with the corresponding tested specimens for intermediate length beam column specimens ($L = 610$ mm) for sample 7 to 12.	113
5.16	Load displacement curves from the FEM together with the corresponding tested specimens for long length beam column specimens ($L = 1219$ mm) for sample 1 to 6.	114
5.17	Load displacement curves from the FEM together with the corresponding tested specimens for long length beam column specimens ($L = 1219$ mm) for sample 7 to 12.	114
5.18	Load displacement curves from the FEM together with the corresponding tested specimens used Z1 & Z2).	115
6.1	Type of sections used in this study.	117
6.2	Effect of length-to-web plate depth ratio (L / h) on different frame elements.	119
6.3	Effect of plate slenderness ratio on different frame elements.	120
6.4	Effect of lip to flange plates length ratio (d/b) on different frame elements.	121
6.5	Effect of web-to-flange plate length ratio (h/b) on different frame elements.	122
6.6	Effect of Yielding stress (F_y) on different frame elements.	123
6.7	Comparison between EWM and DSM for CFS compression members.	126
6.8	Comparison between EWM and DSM for CFS Flexure members.	126
6.9	Effect of length-to-web plate depth ratio (L / h) on CFS member under compression loads with eccentricity.	131

LIST OF FIGURES

6.10	Effect of web plate slenderness ratio (h/t) on CFS member under compression loads with eccentricity.	132
6.11	Effect of lip-to-flange plates length (d/b) on CFS member under compression loads with eccentricity.	133
6.12	Effect of web-to-flange plate length ratio (h/b) on CFS member under compression loads with eccentricity.	134
6.13	Effect of yielding stress (F_y) on CFS member under compression loads with eccentricity.	135

LIST OF TABLES

Table	Title	Page
2-1	Comparison of Durations of RC and CFS Constructions.	13
2-2	Comparison of environmental considerations of RC and CFS constructions.	13
3-1	Different codes dimensional limits and considerations.	30
3-2	Comparison between resistance factors.	32
3-3	The EWM factors in different codes.	33
3-4	Plate buckling coefficient (K).	34
3-5	The nominal design of compression strength (resistance).	41
3-6	The nominal design of flexural strength (resistance).	43
4-1	Different sections used in the different codes parametric study.	59
5-1	The target and measured eccentricities in test.	67
5-2	Cross-section dimensions for test specimens used.	69
5-3	Nominal and measured material properties obtained from tensile coupon tests for test specimens used section columns	69
5-4	Analysis of Strengths Based on different element size.	71
5-5	Analysis of Column Strengths Based on different Geometric Imperfections and different element size.	78
5-6	Comparison between the elastic buckling outputs from CUFSM and ABAQUS.	80
5-7	Peak ultimate loads (experimental and FEM results) for three different lengths.	82
5-8	Peak ultimate loads (experimental and FEM results) for Z-section.	82
5-9	Failure modes from the FEM together with the corresponding tested specimens for short length beam column specimens (L =305 mm).	83
5-10	Failure modes from the FEM together with the corresponding tested specimens for Intermediate length beam column specimens (L = 610 mm).	87
5-11	Failure modes from the FEM together with the corresponding tested specimens for long length beam column specimens (L =1219 mm).	91
5-12	Failure modes from the FEM for specimens.	95

LIST OF TABLES

5-13	Load displacement curves from the FEM together with the corresponding tested specimens for short length beam column specimens ($L = 305$ mm).	97
5-14	Load displacement curves from the FEM together with the corresponding tested specimens for intermediate length beam column specimens ($L = 610$ mm).	101
5-15	Load displacement curves from the FEM together with the corresponding tested specimens for long length beam column specimens ($L = 1219$ mm).	105
5-16	Load displacement curves from the FEM together with the corresponding tested specimens.	109
6-1	CFS sections used in the research.	118
6-2	Different parameters used in this study.	118
6-3	Different sections used in EWM and DSM comparison study.	125
6-4	Comparison between EWM and DSM for CFS compression channel sections.	127
6-5	Comparison between EWM and DSM for CFS compression Z-sections.	127
6-6	Comparison between EWM and DSM for CFS flexure channel sections.	127
6-7	Comparison between EWM and DSM for CFS flexure Z-sections.	127
6.8	Different sections with combined bending and compression forces used in this study.	130
6-9	Comparison between interaction equations results for CFS channel sections.	136
6-10	Comparison between interaction equations results for CFS Z-sections.	137

LIST OF ABBREVIATIONS

Symbol	Definition
A_e	Effective area based on sections 4.2.2.1 & 4.2.2.2 in ECP ($A_e \neq A_{eff}$).
A_{eff}	Effective area of cross section by applying uniform compressive stress = F_y .
A_g	Gross area of cross section.
AISI	North American Specification.
A_n	Effective area of cross section by applying uniform compressive stress equal to F_n .
B	Total width of flange.
b	Flat width of flange.
C^*	Coefficient in ECP equal to 817 for rolled sections, and 470 for welded sections.
C_b	Bending moment coefficient [in ECP = 1].
CFS	Cold-formed steel.
D	Total width of lip.
d	Flat width of lip.
D'	Distortional buckling.
DSM	Direct Strength Method.
E	Young's modulus of steel material.
EC3	Eurocode-3_part1.3.
ECP	Egyptian Code of Practice (ECP-205).
EWM	Effective Width Method.
f	Compressive stress in element.
F	Flexural buckling
F_{cr}	Minimum critical buckling (elastic and inelastic) stress.
F_e	Minimum of elastic flexural, torsional, and flexural–torsional.
FE	Finite element.
FEM	Finite element model.
F_L	Coefficient in ECP equal to $0.75 F_y$ for rolled sections, and $0.6 F_y$ for built up sections.

LIST OF ABBREVIATIONS

FSA	Finite Strip Analysis.
FT	Flexural-torsional buckling.
F_y	Yielding strength of steel.
H	Total depth of web.
h	Depth of web.
HRS	Hot-rolled steel.
I_a	Adequate moment of inertia of the stiffener.
I_s	Moment of inertia of the full stiffener [$I_s = (d^3 t) / 12$].
K	Plate buckling coefficient.
L	Local buckling.
LGS	Light gauge steel construction.
LT	lateral-torsional buckling.
M_{cr}	Critical elastic moment, as calculated in section 5.1.3 in ECP.
M_{crd}	Critical elastic distortional buckling moment.
M_{cre}	Critical elastic global buckling moment.
M_{crL}	Critical elastic local buckling moment.
M_n	Nominal bending strength.
M_{nd}	Buckling resistance for distortional buckling in beam
M_{ne}	Buckling resistance for global buckling in beam.
M_{nL}	Buckling resistance for local buckling in beam.
M_p	Plastic moment, as calculated in section 5.1.3 in ECP.
M_u	Flexural design strengths.
M_y	Yield moment.
P_{crd}	Critical elastic distortional buckling load.
P_{cre}	Critical elastic global buckling load.
P_{crL}	Critical elastic local buckling load.
P_{EX}	Euler loads in x direction.
P_{Ey}	Euler loads in y direction.
P_n	Nominal axial strength.
P_{nd}	Buckling resistance for distortional buckling in column.
P_{ne}	Buckling resistance for global buckling in column.

LIST OF ABBREVIATIONS

P_{nl}	Buckling resistance for local buckling in column.
P_u	Axial design strengths.
P_y	Squash (yield) load.
Q	Reduction factor for slender sections in ECP ($Q = A_e / A_g$).
RCC	Reinforced concrete construction.
RI	Ratio between Adequate moment to moment of inertia of the full stiffener [$I_s / I_a \leq 1$].
s.c.e	Stiffened compression element.
S_e	Elastic section modulus of effective section calculated at F_n .
S_{eff}	Elastic section modulus of effective section calculated at F_y .
T	Torsional buckling.
t	Thickness of section.
u.c.e	Unstiffened compression element.
x	Reduction factor as in EC3 to determine the buckling resistance.
X_{LT}	Reduction factor for lateral torsional buckling, obtained from section 6.2.4 in EC3.
α	Imperfection factor from buckling curve in EC3.
λ_p	Normalized plate slenderness.
λ'	Non-dimensional slenderness defined in EC3.
λ_c	Slenderness as defined in AISI.
ρ	Reduction factor.
Φ_b	Resistance factor for bending.
Φ_c	Resistance factor for compression.
Ψ	Stress ratio.

CHAPTER (1)

INTRODUCTION

1.1 BACKGROUND

Cold formed steel (CFS) sections are one of the most widely used sections in different industrial and civil engineering fields, and their use is increasing day by day. Steel frame domestic houses, low rise office buildings , industrial warehouses [1], bridges, storage racks, car bodies, railway coaches, transmission towers and poles [2] depend mainly on CFS for their construction and composition.

The history of using CFS sections in construction dates to the early 19th century, when the first iron bridges were built using cold-formed steel sections. However, it wasn't until the mid-20th century that the use of CFS started to gain widespread acceptance in the construction industry [3].

In the 1930^s, the American Iron and Steel Institute (AISI) began conducting research on the use of CFS in building construction. This research led to the development of the first CFS design specification in 1946, which was based on the use of sheet steel with a thickness of up to 1.626 mm [3].

The role of cold-formed steel (CFS) in World War II, which occurred from 1939 to 1945, was significant, particularly in the construction of military equipment and infrastructure. CFS was used to make various components of aircraft, such as wing spars, fuselage frames, and engine mounts. It was also used in the construction of military vehicles, such as tanks and armored personnel carriers. In addition, CFS was used in the construction of military infrastructure, such as barracks, hangars, and storage facilities [3].

In the 1950^s and 1960^s, advances in manufacturing technology, such as the development of high-speed roll-forming machines, made it possible to produce CFS sections with greater precision

and at a lower cost. This, in turn, led to the increased use of CFS in construction, particularly in the design of roof and floor systems for low-rise buildings [3].

In the 1970^s and 1980^s, the use of CFS expanded to include the construction of mid-rise and high-rise buildings, as well as the development of new applications such as load-bearing walls and curtain walls. During this time, new design specifications were developed to address the unique properties of CFS, including its high strength-to-weight ratio and its susceptibility to buckling under compressive loads [3].

In the 1990^s and 2000^s, the use of CFS continued to expand globally, driven by increasing demand for sustainable and cost-effective building materials. In addition, new manufacturing techniques such as cold-formed steel framing software and computer-aided design tools made it possible to design and fabricate complex CFS structures with greater ease and precision [3].

The number of residential and low-rise structures constructed using cold formed steel in the United States was estimated to be over 75000 in 1994. In 2002, this number increased by five times [4]. Nowadays, there are many attempts and researches that have been done to find out the potential and ability of using the CFS sections with larger spans and higher loads [5].

Today, CFS is used extensively in the construction of buildings, bridges, and other infrastructure projects around the world. The high demand for the use of these sections is due to several advantages, including:- their high strength to weight ratio, simplicity and adaptability in their fabrication, their various cross-sectional shapes (Z-section, C-section, hat-section, and Σ -section) which make them suitable for various works [6], economic design and forming process [7], light weight making them easy to transport and erect , high resistance to corrosion with an attractive surface finish and all traditional jointing techniques (riveting ,bolting , welding and adhesives) can be used [4] . In addition, CFS meet the standards of sustainability. In fact, the use of recyclable and light gauge materials, system flexibility, the dry building process, and the ability to reuse elements at the end of the life cycle all help to reduce environmental impacts.

Research has been conducted on the disparities in time and expenses between utilizing reinforced concrete (RC) frames and light gauge steel construction (LGS). The research shows that CFS construction is 40% more cost-effective than regular concrete construction for a one-story

structure with an area of 81 m². In addition, it was discovered that CFS is four times quicker and considerably more effortless to fabricate than RC [8].

Satpute and Varghese (2012) delved deep into analyzing a single-level industrial structure spread across an area of 750 m² to draw a comparison between the expenses and weight of hot-rolled steel (HRS) and CFS. Their research revealed that replacing HRS with CFS components resulted in a significant decrease of 35% in overall cost and material consumption [9].

Using RC for construction yields a significant increase in total cost and construction time by up to three times compared to CFS. Additionally, CFS may offer up to 86% more benefits compared to using HRS [10].

Based on all these advantages, it was necessary to know the different methods of designing CFS sections and study their behavior under the influence of different loads and this is the purpose of our research.

Although the utilization of CFS symmetric shapes of compound sections is generally preferred because of their ability to eliminate eccentricities between shear and gravity centers, thus contributing to higher member stability [11], the focus of this research has been directed toward single sections. This shift in attention is due to the more complex failure behavior associated with single sections. Moreover, predicting the type of buckling that may occur when utilizing a single section can present significant challenges [12]. The utilization of channel and Z-sections encompasses various metal building roof and wall systems. These systems may comprise through-fastened roofs (walls), bracing system or standing-seam roofs that are subjected to either gravity (pressure) or uplift (suction) loading [13]. In addition, these sections are used in purlins and girts that are subject to flexural load.

Two methods commonly used for designing CFS sections are the Effective Width Method (EWM) and the Direct Strength Method (DSM). The EWM, introduced by Von Karman [14] and amended by Winter [15], is widely adopted for CFS member design. This method reduces the efficacy of buckled plates within a cross-section by reducing each plate to its effective width. The model of the effective cross-section accurately represents areas where the material's load-bearing capacity is insufficient. However, it does not consider inter-element equilibrium and compatibility, making the analysis of elastic buckling more complex. Moreover, the EWM lacks sufficient

guidelines for anticipating distortion buckling failure. It necessitates multiple iterations to ascertain the basic strength of the element, thereby augmenting the intricacy of section optimization [16].

The DSM is another design method for CFS members. Schafer [17] did a review on the utilization of DSM in CFS design. It was adopted in 2004 as Appendix 1 of the North American Specification [18]. It is an alternative to EWM for estimating CFS strength. It considers buckling modes and avoids iterations or calculations of effective width [19]. It uses the cross-section's properties and elastic buckling behavior to calculate strength. It is based on member elastic stability. The section's strength can be determined directly [16].

This study compares CFS capacities (compression, flexure, and their combination) between Egyptian [20], American [21] and European [22] codes to identify the extent of incompatibility and compatibility between their method for determining CFS capability and encourage accelerated education with previously knowledge of one code.

This study includes computer software to assist designers in design and check the safety of CFS sections and determining CFS capacity using different aforementioned codes. Furthermore, it functions effectively under varied conditions and immediately gives complete calculation sheets.

1.2 RESEARCH OBJECTIVE:

The fundamental objective of the project is to create software for designing CFS sections in various codes, as well as to highlight similarities and differences between various steel structure codes. This software streamlined the analysis, enabling more efficient and accurate evaluations of the innovative CFS sectional profiles' capacities. This research offers valuable insights into the performance of innovative CFS channels and Z-profiles, facilitating a deeper understanding of their structural capacities and providing a foundation for potential applications in modern engineering design and construction practices. With the help of this program, we can obtain for each code a safe, economical and fast design of CFS sections and a comparison between the Egyptian [20], American [21] and European [22] codes.

The second objective is to investigate strengths exhibited by CFS members with channel and Z-profiles and assess the influence of various parameters on the capacities of these CFS members.

The third aim of this study is to investigate the performance of CFS members with channel and Z-profiles subjected to bending, compression, or both, and to evaluate the impact of different parameters on the behavior of these CFS elements.

1.3 RESEARCH METHODOLOGY:

The computer software was created to program the calculation procedure for the different aforementioned codes with the aim of improving the computational speed of the calculation process. This software was created in the C⁺ programming language and can design, check, and determine the maximum strength of CFS sections, specifically those with channel or z-profile that are subjected to axial load, bending moment, or a combination of both, along with providing calculation sheets.

The Finite Element Model (FEM), which has become indispensable in the engineering field due to its relative affordability and time savings compared to physical and practical live lab experiments, especially during the parametric study of cross-section geometries, was created using the ABAQUS [23] program, which is a nonlinear finite element analysis tool.

1.4 ARRANGEMENT OF THE THESIS:

This section explains how the seven chapters of this study are organized.

Chapter (1): INTRODUCTION

This chapter includes the introduction, research objective, and arrangement of the thesis.

Chapter (2): LITERATURE REVIEW

This chapter includes CFS steel design standards and provisions, an overview of CFS and a detailed review of the previous research worked in the field of CFS.

Chapter (3): STUDY ON DIFFERENT CODES

This chapter includes several code equations and formulas for comparison purposes based on Egyptian [20], American [21], and European [22] codes .

Chapter (4): THE PRESENT PROGRAMME

This chapter has a guidebook that covers the whole software manual and gives the user tips on how to use the software more successfully. In addition to verifying the validity and accuracy of the program results, it also contains parametric study based on different codes.

Chapter (5): FINITE ELEMENT MODEL

This chapter describes the numerical models using a finite element (FE) package and the verification of the results.

Chapter (6): PARAMETRIC STUDY

This chapter generates further data by conducting parametric studies on ultimate CFS capacities using the verified FE model. Additionally, it presents a comparative analysis between different codes and the FE model.

Chapter (7): SUMMARY, CONCLUSIONS AND RECOMMENDATIONS

This chapter includes summary, conclusions, and recommendations for future work.

Reference:

Reference contains the references which are used in this thesis.

Appendix (A):

This appendix includes details of different FE Modes and the comparisons between Effective Width and Direct Strength Methods used in the parametric study in chapter 6.

Chapter (2)

LITERATURE REVIEW

2.1 INTRODUCTION

This chapter provides an overview of cold-formed steel sections, covering several key aspects. It starts with a background on the topic and then delves into the various design methodologies and philosophies that are used for cold formed steel sections. Additionally, it includes a review of existing research on cold-formed steel sections, as well as an examination of different design specifications and software programs that are available for their use. Overall, this chapter serves as a resource for anyone seeking to gain a deeper understanding of cold-formed steel sections and their design principles.

2.2 COLD FORMED STEEL SECTIONS OVERVIEW

Cold-formed steel (CFS) sections are unique structural elements crafted from thin sheets of steel. The thickness of steel sheet or strip utilized in CFS structural members usually ranges from 0.378 mm to around 6.35 mm, with steel plates and bars as thick as 25.4 mm being successfully cold formed into structural shapes [24]. To prevent corrosion, the steel is often coated with a protective layer such as zinc. The steel sheets are carefully fed into a roll-forming machine, which gradually bends and shapes the steel into the intended profile [25]. An extensive range of shapes, including C-sections, Z-sections, Σ -section, hat sections, and angle sections, may be effortlessly produced by using roll-forming machines, as illustrated in **Figure 2.1**.

Once the CFS sections have been formed, they can be cut to length and further processed as needed. Additional processing may include punching, drilling, or welding to create finished products.

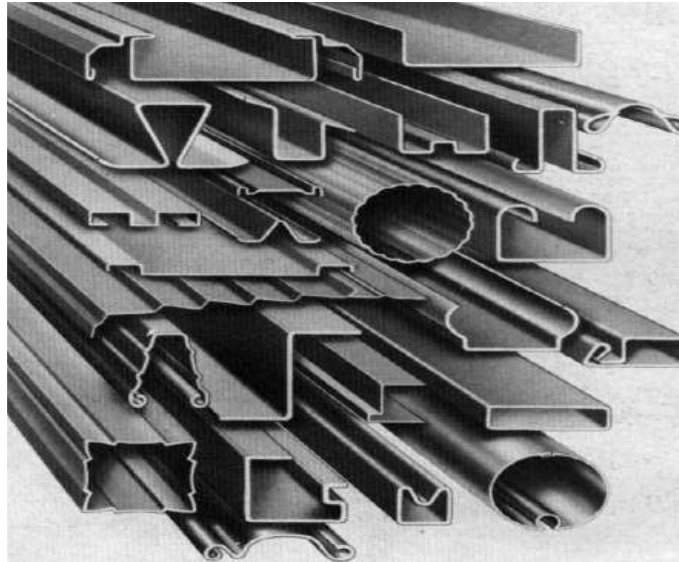


Figure 2.1: Various shapes of cold-formed sections [26].

While CFS sections have a wide range of applications, including car bodies, railway coaches, storage racks, grain bins, highway products, transmission towers, transmission poles, drainage facilities, and bridge construction [1, 2, 24], the discussions in the following chapters primarily concentrate on their use in construction industry.

In the 1850s, the utilization of CFS members in the construction of buildings was first observed in both the United States and Great Britain. However, it was not until approximately 1940 that such steel components became commonplace in constructions [24]. Winter meticulously examined the early development of steel structures [27, 28]. Following the issuance of numerous editions of the "Specification for the Design of Cold-Formed Steel Structural Members" by the American Iron and Steel Institute (AISI), the use and advancement of thin-walled CFS construction in the United States have been expedited since 1946. The initial versions of the standard were predominantly derived from AISI-funded research studies conducted at Cornell University under the watchful guidance of George Winter since 1939 [24].

2.2.1 Manufacturing of Cold-Formed Sections

CFS members are commonly produced through either of two techniques. These techniques include roll forming and the process of folding and press braking.

Roll forming involves the continuous feeding of a steel strip through a series of opposing rolls. This process gradually deforms the steel in a plastic manner to achieve the desired shape. Each set of rolls applies a fixed amount of deformation in a specific sequence, as illustrated in **Figure 2.2**.

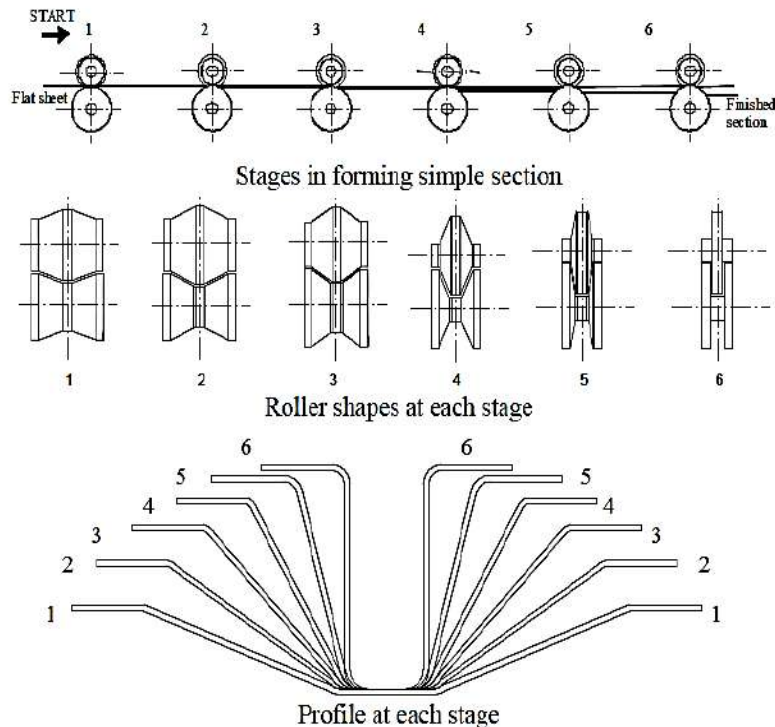


Figure 2.2: Roll forming [24].

Folding is a relatively straightforward technique used to produce specimens of short lengths and simple geometries from a sheet of material. This is accomplished by creating a series of bends, as shown in **Figure 2.3 (a)**. However, the application of this process is quite limited. In contrast, press braking is a more widely employed method that allows to produce a greater variety of cross-sectional forms. In this process, a section is formed by pressing a length of strip between shaped dies, resulting in the desired profile shape, as illustrated in **Figure 2.3 (b)**. Typically, each bend is formed individually.

Roll forming is commonly used for the fabrication of sections in circumstances where there is a significant requirement for a particular shape. While the initial expenses associated with tooling are substantial, the subsequent costs related to labor are minimal. On the other hand, brake

pressing is typically utilized for production on a smaller scale, where a diverse array of shapes is necessary, and the costs associated with roll forming cannot be reasonably justified.

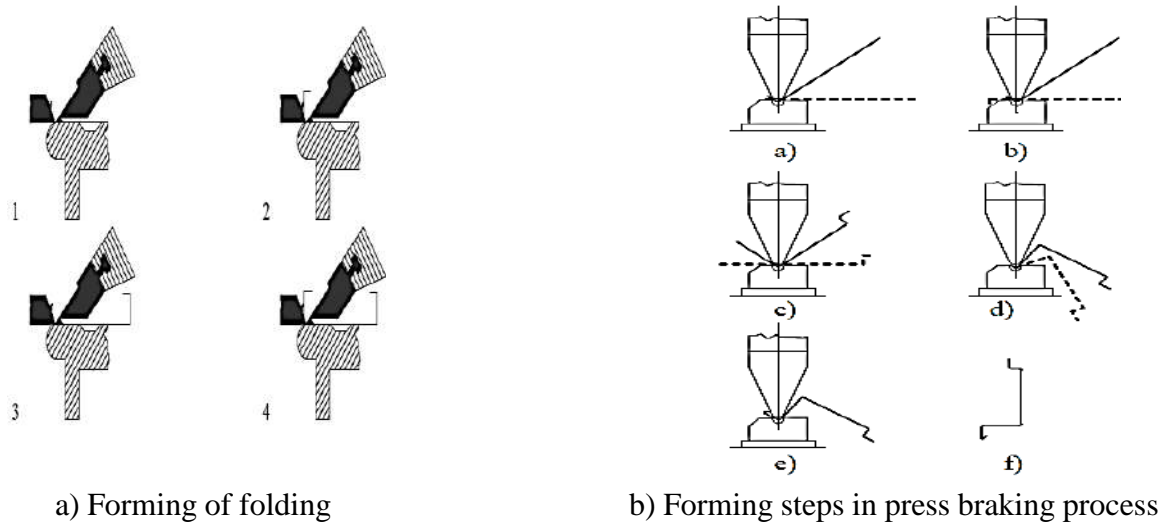


Figure 2.3: folding and press braking [24].

2.2.2 Types of Cold Formed Steel Sections

Cold-formed sections and profiled sheets are steel products that are manufactured from flat strips or coils of hot-rolled or cold-rolled steel, with or without a protective coating. These products have a variable or constant cross-sectional shape, falling within the allowable range of tolerances [25]. There are two main types of cold-formed structural members: -

- Individual structural members
- Panels and decks

2.2.2.1 Individual Structural Members

Individual structural members, also known as bar members, can be obtained from "long products" and include the following types [25]:

- Single open sections, as shown in **Figure 2.4 (a)**.
- Open built-up sections, as shown in **Figure 2.4 (b)**.
- Closed built-up sections, as shown in **Figure 2.4 (c)**.
- Closed sections, as shown in **Figure 2.4 (d)**.

These sections are suitable for using as primary framing members in buildings up to six stories height [29] and can be used as chord and web members of open web steel joists, space frames, arches, and storage racks [24].

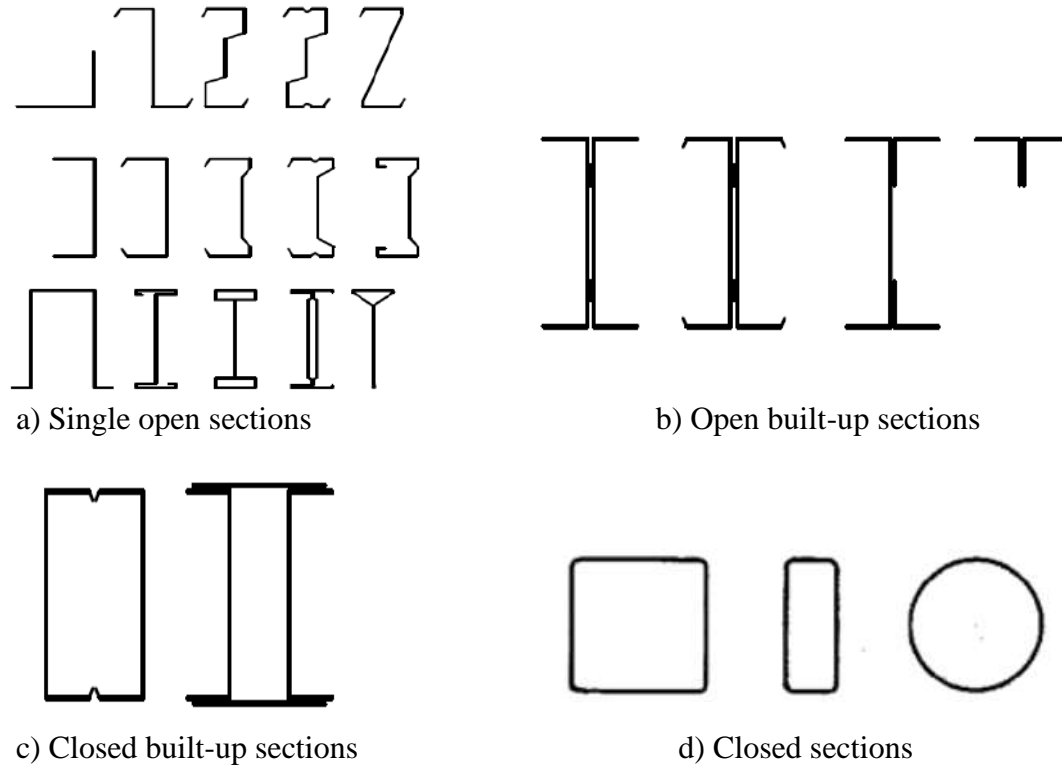


Figure 2.4: Typical forms of sections for cold-formed structural members [25].

Cold-formed individual framing members are typically between 51 and 305 mm deep, with a thickness of material between 1.2 to about 6.4 mm. However, some members may be as deep as 457 mm and have a thickness of 13 mm, particularly for transportation and building. Additionally, steel plate sections with thicknesses up to about 19 or 25 mm have been used for various applications such as transmission poles and highway-sign support structures. The possibilities for cold-formed steel are vast and continue to expand in construction and engineering [24].

2.2.2.2 Panels and Decks

Panels and decks have a widespread application in the construction industry for creating roof and floor decks, wall panels, siding material, and bridge forms [25]. To manufacture these

panels and decks, profiled sheets and linear trays (cassettes) are commonly used, as depicted in **Figure 2.5**. The panels have a depth range between 38 to 191 mm and are composed of materials with thickness varying from 0.5 to 1.9 mm [13].

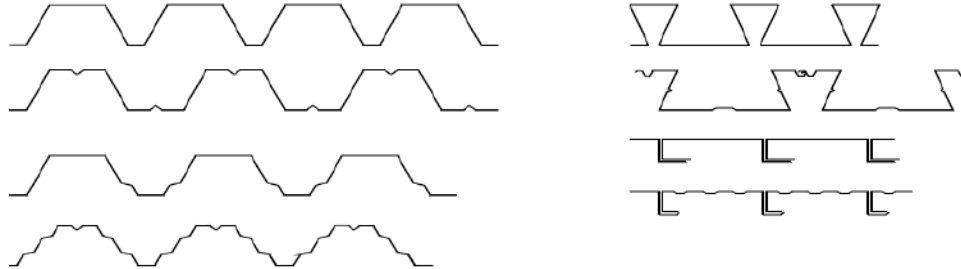


Figure 2.5:- Profiled sheets and linear trays [25].

To enhance the rigidity of cold-formed steel sections as well as sheeting, the utilization of edge and intermediate stiffeners is demonstrated in **Figure 2.6**.

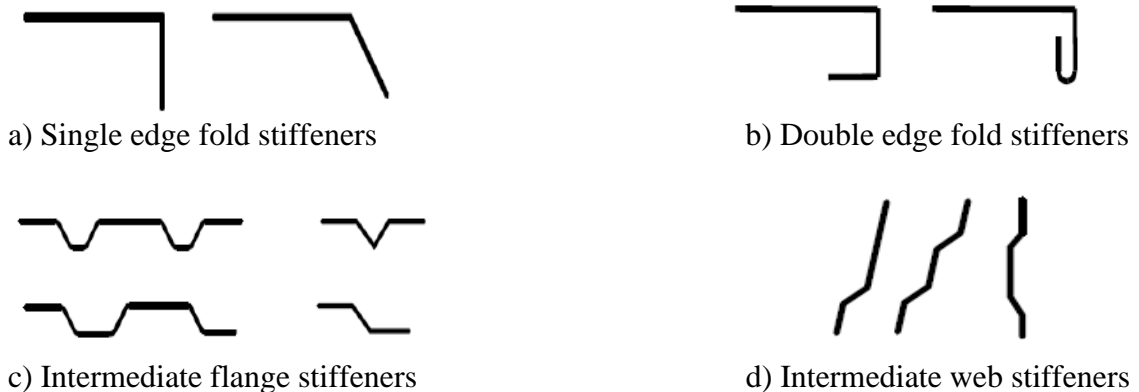


Figure 2.6:- Typical forms of stiffeners for cold-formed members and sheeting [25].

Our research will focus on studying the behavior of single open cold formed sections with channel and Z-profile and have Single and vertical edge fold stiffeners under static compressive and flexural loads.

2.2.3 Advantages of Cold-Formed Steel Sections

In 1997, Grub and Lawson authored a guide titled "Building Design Using Cold-Formed Steel Sections: Construction Detailing and Practice" which was released by the Steel Construction Institute (SCI). The guide highlights the benefits of utilizing cold-formed steelwork for construction purposes and service, providing a comprehensive list of advantages [30].

The research by Qureshi et al. reveals that the creation of a single level edifice with a total area of 81 m² with cold-formed steel (CFS) is 40% more economical than using reinforced concrete (RC). Not only that, but the CFS construction method is also four times quicker and simpler to produce compared to RC. This is demonstrated in **Tables 2.1 & 2.2**, which provide a thorough comparison of timeframes and ecological considerations between RC and CFS for the examined structure [8].

Table 2.1: Comparison of Durations of RC and CFS Constructions [8].

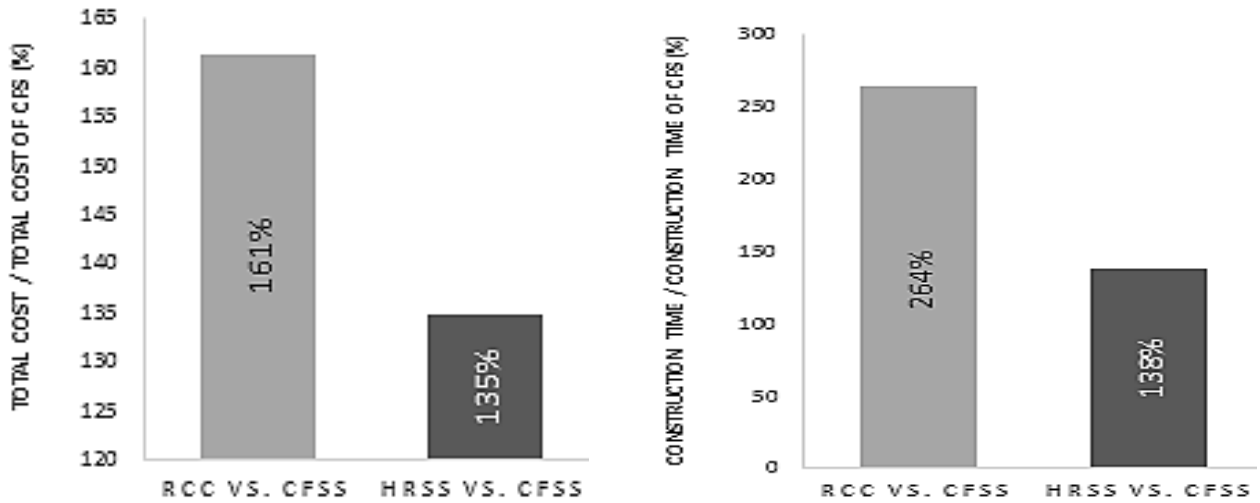
Comparison factor	RC construction	CFS construction
Duration	66 days	16 days

Table 2.2 : Comparison of environmental considerations of RC and CFS constructions [8].

Comparison factor		RC constructions	CFS constructions
Recycling	Recycled content	0%	60%
	End of lifetime recycling rate	50%	98%
Noise pollution		No preventive measures	Sensitive to the audio frequency ranging 250-1000 Hz

A study conducted on a four-story office building with a total area of 960 m² has revealed that the use of CFS sections in mid-rise structures can result in substantial savings in terms of material, building costs, and construction time when compared to reinforced concrete construction (RCC) and hot rolled section (HRS) structures [10]. The advantages of constructing a CFS building are manifold, with savings of 61% and 35% in overall cost (material + construction) when compared to RC and HRS respectively. The construction time of a CFS building is also significantly less, taking 38% and 164% less time than HRS and RC respectively. **Figure 2.7** illustrates the differences between CFS and other building types. In comparison to RC, Using RC for construction yields a significant increase in total cost and construction time by up to three times

compared to CFS. Furthermore, the use of CFS may also provide up to 86% more benefits than HRS, as shown in **Figure 2.8**.



a) the construction total costs

b) the construction duration.

Figure 2.7:- Relative differences between CFS building and other building types regarding [10].

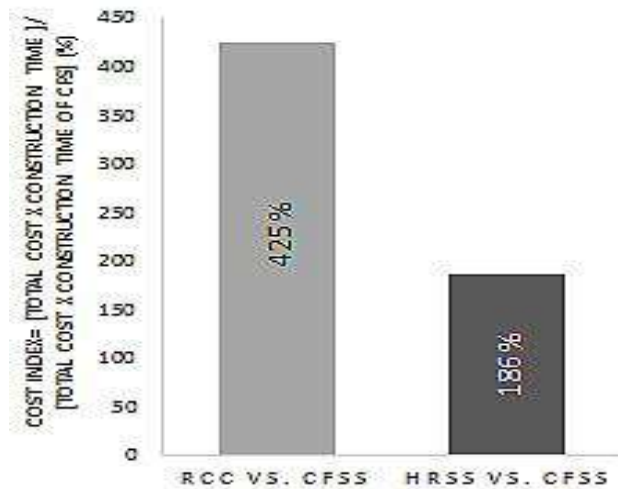


Figure 2.8 :- Relative differences between CFS building and other building types regarding both total costs and the construction duration [10].

A study conducted by Sangave et al. [31] revealed that when it comes to constructing buildings with ground plus six stories (G+6), reinforced concrete (RC) frames are more cost-effective compared to hot-rolled steel (HRS) frames. The study showed that the bare steel frame for a G+6 building costs 31% more than the RC frame. However, for ground plus ten stories (G+10) buildings, the RC frame costs 34% less than the bare steel frame. On the other hand, a 2012 analysis [9] by Satpute and Varghese demonstrated that the use of CFS members instead of HRS resulted in a 35% reduction in total material and cost for a one-story industrial building of 750 m², as depicted in **Figure 2.9**.

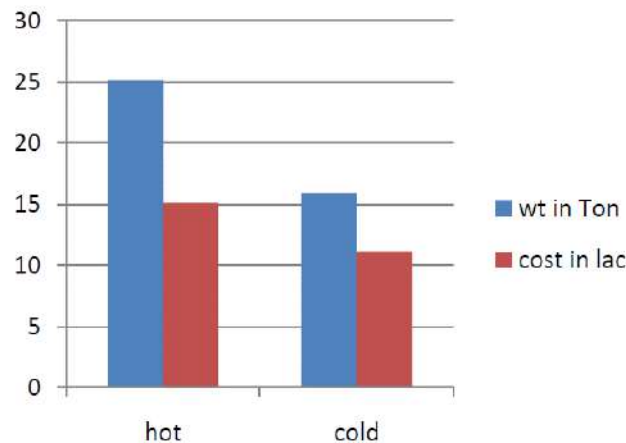


Figure 2.9 :- Relative differences between cost and weight of CFS and HRS [9].

The following are some of the major advantages of using CFS sections in construction:

1. **High strength-to-weight ratio:** The CFS sections, with their lightness and remarkable strength-to-weight ratio, have emerged as the perfect candidate for erecting edifices and constructions that demand a high strength-to-weight ratio.
2. **Cost-effective:** CFS sections are cost-effective compared to other materials like concrete and masonry. They can be manufactured quickly and easily, which reduces labor costs and construction time.
3. **Versatility:** CFS sections can be easily shaped and cut to fit any design requirement, making them highly versatile. They can be used in a variety of applications, including walls, roofs, floors, and frames.
4. **Sustainability:** CFS sections are not only eco-friendly but also sustainable. These sections are crafted from reused materials and can be reused again when their life span is

over. Additionally, they require less energy to manufacture, thereby diminishing their carbon footprint, as compared to other materials.

2.2.4 Disadvantages of Cold-Formed Steel Sections

While cold-formed steel (CFS) has many advantages in construction industry, there are also some disadvantages that should be considered, including:

1. **Susceptibility to corrosion:** CFS is vulnerable to corrosion if it is not properly coated or protected. This can lead to structural damage and reduced lifespan if not addressed. To prevent corrosion in cold-formed steel, follow these steps: select appropriate coating, handle and store properly, ensure proper ventilation, consider design factors, and perform regular maintenance.
2. **Limited fire resistance:** CFS is not as fire-resistant as other materials such as concrete or masonry. It can deform or even collapse under high temperatures, which can pose a safety risk in some applications. Increasing the fire resistance of cold-formed steel (CFS) structures can be achieved by increasing steel thickness, adding fire-resistant insulation, using fire-resistant coatings, incorporating fire barriers, and properly designing and installing fire protection systems.
3. **Limited structural stiffness:** CFS is not as stiff as other materials such as concrete or timber, which can limit its suitability for certain applications. Additional bracing or reinforcement may be required to achieve the necessary structural stiffness.
4. **Noise transmission:** CFS can transmit noise more easily than other materials such as concrete or timber. This can be a concern in some applications, such as multi-unit residential buildings.
5. **Higher skill level required for installation:** The installation of CFS requires a higher level of skill and precision compared to other materials, which can result in higher labor costs and longer installation times.

Overall, while CFS offers many advantages in the construction industry, it also has some limitations and disadvantages that should be considered when selecting construction material.

2.3 DESIGN METHODS OF COLD-FORMED SECTIONS

In the design of CFS members, two widely used methods exist. The first one, referred to as the Unified Method or the Main Specification Method, is commonly known as the Effective Width Method. This traditional approach is utilized in design specifications all over the world. The second technique, the Appendix 1 Method, is known as the Direct Strength Method, and is only employed in North America, Australia, and New Zealand.

Multiple design methods are available, including the Reduced Stress Method, Effective Thickness, the Q-factor approach, and the Erosion of Critical Bifurcation Load approach. While these methods are worth mentioning, their comprehensive discussion is beyond the scope of this text.

2.3.1 Effective Width Method

The Effective Width Method (EWM) is a commonly used design approach for CFS members. This method is explained in detail in different codes, textbooks, and specifications. EWM was originally introduced by Von Karman [14] and subsequently amended by Winter [15], and has been widely adopted as the primary design method for CFS members. The fundamental concept underlying this method is that when plates within a cross-section buckle locally, their efficacy is reduced. The essential step of this method is to reduce each plate to its effective width as illustrated in the following **Figure 2.10**. The model of the effective cross-section is a precise representation of locations where the load-bearing capacity of the material is insufficient. Despite this, it fails to take into account the vital aspects of inter-element equilibrium and compatibility, thereby making the analysis of elastic buckling more intricate. Furthermore, the EWM does not provide adequate guidelines to predict the failure of distortion buckling. Determining the essential potency of a member necessitates several iterations, inevitably intensifying the intricacy of optimizing the section [16].

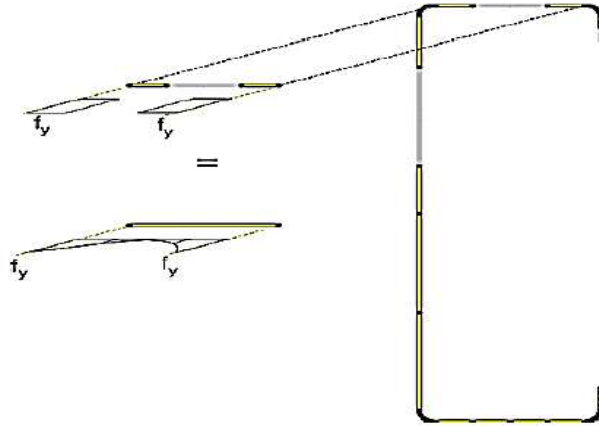


Figure 2.10 :- Fundamental step for the Effective Width Method [16].

For more than six decades, the conventional EWM has been the fundamental approach towards gauging the potency of CFS components. Nonetheless, with the growing intricacy of structural shapes, including lips and intermediate stiffeners, the precise computation of effective widths of individual constituents within these shapes has become more arduous and less precise [32]. Consequently, to tackle this challenge, the Direct Strength Method (DSM) was formulated.

2.3.2 Direct Strength Method

The DSM is an innovative technique for designing CFS components. Schafer [17] was a pioneer in examining the DSM's application in CFS design, and it was subsequently included as Appendix 1 in the North American Specification [18], providing an alternative to the EWM for determining CFS strength. By taking into account various buckling modes and eliminating the need for iterations or effective width calculations [19], this approach considers the interaction of these modes. Instead of relying on effective width, the DSM employs the cross-section's gross properties and its elastic buckling behavior to determine section or member strength. It is based on accurate member elastic stability, so the section's strength can be determined directly [16], as illustrated in **Figure 2.11**.

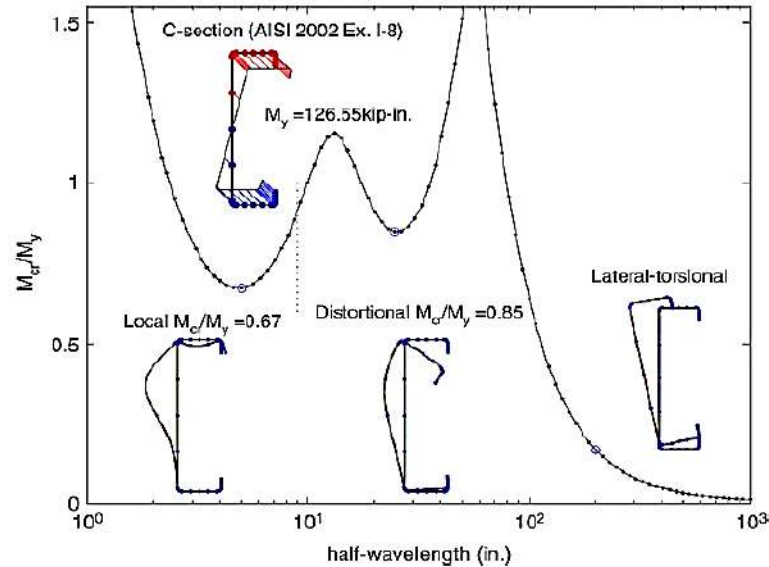


Figure 2.11:- Fundamental step for the DSM Method [16].

2.4 SOFTWARE PROGRAMS

There are several software programs available for the design of CFS sections, which help structural engineers and designers in analyzing and designing CFS members and systems efficiently and accurately. These programs are divided into two basic types based on their reliance on either Finite Element or Finite Strip Analysis.

2.4.1 Finite Element Analysis (FEA) Software Programs

Finite element analysis (FEA) software programs are computer programs modeling and analysis tools for complicated engineering problems. These programs utilize numerical approaches to predict a system's behavior and forecast its response to different loads and boundary conditions. These software programs may be used to analyze the behavior of CFS structures and to determine stresses, strains, and displacements in the structures under different loading conditions. There is many popular FEA software such as ABAQUS, ANSYS, and SAP [23, 33-36].

2.4.2 Finite Strip Analysis (FSA) Software Programs

The finite strip (FS) method is a numerical approach for analyzing thin-walled structures, such as cold-formed steel (CFS) sections. There are many popular FS software such as CUFSM, CFS, and THIN WAL [37, 38].

2.5 COLD-FORMED STEEL BUCKLING STRENGTH

When it comes to designing structures using thin-walled sections and cold-forming manufacturing techniques, there are some distinctive design challenges that are not usually encountered when using thicker hot-rolled sections. These challenges can include issues with buckling strength.

Steel sections are susceptible to various types of buckling, namely local, global, distortional, and shear. In the case of cold-formed steel sections, local buckling (L) is commonly observed, which arises from the short-wavelength buckling of individual plate elements. The term "global buckling," on the other hand, pertains to flexural (F) and flexural-torsional (FT) buckling of columns, as well as lateral-torsional buckling (LTB) of sections. This type of buckling is also known as "rigid body" buckling since the entire cross-section moves as a rigid body without any distortion. Distortional (D) buckling, meanwhile, is recognized by the relative movement of the fold-lines of the cross-section, with its wavelength generally between that of local and global buckling [24, 25]. **Figure 2.12** provides a visual representation of compression single buckling modes.

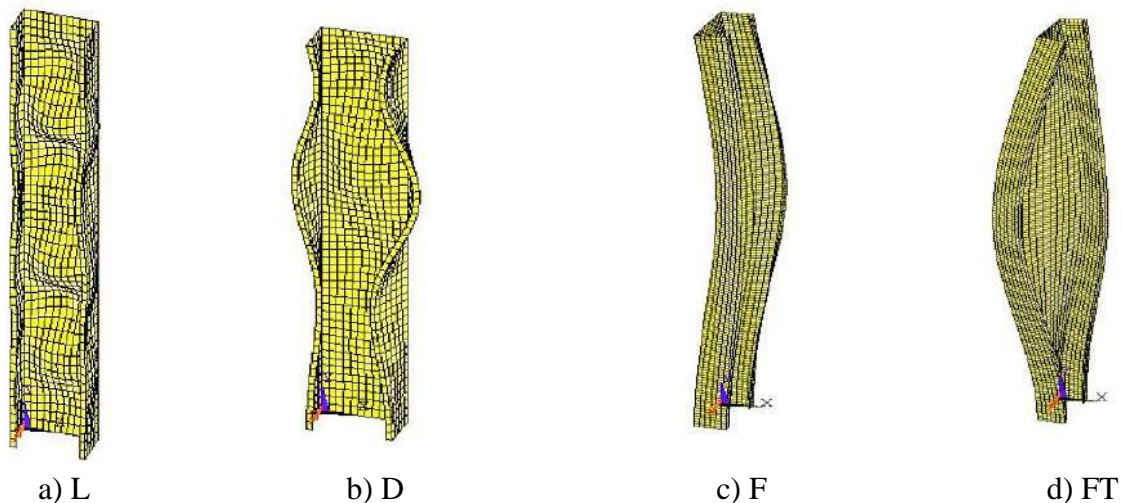


Figure 2.12: - Compression single buckling modes [25].

Local buckling (L) refers to the instability of a small portion of the member, typically near the ends or at points of high stress. Local buckling can occur in the flanges or in the web of cross sections. It involves deflection of the plate out of its initial plane. Distortional buckling (D) happens when the section's flanges begin to deform out of plane due to compressive loads and can lead to a reduction in strength and stiffness. Overall column buckling refers to the instability of the entire member. It can occur in different modes, including flexural, torsional, and flexural-torsional buckling modes. Flexural buckling (F) happens when a compression member bends about a principal axis. This mode of instability is more common in members that are slender or have a low flexural rigidity relative to their length. It involves transverse displacements of the member cross section. Torsional buckling (T) occurs when a compression member twists about its shear center. This mode of instability is more common in members that have a low torsional rigidity relative to their length. It involves twist rotations of the member cross section. Flexural-torsional buckling (FT) happens when a compression member both bends and twists simultaneously. This mode of instability is more common in members that are both slender and have a low flexural and torsional rigidity relative to their length. It involves both transverse displacements and twist rotations of the member cross section. Lateral torsional buckling (LT) occurs when a flexural member is subjected to a combination of bending and twisting moments. This can cause the member to buckle laterally, reducing its load-carrying capacity and potentially causing failure. Lateral torsional buckling is particularly common in thin-walled CFS members, which have a relatively low torsional stiffness.

As the shapes of sections become more intricate, the calculations for local buckling become more intricate as well, and distortional buckling becomes more significant. These modes of local and distortional buckling are deemed "sectional" and can interact with one another, as well as with global buckling, as stated by Dubina [25]. The coupled buckling modes of compression interactive are depicted in **Figure 2.13**.

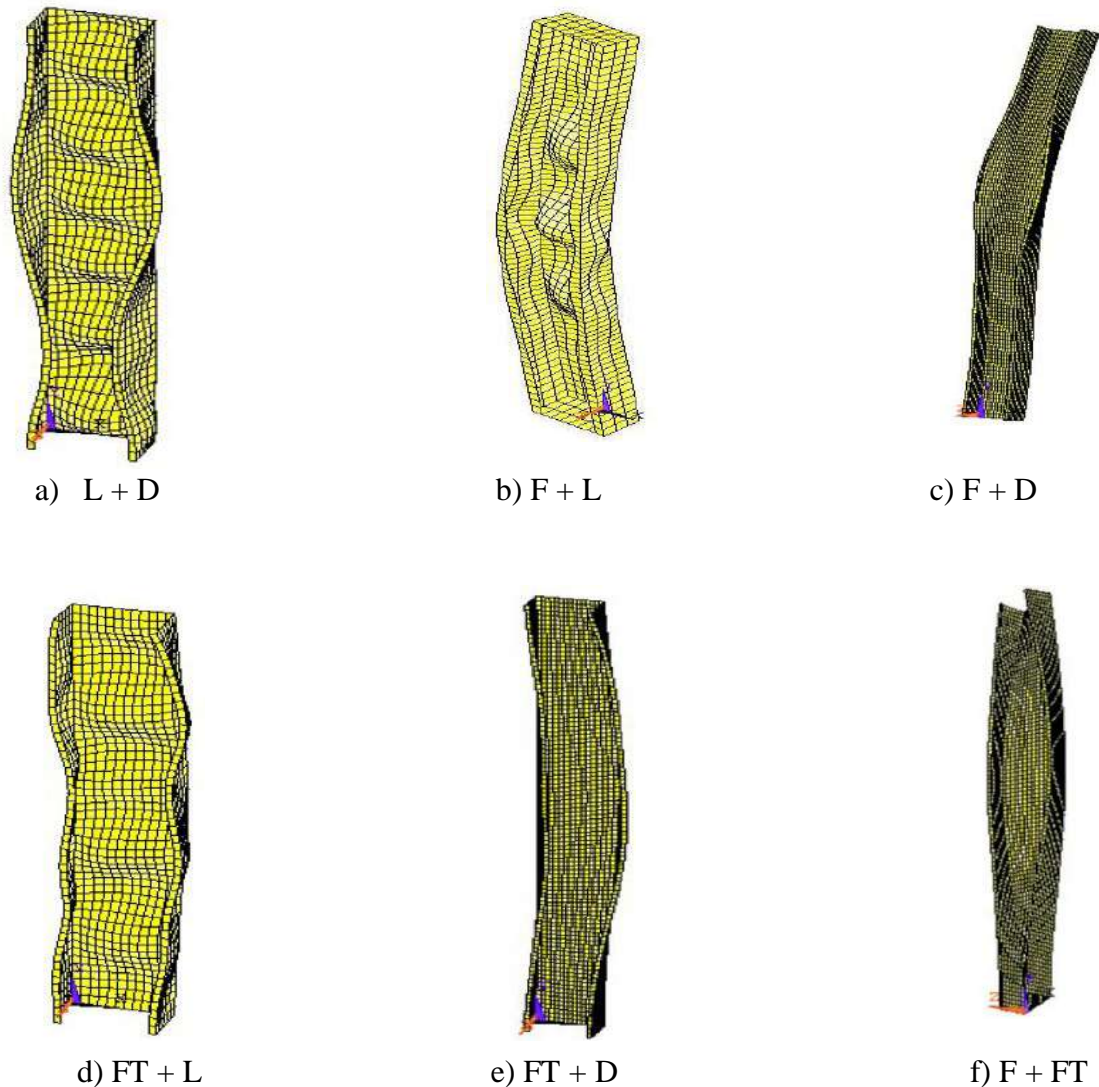


Figure 2.13: - Compression interactive (coupled) buckling modes [25].

2.6 COLD FORMED SECTION RESEACHES

CFS is of great interest to researchers, as there are many studies that have dealt with it, and these studies can be divided according to their field of interest as follows: -

2.6.1 Research on CFS Member Behavior

The behavior of built-up channel sections has been extensively studied in previous research [39-47]. Various studies have been conducted on closed-compound sections [48-51]. Furthermore, some studies have investigated the impact of web openings [52-54].

Manikandan et al. [43] conducted a study on the bending behavior of innovative cold-formed steel (CFS) back-to-back channel sections with folded flanges and complex edge stiffeners, using both experimental and numerical methods. Their findings showed that the sections with complex edge stiffeners and folded flanges exhibited the highest bending strength.

Wang and Young [40] conducted an investigation on the behavior of simply supported built-up section beams with various web intermediate stiffeners under both four-point bending and three-point bending tests.

Poologanathan and Mahendran [47] studied the shear behavior and strength of an innovative CFS Beam section with box flanges. The specimens were tested in both a single and back-to-back configuration, and the results showed significant improvement in shear strength compared to conventional lipped channel sections.

In Yener et al. [55], a failure criterion was established for beams with uniform moment and moment gradient, which was based on the ultimate compressive strain. Subsequently, the researchers expanded their investigation to explore the load-bearing capacity of cold-formed steel beams with compression flanges reinforced with stiffeners. Two years later, the authors shared their discoveries on the application of partial section classification in cold-formed steel flexural elements. Additionally, they provided equations for determining the ultimate moment capacity of cold-formed steel sections that are utilized in design and analysis, as noted in [56].

The study conducted by Maduliat and colleagues [57] primarily concentrated on the inelastic bending capability of cold-formed channel sections. They undertook both experimental and analytical analyses on a total of 42 cold-formed channel sections, classifying them into three distinct geometric groups.

Various studies have also studied the performance of CFS , for column design [58-61] [62], for beam/purlin design [63-69]. Cheng et al. [70] has investigated CFS subjected to combined bending and compression.

In order to explore the capacity of inelastic bending and the method of designing bending members, Xingyou & Yanli [71] carried out experimental tests on 30 members of cold-formed

steel-lipped channels. Furthermore, they analyzed the modes of failure in the bending members through the application of shell finite element analysis.

2.6.4 Research on CFS Buckling Behavior

Numerous studies have been conducted on the CFS buckling modes. These studies include investigations of CFS buckling behavior under axial compression and bending loads and the effect of section shape on CFS buckling behavior [70, 72-79]. Much research has been conducted on the buckling failure behavior of single plain channels [80, 81], lipped channels [82, 83] [70, 72-78], and more intricate channel sections [84-87].

Schafer & Pekoz [88] investigated a cold-formed steel flexure member with edge-stitched flanges that is laterally braced. The study aimed to determine the buckling stress in both local and distortional modes. The standard design process does not consider distortion buckling. As a result, the authors proposed a modified design approach that incorporates distortionary buckling into a unified and effective width strategy.

Zhao and Schafer [89] described a rig for measuring and classifying global, distortional, and local imperfections in cold-formed members.

2.6.1 Research on CFS Strengthening

The utilization of diverse forms of stiffeners, such as edge stiffeners and intermediate stiffeners within the web, would bring about significant advantages for cold-formed light-gauge steel open section members. Edge reinforcements play a crucial role in providing sufficient support for slim-walled compression flanges and impeding the occurrence of distortional buckling in the flanges, as studied by Schafer et al. [74].

The structural efficiency of light-gauge steel sections with reinforcements, encompassing simple lipped sections, sections with intricate edge reinforcements, and sections with intermediate reinforcements, has been extensively examined through theoretical, empirical, and numerical investigations [90-95] [62, 74, 90, 96-102].

Bambach & Rasmussen [103] introduced an innovative method for constructing elements without stiffener. When evaluating the strength of cold-formed steel (CFS), they neglected to

consider lateral-torsional buckling, local buckling, or distortional buckling. Wang et al. [99] carried out experiments on CFS channel columns, incorporating intermediate V-shaped web stiffeners and return lip stiffeners. These columns were subjected to pin-ended boundary conditions during testing. Yu [104] discovered that the strength of cold-formed steel channel sections is significantly influenced by the ratio of edge-stiffener length to the flat portion of the web.

2.6.2 Research on CFS Simulation

Numerous research papers have been published on the topic of simulating CFS sections [2, 36, 96, 105].

To investigate the impact of uniform bending on the lateral-torsional buckling behavior of cold-formed steel-lipped channel beams, Kankanamge and Mahendran [106] developed a numerical model. They employed reduced integration (S4R) and four-node shell elements with five degrees of freedom per node in ABAQUS for this purpose.

Keerthan & Mahendran [107] examined the post-buckling and shear buckling behavior of an advanced cold-formed steel beam. They utilized the same numerical investigation approach in ABAQUS.

Abhishek [108] conducted a numerical study on the performance of cold-formed steel (CFS) Z purlins when subjected to bending applied at the shear center of the proposed section.

G. Beulah [109] performed non-linear finite element analysis (FEA) using ABAQUS software to predict the structural behavior of built-up cold-formed steel (CFS) sections under axial loading.

Krishanu [110] proposed an improved version of design rules for back-to-back built-up cold-formed steel channel sections subjected to axial compression. They validated the accuracy of their proposed design rules through finite element analysis (FEA) using ABAQUS and ANSYS software and by conducting test results.

Marsel [111] provides the nonlinear buckling analyses results of light gauge C-shaped compressed columns and then calculates the load-bearing capacity of the column members and its influence of the imperfections on the columns.

Nagesh [112] presents the theoretical and analytical investigations on the maximum load carrying capacity and the behavior of light gauge un-lipped channel sections with ends being fixed then subjected to axial compression.

Karim [113] was able to enhance the efficiency of hat, I, and Z-shaped cross-sections through the implementation of the neural network method. Lee et al. [114, 115] delved into the exploration of the most optimal design for channel beams and columns by utilizing micro-genetic algorithms.

Lu [116], on the other hand, focused on investigating the minimum weight of cold-formed C-channel sections, both with and without lips. These sections had a fixed coil width and were subjected to a prescribed axial compressive load. Leng et al. [117] combined various techniques such as the Direct Strength Method (DSM), the gradient-based steepest descent method, as well as genetic and simulated annealing algorithms to obtain cold-formed steel (CFS) sections with maximum capacity.

In a separate study, Madeira et al. [118] conducted a multi-objective optimization of CFS elements in compression. Uzzaman et al. [119] developed a finite element model that accurately predicted the ultimate loads and failure modes of channel sections, whether they had web holes or not, and were subjected to web crippling.

2.6.5 Other Investigations

Ye et al. [120] successfully implemented a framework to achieve the most optimal sections for cold-formed steel (CFS) beams that align with the design requirements of Eurocode 3, while also considering constraints associated with manufacturing and construction. Dundu [121] presented an analytical study showcasing the potential utilization of CFS sections in portal frames with a span of 12 m and a spacing of 4.5 m. Ongoing efforts and research are being conducted to explore the application of cold-formed steel sections with larger spans and higher loads [5]. In

[122], the authors made predictions regarding the inelastic reserve capacity of bending members, taking into account both lateral-torsional and local buckling modes. Numerous studies aim to enhance the corrosion protection of CFS sections by leveraging the benefits of galvanization and other coating technologies [4].

While significant progress has been made in understanding the behavior and properties of CFS elements under various loading conditions, there is still much to be learned and improved upon. Ongoing research in CFS includes investigating the use of new materials and coatings to improve corrosion resistance, developing new connections and fasteners to improve performance, and exploring the use of CFS in new and innovative structural systems. As such, research on CFS elements is far from finished, and is likely to continue for many years to come.

CHAPTER (3)

STUDY ON DIFFERENT CODES

3.1 INTRODUCTION

The codes that govern the structural design of various countries offer engineers a wealth of information and guidelines for constructing diverse structural elements. These codes may vary significantly in the data provided for actions, such as loads, as well as for assessing the resistance of sections, in addition to other durability and detailing requirements. This chapter presents a comparative analysis between Eurocode-3_part1.3 (EC3), the North American Specification (AISI), and the Egyptian Code of Practice (ECP-205) for designing CFS members with channel and Z-section profiles. This chapter recognizes the resemblances and diversities found in the measurements of strength, thus aiding the acquisition of knowledge in the realm of codes. Moreover, it acknowledges the presence of expressions and boundaries outlined in the ECP-205, EC3, and AISI codes.

3.2 STUDY ON DIFFERENT CODES

Numerous design guidelines at the national level have been formulated for cold-formed steel (CFS) sections and structures, owing to extensive research and product advancement in the past. Each global steel code of conduct consistently aims to enhance the analysis and design of steel structural systems. These enhancements undergo a series of stages that are uniformly implemented worldwide.

This study focuses on commonly different CFS steel codes including Eurocode-3_part1.3 (EC3) [22], the North American Specification (AISI) [21], and the Egyptian Code of Practice (ECP-205) [20].

Comparison between the European, Egyptian, and American codes is present herein. The design methods for the European and Egyptian codes are summarized in EN 1993 [22] and ECP-205 [20], respectively. The American code refers to both the EWM and DSM provided in AISI 100-16 [21]. These codes are respectively referred to as EC3, ECP-205, AISI_{EWM}, and AISI_{DSM} in the rest of the study. It is important to mention that, in order to make things easier, the symbols utilized in the analytical equations have been adjusted to ensure consistency across various codes. Therefore, they may not necessarily match the symbols used in each individual standard.

3.2.1 Comparison Between Dimensional Limits and Considerations

In the design of CFS structures, there are general terms and concepts that are commonly used. These terms include the following definitions:

- **An unstiffened compression element (u.c.e.)** is a compression element that has a flat shape and is stiffened only at one edge, which runs parallel to the direction of stress. This is illustrated in **Figure 3.1**.
- **A stiffened or partially stiffened compression element (s.c.e.)** is a type of flat structural component that is designed to resist compressive forces. This element has reinforcing elements such as webs, flanges, stiffening lips, intermediate stiffeners, or similar features along both edges that are parallel to the direction of stress, as shown in **Figure 3.2**. These reinforcements provide additional stiffness and strength to the compression element, helping it to better resist buckling under load. Such compression elements are commonly used in various structural applications, such as buildings, bridges, and other large-scale infrastructure projects [24].

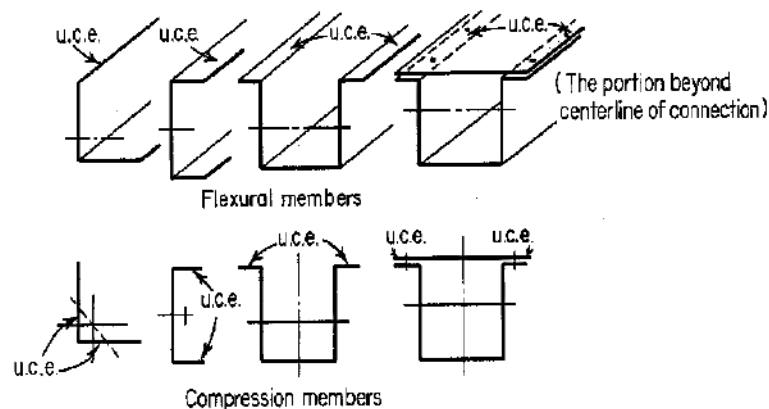


Figure 3.1 :- Sections with unstiffened compression elements [24].

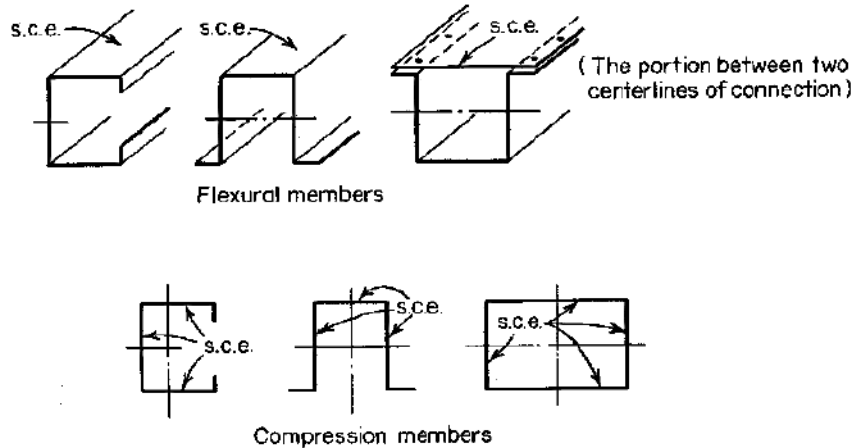


Figure 3.2: - Sections with stiffened or partially stiffened compression elements [24].

When designing CFS sections, there are several dimensional limits and considerations in each code that must be met before using the code, as shown in Table 3-1 and Figure 3.3. There are several additional considerations in EC3 that should be noted. For instance, if $\frac{d}{b} \leq 0.2$, the stiffening lip should be disregarded ($d = 0$). Additionally, if $r \leq 5 t$ and $r \leq 0.10 b$, the impact of rounded corners on the cross-section resistance may be ignored. In such cases, the cross-section can be assumed to be composed of planar elements with sharp corners [22].

Table 3-1: - Different codes dimensional limits and considerations.

Criteria	Different codes			
	AISI _{DSM}	AISI _{EWM}	EC3	ECP-205
Compressed stiffened element	$\frac{h}{t} \leq 500$		$\frac{H}{t} \leq 500$	$\frac{h}{t} \leq 300$
Compressed edge stiffened element	$\frac{b}{t} \leq 160$	$\frac{b}{t} \leq 90$ for $I_s \geq I_a$ $\frac{b}{t} \leq 60$ for $I_s < I_a$	$\frac{B}{t} \leq 60$	$\frac{b}{t} \leq 60$
Compressed unstiffened element	$\frac{d}{t} \leq 60$		$\frac{D}{t} \leq 50$	$\frac{d}{t} \leq 40$
Stiffened element in bending	$\frac{h}{t} \leq 300$	$\frac{h}{t} \leq 200$	$\frac{H}{t} \leq 500$	$\frac{h}{t} \leq 200$
Inside radius	$\frac{r}{t} \leq 20$	$\frac{r}{t} \leq 10$	$r \leq 0.04 t.E / F_y$	Not exist
Simple edge stiffener	$\frac{D}{B} \leq 0.7$		$0.2 \leq \frac{D}{B} \leq 0.6$	Not exist
Edge stiffener type	Simple and complex	Simple only	Simple only	Not exist
Nominal yield stress (F_y)	$F_y < 655$ Mpa	$F_y < 552$ Mpa	$F_y > 140$ Mpa	Not exist
Angle of stiffener (θ)	$40^\circ \geq \theta \geq 140^\circ$		$45^\circ \geq \theta \geq 135^\circ$	$40^\circ \geq \theta \geq 140^\circ$

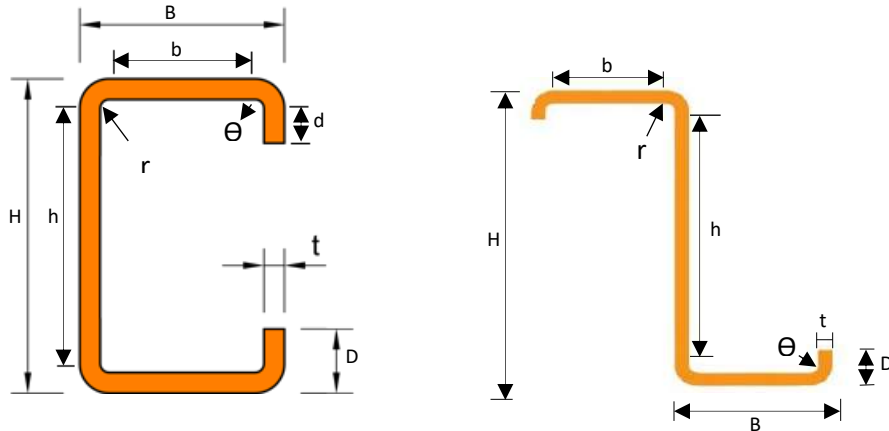


Figure 3.3: - Sections used in this study.

All abbreviations and symbols in the previous table will be explained here as follows: -

- t = Thickness of element.
- B = Total width of element with edge stiffeners.
- b = Flat width of element with edge stiffeners.
- D = Total width of unstiffened element.
- d = Flat width of unstiffened element.
- H = Total depth of web measured along plane of web.
- h = Flat depth of flat portion of web measured along plane of web.
- r = inside bend radius.
- F_y = Nominal yield stress.
- E = Young modulus.
- I_s = Moment of inertia of the full stiffener about its own centroidal axis parallel to the element to be stiffened.
- I_a = Adequate moment of inertia of stiffener.

3.2.2 Resistance Factors

The general equation for determining the axial (P_u) and flexural (M_u) design strengths in any codified design method is as in Equations (3.1) and (3.2). The resistance factors used in different codes can vary depending on the design philosophy and safety requirements of the code. **Table 3-2** explores resistance factors in different codes.

$$P_u = \Phi_c P_n \quad (3.1)$$

$$M_u = \Phi_b M_n \quad (3.2)$$

Table 3-2: - Comparison between resistance factors.

Stress	AISI	EC3	ECP-205
Compression (Φ_c)	0.85	1	0.8
Bending (Φ_b)	0.9	1	0.85

3.2.3 Comparison Between CFS Different Methods

There are two basic design methods for analyzing and designing cold-formed steel (CFS) members, each with its own strengths and limitations. There are the traditional Effective Width Method (EWM) and the Direct Strength Method (DSM). The EWM is spread in different forms almost all over the world for formal use in design, while the direct strength method is only available in AISI [21].

3.2.3.1 Design Resistance of Cross Section

This part of the study focuses on how to design the **resistance of CFS members** using different methods.

3.2.3.1.1 Effective Width Method

The Effective Width Method (EWM) is a commonly used approach for designing Cold Formed Steel (CFS) sections. The EWM involves the determination of the effective width of the section based on the distribution of stresses across the cross-section of the beam. The effective width is then used to calculate the moment of resistance of the section, which is the maximum bending moment that the section can withstand without failure.

Effective width refers to the width of a beam or structural element that is actually effective in resisting the applied loads. In other words, it is the width of the beam or element that is contributing to the strength and stiffness of the structure. A method of effective width is utilized where unproductive parts of a cross-section are eliminated, and the properties of the remaining effective parts are used to determine section properties.

Clause 4.4 of EN 1993-1-5 [123] defines the effective area of a flat compression element ($A_{c;eff}$) as the product of the gross area of the compression element, denoted as A_c , and a plate buckling reduction factor (ρ). The value of ρ must be less than or equal to one, as shown in equation (3.3). The plate buckling reduction factor (ρ) is taken as the following **Table 3-3**.

$$A_{c;eff} = \rho A_c \tag{3.3}$$

Table 3-3: - The EWM factors in different codes.

		Different codes		
		AISI _{EWM}	EC3	ECP-205
The reduction factor (ρ)		$\rho = 1$ For $\lambda_p \leq 0.673$ (3.4) $\rho = \frac{1 - .22}{\lambda}$ For $\lambda_p > 0.673$	For stiffened element (3.5) $\rho = \frac{\lambda_p - .055(3+\Psi)}{\lambda_p^2} \leq 1$ For unstiffened element $\rho = \frac{\lambda_p - .188}{\lambda_p^2} \leq 1$	For stiffened element (3.6) $\rho = \frac{1.1\lambda_p - .16 - .1\Psi}{\lambda_p^2} \leq 1$ For unstiffened element $\rho = \frac{\lambda_p - .15 - .05\Psi}{\lambda_p^2} \leq 1$
The normalized plate slenderness (λ_p)		$\lambda_p = \sqrt{\frac{f}{F_{cr1}}}$ (3.7) Where: - $F_{cr1} = K \frac{\pi^2 E}{12(1-\mu^2)} \left(\frac{t}{b}\right)^2$	$\lambda_p = \sqrt{\frac{f_y}{\sigma_{cr}}} = \frac{\left(\frac{b}{t}\right)}{28.4 \cdot \xi \cdot \sqrt{K}}$ (3.8) Where: - ξ is the ratio $\sqrt{\frac{235}{f_y}}$ with f_y in N/mm ²	For stiffened element (3.9) $\lambda_p = \frac{\left(\frac{b}{t}\right)}{44} \left[\sqrt{\frac{F_y}{K}} \right]$ for unstiffened element $\lambda_p = \frac{\left(\frac{b}{t}\right)}{59} \left[\sqrt{\frac{F_y}{K}} \right]$
Plate buckling coefficient (K)	in compressed Stiffened	$K = 4$ (3.10)		
	in compressed unstiffened	$K = .43$ (3.11)		
	in flexural Stiffened	$k = 4 + 2(1 + \Psi)^3 + 2(1 + \Psi)$ (3.12)	$k = 7.81 - 6.29 \Psi + 9.78 \Psi^2$ (3.13)	

Where: - ψ is the stress ratio.

In the case of designing plane elements with an edge stiffener (lipped flange), the ECP-205 standards follow the AISI_{EWM} except for how to calculate the plate buckling coefficient (K), as shown in **Table 3-4**, the adequate moment of inertia of the stiffener (I_a), as shown in equations (3.14) and (3.15), and the calculations of the reduction factor (ρ), as mentioned before.

$$I_a = 399 t^4 \left(\frac{b/t}{S} - .328 \right)^3 \leq t^4 \left(115 \frac{b/t}{S} + 5 \right) \quad \text{in AISI}_{EWM} \quad (3.14)$$

$$\left. \begin{aligned} &= 399 t^4 \left(\frac{b/t}{S} - .328 \right)^3 \quad \text{if } .25 < b/t \leq S \\ &= t^4 \left(115 \frac{b/t}{S} + 5 \right) \quad \text{if } b/t \geq S \end{aligned} \right\} \text{in ECP} \quad (3.15)$$

Where: - $S = 1.28 \sqrt{E/f}$ (3.16)

Table 3-4 :- Plate buckling coefficient (K).

Codes		Simple Lip Edge Stiffener	
		d/b ≤ 0.25	0.25 < d/b ≤ 0.8
AISI _{EWM}		3.57 (R _I) ⁿ + 0.43 ≤ 4 (3.17)	(4.82 - 5d/b) (R _I) ⁿ + 0.43 ≤ 4 (3.18)
ECP-205	S/3 < b/t < S	3.57 (R _I) ^(1/2) + 0.43 ≤ 4 (3.19)	(4.82 - 5d/b) (R _I) ^(1/2) + 0.43 ≤ 5.25-5 (d/b) (3.20)
	b/t ≥ S	3.57 (R _I) ^(1/3) + 0.43 ≤ 4 (3.21)	(4.82 - 5d/b) (R _I) ^(1/3) + 0.43 ≤ 5.25-5 (d/b) (3.22)

Where: -

- $n = \left(0.582 - \frac{b/t}{4S} \right) \geq \frac{1}{3}$ (3.23)

- I_s = The moment of inertia of the full section of stiffener about its own centroidal axis parallel to the element to be stiffened. [I_s = (d³·t)/12] (3.24)

- R_I = I_s / I_a ≤ 1 (3.25)

In EC3, the stiffener behaves as a compression member with continuous partial restraint, which is represented by a linear spring (with stiffness K) that is located at the centroid of the effective stiffener section, as illustrated in **Figure 3.4**. It functions as a partially restrained compression member, and its spring stiffness is affected by the flexural stiffness and boundary conditions of adjacent plane elements.

Section 5.5.3 of EC3 outlines a recommended step-by-step procedure for designing compression elements with edge or intermediate stiffeners. The first step is to determine an initial effective cross section for the stiffener by assuming that it provides full restraint and using effective widths. The second step is to calculate the reduction factor for distortional buckling (also known as flexural buckling of the stiffener) using the initial effective cross section, while accounting for the effects of continuous spring restraint. Optionally, the reduction factor can be refined through iteration. To determine initial values for the effective widths, consult **Figure 3.5** and assume that the plane element is supported on both longitudinal edges. Finally, the effective cross section of the stiffener and the reduction factor are used to determine the design strength of the stiffener.

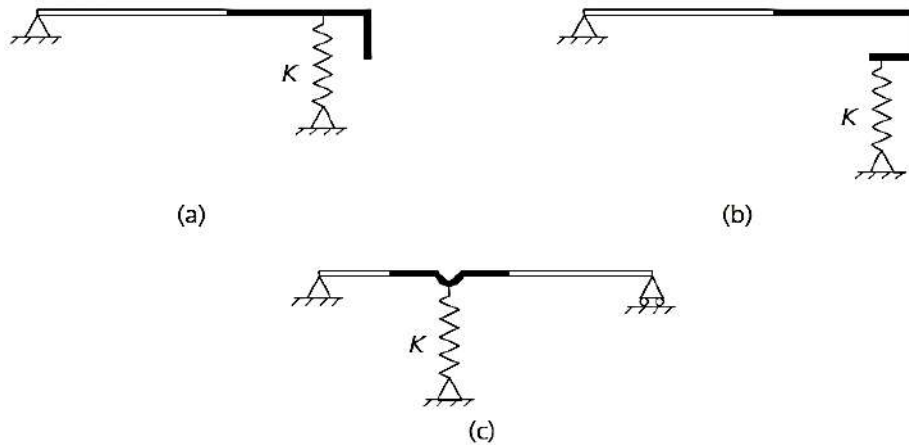


Figure 3.4 :- Assumed model for edge and intermediate stiffeners. (a) Single-fold edge stiffener. (b) Double fold edge stiffener. (c) Intermediate stiffener [124].

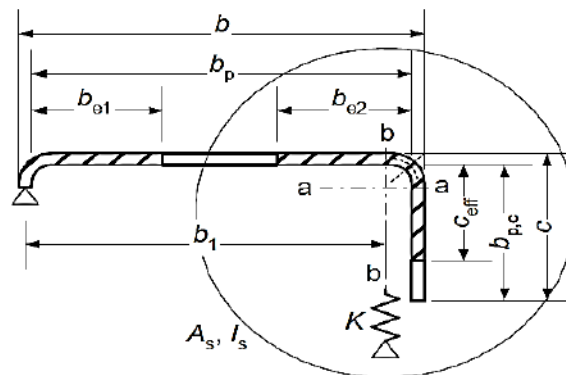


Figure 3.5 :- Edge stiffener [25].

The reduction factor X_d for distortional buckling resistance (i.e., stiffener flexural buckling) can be found by calculating the relative slenderness λ_d using the following equations: -

$$X_d = 1 \quad \text{if} \quad \lambda_d \leq .65 \quad (3.26)$$

$$X_d = 1.47 - .723 \lambda_d \quad \text{if} \quad .65 < \lambda_d \leq 1.38 \quad (3.27)$$

$$X_d = \frac{.66}{\lambda_d} \quad \text{if} \quad \lambda_d \geq 1.38 \quad (3.28)$$

Where:-

- $\lambda_d = \sqrt{\frac{f_y}{\sigma_{cr,s}}}$ (3.29)

- $\sigma_{cr,s}$ is the elastic critical stress for the stiffener

$$= \frac{2 \cdot \sqrt{K \cdot E \cdot I_s}}{A_s} \quad (3.30)$$

For a single edge fold stiffener, initial values of the effective width (C_{eff}), refer to **Figure 3.5**, should be obtained as follows:

$$C_{eff} = \rho b \quad (3.31)$$

The value of the buckling factor k_σ used to calculate the reduction factor for buckling of the stiffener is given by a specific expression, while ρ is obtained as mentioned before. This expression is used in place of the value of the plate buckling coefficient (K)

- if $d/b \leq 0.35$ $k_\sigma = 0.5$ (3.32)

- if $0.35 < d/b \leq 0.6$ $k_\sigma = 0.5 + \sqrt[3]{\left(\frac{d}{b} - .35\right)^2}$ (3.33)

3.2.3.1.2 Direct Strength Method

The Direct Strength Method (DSM) is a design approach used in the North American specification (AISI) [21] for cold-formed steel structures. The DSM approach is a relatively new method for designing cold-formed steel structures that is based on the principles of mechanics and engineering, and it has been shown to provide a more accurate prediction of the structural behavior of cold-formed steel members than traditional design methods.

The DSM method allows for the direct calculation of the strength and stiffness of cold-formed steel members, without the need for empirical adjustments or safety factors. This is accomplished by using finite element analysis (FEA) to model the behavior of the member under load, and then using the calculated stresses and strains to determine the member's strength and stiffness.

The Direct Strength Method (DSM) is often preferred for designing optimized cold-formed steel shapes over the main Specification. DSM provides a design method for complex shapes that is as easy as for normal shapes, while the main Specification may be difficult or inapplicable. DSM has practical advantages, such as no effective width calculations, no required iterations, and the use of gross cross-sectional properties. It integrates elastic buckling analysis through computer software, allowing for a general method of designing cold-formed steel members with broader extensions than traditional Specification methods. Theoretical advantages of DSM include explicit design for distortional buckling, element interaction inclusion, and exploration of all stability limit states. DSM also encourages cross-section optimization, provides a rational basis for analysis extensions, has a wider applicability and scope, and focuses on elastic buckling behavior determination rather than empirical effective widths [17].

The use of DSM in AISI [21] has certain limitations, such as the absence of shear provisions and web crippling provisions. It also does not provide any guidelines for members with holes and has a limited number and geometry of pre-qualified members. Additionally, it does not incorporate any provisions for enhancing strength due to cold work of forming.

The direct strength method depends mainly on the idea of the accurate member elastic stability. It is mainly based on an idea of determining all of the elastic instabilities for the gross section, i.e. local (M_{crL} or P_{crL}), distortional (M_{crd} or P_{crd}), global buckling (M_{cre} or P_{cre}) and also calculating the yielding straining action (M_y or P_y), then the nominal strength can be directly defined, i.e. $M_n = \mathcal{F}(M_{crL}, M_{crd}, M_{cre}, M_y)$ & $P_n = \mathcal{F}(P_{crL}, P_{crd}, P_{cre}, P_y)$.

3.2.3.2 Design of Different Buckling Resistances

Compression members are structural elements that experience compressive forces, such as columns, struts, and beams subjected to axial compression. The limit states for compression members refer to the conditions under which a member is considered to have failed or reached its capacity. The limit states for compression members include yielding, overall column buckling, local buckling of individual compression elements and distortional buckling of open sections with edge stiffened flanges [24].

Flexural members are structural elements that are designed to resist bending or flexure. Some common examples of flexural members include beams and joists. They are typically

horizontal members that are designed to resist bending and support loads perpendicular to their length. They are often used to support floors, roofs, or bridges. Local, distortional, and lateral torsional buckling are failure modes of cold-formed flexural members.

Yielding occurs when the stress in a compression member exceeds the yield strength of the material. At this point, the material will begin to deform plastically, meaning it will experience permanent deformation even after the load is removed. Yielding can cause failure only in a very short, compact column under axial load, so it doesn't occur in slender sections like CFS, that is why it is not discussed in this study.

It is worth noting that the EC3 is unique EWM code in that it accounts for distortional buckling and the interaction between local and distortion buckling modes by assuming that the stiffener behaves as a compression member with continuous partial restraint, which is represented by a linear spring (with stiffness K) that is located at the centroid of the effective stiffener section, as illustrated in Section 5.5 of the EC3.

There are several methods for determining the interaction between local and overall column buckling modes for slender sections such as Q-factor method and unified approach. The AISI [21] was used Q-factor method in old versions and has been replaced it by the unified approach method in new versions of the code. However, the Egyptian code [20] still follows the old versions of the AISI in the use of semi Q-factor method.

The Q-factor method was considered in the AISI specification during the period from 1946 through 1986 [24]. It is a simplified approach that can be used to determine the axial capacity of CFS columns and beams. The Q-factor method uses a Q factor that is based on the slenderness ratio of the member. The Q factor is a dimensionless factor that is used to account for the reduction in strength of the member due to buckling.

The Q factor was eliminated in the 1986 edition of the AISI Specification [24]. The unified approach is recommended by the North American Specification for the Design of Cold-Formed Steel Structural Members and is used extensively in the United States and Canada. It provides a more accurate and reliable design method for CFS members subjected to compression and can be used for a wide range of member types and loading conditions. It is a more advanced and comprehensive method compared to the Q-factor method, as it takes into account the effects

of local buckling and distortional buckling, as well as the interaction between different components of the member.

The unified approach considers the interaction between different components of the member, such as the flanges and the web, which can affect the overall strength and stiffness of the member. It also uses a series of equations to determine the reduction factors for local buckling. These reduction factors account for the reduction in strength and stiffness of the member. In order to reflect the effect of local buckling on column strength, the nominal column load is determined by the governing critical buckling stress and the effective area instead of the full sectional area.

On the other hand in EC3 [22] structural design, the resistance of compressed members is determined using the "European design buckling curves," which were established by ECCS in 1978 [125]. These curves relate the reduction factor (χ) to non-dimensional slenderness parameter ($\bar{\lambda}$). **Figure 3.8** shows the five curves that were derived from an extensive research program conducted by ECCS in 1976 [126].

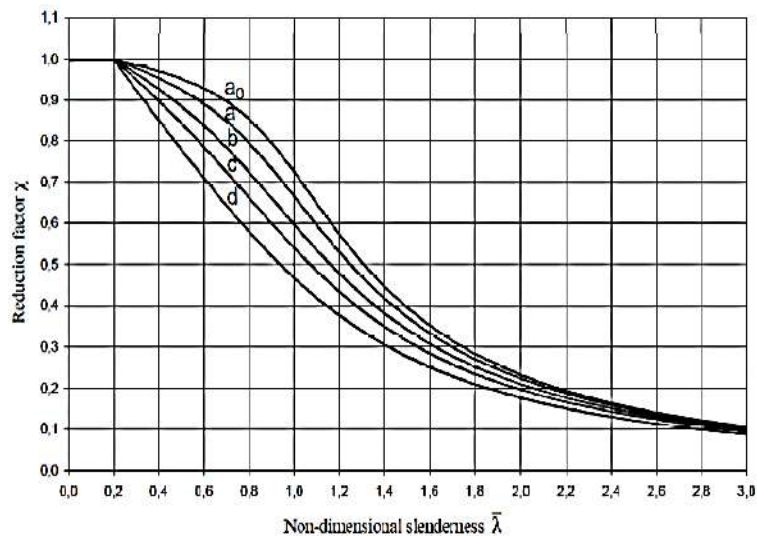


Figure 3.6: - European design buckling curves [25].

The first step of the Direct Strength Method is finding buckling straining actions (moment or load), i.e. local (M_{crL} or P_{crL}), distortional (M_{crd} or P_{crd}), global (M_{cre} or P_{cre}) buckling. It simply became easy to get the elastic buckling straining actions of any cold-formed steel cross-section by freely, available, open-source software, such as CUFSM, CFS and THIN-WALL or by manual elastic buckling calculation.

The cross-section can achieve its full capacity in all buckling modes, such as local, distortional, and global, if the elastic buckling value is high enough. This value determines whether the cross-section can achieve the yield moment in bending (M_y) or the squash load in compression (P_y). The limits for these conditions can be generated using the Direct Strength predictor equations provided in Appendix 2 of AISI [21].

Flexural Members

- if $M_{cr1} > 1.66M_y$ then local buckling will not cause any reduction in the structure's strength or capacity.
- if $M_{crd} > 2.21M_y$ then distortional buckling will not cause any reduction in the structure's strength or capacity.
- if $M_{cre} > 2.78M_y$ then global buckling will not cause any reduction in the structure's strength or capacity.

Compression Members

- if $P_{cr1} > 1.66P_y$ then local buckling will not cause any reduction in the structure's strength or capacity.
- if $P_{crd} > 3.18P_y$ then distortional buckling will not cause any reduction in the structure's strength or capacity.
- if $P_{cre} \geq 3.97P_y$ then global buckling may cause a reduction of 10% or less in the strength or capacity of the structure.
- if $P_{cre} \geq 8.16P_y$ then global buckling may cause a reduction of 5% or less in the strength or capacity of the structure.
- if $P_{cre} \geq 41.64P_y$ then global buckling may cause a reduction of 1% or less in the strength or capacity of the structure.

The nominal strength of the member is determined by taking the minimum of different buckling resistances, such as local, distortional, and global buckling. The different buckling resistance formulas for columns and beams are shown in **Tables 3-5** and **Tables 3-6**, respectively.

Table 3-5: - The nominal design of compression strength (resistance).

Mode	Different codes			
	AISI _{DSM}	AISI _{EWM}	EC3	ECP-205
Local buckling	For $\lambda_L \leq 0.776$ $P_{nL} = P_{ne}$ (3.34) For $\lambda_L > 0.776$ $P_{nL} = \left[1 - 0.15 \left(\frac{P_{crL}}{P_{ne}} \right)^4 \right] \left(\frac{P_{crL}}{P_{ne}} \right)^4 P_{ne}$ Where: - $\lambda_L = \sqrt{\frac{P_{ne}}{P_{crL}}}$	$P_{nl} = A_{eff} \cdot f_y$ (3.35)		
Distortion buckling	For $\lambda_d \leq 0.561$ $P_{nd} = P_y$ (3.36) For $\lambda_d > 0.561$ $P_{nd} = \left[1 - 0.25 \left(\frac{P_{crd}}{P_y} \right)^6 \right] \left(\frac{P_{crd}}{P_y} \right)^6 P_y$ Where: - $\lambda_d = \sqrt{\frac{P_y}{P_{crd}}}$	-	For $\lambda_d \leq 0.65$ (3.37) $X_d = 1$ For $0.65 < \lambda_d \leq 1.38$ $X_d = 1.47 - 0.723 \lambda_d$ For $\lambda_d \geq 1.38$ $X_d = \frac{.66}{\lambda_d}$	-
Global buckling	For $\lambda_c \leq 1.5$ (3.38) $P_{ne} = (.658^{(\lambda_c)^2}) P_y$ For $\lambda_c > 1.5$ $P_{ne} = \left(\frac{.877}{(\lambda_c)^2} \right) P_y$	$P_{ne} = A_n \cdot F_n$ (3.39) Where: - For $\lambda_c = \sqrt{\frac{F_y}{F_{cr}}} \leq 1.5$ $F_n = (0.658^{\lambda_c^2}) F_y$ For $\lambda_c = \sqrt{\frac{F_y}{F_{cr}}} > 1.5$ $F_n = \left[\frac{0.877}{\lambda_c^2} \right] F_y$	$P_{ne} = X A_{eff} F_y$ (3.40) Where: - $X = \frac{\phi - \sqrt{\phi^2 - \lambda'^2}}{\lambda'^2} \leq 1$ $\phi = 0.5 [1 + \alpha(\lambda' - 0.2) + \lambda'^2]$ $\lambda' = \sqrt{\frac{A_{eff} \cdot F_y}{F_{cr}}}$	$P_{ne} = A_g \cdot F_{cr}$ (3.41) Where: - For $\lambda_c \sqrt{Q} \leq 1.1$ $F_{cr} = F_y \cdot Q (1 - 0.384 Q (\lambda_c)^2)$ For $\lambda_c \sqrt{Q} > 1.1$ $F_{cr} = 0.648 F_y / (\lambda_c)^2$

Where:-

- A_{eff} is the effective area of cross section by applying uniform compressive stress equal to F_y .
- F_y is the yield strength.
- Q is a reduction factor for slender sections. [$Q = A_e / A_g$]
- A_e is an effective area based on sections 4.2.2.1 & 4.2.2.2 in ECP-205.
- A_g is gross area of member.
- X is the reduction factor in EC3.
- α is the imperfection factor for buckling curve.
- λ is a non-dimensional slenderness parameter.
- F_{cr} is the minimum elastic global buckling stress.
- A_n is the effective area of cross section by applying uniform compressive stress equal to F_n .
- P_{ne} is the nominal axial strength for flexure, torsional or torsional flexural buckling.
- P_{nL} is the nominal axial strength for local buckling.
- P_{nd} is the nominal axial strength for distortional buckling.
- P_{crl} is the critical elastic local column buckling load.
- P_{cre} is the critical elastic global buckling load.
- P_{crd} is the critical elastic distortional buckling load.

Table 3-6: - The nominal design of flexural strength (resistance).

Mode	Different codes			
	AISI _{DSM}	AISI _{EWM}	EC3	ECP-205
Local buckling	For $\lambda_L \leq 0.776$ $M_{nL} = M_{ne}$ (3.42) For $\lambda_L > 0.776$ $M_{nL} = \left[1 - 0.15 \left(\frac{M_{crL}}{M_{ne}} \right)^4 \right] \left(\frac{M_{crL}}{M_{ne}} \right)^4 M_{ne}$ Where: - $\lambda_L = \sqrt{\frac{M_{ne}}{M_{crL}}}$	$M_{nl} = Z_{eff} \cdot f_y$ (3.43)		For $\frac{b}{t} \leq 30$ (3.44) $M_{nl} = \begin{cases} C * \frac{S_x}{\lambda^2} \\ F_L S_e \end{cases}$ For $\frac{b}{t} > 30$ $M_{nl} = Z_{eff} F_y$
Distortion buckling	For $\lambda_d \leq 0.673$ $M_{nd} = M_y$ (3.45) For $\lambda_d > 0.673$ $M_{nd} = \left[1 - 0.22 \left(\frac{M_{crd}}{M_y} \right)^5 \right] \left(\frac{M_{crd}}{M_y} \right)^5 M_y$ Where: - $\lambda_d = \sqrt{\frac{M_y}{M_{crd}}}$	-	For $\lambda_d \leq 0.65$ (3.46) $X_d = 1$ For $0.65 < \lambda_d \leq 1.38$ $X_d = 1.47 - .723 \lambda_d$ For $\lambda_d \geq 1.38$ $X_d = \frac{.66}{\lambda_d}$	-
Global buckling	For $M_{cre} < 0.56 M_y$ (3.47) $M_{ne} = M_{cre}$ For $2.78 M_y \geq M_{cre} \geq 0.56 M_y$ $M_{ne} = \frac{10}{9} * M_y * \left(1 - \frac{10 * M_y}{36 * M_{cre}} \right)$ For $M_{cre} > 2.78 M_y$ $M_{ne} = M_y$	$M_{ne} = S_e F_n$ (3.48) Where: - For $F_e \geq 2.78 F_y$ $F_n = F_y$ For $2.78 F_y > F_e > 0.56 F_y$ $F_n = \frac{10}{9} F_y \left[1 - \frac{10 F_y}{36 F_e} \right]$ For $F_e \leq 0.56 F_y$ $F_n = F_e$	$M_{ne} = X_{LT} \cdot Z_{eff} \cdot F_y$ (3.49) Where: - $X_{LT} = \frac{1}{\phi_{LT} + (\phi_{LT}^2 - \lambda'^2_{LT})^5} \leq 1$ $\phi_{LT} = 0.5 \left[1 + \alpha_{LT} (\lambda'_{LT} - 0.2) + \lambda'^2_{LT} \right]$ $\lambda'_{LT} = \sqrt{\frac{Z_{eff} \cdot F_y}{M_{cr}}}$	$M_{ne} = C_b M_{cr} \leq M_p$ (3.50)

Where: -

- S_e is elastic section modulus of effective section calculated with extreme compression fiber at F_n .
- F_n is elastic or inelastic critical lateral torsional buckling stress.
- F_e is the elastic critical lateral torsional buckling stress.
- X_{LT} is the reduction factor for lateral torsional buckling.
- Z_{eff} is the elastic section modulus of effective section calculated with extreme compression fiber at F_y .
- X_{LT} is The reduction factor.
- α_{LT} is the imperfection factor for buckling curve a, ($\alpha_{LT} = .21$) [22].
- λ'_{LT} is non-dimensional slenderness.
- M_{cr} is the elastic critical moment for lateral torsional buckling stress.
- C_b is bending moment coefficient [in ECP-205 for cold-formed sections = 1].
- S_x is the gross elastic section modulus.
- $C^* = \begin{cases} 817 & \text{for rolled sections.} \\ 470 & \text{for welded sections.} \end{cases}$
- $F_L = \begin{cases} .75 F_y & \text{for rolled sections.} \\ .6 F_y & \text{for built up sections.} \end{cases}$
- M_{ne} is the nominal flexural strength for lateral torsional buckling.
- M_{nL} is The nominal flexural strength for Local buckling .
- M_{nd} is The nominal flexural strength for Distortional buckling.
- $M_y = S_g * F_y$ (Squash Moment).
- S_g is the gross section modulus referenced to the extreme fiber in first yield.
- M_{cre} is critical elastic lateral torsional buckling moment.
- M_{crl} is critical elastic local buckling moment.
- M_{ne} is the nominal flexural strength for lateral torsional buckling.
- M_{crd} is critical elastic distortional buckling moment.

3.2.3.3 Beam Column Members

Beam column members are typically used in structures where the loads are not purely vertical or horizontal, but instead have a combination of both. For example, in a building with a sloped roof, the beams supporting the roof will also need to support some of the vertical load from the roof, making them beam columns.

Beam column members can be designed using a combination of beam and column design principles, taking into account the effects of both bending and axial compression. The design must ensure that the member can resist the bending and compression forces without buckling or failing.

The equations for beam-column members are a blend of compression and flexure equations that are present in the three codes. The equations have a common form, which mandates that the ratio of applied loads to the member's resistance should not surpass 1.0. This condition is demonstrated in the equations given below: -

For AISI [21]

For $\frac{P_u}{\phi_c P_n} \leq .15$

$$\bullet \frac{P_u}{\phi_c P_n} + \left(\frac{M_{ux}}{\phi_b M_{nx}} + \frac{M_{uy}}{\phi_b M_{ny}} \right) \leq 1 \quad (3.51)$$

For $\frac{P_u}{\phi_c P_n} > .15$

$$\bullet \left\{ \frac{P_u}{\phi_c P_n} + \left(\frac{C_m M_{ux}}{\alpha_x \phi_b M_{nx}} + \frac{C_m M_{uy}}{\alpha_y \phi_b M_{ny}} \right) \right\} \leq 1 \quad (3.52)$$

$$\bullet \left\{ \frac{P_u}{\phi_c P_n} + \left(\frac{M_{ux}}{\phi_b M_{nx}} + \frac{M_{uy}}{\phi_b M_{ny}} \right) \right\} \leq 1 \quad (3.53)$$

For EC3 [22]

$$\bullet \left(\frac{P_u}{P_n} \right)^8 + \left(\frac{M_{ux}}{M_{nx}} + \frac{M_{uy}}{M_{ny}} \right)^8 \leq 1 \quad (3.54)$$

For ECP-205 [20]

For $\frac{P_u}{\phi_c P_n} \geq .2$

$$\bullet \frac{P_u}{\phi_c P_n} + \frac{8}{9} \left(\frac{M_{ux}}{\phi_b M_{nx}} + \frac{M_{uy}}{\phi_b M_{ny}} \right) \leq 1 \quad (3.55)$$

For $\frac{P_u}{\phi_c P_n} < .2$

$$\bullet \frac{P_u}{2 \phi_c P_n} + \left(\frac{M_{ux}}{\phi_b M_{nx}} + \frac{M_{uy}}{\phi_b M_{ny}} \right) \leq 1 \quad (3.56)$$

All abbreviations and symbols in the previous equations will be explained here as follows: -

- P_u requires compressive axial strength.
- $M_{u(x \text{ or } y)}$ are required flexural strengths .
- P_n is nominal compressive strength as discussed in section 3.7.1.2 of this chapter.
- M_n is nominal flexural strength as discussed in section 3.7.1.3 of this chapter.
- ϕ_c and ϕ_b are safety factors as discussed in section 3.6 of this chapter.

$$\bullet \alpha_x = 1 - \frac{P_u}{P_{EX}} \quad (3.57)$$

$$\bullet \alpha_y = 1 - \frac{P_u}{P_{Ey}} \quad (3.58)$$

- P_{EX}, P_{Ey} are Euler loads.
- C_m is a coefficient depending on the sidesway and bending shape of the member.
- The subscripts x and y indicate the axis of bending.

CHAPTER 4

THE DEVELOPED PROGRAM

4.1 INTRODUCTION:

With the aim of improving the computational speed of the calculation process, computer software was utilized to program the calculation procedure for the different aforementioned codes. This chapter presents a comprehensive guide for users of this program, outlining the steps necessary to utilize the software in order to design, check, and determine the maximum strength of cold formed steel sections (CFS), specifically those with channel or z-profile that are subjected to axial load, bending moment, or a combination of both, along with providing calculation sheets. This software was created in the C⁺ programming language and can calculate the axial load and bending moment capacities of CFS Channels.

4.2 PROGRAM INTERFACE

The initial part of the program interface presents a concise explanation of the program's nature and its potential applications. Moreover, the software developers can acquaint themselves with this application by simply pressing button 1. The latter part of the program interface comprises the most widely used CFS design techniques and an uncomplicated description of each. This section is constituted of two principal divisions. The first section, the Effective Width Method, utilizes three codes (Egyptian [20], American [21], and Eurocode [22]). The second section, the Direct Strength Method, employs the American code [21]. Designers must select between the Effective Width Method or the Direct Strength Method by clicking button 2 or 3, respectively, as depicted in **Figure 4.1**.



Figure 4.1: - the developed program interface.

4.2 FORMS OF DIFFERENT METHODS

If one were to make the selection of the first section by simply clicking on button 2 in the esteemed major form of the current program, as is exemplified in the illustrious **Figure 4.1**, then the EWM form shall effortlessly come into view, as it is masterfully presented in the **Figure 4.2**. However, if one were to select for the second section by simply clicking on button 3 in the alluring **Figure 4.1**, then the DSM form would majestically manifest itself, as is depicted in **Figure 4.3**.

Figure 4.2: - Form of Effective Width Method.

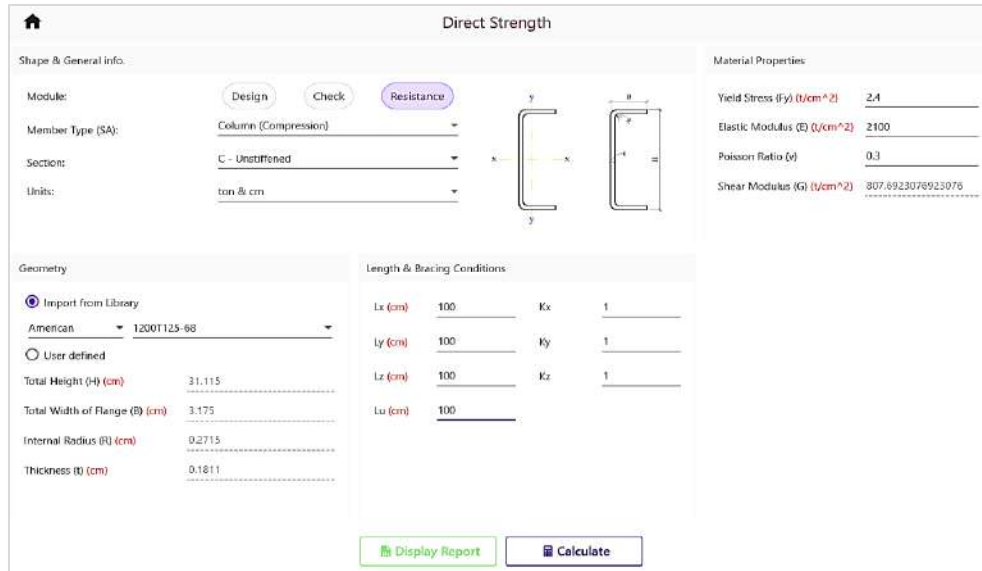


Figure 4.3: - Form of Direct Strength Method.

Input data (cross section geometry, length, bracing conditions, material properties, type of influential load, and code required) were entered, and output data (CFS Capacity) were obtained. in case the designer wants to design or check CFS section, the input data includes all the above input data in addition to the values of the loads affecting the section. It should be noted that the screens for EWM and DSM forms are divided into 5 sections, namely "Form and General Info.", "Geometry", "Length and bracing Conditions", "Material Properties", and "ultimate loads" appeared only in case of design or check CFS section, as shown in **Figure 4.4**.

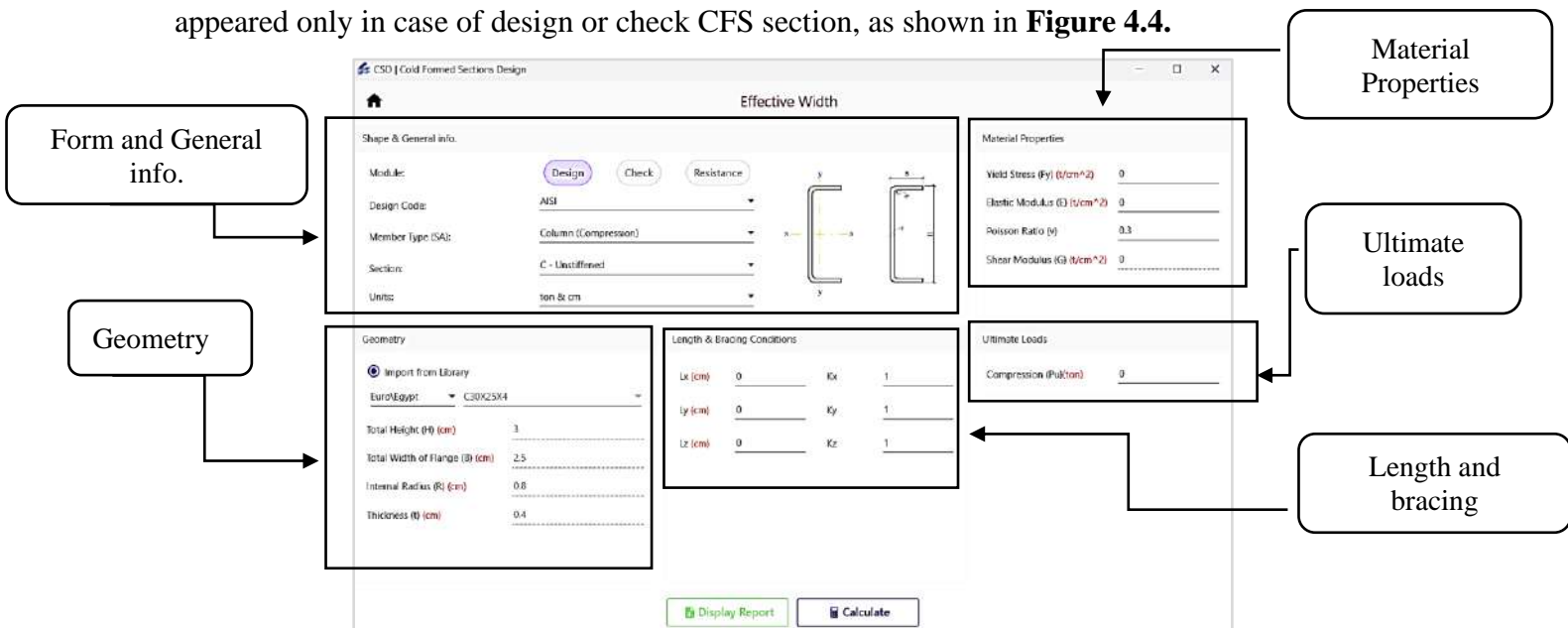


Figure 4.4: - Form sections of CFS design in the program.

4.2.1 Shape & General info.

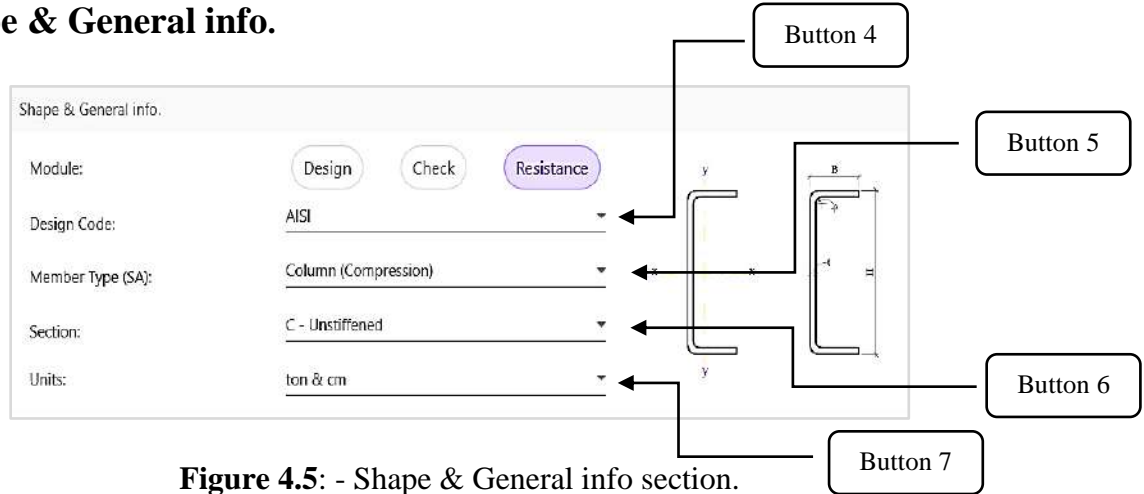


Figure 4.5: - Shape & General info section.

Whether you choose EWM or DSM, the first section on the program screen is called “Shape & General info.”, as shown in **Figure 4.4**. To enter information related to this section, you should follow the following steps: -

The first step the designer should choose what he needs to do; Design CFS section or check the safety of section or finding resistance of CFS section by simply clicking in the buttons called “Design”, “Check” or “Resistance”, respectively, as shown in **Figure 4.5**.

The second step is to specify the code that you want to use, whether it is the Egyptian, European, or American code, and this is done by pressing button 4, as shown in **Figure 4.6**. It should be noted that this button does not exist on the screen of DSM form.



Figure 4.6: - Different codes in Button 4.

The next step is to determine the type of section that the designer wants, either to be a column, a beam, or beam-column, or in other words, to determine the type of straining actions (axial load, bending moment or both) affecting the section, and this is done by pressing button 5, as shown in **Figure 4.7**.

Next, determining the shape of section that the designer wants, either to be a lipped channel, an unstiffened channel, lipped Z-section, and unstiffened Z-section, and this is done by pressing button 6, as shown in **Figure 4.8**.

Finally, the designer should choose which units of load and dimensions he wants to deal with in data entry as well as the solution resulting from the program. The available units are ton & cm, newton & mm, and Kips & inch by simply clicking button 7, as shown in **Figure 4.9**.

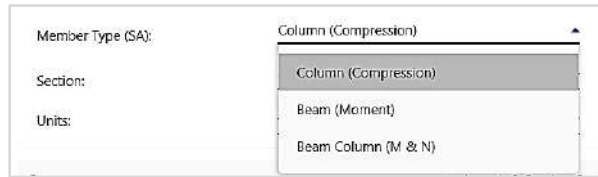
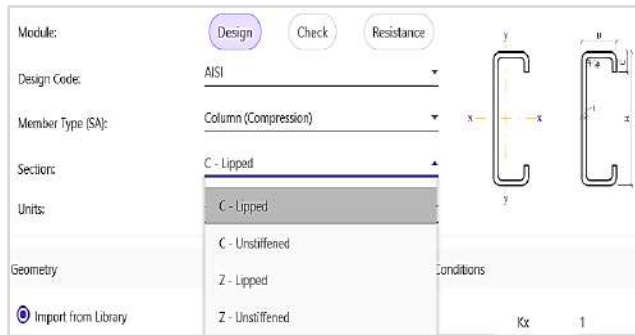
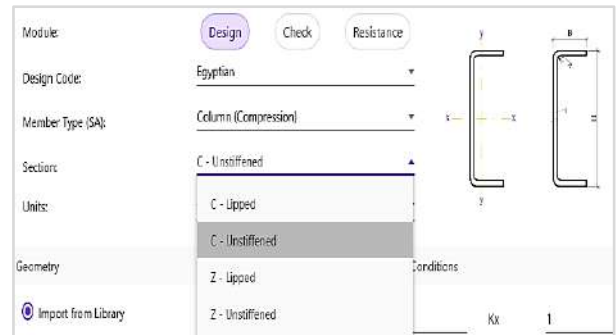


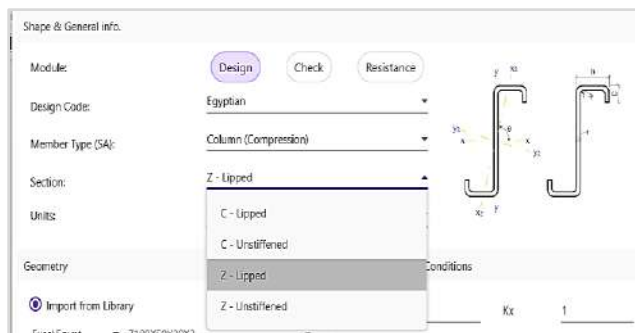
Figure 4.7: - Different frame elements in button 5.



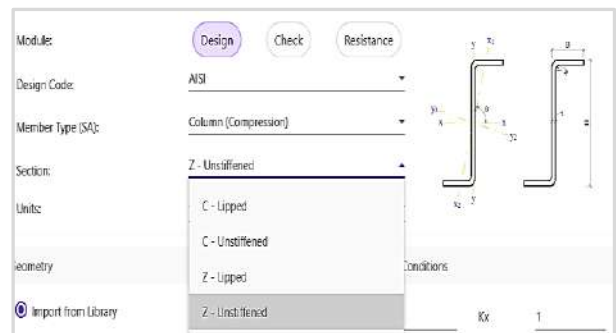
a) Lipped channel



b) Unstiffened channel



c) Lipped Z-section



d) Unstiffened Z-section

Figure 4.8: - Different sectional shapes in button 6.

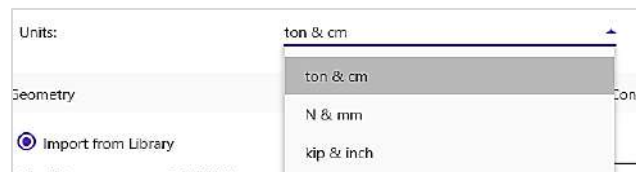


Figure 4.9: - Different units in button 7.

4.2.2 Geometry

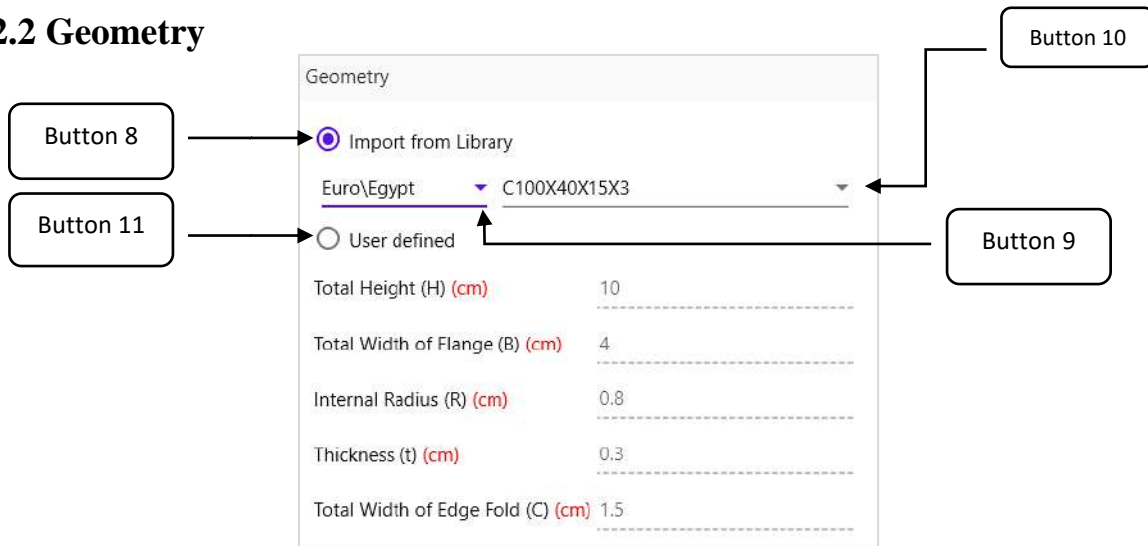


Figure 4.10: - Geometry section.

Whether you choose EWM or DSM, the second part on the program screen is called “Geometry” as shown in **Figure 4.4**. This part is concerned with determining the dimensions of the section to be checked or finding the maximum design load that this section can bear. In the case of the program being required to design, this part is concerned only with specifying the type of steel sections tables from which the design section chooses. The designer can enter the dimensions directly by selecting one of the well-known sections from the different steel tables, as shown in **Figure 4.11**, by pressing button 8, then pressing button 9 to choose which steel tables the designer wants, finally pressing button 10 to choose the section in that table or entering the dimensions manually for each part separately by pressing button 11, as shown in **Figure 4.12**.

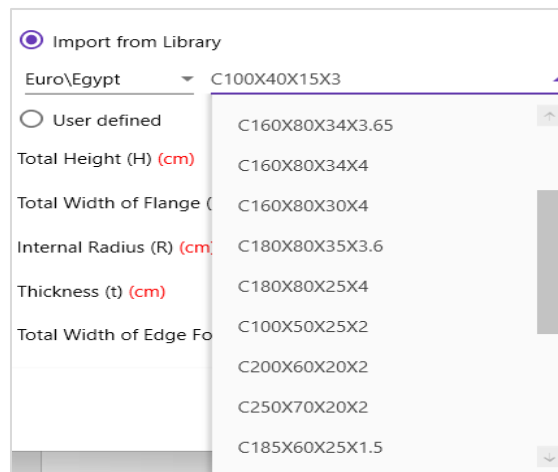


Figure 4.11: - Choose section from the table of the steel tables.

Geometry	
<input type="radio"/> Import from Library	
<input checked="" type="radio"/> User defined	
Total Height (H) (cm)	10
Total Width of Flange (B) (cm)	4
Internal Radius (R) (cm)	0.8
Thickness (t) (cm)	0.3
Total Width of Edge Fold (C) (cm)	1.5

Figure 4.12: - Entering the dimensions manually.

4.2.3 Material Properties

Material Properties	
Yield Stress (F _y) (t/cm ²)	2.4
Elastic Modulus (E) (t/cm ²)	2100
Poisson Ratio (ν)	0.3
Shear Modulus (G) (t/cm ²)	807.6923076923076

Figure 4.13: - Material properties section.

Whether you choose EWM or DSM, the third part on the program screen is called “Material Properties” as shown in **Figure 4.4**. Material properties refer to the characteristics or attributes of a steel material that determine its behavior and response to various external conditions and forces. The steel material exhibits distinct properties, notably the yield strength (F_y), Young's modulus (E_0), Poisson's ratio (ν), and shear modulus. Yield Strength (F_y) refers to the maximum stress a steel material can withstand before it undergoes permanent deformation or starts to exhibit plastic behavior. It indicates the material's ability to resist deformation under load. Young's Modulus (E_0), also known as the elastic modulus or modulus of elasticity, represents a material's stiffness or rigidity. It quantifies the material's ability to deform elastically in response to an applied stress and is defined as the ratio of stress to strain within the elastic limit. Poisson's Ratio (ν) measures the ratio of lateral strain (strain perpendicular to the applied load) to the axial strain

(strain parallel to the applied load) in a material. It characterizes the material's tendency to contract in the transverse direction when subjected to axial loading or vice versa. Shear Modulus (G), also known as the modulus of rigidity or elastic modulus in shear, reflects a material's resistance to shear deformation. It quantifies the material's ability to withstand shearing forces without undergoing permanent deformation. The shear modulus is defined as the ratio of shear stress to shear strain within the elastic limit. The designer enters these mentioned properties of steel material to be used in order in this part of the screen, as shown in **Figure 4.13**.

4.2.4 Length and bracing conditions

Length & Bracing Conditions	
Lx (cm)	120
Ly (cm)	120
Lz (cm)	120

a) column

Length & Bracing Conditions	
Lx (cm)	120
Ly (cm)	120
Lz (cm)	120
Lu (cm)	50
Cb	1

b) beam and column-beam

Figure 4.14: - Length and bracing Conditions section.

In this part of the form, the designer enters the length and bracing conditions of the desired member, taking into account that the program deals with member local axis. local axis refers to a coordinate system that is specific to an individual structural member. It is typically aligned with the member's geometry and is used to define local directions and orientations within that member. The designer should enter different effective lengths (L) in different local axes (x , y , z) of the compressive member, as shown in **Figure 4.14 (a)**. in case of the member is subject to bending, He should also enter the unsupported length (L_u) and the bending coefficient (C_b), as shown in **Figure 4.14 (b)**.

The effective length (L) is a concept used in structural analysis and design to account for the influence of the member's boundary conditions on its behavior. The unsupported length (L_u) is a measure of the effective unsupported length of the member and affects its buckling and deflection characteristics. The bending coefficient (C_b) is a parameter used in the design of steel beams to account for the influence of lateral-torsional buckling.

4.2.5 Ultimate loads

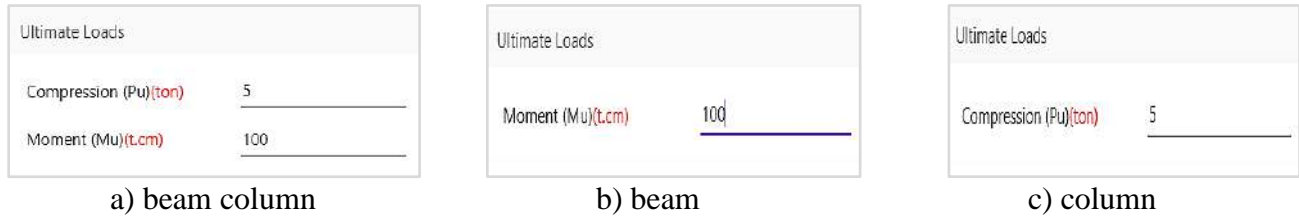


Figure 4.15: - Ultimate loads section in different frame elements.

If the user wants to design the section or make a check for it, he must enter the value of loads affecting the section, whether this load is compression or bending or both in this part of the form, as shown in Figure 4.15. It should be noted that this section “Ultimate loads” does not appear at all in the case of the user wants to find the maximum resistance of the section.

4.3 EXTRACT RESULTS

The required result is easily obtained, whether it is required to design, test, or find the largest bearing strength for the section by pressing button “calculate” in the bottom middle of the screen, as this result appears on the left of the screen, as shown in Figure 4.16. It is also possible to know the details of the solution by obtaining the calculation sheet by pressing the “Display report” button, and this report can also be printed by pressing the “Print Report” button in the bottom middle of the calculation sheet, as shown in Figure 4.17.

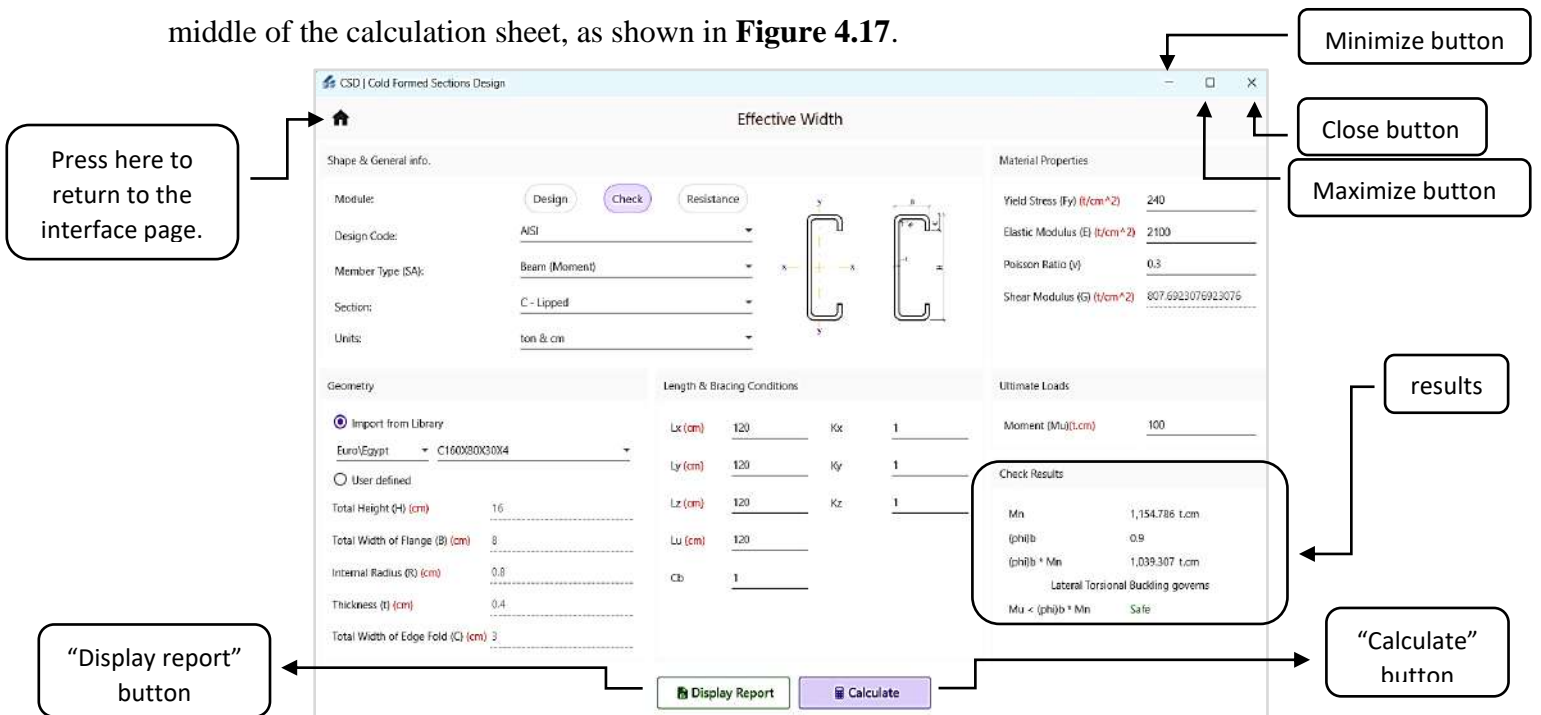


Figure 4.16: - Extract the check results.

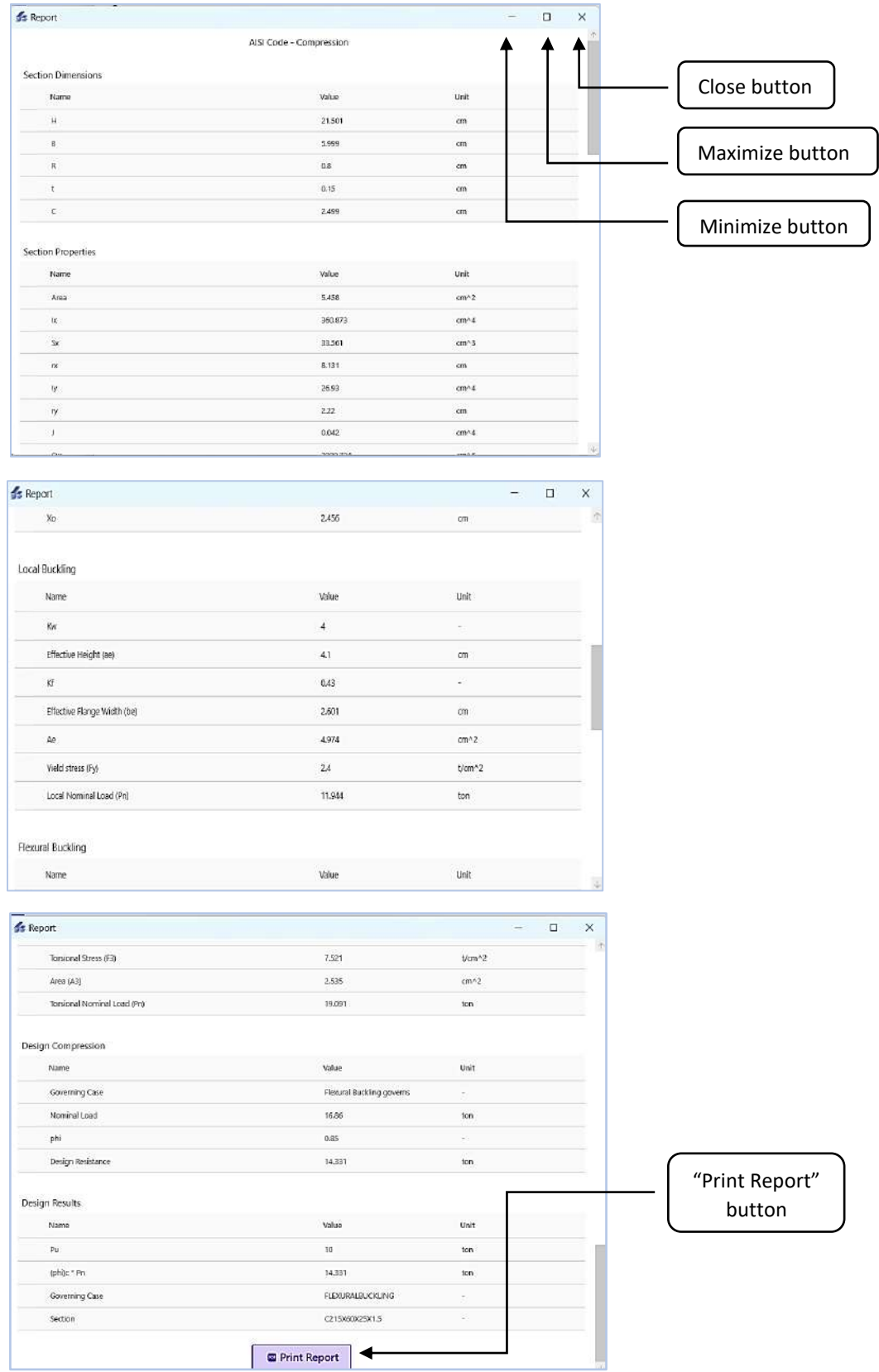


Figure 4.17: - Calculation sheet report.

If the user wants to go back to re-enter the data for the same method, whether it is EWM or DSM, all he has to do is close the report of calculation sheet from the “x” sign above the screen, as shown in Figure 4.17, and change the data he wants. On the other hand, if he wants to re-enter the data for another method, he can click on the house sign at the top on the left, as shown in Figure 4.16, then he will return to the program interface page, where he can select any methods Wants.

4.4 PROGRAM RESULTS VERIFICATION

It is important to check the results of the program before using it. This confirmation is achieved by taking some of the resolved examples from some references [3, 24, 26, 29, 30, 124, 127-130] and comparing them with the results of the program.

The average ratio of references-to-program solution for AISI_{DSM}, AISI_{EWM}, ECP, and EC3 are 1.00, 1.00, 1.02 and 1.00, with coefficients of variation of 0.02, 0.00, 0.02, and 0.00, respectively, in the case of compressive member. On other hand, in case of flexural member, the average ratio of references-to-program solution for aforementioned codes are 1.00, 1.00, 1.00 and 1.00, with coefficients of variation of 0.00, 0.00, 0.00, and 0.01, respectively.

The maximum resistances resulted by the program matched well with manual results from different references, providing additional credibility and reliability to the program. These results show that the suggested program can accurately calculate the maximum flexural and compressive resistances, enabling precise prediction of design and check of the buckling behavior and ultimate loads of thin-walled members.

4.5 DIFFERENT CODES PARAMETRIC STUDY

Various codes were utilized to carry out parametric analyses on the ultimate capacities of CFS for the channel section. These parameters include the member slenderness ratio (λ), which ranges from 5 to 62 for compression members, and the member torsional slenderness ratio (L/r_t), which varies from 10 to 173 for flexural members. Additionally, the web plate slenderness ratio (h/t) was examined at 50, 80, 100, 114, 150, 180, 200, 220, 250, and 280 for compression members and at 50, 80, 100, 114, 150, and 180 for flexural members to avoid exceeding the maximum limit of the h/t ratio according to the different codes. Similarly, the flange plate slenderness ratio (b/t) was analyzed across a range of values, including 30, 35, 37, 40, 45, 50, and 55 for compression members and 30.5, 35, 37, 40, 45, 50, and 55 for flexural members. Furthermore, the lip-to-flange plate width ratio (d/b) varied at 0.2, 0.25, 0.3, 0.35, and 0.4. Lastly, the yielding stress (F_y) was studied using recommended values by European codes for cold-rolled flat products: 240, 280, 320, 360, and 400 MPa. This study focused only on the effect of b/t ratios greater than 30 on the CFS flexural strength because the Egyptian Code Committee is currently reviewing ECP in the case of CFS flexural members with b/t ratios smaller than 30.

Except for the yielding stress (F_y) parameter, the material characterized during the study of various parameters has a yield strength (F_y) of 360 MPa. The Young's modulus (E_0) is 210 GPa. The studied members have hinged boundary conditions at both ends. The cross-section used in the study is presented in **Table 4-1** and the dimensions “H, B, D, t and r” are shown before in **Figure 3.3**.

Table 4-1: - Different sections used in the different codes parametric study.

Dimensions (mm)				
H	B	D	t	r
304.8	101.6	22.5	1.7	4.8
304.8	101.6	22.5	2.0	4.8
304.8	101.6	22.5	2.5	4.8
304.8	101.6	22.5	2.7	4.8
304.8	101.6	22.5	3.0	4.8
304.8	101.6	22.5	3.5	4.8
304.8	101.6	22.5	4.0	4.8
666.8	101.6	22.5	2.7	4.8
400.0	101.6	22.5	2.7	4.8
450.0	101.6	22.5	2.7	4.8
800.1	101.6	22.5	2.7	4.8
533.4	101.6	22.5	2.7	4.8
304.8	82.7	18.4	2.7	4.8
304.8	96.0	21.3	2.7	4.8
304.8	109.3	24.1	2.7	4.8
304.8	122.7	27.0	2.7	4.8
304.8	136.0	29.8	2.7	4.8
304.8	149.4	32.7	2.7	4.8
304.8	101.6	26.1	2.7	4.8
304.8	101.6	31.0	2.7	4.8
304.8	101.6	36.0	2.7	4.8
304.8	101.6	40.9	2.7	4.8

4.5.1 Effect of Member Slenderness Ratio (λ) Parameter

Figure 4.18 (a) demonstrates an indirect correlation between the member slenderness ratio (λ) and nominal axial load capacities in different design codes. This is because when increasing

the member slenderness ratio (λ), the incidence of global (flexural) buckling increases, and the member slenderness ratio (λ) is inversely proportional to the nominal global buckling resistance, as shown in Eqs. (3.38) to (3.41).

In **Figure 4.18 (b)**, there is a shift from a stable to an indirect relationship between the nominal flexural capacity and torsional slenderness ratio (L/r_t) in AISI_{DSM}, AISI_{EWM}, and ECP at L/r_t ratios of 12, 11, and 8, respectively. This phenomenon can be attributed to the transition of failure buckling modes from local to global buckling. The shift from local to global buckling modes means moving from a buckling mode that relies on the sectional dimension to one that relies on the length. During this parameter study, the same section with different lengths was used; therefore, the nominal local buckling strength (M_{nL}) was constant, as expressed in equations (3.42), (3.43), and (3.44). Consequently, a stable relationship exists between the CFS flexural capacity and torsional slenderness ratio (L/r_t) in AISI_{DSM}, AISI_{EWM}, and ECP as long as the local buckling failure mode occurs. The indirect correlation between the torsional slenderness ratio (L/r_t) and the nominal global buckling resistance (M_{ne}) owing to the increasing length, which means increasing the torsional slenderness ratio (L/r_t), causes a decrease in the critical elastic global buckling (M_{cre} & F_{cre}), and consequently, an increase in the nominal global buckling resistance (M_{ne}), as shown in equations (3.47), (3.48), and (3.50). It is also noted that the ECP gives a more conservative result compared to the other codes when the member is subjected to global buckling because the ECP contains some criticism, such as that the bending moment coefficient (C_b) remains constant at a value of 1, and the nominal global buckling resistance (M_{ne}) is always equal to the critical elastic global buckling (M_{cre}), regardless of the member length or the boundary conditions, while applying Eq. (3.50).

In contrast, an indirect correlation was observed between the nominal flexural capacity in EC3 and the torsional slenderness ratio (L/r_t). EC3 considers the effect of the combination of the different buckling modes: local, distortion and global buckling, irrespective of the member length, as shown in equation (3.49). Since varied lengths of the same section were studied, the effects of local buckling, and distortion buckling were constant. Therefore, the CFS flexural strength (M_n) depends only on global buckling, which is inversely proportional to the torsional slenderness ratio (L/r_t).

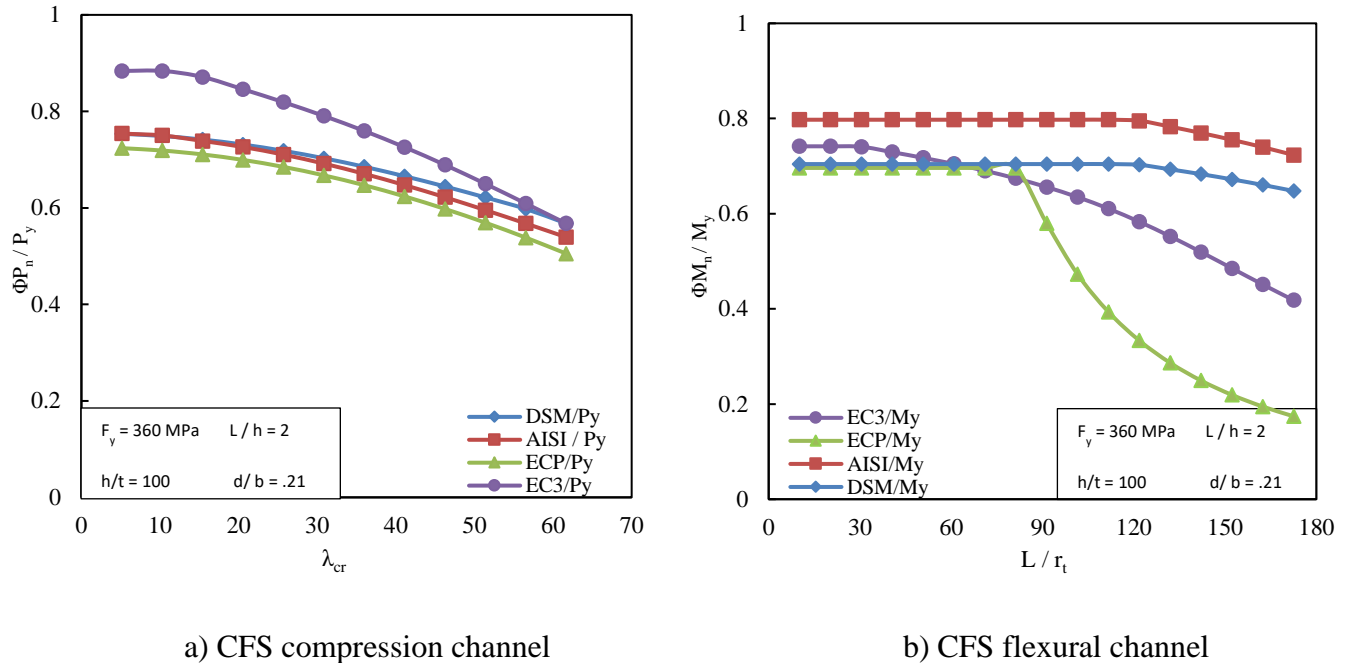


Figure 4.18: - Effect of member slenderness ratio (λ) parameter on CFS channel.

4.5.2 Effect of Web Slenderness Ratio (h/t) Parameter

As shown in **Figure 4.19 (a)**, there is an indirect relationship between the web slenderness ratio (h/t) and the nominal axial capacities in different design codes. The reason behind this correlation is that all the studied sections failed because of local buckling, which is indirectly related to the h/t ratio, as shown in equations (3.4) to (3.13). When the h/t ratio increases in the AISI_{EWM}, EC3, and ECP codes, the web's reduction coefficient (ρ) increases, resulting in a decrease in the effective area (A_{eff}) and a reduction in local buckling resistance. Additionally, in AISI_{DSM}, the critical local buckling (P_{cr1}) decreases, causing a decrease in local buckling resistance, as demonstrated in equations (3.34) and (3.35).

As shown in **Figure 4.19 (b)**, a slight variation in the flexural capacities from different design codes was observed with a change in h/t until the ratio reached 100. However, after this ratio, the relationship between them became inverse. This is because all the studied sections failed owing to local buckling. In the case of EWM codes, when the h/t ratio is less than 100, the sectional area has almost no reduction as the web's reduction coefficient (ρ) approaches the unit value, causing the web's effective width to equal the web's total width; thus, the effective sectional area is similar to the total sectional area. However, when the h/t ratio is greater than 100, the web's

reduction coefficient (ρ) is less than the unit value. Consequently, the web's effective width is less than the web's total width; therefore, the effective cross-sectional area is less than the total cross-sectional area. In contrast, according to DSM, when the h/t ratio is less than 100, λ_L is typically less than 0.776, causing the nominal local buckling resistance (M_{nL}) to be equal to the critical elastic global buckling (M_{cre}), as shown in Eq. (31), and because the lengths in all the studied sections are constant, M_{cre} is almost constant. However, when the h/t ratio exceeded 100, λ_L was typically greater than 0.776, and M_{nL} changed depending on the critical elastic local buckling (M_{crL}) and critical elastic global buckling (M_{cre}), as shown in equation (3.42). M_{cre} is almost constant; therefore, M_{nL} depends only on M_{crL} . M_{crL} decreases owing to the decrease in the connection strength between the web and flange as the web height increases, causing a decrease in M_{nL} . This is because AISI_{DSM} is the only code that takes into account the interaction between different section elements, like flange-to-web.

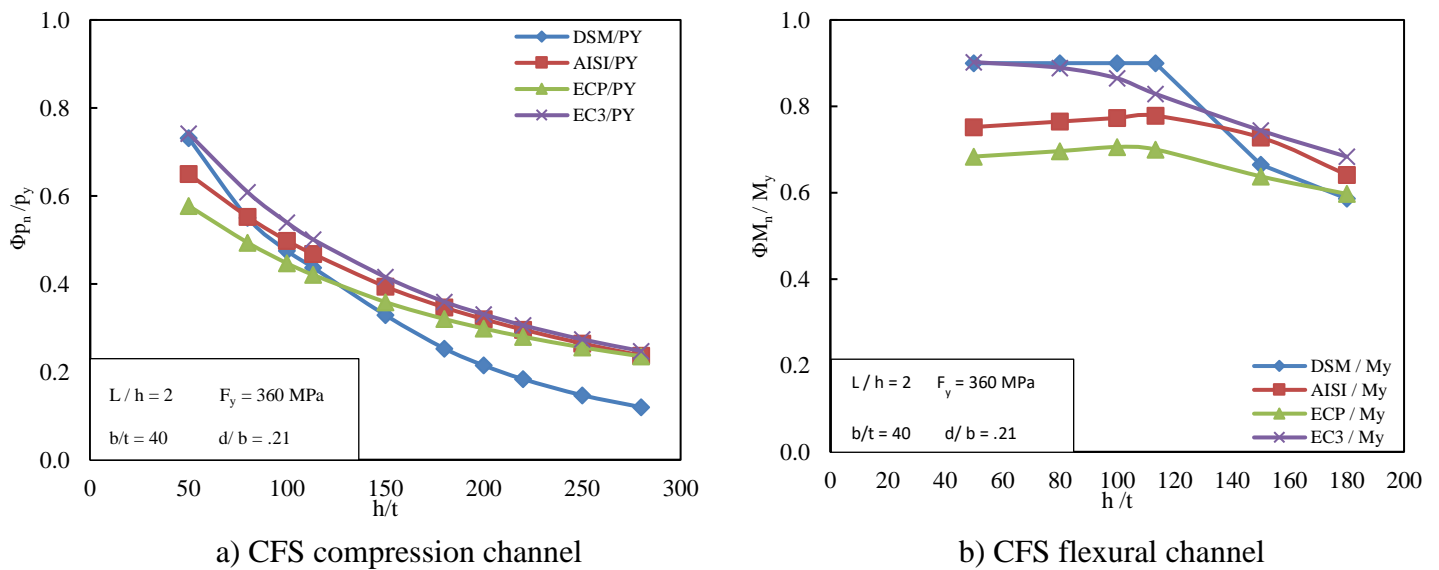


Figure 4.19: - Effect of Web Slenderness Ratio (h/t) Parameter on CFS channel.

4.5.3 Effect of Flange Slenderness Ratio (b/t) Parameter

As shown in Figure 4.20 (a), there is a slight indirect relationship between the CFS compressive capacities in different codes and the flange slenderness ratio (b/t). This can be explained in the AISI_{EWM}, EC3, and ECP codes as, when there is an increase in the b/t ratio, there is a corresponding increase in plate slenderness (λ_p), as shown in equations (3.7), (3.8), and (3.9), respectively, which causes a decrease in the flange's reduction coefficient (ρ), as demonstrated in

equations (3.4), (3.5), and (3.6). This leads to a decrease in the effective area (A_{eff}) and local buckling resistance, as shown in equation (3.35). It is observed that the compressive capacity of the AISI_{DSM} exhibits a positive correlation with b/t when the b/t ratio is less than 35, but a slight negative correlation beyond that point. This can be attributed to a shift in the failure mode from distortion buckling caused by equation (3.36) to the local buckling resulting from equation (3.34).

As illustrated in **Figure 4.20 (b)**, the b/t ratio was found to have an indirect correlation with the flexural CFS capacities according to AISI_{EWM} , ECP and EC3. This can be explained as follow: when there is an increase in the b/t ratio, there is a corresponding increase in the plate slenderness (λ_p), as shown in equations (3.7), (3.8), and (3.9), respectively, which causes a decrease in the flange's reduction coefficient (ρ), as demonstrated in equations (3.4), (3.5), and (3.6), which led to a decrease in the effective section modulus (S_{eff}) and a reduction in the local buckling resistance, as shown in equation (3.43). According to AISI_{DSM} , it has been observed that when b/t is less than 45, the flexural capacity remains unaffected by changes in the b/t ratio owing to member failure occurring via the global buckling failure mode, which results from applying equation (3.47). Moreover, the cross-sectional dimensions have no impact on the critical elastic global buckling (M_{cre}), as long as there is no change in length. However, when the b/t ratio is greater than 45, it has been discovered that an indirect relationship exists between the CFS flexural capacities and the b/t ratio as member failure occurs via the local buckling mode, which results from applying equation (3.42).

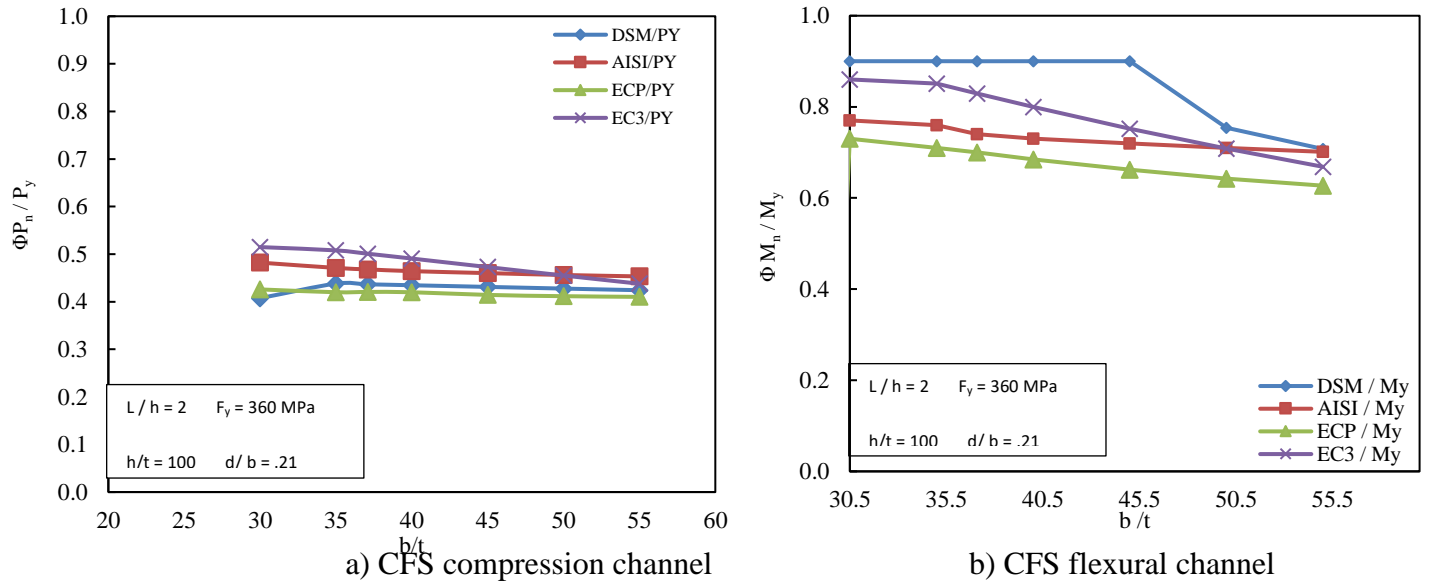
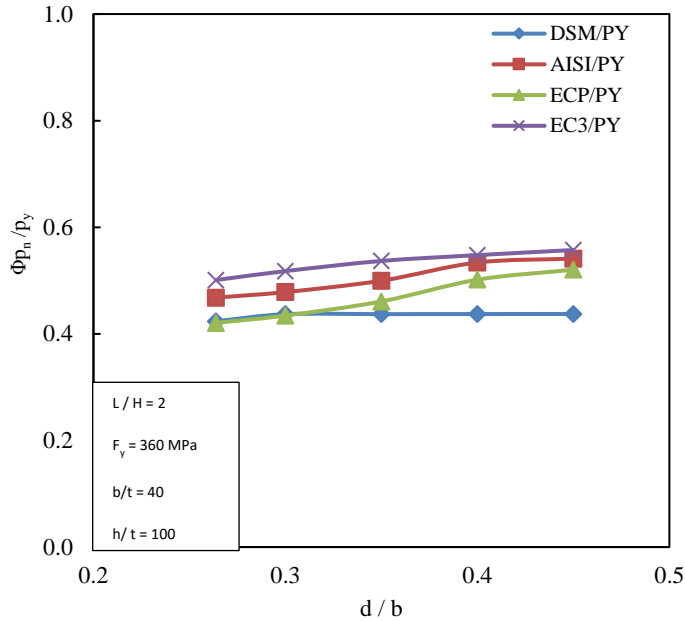


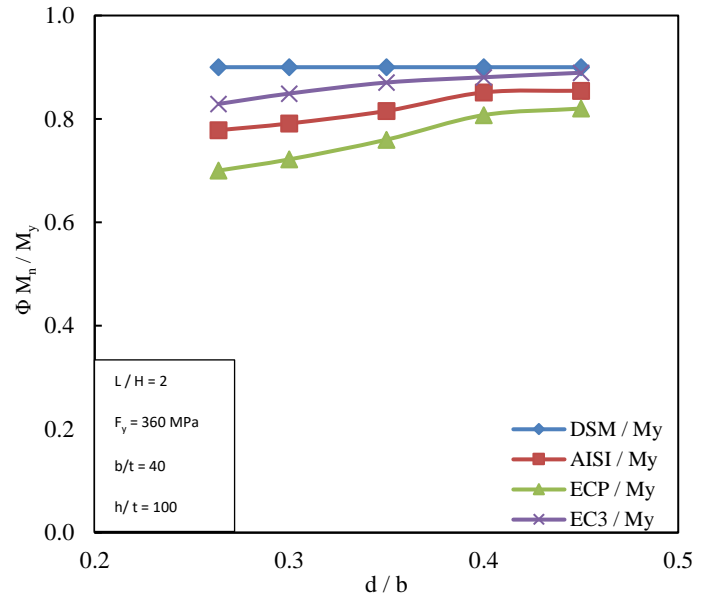
Figure 4.20: - Effect of flange slenderness ratio (b/t) parameter on CFS channel.

4.5.4 Effect of Lip-to-Flange Length Ratio (d/b) Parameter

It can be observed from **Figure 4.21** that there is a slight variation in the CFS capacities resulting from the $AISI_{DSM}$ owing to the change in the lip-to-flange width (d/b) ratio. Conversely, a direct correlation exists between the CFS capacities in $AISI_{EWM}$, EC3, and ECP with the same change in the d/b ratio. This is because $AISI_{DSM}$ considers the interaction between different section elements, such as the flange-to-web and flange-to-lip interactions. The studied sections failed owing to local buckling, and the flange-to-web local buckling consistently proved to be more critical than the flange-to-lip local buckling. Hence, changing the lip-to-flange width ratio (d/b) had no impact on the $AISI_{DSM}$ results. Additionally, in $AISI_{EWM}$, EC3, and ECP, an increase in the d/b ratio results in a flange buckling coefficient (K) reduction, consequently leading to an increase in the normalized flange plate slenderness (λ_P), which ultimately causes a decrease in the flange reduction factor (ρ), as shown in equations (3.4) to (3.13). This leads to a decrease in the flange effective length, causing a reduction in A_{eff} and Z_{eff} , ultimately leading to a decrease in CFS compressive and flexural capacities.



a) CFS compression channel



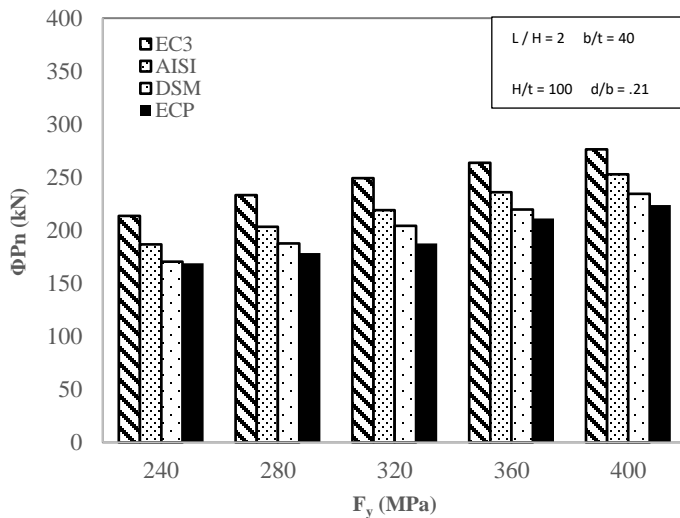
b) CFS flexural

channel

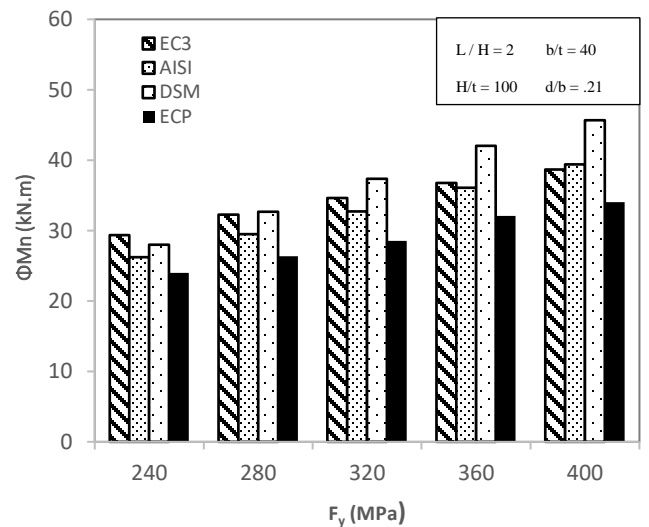
Figure 4.20: - Effect of lip to flange length ratio (d/b) parameter on CFS channel.

4.5.5 Effect of Steel Yielding Stress (F_y) Parameter

As anticipated, there is a clear direct correlation between the steel yield stress (F_y) and the capacities of the CFS channels of different frame members in various codes, which is clearly illustrated in Figure 4.21.



a) CFS compression channel



b) CFS flexural channel

Figure 4.21: - Effect of steel yielding stress parameter on CFS channel.

CHAPTER (5)

FINITE ELEMENT MODEL

5.1 INTRODUCTION

The Finite Element Model (FEM) has become essential in the field of engineering due to its relatively affordable nature and time-saving properties when compared to physical experiments conducted in live labs. This is especially true during the parametric examination of cross-section geometries. Moreover, performing an empirical analysis on the impact of geometric imperfections and residual stresses on structural elements is a challenging task [7]. Consequently, it has become crucial to establish a simplified version of FEM that can accurately forecast the axial capacity of CFS [6]. This prediction can then be used for future reference and comparison with other analytical studies. The FEM created in this study is thoroughly elucidated in the subsequent sections.

5.2 SUMMARY OF EXPERIMENTAL STUDIES

The Finite Element model (FEM) was created using ABAQUS software [23]. To ensure the accuracy of the FEM, it was validated against the previous test results obtained by Torabian et al. [131] and Chen et al. [1].

Torabian et al. (2014) [131] conducted an experimental study in which they tested 55 lipped channel specimens under different eccentric compressions. The 600S137-54 lipped channel with a yield strength (F_y) of 345 MPa was chosen for that experimental study. The specimens experienced a vast array of peculiarities which led to significant and/or insignificant curvatures along the main and secondary axes. In order to explore the strength of the cross-section, the compromised strength caused by distortional buckling, and the overall buckling, three distinct lengths were examined: 305 mm (short), 610 mm (intermediate), and 1219 mm (long).

Figure 5.1 portrays the average stress-strain curve of the material, showcasing the yield strength and ultimate strength. The measurement of Young's modulus was not directly obtained from the tensile tests. Consequently, a nominal Young's modulus of 203.4 MPa was assumed for the specimens based on AISI [132]. The eccentricities can be found in Table 5-1. For more comprehensive information regarding the test, please consult the research conducted by Torabian et al. [131].

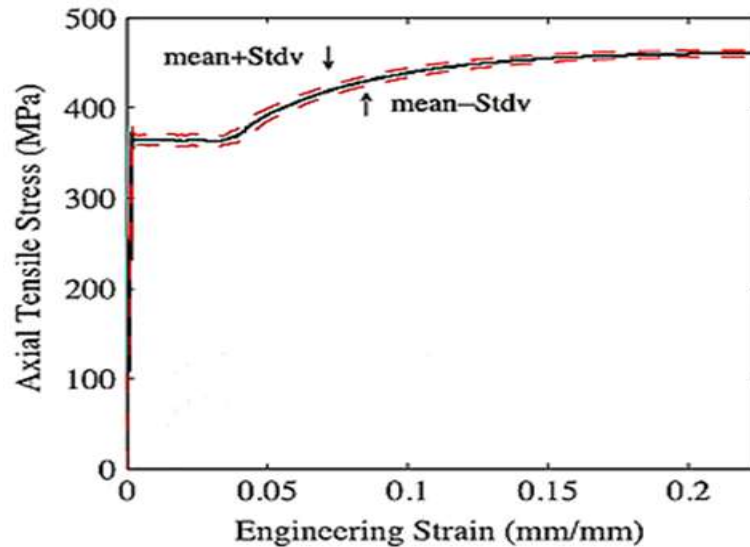


Figure 5.1: - Tensile test results in Torabian (2014) [131].

Table 5-1: - The target and measured eccentricities in Torabian (2014) [131].

No.	Loading Condition	L = 305 mm		L = 610 mm		L = 1219 mm	
		Eccentricities (mm)		Eccentricities (mm)		Eccentricities (mm)	
		e_y	e_x	e_y	e_x	e_y	e_x
1	Minor axis bending	0	-27.3	0	-32.6	0	-39.7
2		0	-13.7	0	-15.3	0	-16.6
3		0	-4.7	0	-3.8	0	-4.9
4		0	2.8	0	3.8	0	5.2
5		0	7.8	0	15.4	0	16.7
6		0	24.1	0	31.3	0	38.3
7	Major axis bending	-25.4	-1.1	-22.1	.3	-15.2	0.1
8		-88.9	-.33	-76.2	0.1	-50.8	1.2
9		-190.5	0	-165.1	-0.1	-139.7	0
10	Biaxial axis bending	-38.1	2.7	-31.8	2.3	-25.4	2.0
11		-127.0	8.6	-114.3	8.8	-101.6	6.8
12		-20.6	4.2	-19.1	4.3	-17.8	3.7

Chen and colleagues (2019) [1] ventured into an exploratory inquiry of stub column examinations on frigid-formed steel Channel and Zee sections with an assortment of stiffeners. The investigation encompassed 30 firmly ended column examinations, involving 6 sequences of C-sections and 4 sequences of Z-sections. The stiffener configurations embraced uncomplicated edge stiffeners, uncomplicated lips with inward or outward return lips, and intervening web stiffeners. An oppressing axial force was employed to the specimens utilizing a servo-controlled hydraulic testing apparatus. The specimens were fashioned through the application of brake-pressing to high-strength zinc-coated grades G450 and G550 structural steel sheets, and the material characteristics were appraised through tensile coupon examinations.

The samples were marked in a manner that allowed for the identification of their cross-section progression and stated thickness. This accomplishment was made by assigning a letter (C or Z) and a number to indicate the cross-section progression, followed by the letter T and another number to indicate the stated thickness. For example, a sample from Progression Z2T1.5, which is a straightforward lipped Zee-section with outward return lips and a stated thickness of 1.5 mm, would be marked as Z2T1.5.

In that experimental investigation [1], four cross-section profiles are integrated (Progression Z1-Z4) for Z-sections. However, the test samples employed in our investigation only consisted of a plain Z-section (Z1) and a straightforward lipped Z-section (Z2). The cross-section configuration of the test samples is illustrated in **Figure 5.2**, and their respective dimensions are specified in **Table 5.2**.

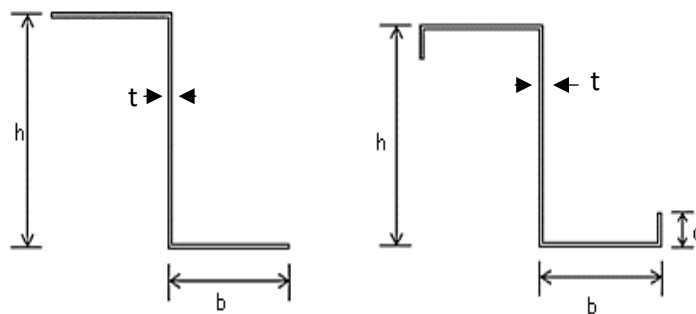


Figure 5.2:- The cross-section Profile for test specimens used in Chen (2019) [1].

Table 5-2: - Cross-section dimensions for test specimens used in Chen (2019) [1].

Specimen	Dimensions (mm)				
	L	d	b	h	t
Z1T1.0	480	-	102.6	159.6	1.02
Z1T1.5	480	-	103.0	160.0	1.52
Z1T1.9	480	-	103.8	160.2	1.92
Z2T1.0	481	23.1	102.4	159.0	1.02
Z2T1.5	480	23.3	102.8	160.6	1.50
Z2T1.9	482	23.7	103.3	160.4	1.90

Chen et al. (2019) ascertained the material characteristics of every set of samples through the execution of tensile coupon tests. These coupons were obtained from the identical set of samples employed in the stub column tests for each individual cross-section. To procure them, we meticulously machined the coupons lengthwise along the very core of the planar section of plate elements boasting the widest breadth within a given section.

The values denoting the nominal and measured 0.2% tensile proof stress ($\sigma_{0.2}$), initial Young's modulus (E), ultimate tensile strength (σ_u), as well as the elongation at fracture (ϵ_f) have been systematically arranged in Table 5-3, exclusively for the examination specimens that were harnessed in our inquiry. For a more comprehensive understanding of the test, kindly consult the research undertaken by Chen et al. (2019) [1].

Tables 5-3: - Nominal and measured material properties obtained from tensile coupon tests for test specimens used section columns [1].

Specimen	Nominal	Measured			
	$\sigma_{0.2}$ (MPa)	E (Mpa)	$\sigma_{0.2}$ (MPa)	σ_u (MPa)	ϵ_f %
Z1T1.0	550	212	594	615	10
Z1T1.5	450	209	534	560	16
Z1T1.9	450	196	500	527	17
Z2T1.0	550	216	573	581	12
Z2T1.5	450	216	530	555	15
Z2T1.9	450	202	500	529	15

5.3 NUMERICAL INVESTIGATION

5.3.1 Description

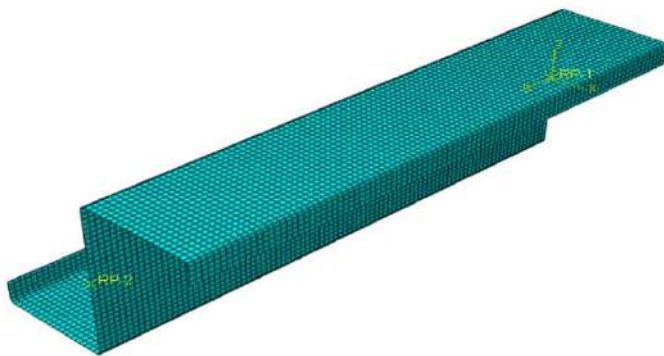
The ABAQUS [23] program, a nonlinear analysis tool based on finite element principles, has been utilized to construct a model for finite element analysis (FEA). The simulation itself occurs in a dual-stage process. The initial stage involves an eigenvalue elastic buckling analysis, alternatively referred to as a linear perturbation analysis, to ascertain the potential modes of buckling for the column, utilizing a flawlessly defined geometry. Subsequently, in the subsequent stage, a non-linear analysis is carried out, encompassing both geometric and material nonlinearities, with the intention of determining the ultimate load and failure modes of CFS sections through the implementation of the modified Riks analysis.

5.3.2 Element Type and Mesh

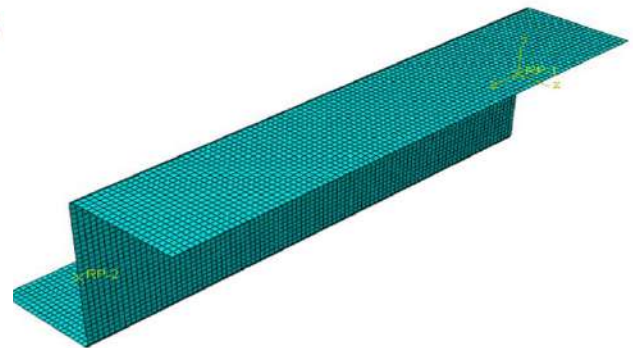
The CFS section elements have been replicated through the usage of the S4R shell element, a versatile four-noded element handpicked from the ABAQUS [23] program library. This segment possesses the capability to imitate the behavior of shells that are slender, bulky, and doubly curved. We attain a reduced integration and a curvaceous control by employing six degrees of freedom per node (three translations and three rotations). In order to establish the finite element mesh utilized in the model, diverse finite element dimensions were scrutinized. The outcomes of the analysis are exhibited in **Table 5-4** for the initial instance of loading in a short column in the experimental exploration [131]. In **Table 5-4**, P_{EXP} signifies the experimental ultimate load, while P_{FEA} denotes the ultimate load produced by the FEA. The study revealed that using an element size of 5 mm × 5 mm (length by width), with an aspect ratio (length to width) equal to one unit yielded good simulation results. **Figures 5.3& 5.4** illustrate typical finite element meshes of CFS used in this study.

Table 5-4: - Analysis of Strengths Based on different element size.

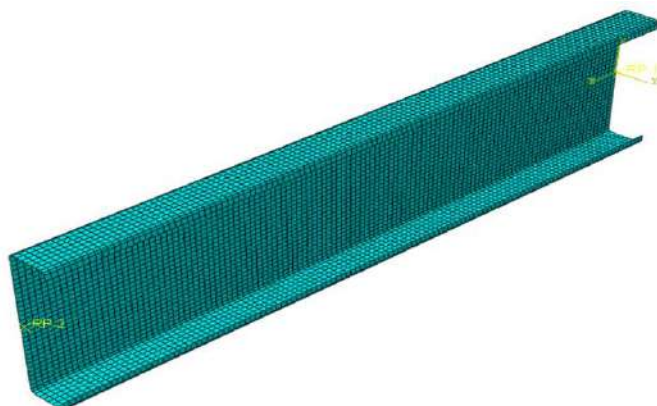
Element size (mm)	P_{FEA} (kN)	P_{FEM} / P_{EXP}
2×2	23.55	0.93
3×3	23.5	0.93
5×5	23.96	0.95
8×8	23.34	0.92
10×10	23.23	0.92
12×12	22.21	0.91



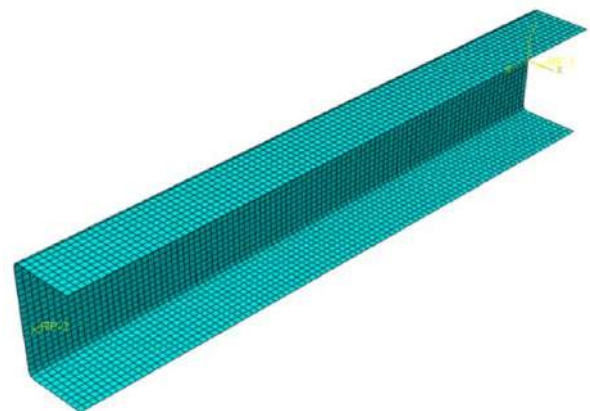
a) lipped CFS Z-shape



b) plain CFS Z-shape

Figure 5.3: - Meshing of Zee CFS sections.

a) lipped CFS channel shape



b) plain CFS channel shape

Figure 5.4: - Meshing of channel CFS sections.

5.3.3 Boundary Condition

The FEM has been employed for the representation of CFS with hinged roller supports at the extremities. The boundary conditions at the ends were applied to the column ends through two reference points situated at specific positions of the column end cross sections, which were utilized in the experiments mentioned in [1, 131]. The hinged end boundary condition was modeled by restraining all the translational degrees of freedom (d_x , d_y , d_z) and releasing all the rotational degrees of freedom (Θ_x , Θ_y , Θ_z), except for the degree of freedom in the axial direction (Θ_z) of the node at that point. The roller end boundary condition is simulated as a hinged boundary condition, except for releasing the translational degree of freedom in the axial direction (d_z), since this is the end where the axial load is applied to the column. Consequently, the nodes at that end were permitted to translate freely in the axial direction. **Figures 5.5** illustrate typical finite element interaction and boundary conditions of CFS sections used in this study.

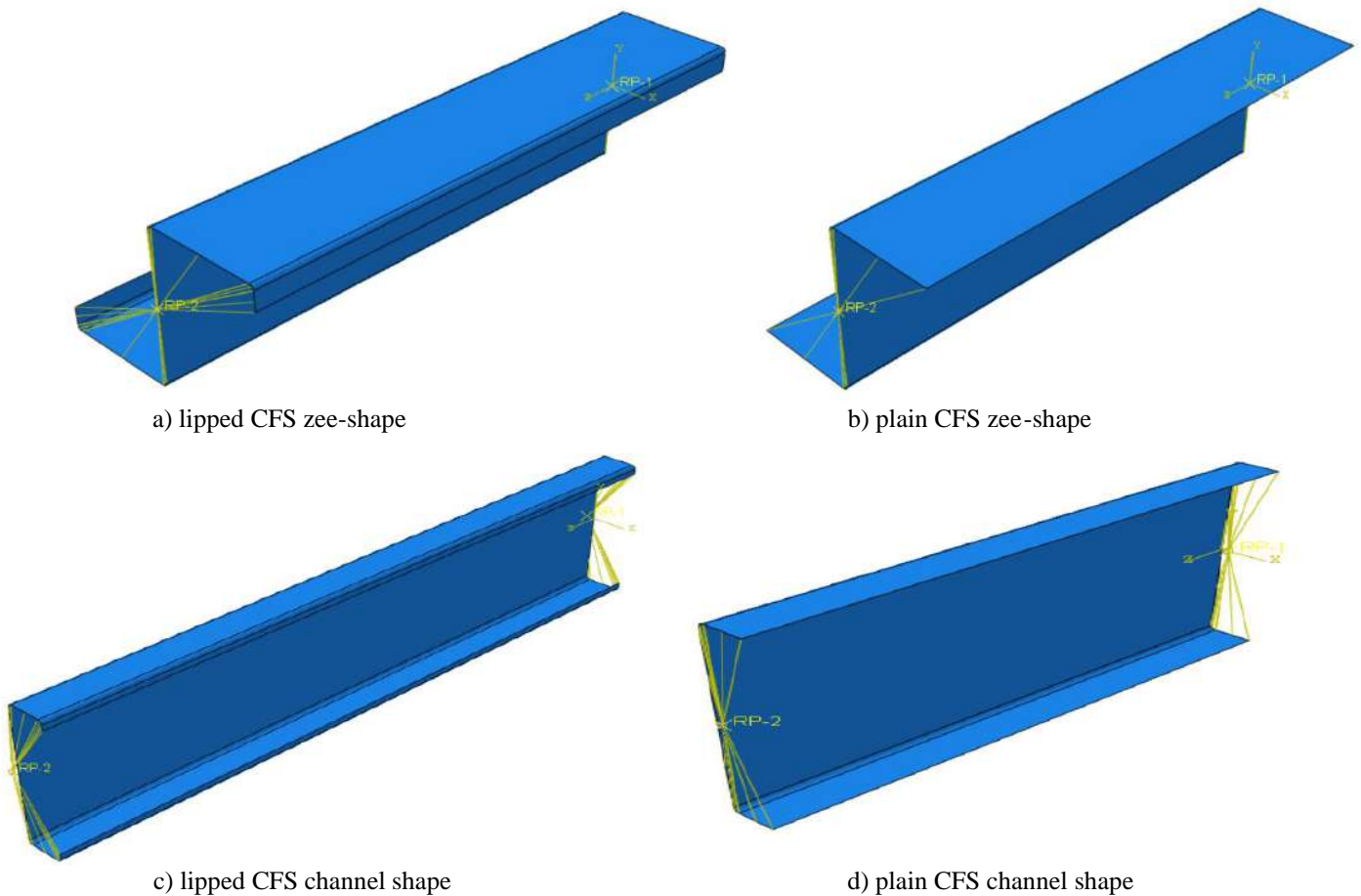
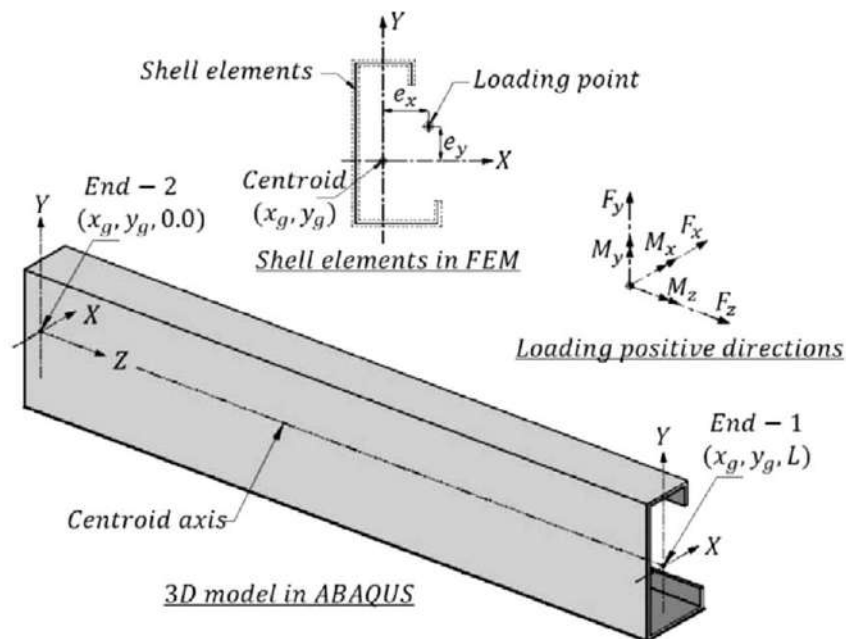


Figure 5.5: - Interaction and boundary conditions.

5.3.4 Method of Loading

The technique used for loading in the FEA is identical to the one employed in the tests mentioned in [1, 131]. When analyzing the columns, the load control technique utilized was the modified Riks analysis [23]. In this method, a compressive load was applied axially on the ends of the column through two reference points positioned at the centroid or center of gravity (CG) of the cross sections of the column ends. These reference points were connected to the adjacent column end, as depicted in the previous **Figure 5.5**. The loading point, member axes, and orientations in the FE model are illustrated in **Figure 5.6**, exactly as they appear in the tests



mentioned in [1, 131].

Figure 5.6: - Illustration of the member axes and orientations in the FE model [36].

5.3.5 Residual Stresses and Corner Enhancement

Many studies have demonstrated that the residual stress does not significantly affect the ultimate capacity [133-135]. Furthermore, there have been indications that the rise in yield strength that arises from corner enhancement during cold-forming operations compensates for the impact of residual stress, provided the ultimate capacity remains the top priority. Abdel-Rahman and

Sivakumaran concluded that corner enhancement and residual stress only affect the behavior of the member, particularly in the post-ultimate stage, rather than the ultimate capacity value [133].

Since this study focuses on the ultimate capacity of the CFS and not the post-ultimate stage, it was determined that the finite element model does not consider residual stresses and corner enhancement.

5.3.6 Material Properties

As previously stated, the initial phase of the numerical simulation involves a linear analysis with a direct correlation between the applied loads and the structure's response. Throughout this analysis stage, the rigidity of the structure remains unchanged, and the qualities of the substance are solely determined by the density, Young's modulus, and Poisson's ratio. However, in the subsequent stage of the numerical simulation, a non-linear examination is carried out, with the rigidity of the structure fluctuating as it undergoes deformations. The non-linearity of the substance is incorporated in the finite element method by specifying actual stresses and strains. A mathematical representation, known as the incremental plasticity representation, was employed to replicate the plasticity of the material. A mathematical model, referred to as the incremental plasticity model, was utilized to simulate the plasticity of the material. the calculation of the incremental plasticity model, true stress (σ_{true}) and true plastic strain (\sum_{true}^{pl}) as follow in equations 5.1 & 5.2.

$$\sigma_{true} = \sigma (1 + \xi) \quad (5.1)$$

$$\sum_{true}^{pl} = \ln(1 + \varepsilon) - \sigma_{true} / E \quad (5.2)$$

The equations use the measured engineering stress and strain, denoted by σ_{true} and (\sum_{true}^{pl}) respectively, which are based on the original cross-sectional area of the coupon specimens, as described in [81, 82]. E represents the Young's modulus. It should mention that the study used stress strain curve, which was elastic perfect plastic.

5.3.7 Geometric Imperfections and Sensitivity Analysis

Similar to any other structure created by humans, cold-formed steel structures have the potential to possess imperfections. These imperfections can occur during the process of

manufacturing, transportation, storage, or construction. The term "geometric imperfections" relates to the differences between the actual geometry of a structural element and its ideal geometry [135].

Geometric imperfections resulting from the manufacturing process may arise because of the coiling process, which has a significant impact on the curvature of the structural elements. They can also occur during the cold-forming process, which may introduce various types of imperfections, such as camber, twist, and waviness. To accurately replicate these geometric imperfections, it is essential to consider their magnitude and distribution. **Figure 5.7** illustrates that these imperfections can manifest as bowing, warping, and twisting, as well as localized deviations like dents and regular undulations in the plate.

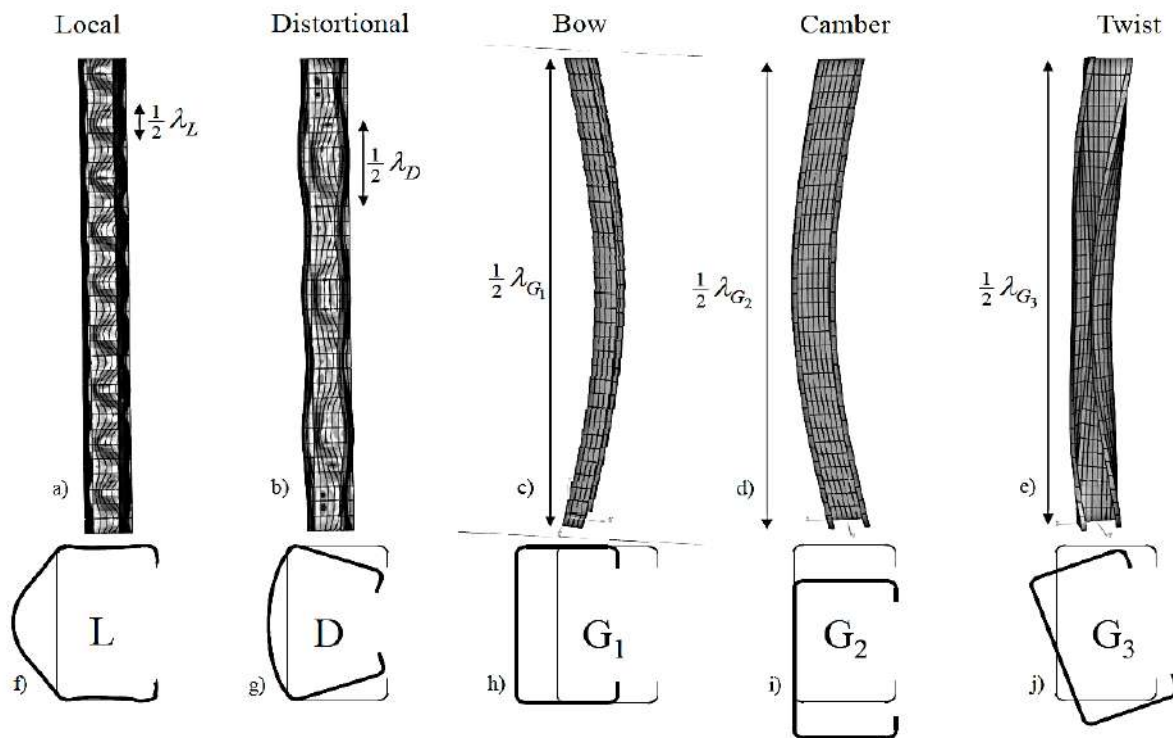


Figure 5.7:- Five mode shapes used in the Traditional Modal Approach, a-e) 3D buckling mode shape and the corresponding wavelength, f-j) 2D cross-sectional mode shape, λ is buckling wavelength [136].

To account for geometric imperfections in the FEM, A perturbation analysis of a linear nature was employed in order to accomplish the task at hand. The primary objective of this

particular analysis was to discern and delineate the potential modes of buckling (or eigenmodes, as they are often referred to) that could conceivably manifest within the column. Subsequently, these eigenmodes were subjected to a scaling factor, which in turn generated a perturbed mesh that could then be utilized in the subsequent non-linear analysis. For the finite element model, it was eigenmode 1 that was specifically chosen and employed [7]. **Figures 5.8, 5.8, 5.10 & 5.11** illustrate the typical buckling (Eigen mode 1) of some samples used in FEM as a simulation of that in the tests.

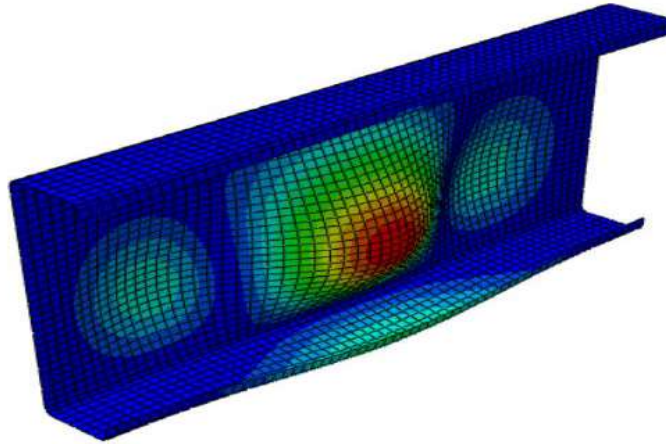


Figure 5.8 :-Typical finite element mesh and buckling (eigenmode 1) of 2nd case of loading on short columns as a simulation of that in the experimental study [131].

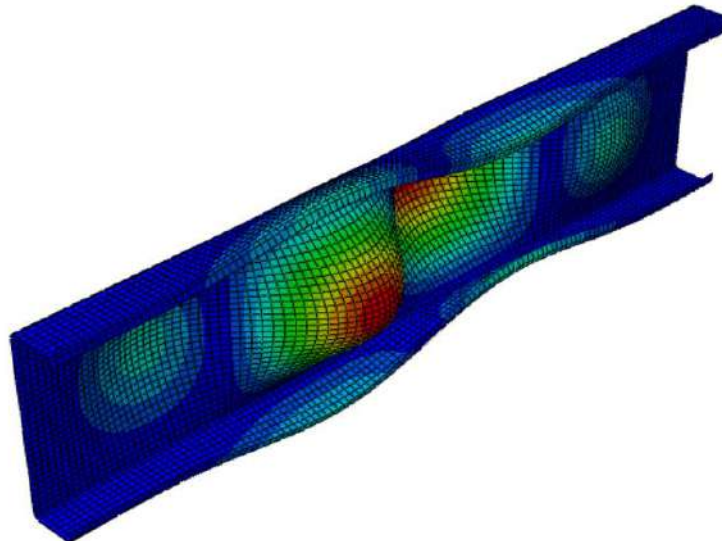


Figure 5.9 :- Typical finite element mesh and buckling (eigenmode 1) of 4th case of loading on intermediate columns as a simulation of that in the experimental study [131].

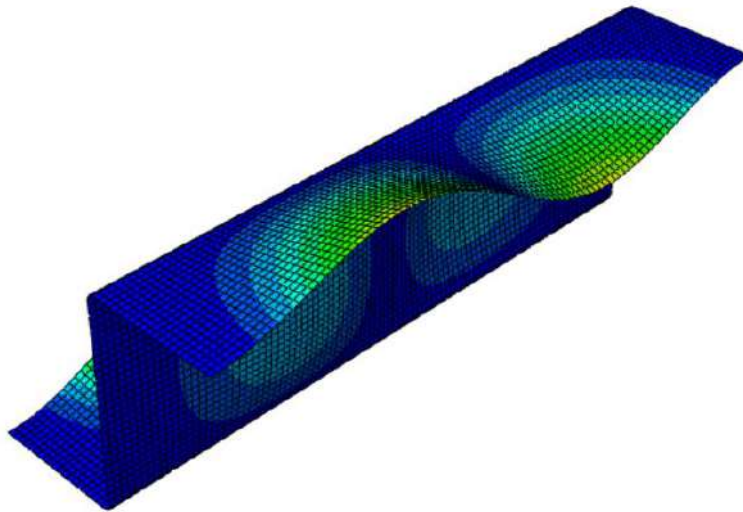


Figure 5.10 :- Typical finite element mesh and buckling (eigenmode 1) of Z1T1.5 sample as a simulation of that in the experimental study [1].

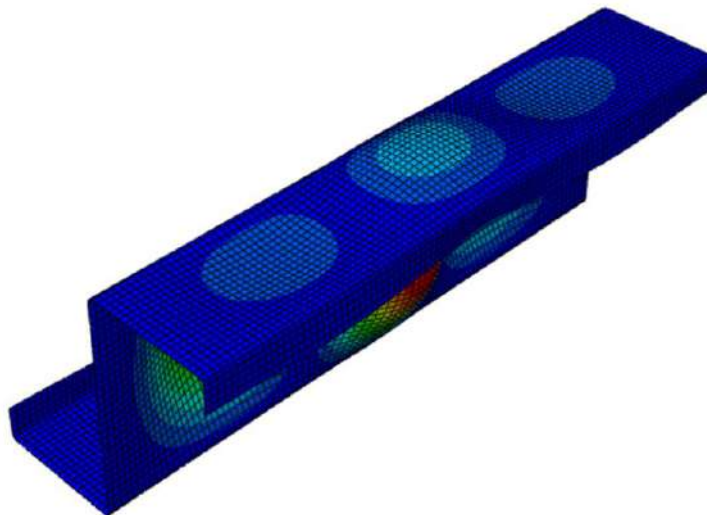


Figure 5.11:- Typical finite element mesh and buckling (eigenmode 1) of Z2T1.9 sample as a simulation of that in the experimental study [1].

Geometric imperfections can be broadly categorized as global imperfections and cross-sectional imperfections. To approximate global imperfections, a magnitude of $L/1000$ (although it is actually $L/960$ based on Galambos, 1998 [137]) is typically utilized, along with a global buckling mode shape as the distribution shape.

When looking at cross-sectional imperfections, one popular approach is to use a part of the member's thickness as the size and the local and distortional buckling mode shapes as the pattern of these imperfections. This approach has been adopted by various studies, including [135, 138-144].

A multitude of proportional ratios, denoted as 100%, 75%, 50%, 25%, 10%, 5%, 2%, and 0.02%, were meticulously examined in relation to the ascertained thickness of the plate (t) as per reference [7]. Additionally, a separate investigation was conducted on the quotient of a divided by 400, where a represents the unobstructed altitude of the web, as based on [36]. The results of the analysis are shown in **Table 5-5** for the first case of loading in short column in in the experimental study [131]. The study revealed that using an imperfection of $a / 400$ and element size of $5 \text{ mm} \times 5 \text{ mm}$ yielded good simulation results and the most accurate ultimate load resulted by the FEA. So, the imperfection of $a/400$ with element sizes $5 \text{ mm} \times 5 \text{ mm}$ were chosen for the parametric study.

Table 5-5: - Analysis of Column Strengths Based on different Geometric Imperfections and different element size.

Imperfection	P_{FEA} (kN)	P_{FEM} / P_{EXP}
.02% t	23.54	0.93
2 % t	23.54	0.93
5 % t	23.56	0.93
10 % t	23.56	0.93
25 % t	23.55	0.93
50 % t	23.5	0.93
75 % t	23.34	0.92
100% t	23.23	0.92
$h / 400$	23.96	0.95

5.4 ELASTIC BUCKLING OF FINITE ELEMENT MODEL

Elastic buckling is a type of buckling that occurs when a slender member, such as a cold-formed steel (CFS) section, is subjected to compressive loads and the material reaches its elastic limit. When the compressive load exceeds a critical value, the member will suddenly buckle and fail under the applied load.

For CFS sections, elastic buckling can occur due to several factors such as the cross-sectional shape, slenderness ratio, and boundary conditions. The buckling behavior of cold-formed steel sections is typically different from hot-rolled steel sections due to the thinness of the material and the presence of residual stresses.

In ABAQUS [23], the main purpose of a linear perturbation analysis was to identify the probable buckling modes (eigenmodes) of the column. Eigenmode 1, which is the specific mode utilized in the ABAQUS, expresses elastic / critical buckling.

There are many specialized programs in determining elastic buckling for CFS Which can be used to find the elastic buckling to compare it to that in FEM program. The analyses used in this research deal with CUFSM [145] program which depend on the finite strip method, as shown in **Appendix (A)**.

A comparison between the elastic buckling outputs of the CUFSM [145] and the ABAQUS [23] programs are made to make sure that we can rely on the FEM elastic buckling results. **Table 5-6** illustrates that comparison for some random samples in American specification [132] with $F_y = 55 \text{ Ksi}$ (378.9 kN /mm^2), $E = 29500 \text{ Ksi}$ ($203225.5 \text{ kN /mm}^2$) and length 56.2 inch (500 mm).

From the **Table 5-6**, it is clear to us that the elastic buckling results of the two programs (CUFSM and ABAQUS) are close where the means ABAQUS to CUFSM results ratio for all tested specimens are 1.08 and 1.1 and the associated coefficients of variation (COV) are .03 and .07 in compression and flexure, respectively. Therefore, we can rely on and trust the elastic buckling results of our FEM (ABAQUS) model.

Table 5-6: - Comparison between the elastic buckling outputs of the CUFSM and the ABAQUS.

NO.	ID	Liner result							
		Compression (kN)		$\frac{\text{ABAQUS}}{\text{CUFSM}}$	Flexure (kN.mm)		$\frac{\text{ABAQUS}}{\text{CUFSM}}$		
		CUFSM	ABAQUS		CUFSM	ABAQUS			
1	9CS2.5×105	166.71	167.54	1.00	55.28	57.83	1.05		
2	9CS2.5×085	85.24	88.95	1.04	30.41	30.62	1.01		
3	9CS2.5×070	44.94	49.62	1.10	15.95	17.17	1.08		
4	9CS2.5×065	35.82	39.72	1.11	12.79	13.76	1.08		
5	9CS2.5×059	26.76	29.68	1.11	9.57	10.31	1.08		
6	600S137-97	165.77	168.11	1.01	26.70	27.59	1.03		
7	600S137-68	61.47	63.33	1.03	11.09	12.11	1.09		
8	600S137-54	31.85	33.03	1.04	6.44	6.25	0.97		
9	600S137-43	16.46	17.12	1.04	3.75	3.94	1.05		
10	600S137-33	7.54	7.90	1.05	1.71	1.81	1.05		
12	800T200-68	38.15	40.10	1.05	6.20	6.29	1.01		
13	800T200-54	19.03	20.04	1.05	3.08	3.13	1.02		
				Mean	1.08			Mean	1.04
				COV	0.032			COV	0.033

5.5 VERIFICATION OF THE FEM

This section presents a comparison between the outcomes of the experimental approach and the finite element method (FEM) regarding ultimate loads, failure modes, and load-displacement responses. Two tables, namely **Table 5-7** and **Table 5-8**, provide a comprehensive summary of the maximum ultimate loads achieved using both the proposed framework and the experimental studies for each specimen at three distinct lengths (305 mm, 610 mm, and 1219 mm) and various cross zee sections mentioned in prior experimental studies [1, 131]. The average predicted-to-experimental ratios for ultimate loads across the three different member-lengths are found to be 0.95, 0.96, and 1.03, accompanied by respective coefficients of variation of 0.06, 0.08, and 0.14. Additionally, the average predicted-to-experimental ratio for ultimate loads for the zee sections is determined to be 0.92, with a coefficient of variation of 0.12.

For all tested specimens, the average ratio is 0.97 with a coefficient of variation of 0.097. The FEM accurately forecasts failure modes that align well with the outcomes of the experiments, as evidenced in **Tables 5-9, 5-10, and 5-11**. However, there exists an absence of information regarding the failure modes of Z-sections utilized in the experimental investigation [1]. Hence, we shall solely clarify the FEM failure modes for those sections in **Table 5-12**. Furthermore, **Table 5-13 to Table 5-16** show the load-displacement curves based on FEM and experimental data, providing additional credibility and reliability to the FEM. **Figures 5.12 to 5.18** brief load displacement curves in **Tables 5-13 to 5-16**. These outcomes effectively showcase that the proposed FEM possesses the capability to precisely simulate material and geometric nonlinearities, thus facilitating the accurate prediction of buckling behavior and ultimate loads of thin-walled members.

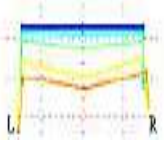

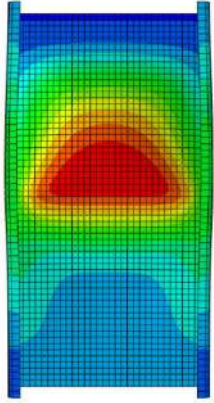
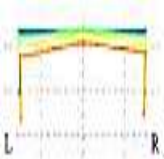

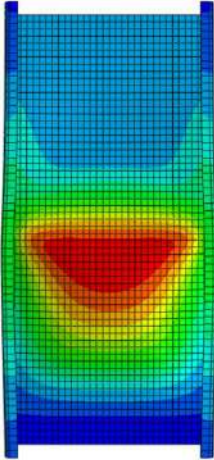
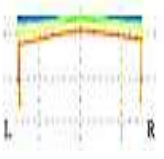

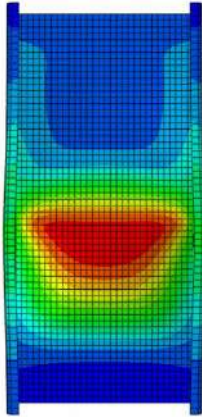
Table 5-7:- Peak ultimate loads (experimental and FEM results) for experimental study [131].

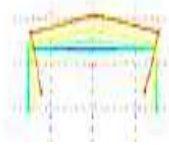

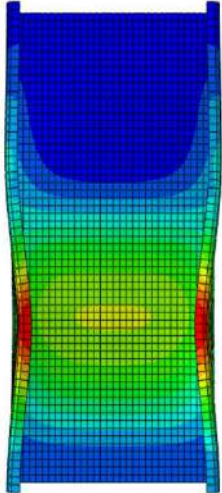
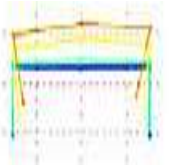

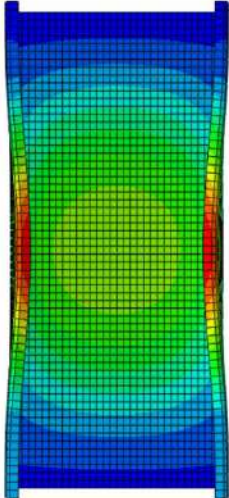
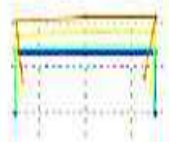

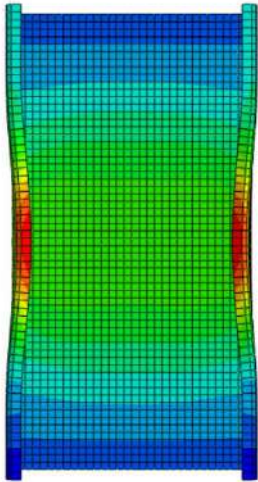
NO.	Loading condition	L =305 mm			L =610 mm			L =1219 mm		
		P _{EXP} (kN)	P _{FEM} (kN)	P _{FEM} / P _{EXP}	P _{EXP} (kN)	P _{FEM} (kN)	P _{FEM} / P _{EXP}	P _{EXP} (kN)	P _{FEM} (kN)	P _{FEM} / P _{EXP}
1	Axial load, Minor axis bending	25.33	24.30	0.96	18.09	18.16	1.00	9.50	11.25	1.18
2		40.81	35.51	0.87	28.25	28.21	1.00	17.59	17.81	1.01
3		51.67	48.82	0.94	43.38	42.21	0.97	25.27	26.09	1.03
4		72.11	65.32	0.91	46.86	49.70	1.06	24.59	28.89	1.17
5		49.29	48.46	0.98	24.99	26.68	1.07	16.01	17.59	1.10
6		26.16	24.89	0.95	16.09	16.23	1.01	10.02	10.60	1.06
7	Major axis bending	54.62	51.07	0.94	57.69	48.14	0.83	48.57	39.22	0.81
8		34.04	31.05	0.91	34.93	31.58	0.90	38.18	34.17	0.89
9		20.56	18.84	0.92	21.43	19.08	0.89	23.44	19.33	0.82
10	Axial load, Biaxial bending	49.25	45.67	0.93	50.10	43.77	0.87	30.34	36.56	1.21
11		21.41	23.80	1.11	22.24	20.90	0.94	18.28	16.96	0.93
12		52.74	53.04	1.01	44.81	44.28	0.99	27.01	32.27	1.19
			Mean	0.95		Mean	0.96		Mean	1.03
			Cov	0.06		Cov	0.08		Cov	0.14

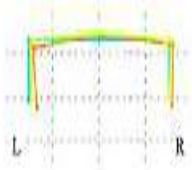

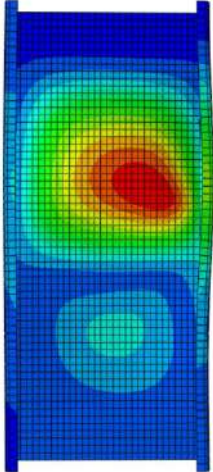
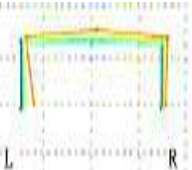

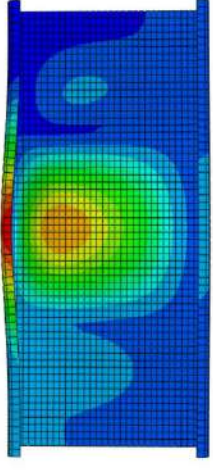
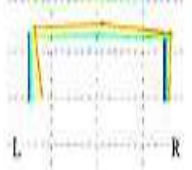

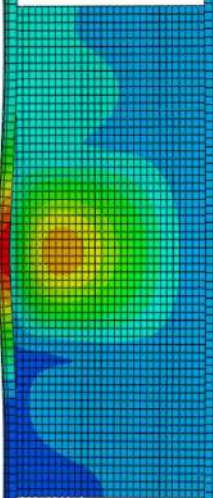
Table 5-8 :- Peak ultimate loads (experimental and FEM results) for experimental study [1].

NO.	Specimen	P _{EXP} (kN)	P _{FEM} (kN)	P _{FEM} / P _{EXP}
1	Z1T1.0	42.10	42.63	1.01
2	Z1T1.5	86.40	80.32	0.93
3	Z1T1.9	129.20	116.32	0.90
4	Z2T1.0	72.20	50.58	0.70
5	Z2T1.5	133.70	134.70	1.01
6	Z2T1.9	205.00	192.85	0.94
			Mean	0.92
			COV	0.12

Table 5-9: - Failure modes from the FEM together with the corresponding tested specimens for short length beam column specimens ($L = 305$ mm).

NO.	Failure mode	Cross-section deformation	Test specimens at the failure load [131]	FEM specimens at the failure load [23]
1	Web-local buckling			
2	Web-local buckling			
3	Web-local buckling			

NO.	Failure mode	Cross-section deformation	Test specimens at the failure load [131]	FEM specimens at the failure load [23]
4	Web-local buckling & flange distortion buckling			
5	Flange distortion buckling			
6	Flange distortion buckling			

NO.	Failure mode	Cross-section deformation	Test specimens at the failure load [131]	FEM specimens at the failure load [23]
7	Web-local buckling & flange distortion buckling			
8	Flange distortion buckling			
9	Flange distortion buckling			

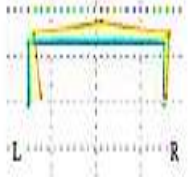

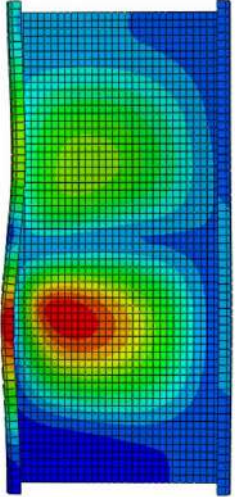
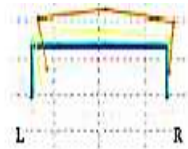

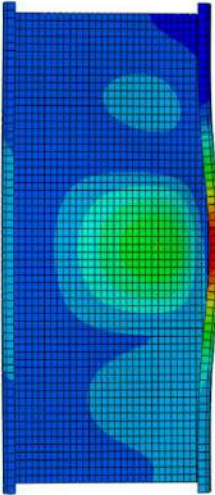
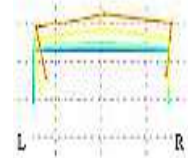

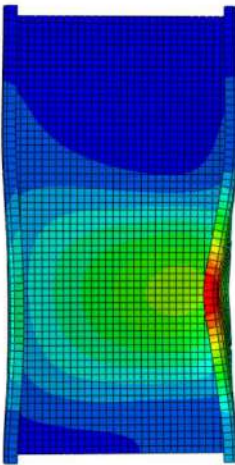
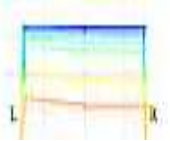

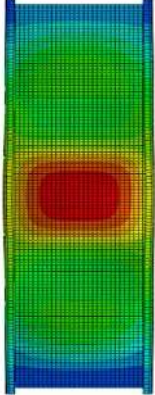
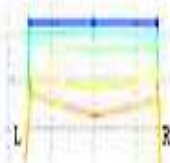

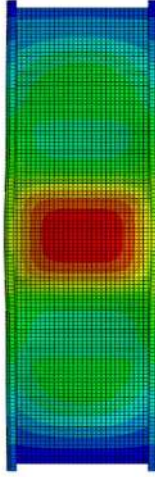
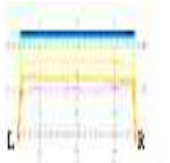

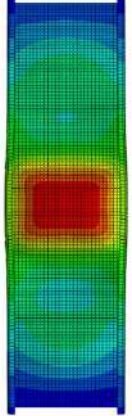
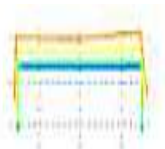

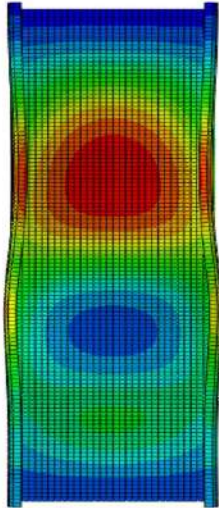
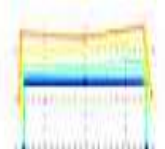

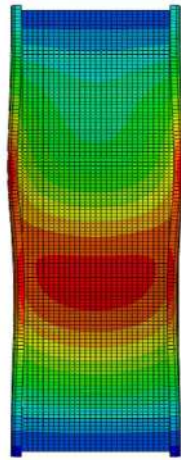


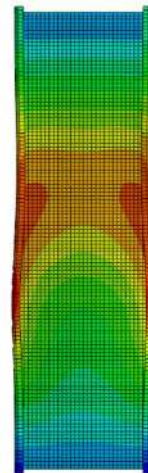
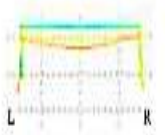

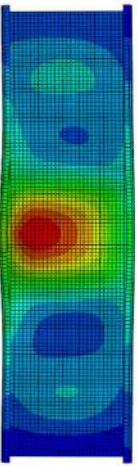
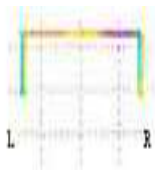

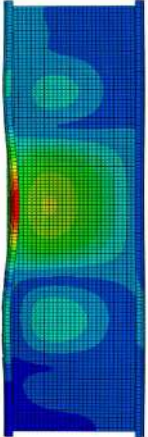
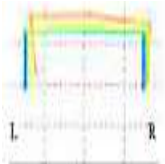

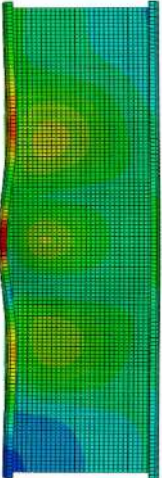
NO.	Failure mode	Cross-section deformation	Test specimens at the failure load [131]	FEM specimens at the failure load [23]
10	Web-local buckling & flange distortion buckling			
11	Flange distortion buckling			
12	Flange distortion buckling			

Table 5-10 :- Failure modes from the FEM together with the corresponding tested specimens for Intermediate length beam column specimens (L = 610 mm).

NO.	Failure mode	Cross-section deformation	Test specimens at the failure load [131]	FEM specimens at the failure load [23]
1	Web-local buckling			
2	Web-local buckling			
3	Web-local buckling			

NO.	Failure mode	Cross-section deformation	Test specimens at the failure load [131]	FEM specimens at the failure load [23]
4	Flange distortion buckling			
5	Flange distortion buckling			
6	Flange distortion buckling			

NO.	Failure mode	Cross-section deformation	Test specimens at the failure load [131]	FEM specimens at the failure load [23]
7	Web-local buckling & flange distortion buckling			
8	Flange distortion buckling			
9	Flange distortion buckling			

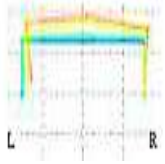

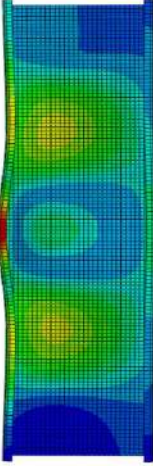
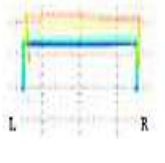

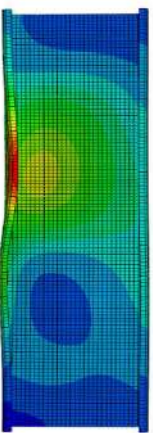
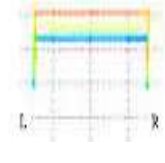

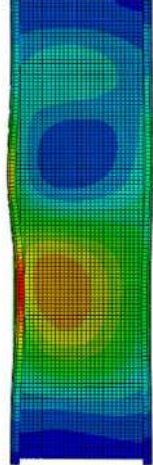
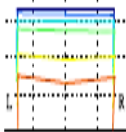


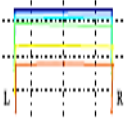

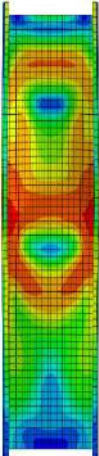
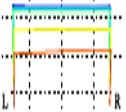

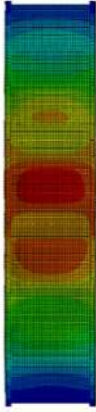
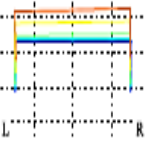


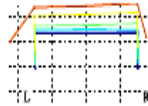


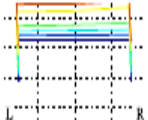


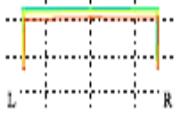


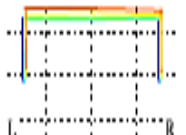


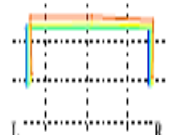

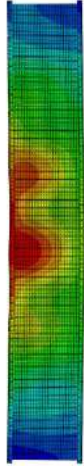
NO.	Failure mode	Cross-section deformation	Test specimens at the failure load [131]	FEM specimens at the failure load [23]
10	Web-local buckling & flange distortion buckling			
11	Flange distortion buckling			
12	Flange distortion buckling			

Table 5-11: - Failure modes from the FEM together with the corresponding tested specimens for long length beam column specimens (L =1219 mm).

NO.	Failure mode	Cross-section deformation	Test specimens at the failure load [131]	FEM specimens at the failure load [23]
1	Web-local buckling			
2	Web-local buckling			
3	Web-local buckling			

NO.	Failure mode	Cross-section deformation	Test specimens at the failure load [131]	FEM specimens at the failure load [23]
4	Flange distortion buckling			
5	Flange distortion buckling			
6	Flange distortion buckling			

NO.	Failure mode	Cross-section deformation	Test specimens at the failure load [131]	FEM specimens at the failure load [23]
7	Web-local buckling & flange distortion buckling			
8	Flange distortion buckling			
9	Flange distortion buckling			

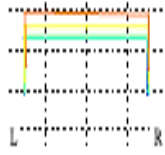

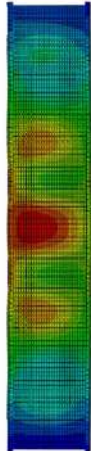
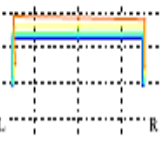

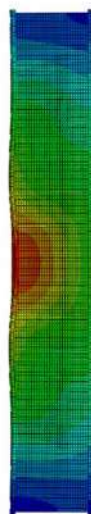
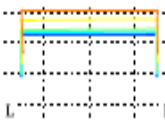



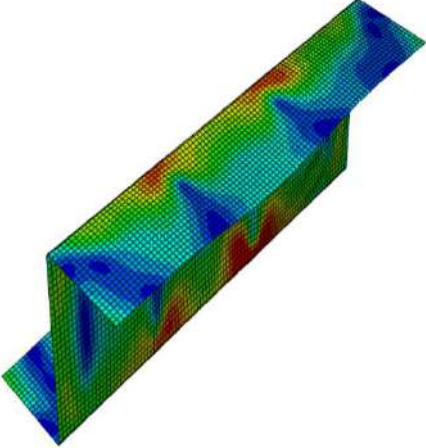

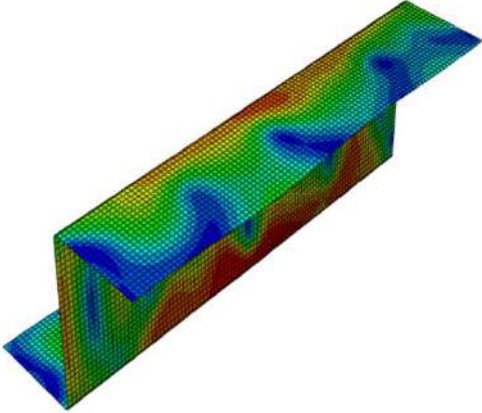

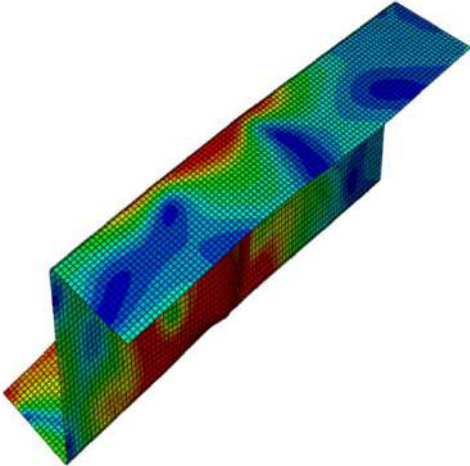
NO.	Failure mode	Cross-section deformation	Test specimens at the failure load [131]	FEM specimens at the failure load [23]
10	Flange distortion buckling			
11	Flange distortion buckling			
12	Flange distortion buckling			

Table 5-12 :- Failure modes from the FEM for specimens in [1].

NO.	Specimens	Failure mode	Cross-section deformation	FEM failure modes
1	Z1T1.0	Local buckling		
2	Z1T1.5	Local buckling		
3	Z1T1.9	Local buckling		


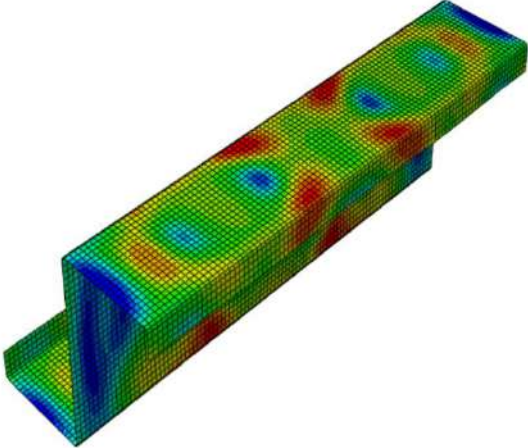

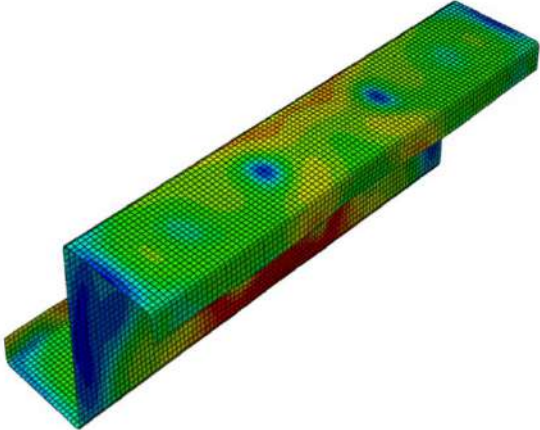
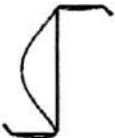
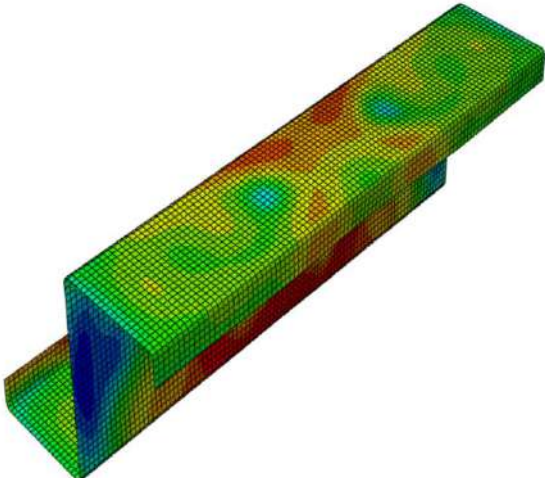
NO.	Specimens	Failure mode	Cross-section deformation	FEM failure modes
4	Z2T1.0	Local buckling & Distorsion buckling		
5	Z2T1.5	Local buckling & Distorsion buckling		
6	Z2T1.9	Local buckling		

Table 5-13:- Load displacement curves from the FEM together with the corresponding tested specimens [131] for short length beam column specimens (L = 305 mm).

Specimen NO.	Load displacement curves from the FEM together with the tested specimens (L = 305 mm) [131]
1	
2	
3	

Specimen NO.	Load displacement curves from the FEM together with the tested specimens (L = 305 mm) [131]
4	
5	
6	

Specimen NO.	Load displacement curves from the FEM together with the tested specimens (L = 305 mm) [131]
7	
8	
9	

Specimen NO.	Load displacement curves from the FEM together with the tested specimens (L = 305 mm) [131]
10	<p>load (kN)</p> <p>displacement (mm)</p> <p>— FEM</p> <p>— Test</p>
11	<p>load (kN)</p> <p>displacement (mm)</p> <p>— FEM</p> <p>— Test</p>
12	<p>load (kN)</p> <p>displacement (mm)</p> <p>— FEM</p> <p>— Test</p>

Table 5-14:- Load displacement curves from the FEM together with the corresponding tested specimens [131] for intermediate length beam column specimens (L = 610 mm).

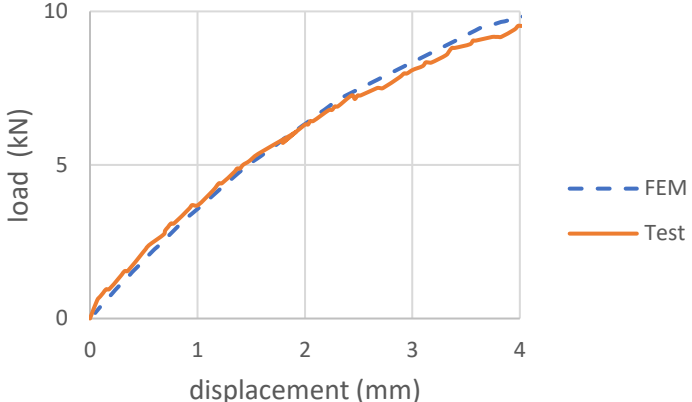
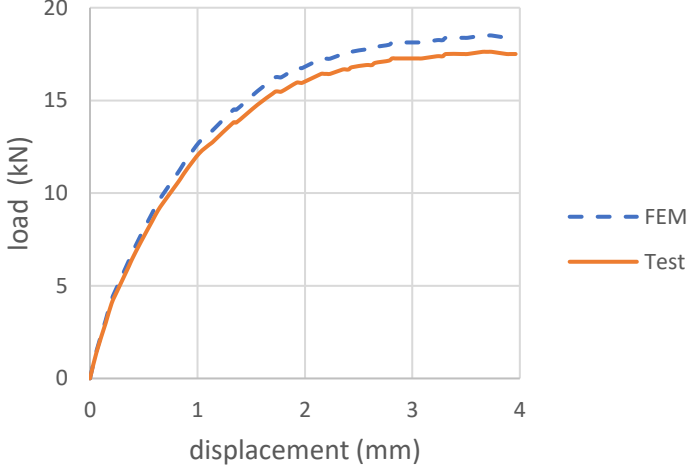
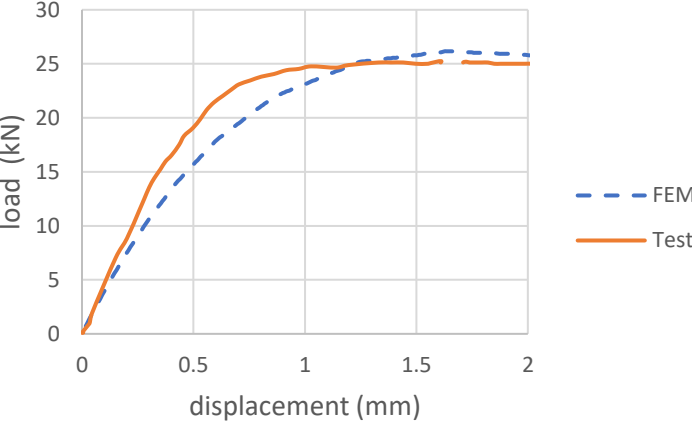
Specimen NO.	Load displacement curves from the FEM together with the tested specimens (L = 610 mm) [131]
1	
2	
3	

Specimen NO.	Load displacement curves from the FEM together with the tested specimens (L = 610 mm) [131]
4	
5	
6	

Specimen NO.	Load displacement curves from the FEM together with the tested specimens (L = 610 mm) [131]
7	<p>load (kN)</p> <p>displacement (mm)</p> <p>--- FEM</p> <p>— Test</p>
8	<p>load (kN)</p> <p>displacement (mm)</p> <p>--- FEM</p> <p>— Test</p>
9	<p>load (kN)</p> <p>displacement (mm)</p> <p>--- FEM</p> <p>— Test</p>

Specimen NO.	Load displacement curves from the FEM together with the tested specimens (L = 610 mm) [131]
10	
11	
12	

Table 5-15:- Load displacement curves from the FEM together with the corresponding tested specimens [131] for long length beam column specimens (L = 1219 mm).

Specimen NO.	Load displacement curves from the FEM together with the tested specimens (L = 1219 mm) [131]
1	
2	
3	

Specimen NO.	Load displacement curves from the FEM together with the tested specimens (L = 1219 mm) [131]
4	
5	
6	

Specimen NO.	Load displacement curves from the FEM together with the tested specimens (L = 1219 mm) [131]
7	<p>Load displacement curve for Specimen 7. The x-axis is displacement (mm) from 0 to 1.5, and the y-axis is load (kN) from 0 to 60. The FEM curve (dashed blue) shows a linear increase to about 38 kN at 1.2 mm, then levels off. The Test curve (solid orange) follows the FEM curve until about 0.8 mm, then continues to rise to about 48 kN at 1.4 mm.</p>
8	<p>Load displacement curve for Specimen 8. The x-axis is displacement (mm) from 0 to 3, and the y-axis is load (kN) from 0 to 40. The FEM curve (dashed blue) rises linearly to a peak of about 34 kN at 1.5 mm, then drops to about 12 kN at 2.5 mm. The Test curve (solid orange) follows the FEM curve until about 1.2 mm, peaks at about 38 kN at 1.5 mm, and then drops to about 14 kN at 2.5 mm.</p>
9	<p>Load displacement curve for Specimen 9. The x-axis is displacement (mm) from 0 to 3, and the y-axis is load (kN) from 0 to 25. The FEM curve (dashed blue) rises linearly to about 19 kN at 3 mm. The Test curve (solid orange) follows the FEM curve until about 2.5 mm, then rises to about 22 kN at 3 mm.</p>

Specimen NO.	Load displacement curves from the FEM together with the tested specimens (L = 1219 mm) [131]
10	
11	
12	

Table 5-16:- Load displacement curves from the FEM together with the corresponding tested specimens in [1].

Specimen NO.	Load displacement curves from the FEM together with the tested specimens [1]
<p style="text-align: center;">Z1T1.0</p>	
<p style="text-align: center;">Z1T1.5</p>	
<p style="text-align: center;">Z1T1.9</p>	

Specimen NO.	Load displacement curves from the FEM together with the tested specimens [1]
Z2T1.0	<p>Load displacement curve for specimen Z2T1.0. The graph plots load (kN) on the y-axis (0 to 80) against displacement (mm) on the x-axis (0 to 0.4). Two curves are shown: FEM (dashed blue line) and Test (solid orange line). Both curves show a non-linear increasing trend, with the test curve slightly higher than the FEM curve.</p>
Z2T1.5	<p>Load displacement curve for specimen Z2T1.5. The graph plots load (kN) on the y-axis (0 to 160) against displacement (mm) on the x-axis (0 to 1.5). Two curves are shown: FEM (dashed blue line) and Test (solid orange line). Both curves show a non-linear increasing trend up to a peak load of approximately 135 kN at 1.0 mm displacement, followed by a decrease.</p>
Z2T1.9	<p>Load displacement curve for specimen Z2T1.9. The graph plots load (kN) on the y-axis (0 to 250) against displacement (mm) on the x-axis (0 to 1.0). Two curves are shown: FEM (dashed blue line) and Test (solid orange line). Both curves show a non-linear increasing trend, with the test curve slightly lower than the FEM curve.</p>

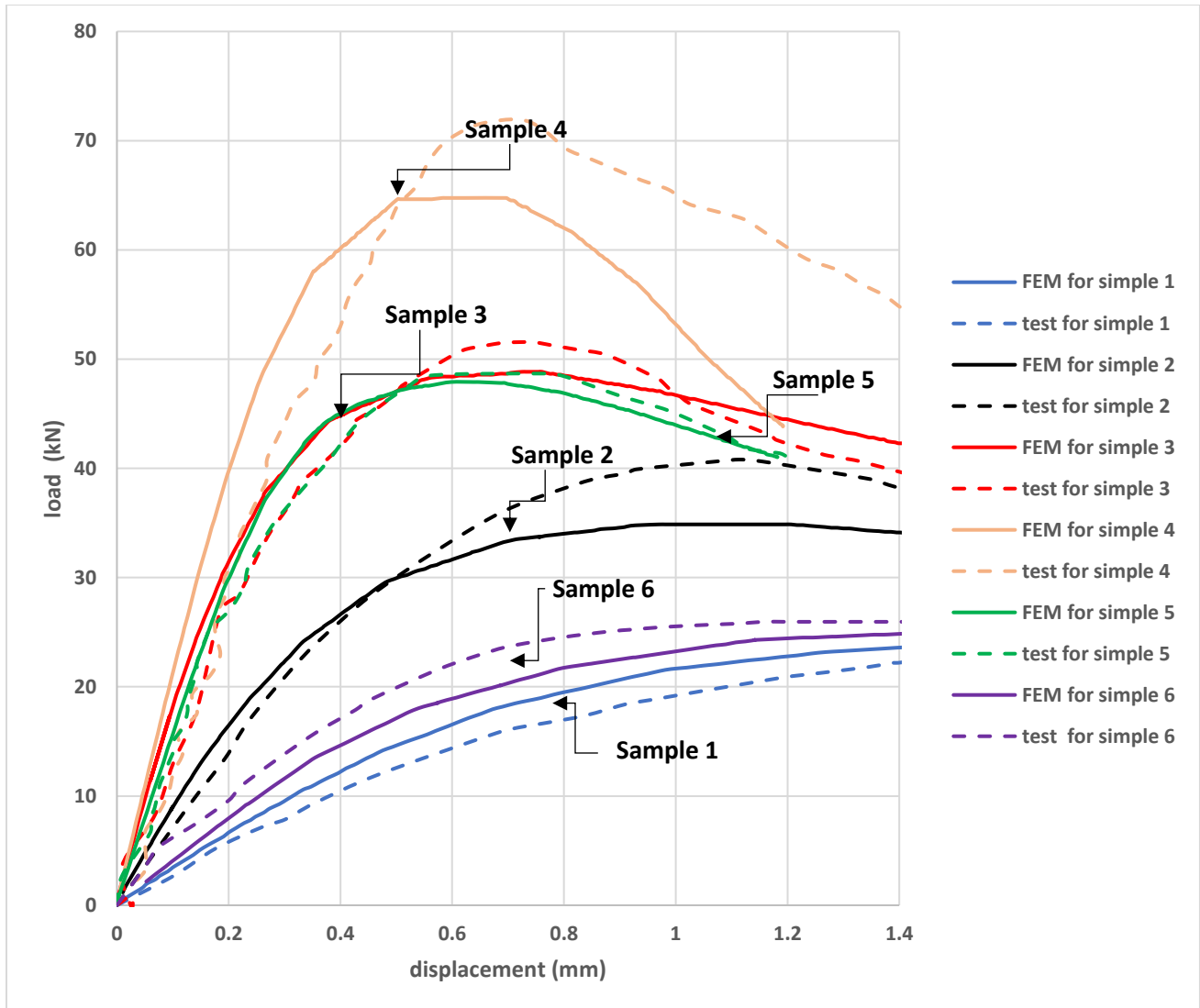


Figure 5.12 :- load displacement curves from the FEM together with the corresponding tested specimens [131] for short length beam column specimens ($L = 305$ mm) from sample 1 to 6.

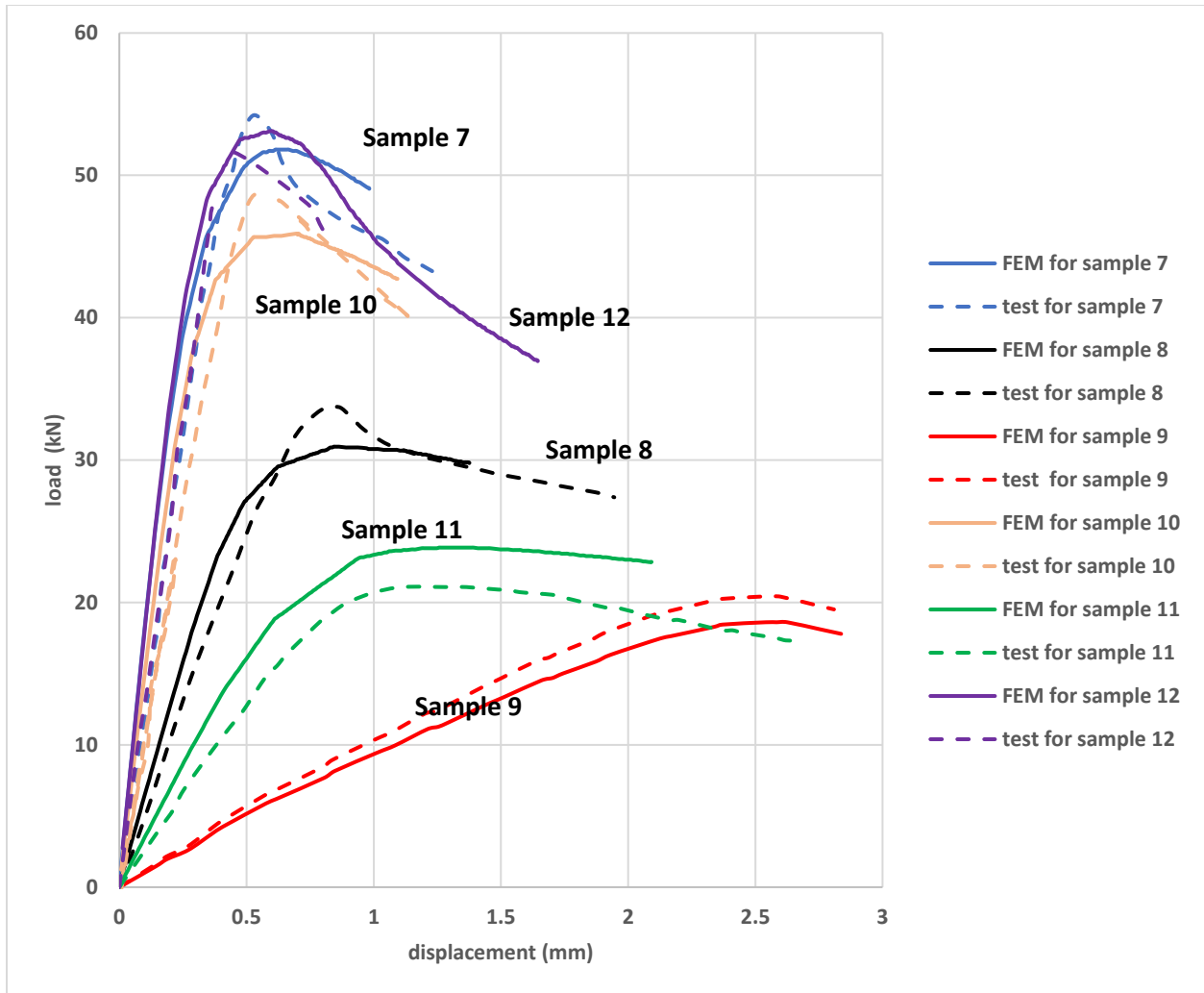


Figure 5.13 :- load displacement curves from the FEM together with the corresponding tested specimens [131] for short length beam column specimens ($L = 305$ mm) from sample 7 to 12.

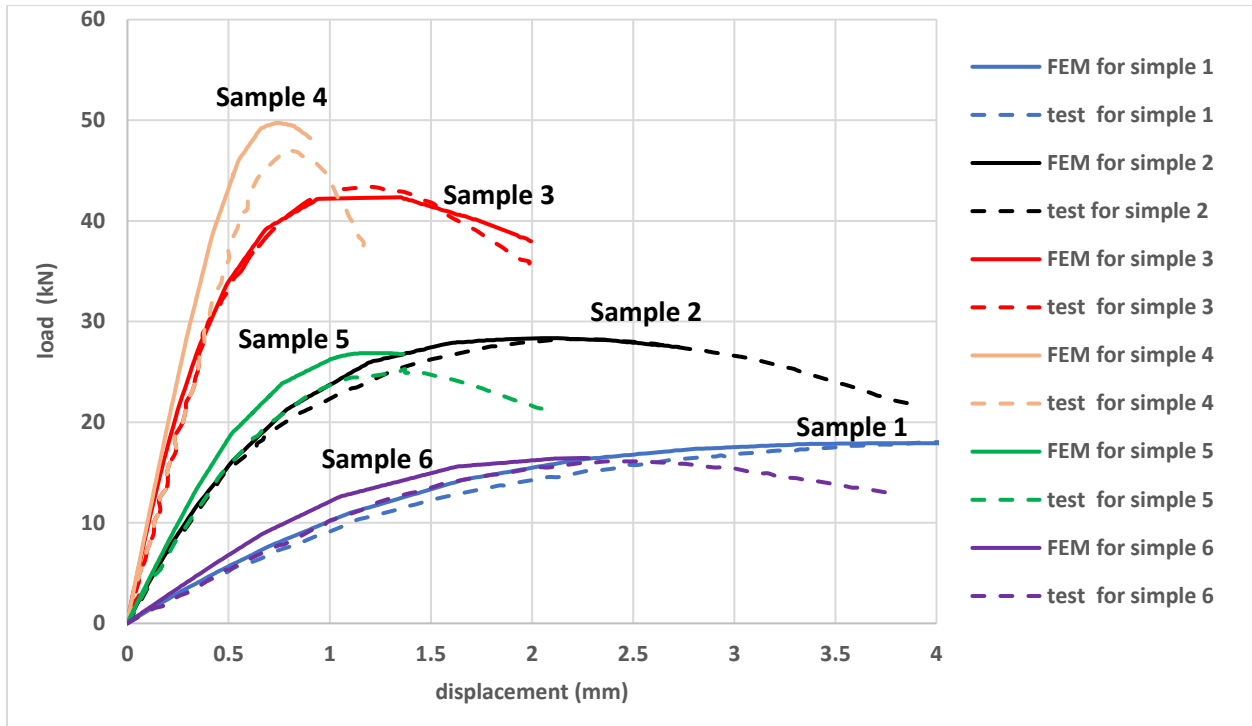


Figure 5.14 :- load displacement curves from the FEM together with the corresponding tested specimens [131] for intermediate length beam column specimens (L =610 mm) for sample 1 to 6.

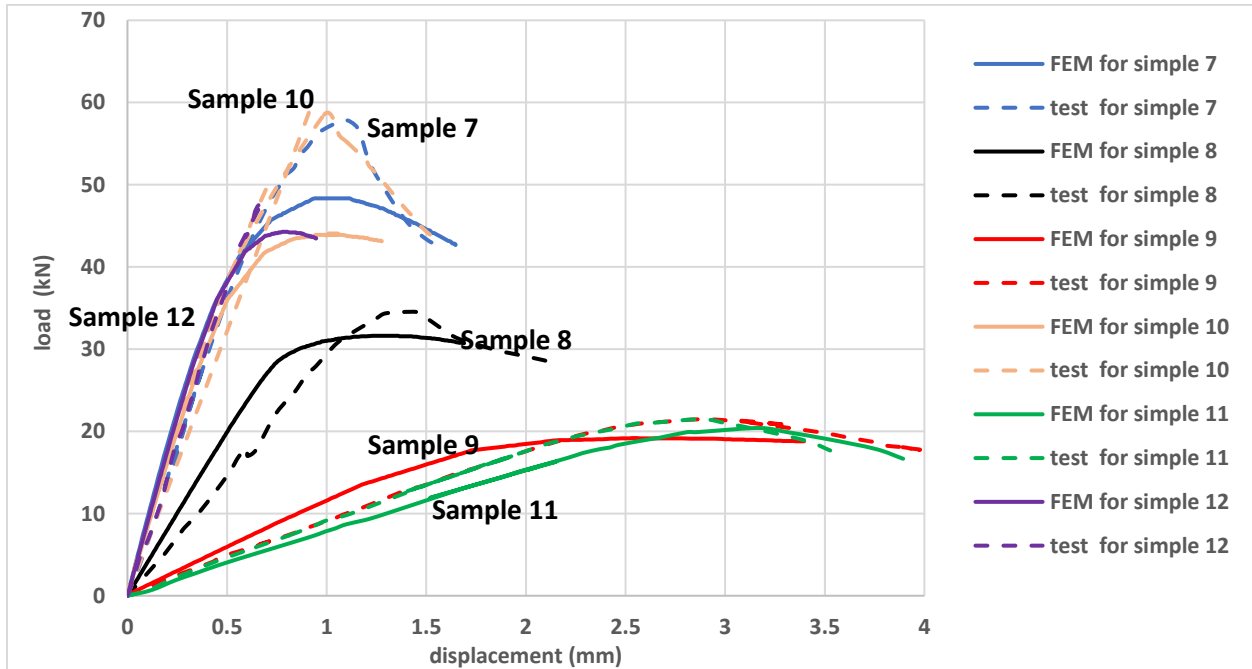


Figure 5.15 :- load displacement curves from the FEM together with the corresponding tested specimens [131] for intermediate length beam column specimens (L =610 mm) for sample 7 to 12.

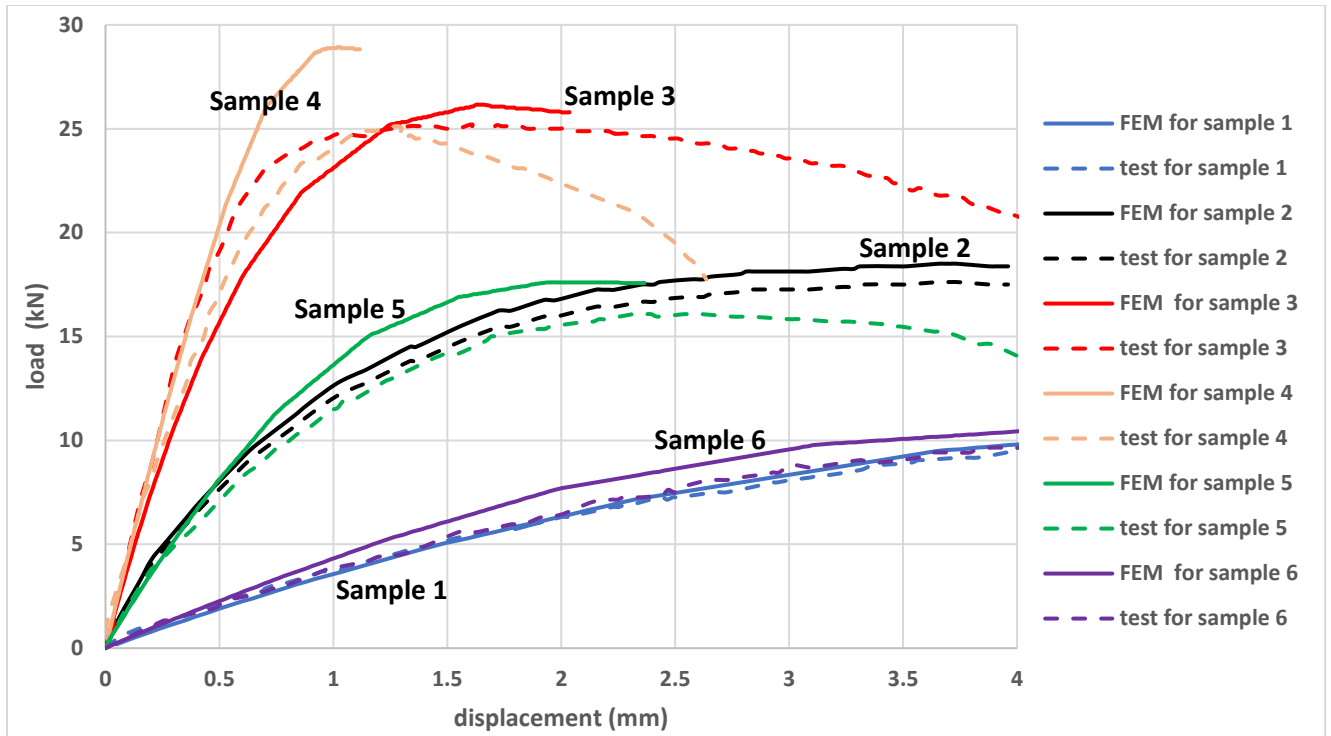


Figure 5.16 :- load displacement curves from the FEM together with the corresponding tested specimens [131] for long length beam column specimens (L = 1219 mm) for sample 1 to 6.

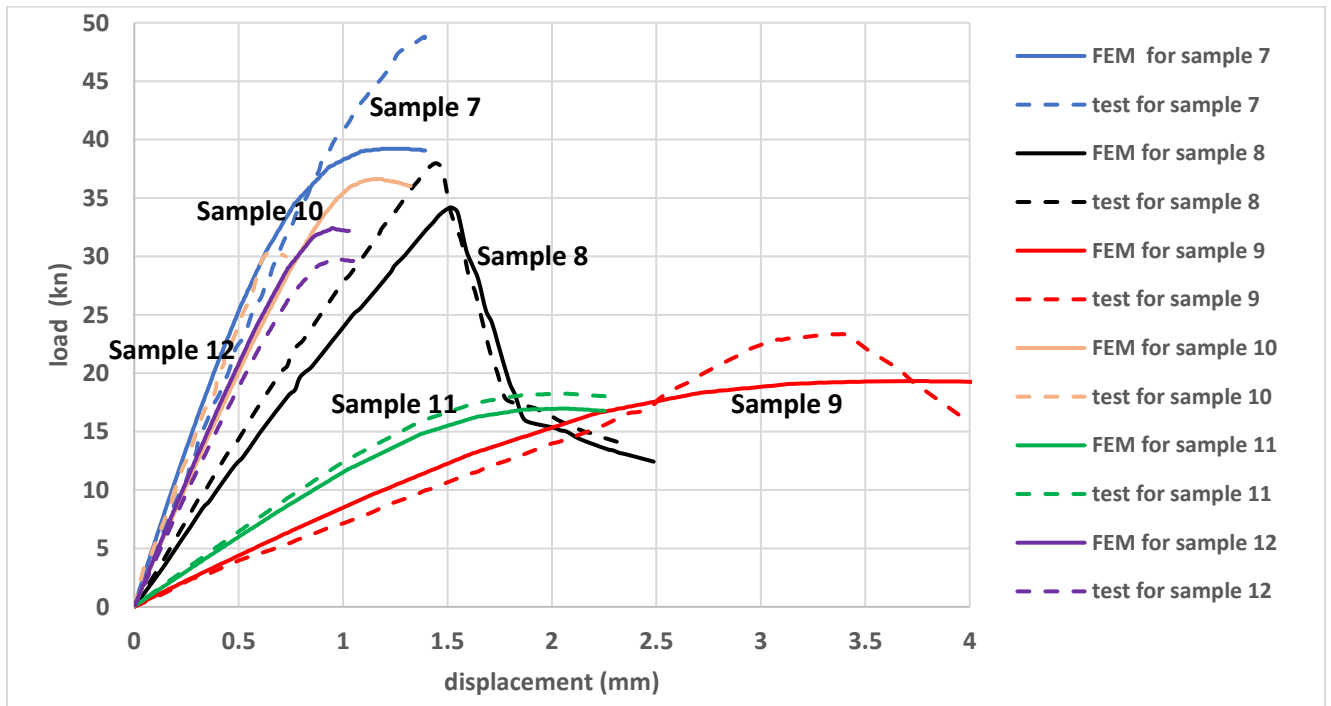


Figure 5.17 :- load displacement curves from the FEM together with the corresponding tested specimens [131] for long length beam column specimens (L = 1219 mm) for sample 7 to 12.

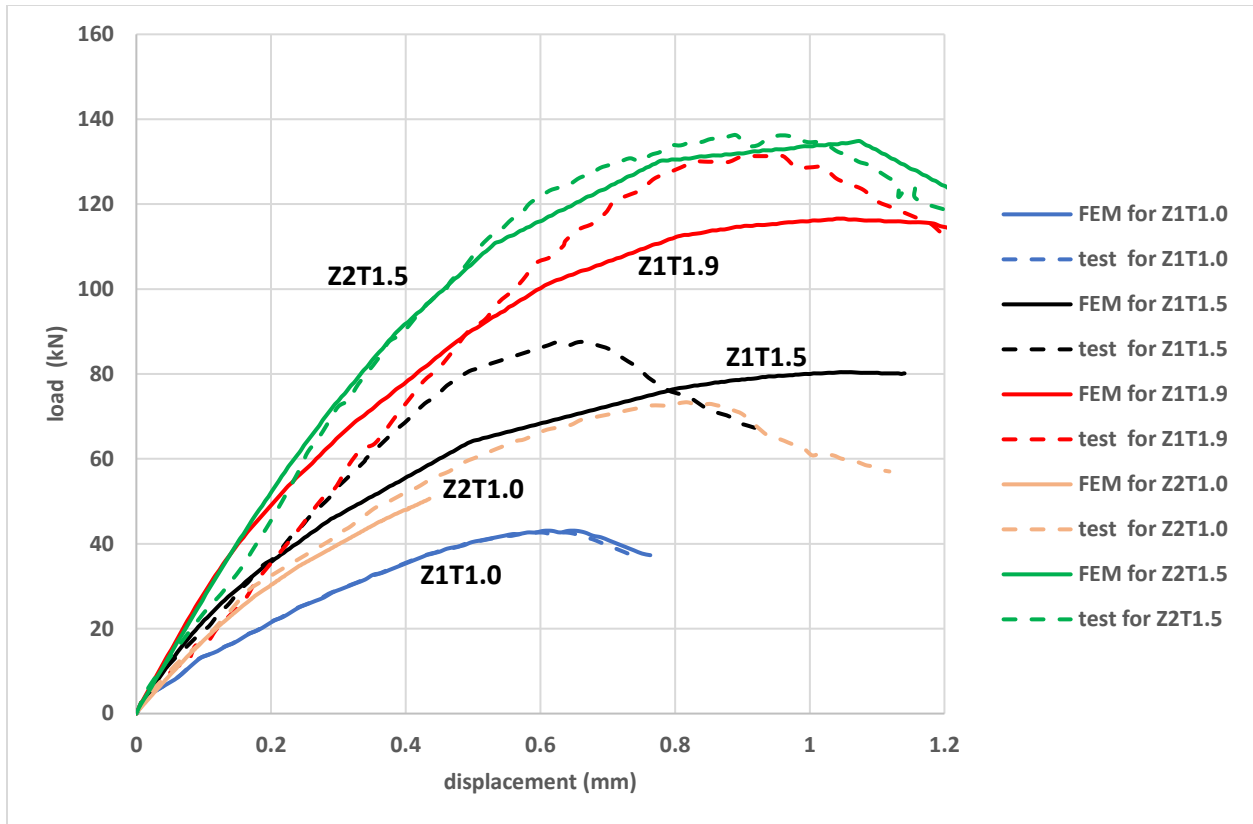


Figure 5.18 :- load displacement curves from the FEM together with the corresponding tested specimens used Z1 & Z2) [1].

CHAPTER (6)

PARAMETRIC STUDY

6.1 INTRODUCTION

Parametric research was conducted as an extension to the current investigation. The primary goal of this study was to investigate the strength of the CFS sections. As a result, the goal of this parametric study was to collect more data points from which to make conclusions and suggestions about the behavior of the CFS sections. This chapter generates further data by conducting parametric tests to study the many variables that impact the strength of CFS sections. Additionally, this section provides a comparison between the EWM and the DSM, which are two different methods for designing CFS sections. As an example of the EWM, the North American Specification (AISI) [21], Eurocode-3_part1.3 (EC3) [22], and the Egyptian Code of Practice (ECP) [20] have been utilized. On the other hand, Appendix 1 in the North American Specification (AISI) [21] is utilized as an example of the DSM.

In recent years, many researchers have increasingly used FE modeling as a cost-effective and time-saving alternative to experimental programs. Additionally, FE modeling has an advantage over analytical models, particularly in simulating the behavior of CFS sections. FE models can accurately solve complex interactive buckling of CFS elements, including important governing parameters such as geometrical imperfections, material nonlinearity, post-buckling behavior, etc. These parameters are often difficult to simulate using analytical methods, as pointed out by Haidarali and Nethercot [146].

Based on the factors explained in the preceding paragraph, it was determined that the validated finite element model (FEM) presented in Chapter 4 was utilized in this parametric study.

6.2 PARAMETRIC STUDIES OF DIFFERENT CFS ELEMENTS

Parametric studies on the ultimate CFS capacities were conducted for the channel and Z-section profiles using the verified FEM, as discussed in the previous section. The investigated parameters include the member length-to-web plate length ratio (L/h), plate slenderness ratio, lip-to-flange plate length ratio (d/b), web-to-flange plate length ratio (h/b) and yielding stress (F_y) on the ultimate axial load and bending moment capacities of different CFS members. The channel and Z-section profiles were studied with the same dimensions to determine the effect of the cross-section profile on the load capacity. This parametric study included 32 different CFS cross-sections.

Table 6-1 and **Figure 6.1** provide the details of the cross-sectional dimensions used in the parametric studies. **Table 6-2** lists the parameters used in this study. **Appendix A** shows details about the FEM results for this parametric study.

Five values of steel yielding strength (F_y) were used in this study; 240, 280, 320, 360 and 400 MPa, as recommended by European codes for cold rolled flat products made of high strength micro-alloyed steels for cold forming. The material defined in Abaqus during the study of different parameters, except for yielding stress (F_y) parameter, has yield strength (F_y) and ultimate strength (F_u) of 360 MPa and 400 MPa, respectively. The Young's modulus (E_0) and Poisson's ratio (ν) are 210 GPa and 0.3, respectively.

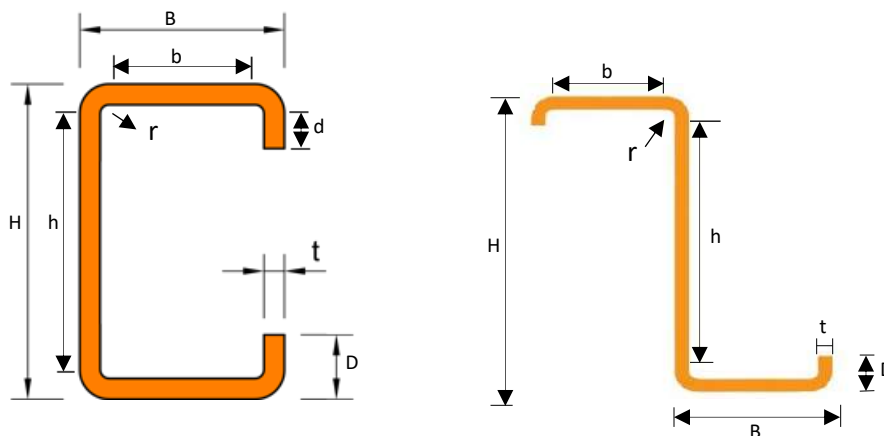


Figure 6.1: - Type of sections used in this study.

Table 6-1: - CFS sections used in this research.

Type	Dimension (mm)					Type	Dimension (mm)				
	H	B	D	t	r		H	B	D	t	r
Compression members	100	50	20	2	8	Flexural members	200	100	40	2	8
	200	100	40	2	8		100	50	20	2	8
	300	150	60	2	8		300	150	60	2	8
	400	200	80	2	8		400	200	80	2	8
	500	250	100	2	8		500	250	100	2	8
	600	300	120	2	8		600	300	120	2	8
	100	100	40	2	3		300	100	40	2	8
	100	33.33	13.33	2	3		400	100	40	2	8
	100	25	10	2	3		500	100	40	2	8
	100	20	8	2	3		600	100	40	2	8
	100	50	12.5	2	8		200	100	20	2	8
	100	50	15	2	8		200	100	30	2	8
	100	50	25	2	8		200	100	50	2	8
	100	50	30	2	8		200	100	60	2	8
	100	50	35	2	8		200	100	70	2	8
	100	50	40	2	8		200	100	80	2	8

Table 6-2: - Different parameters used in this study.

	Parameters used for CFS different frame elements	
	Compression member	Flexural member
The length-to-web plate depth ratio (L/h)	1, 2, 3, 4, 5, 6, 7, 8, 9, 10, 11 & 12	
The web plate slenderness ratio (h/t)	50, 100, 150, 200, 250 & 300	100
The flange plate slenderness ratio (b/t)	25	25, 50, 75, 100, 125 & 150
The lip-to-flange plates length ratio (d/b)	.2, .3, .4, .5, .6, .7 & .8	
The web-to-flange plate length ratio (h/b)	2, 3, 4, 5 & 6	
Yielding stress (F _y) (MPa)	240, 280, 320, 360 & 400	

6.2.1 Effect of Length-to-Web Plate Depth Ratio (L/h) Parameter

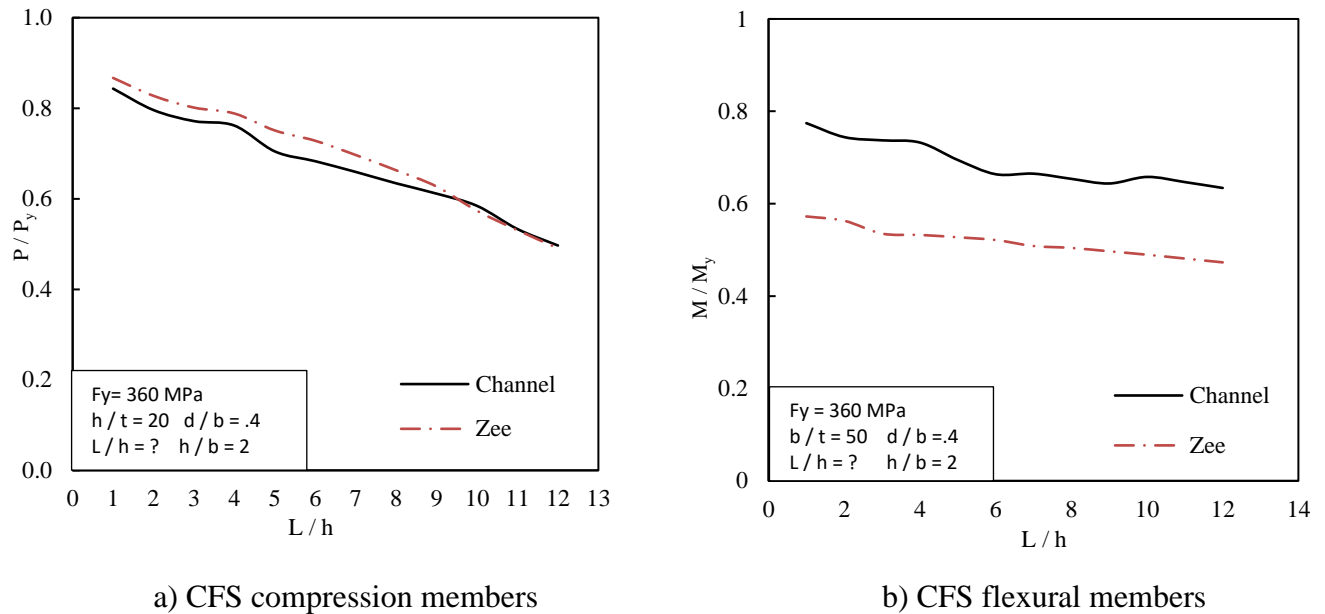


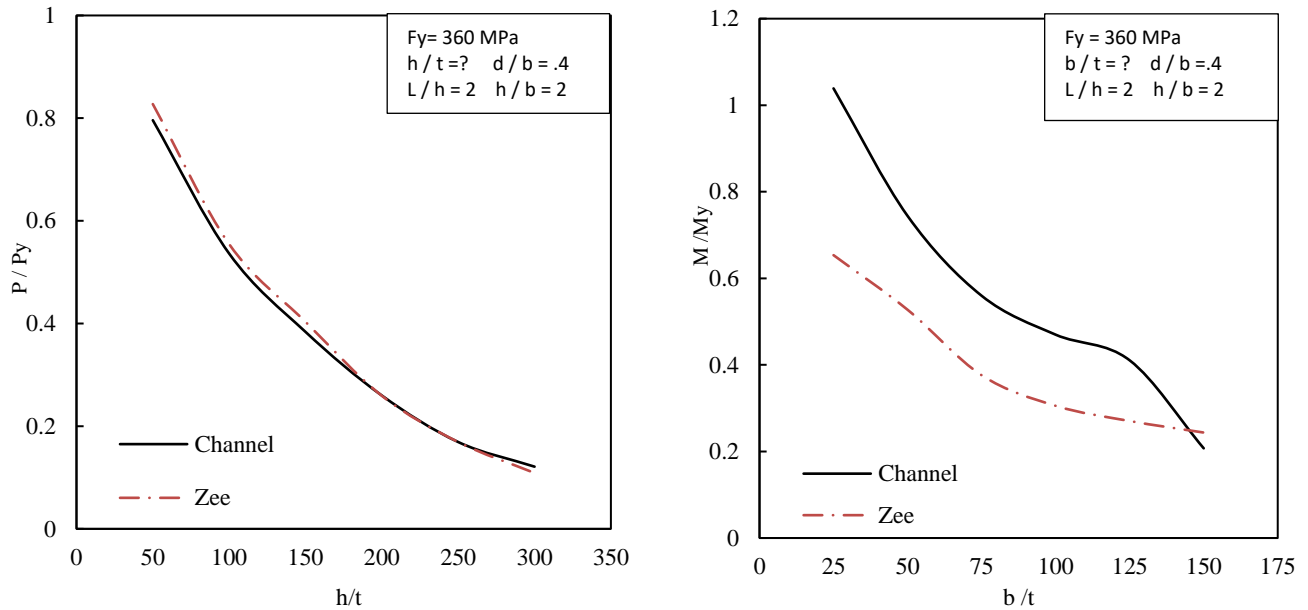
Figure 6.2: - Effect of length-to-web plate depth ratio (L/h) on different frame elements.

Figure 6.2 (a) presents evidence of an inverse relationship between the compressive capacity of the CFS sections and the length-to-web plate depth ratio (L/h). This trend is attributed to the heightened frequency of global buckling as L/h increases. Additionally, it is worth noting that, with increasing length, the axial load capacity of both the channel and Z-sections becomes more similar. This convergence is primarily due to the heightened impact of flexural buckling, which is exclusively dependent on length, given the constant nature of the cross-sectional dimensions and moment of inertia about the minor axis. Consequently, the effects of torsion and distortional buckling diminish, leading to a reduced reliance on shape and symmetry until the axial strengths become perfectly matched at large lengths.

From the observation of **Figure 6.2 (b)**, it is apparent that an inverse correlation exists between the flexural capacity of the CFS sections and the length-to-web plate depth ratio (L/h) owing to the amplified occurrence of lateral torsional buckling. Furthermore, it was demonstrated that as the length increased, the distinction between the flexural load capacity values of each channel and the Z-section remained relatively invariable. This phenomenon occurs because lateral

torsional buckling is solely dependent on the shape and symmetry of the cross-section at a specific length, and the constant value of the cross-sectional dimensions ensures that the shape and symmetry remain constant during the L/h parameter evaluation.

6.2.2 Effect of Plate Slenderness Ratio



a) Effect of the h/t ratio on CFS compression members. b) Effect of the b/t ratio on CFS flexural members

Figure 6.3: - Effect of plate slenderness ratio on different frame elements.

The investigation of critical plate slenderness ratios led to the selection of the web plate slenderness ratio (h/t) in the compression member and the flange plate slenderness ratio (b/t) in the flexural member, as these ratios control the buckling failure mode. It is worth noting that an increase in the h/t ratio resulted in a decrease in the CFS compressive capacity, as illustrated in **Figure 6.3 (a)**. This is because an increase in h/t leads to a higher incidence of web local buckling, which in turn causes weakness and a decline in the CFS compressive capacity. Furthermore, it was observed that the channel and Z-cross-section profiles of the same dimensions exhibited similar compressive capacities, coinciding with the increase in h/t resulting from the amplified effect of local buckling.

The graphical representation shown in **Figure 6.3 (b)** reveals a discernible inverse correlation between the flexural capacity of CFS and the slenderness ratio of the flange plates (b/t).

This is because an elevation in the value of b/t leads to a heightened occurrence of local buckling in the flange, consequently leading to debilitation and attenuation of the CFS flexural capacity. The difference between the flexural capacities of the channel and Z-cross-section profiles decreases with an increase in b/t , owing to the increased effect of local buckling.

6.2.3 Effect of Lip-to-Flange Plates Length Ratio (d/b) Parameter

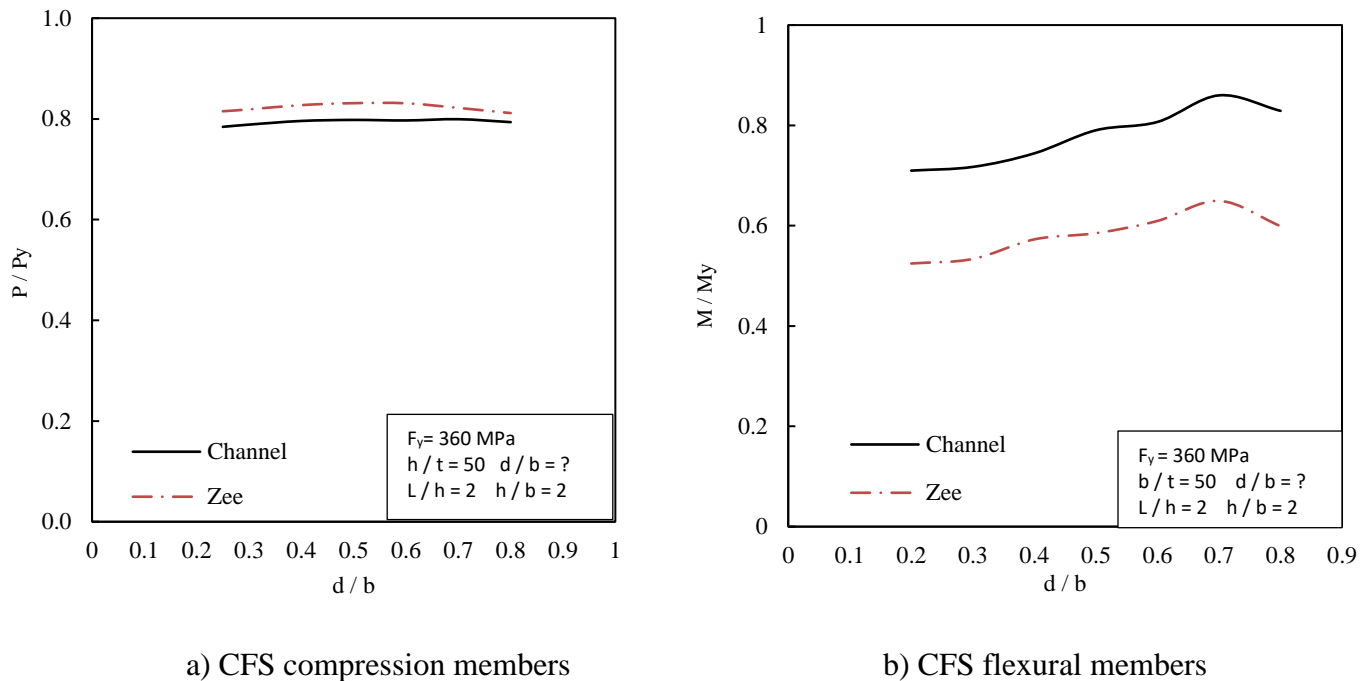


Figure 6.4: - Effect of lip to flange plates length ratio (d/b) on different frame elements.

There is a slight change in the compressive strength of the CFS when changing the lip-to-flange plate length ratio (d/b). This is because the compression members are exposed to local buckling, which critically occurs in the web due to its higher slenderness ratio in comparison to the lip and flange. Furthermore, all the samples studied in this parameter have a constant web plate slenderness ratio (h/t). Additionally, increasing the lip-to-flange plate length ratio causes the flange stiffness to increase; however, this does not affect the web local buckling, as shown in **Figure 6.4 (a)**.

A direct correlation exists between the flexural capacity of CFS and the ratio of the length between the lip and flange plates (d/b). As the aforementioned ratio increased, the stiffness

of the flange was augmented, thereby enhancing the sectional strength of the flexural members in situations where flange local buckling was encountered, as illustrated in **Figure 6.4 (b)**.

6.2.4 Effect of Web-to-Flange Plate Length Ratio (h/b) Parameter

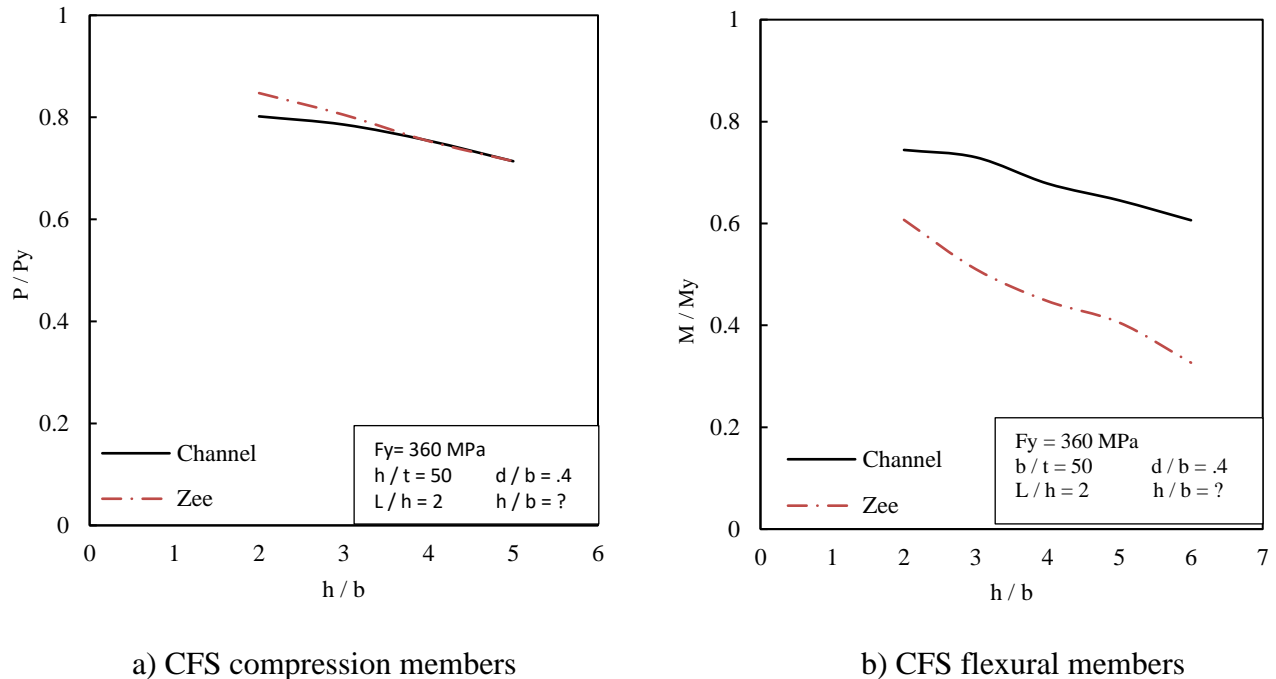


Figure 6.5: - Effect of web-to-flange plate length ratio (h/b) on different frame elements.

Observing **Figure 6.5**, it can be noted that an inverse correlation exists between the capacity of the CFS sections and the web-to-flange plate length ratio (h/b). This is because an increase in h/b leads to a weaker connection between the flange and the web, consequently increasing the likelihood of distortional buckling. Additionally, it is noteworthy that the rate of decrease in the Z-section is significantly higher than that of the channel section. This can be attributed to the higher warping torsional constant (C_w) of the Z-section, which measures the structural member's resistance to non-uniform or warping torsion. As previously demonstrated, this renders the Z-sections more susceptible to collapse resulting from torsional and flexural torsional deformations.

The Channel and Z-section profiles, of identical dimensions, exhibit similar compressive capacities. In addition, their respective capacities align with the increase in h/b due to the increased influence of the web local buckling; this is indicated in **Figure 6.5 (a)**.

The difference between the values of the flexural capacities of each channel and Z-section increases with increasing (h/b) because the greater the value of h/b, the more twisting and bending occur, the more the difference between the Z and channel warping constants happens, and the more we get the difference between their lateral torsional resistance, as illustrated in **Figure 6.5 (b)**.

6.2.5 Yielding Stress (F_y) Parameter

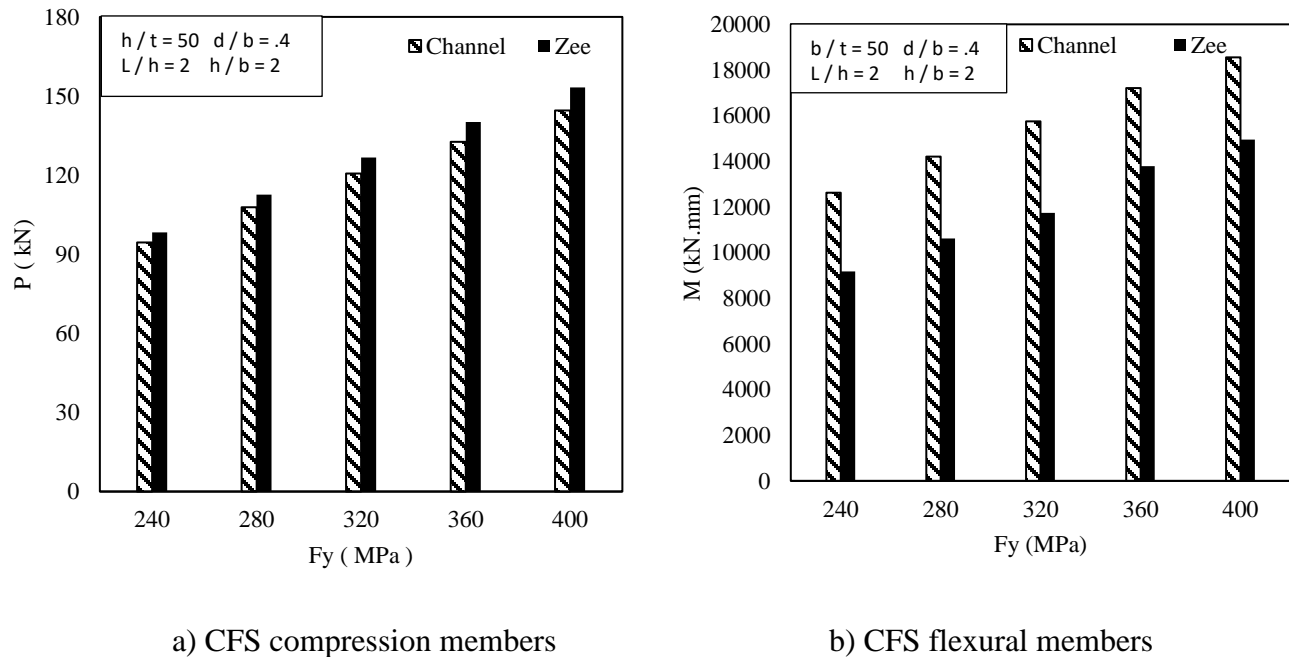


Figure 6.6: - Effect of Yielding stress (F_y) on different frame elements.

As expected, there exists a positive correlation between steel yield stress (F_y) and the CFS capacities of various frame elements, owing to material enhancements, as shown in **Figure 6.6**.

Figures 6.2 to 6.6 indicate that the channel provides lower compressive capacities than Z-sections of the same dimensions and loading conditions because the channel section has a higher value of moment of inertia (I) about its minor local axis than the Z-section, and by dependency, the channel section has a higher value of radius of gyration ($r = \sqrt{\frac{I}{\text{area}}}$) than the Z-section and that the radius of gyration is inversely proportional to the sectional slenderness ratio ($\lambda = L/r$); therefore, we find that the channel slenderness ratio is less than that of the Z-section, and there is an inverse relationship between the compressive capacity and the sectional slenderness ratio (λ). For instance,

the initial compression member sample with a channel profile has $I_y=175660.14 \text{ mm}^3$, $r = 19.46 \text{ mm}$, $\lambda = 10.28$, and its compressive capacity (P_{FEM}) is 128.4 kN. In contrast, if it possesses a Z-profile, the values of I_v , r , λ , and P_{FEM} are 955088.4 mm^3 , 45.37 mm , 13.22 , and 135.7 kN , respectively.

Additionally, **Figures 6.2 to 6.6** also indicate that when considering the same dimensions and loading conditions, channel sections exhibit greater flexural capacities than Z-sections. This is because Z-sections tend to buckle laterally at lower strengths than channel sections, which can be attributed to the lower value of the warping torsional constant (C_w) in channel sections; this is because when a channel section flexural member undergoes lateral torsional buckling, it twists and bends in the weaker direction. Conversely, the Z-section flexural member experiences both twisting and bending, not only in the weaker direction but also in the stronger direction due to the coupling effect between the two directions [13], and For instance, in our investigation, the initial flexural member specimen possessing a channel profile exhibited a C_w value of 15.76 m^6 alongside a flexural capacity (M_{FEM}) of 5405.13 kN.mm . Conversely, the same specimen with a Z-profile demonstrated a C_w value of 18.92 m^6 and a M_{FEM} of 3394.38 kN.mm .

6.3 COMPARISON BETWEEN EFFECTIVE WIDTH AND DIRECT STRENGTH METHODS

This section provides a comparison between the EWM and the DSM, which are two different methods for designing CFS sections. As an example of the EWM, the North American Specification (AISI) [21], Eurocode-3_part1.3 (EC3) [22], and the Egyptian Code of Practice (ECP) [20] have been utilized. On the other hand, Appendix 1 in the North American Specification (AISI) [21] is utilized as an example of the DSM.

It was determined that the EWM and DSM, which are utilized in various codes, will be compared against the validated FEM in various member lengths. To accomplish this, a total of 20 randomly selected sections from diverse CFS sections tables were included, in addition to the sections used in the preceding sections of the parametric study. These supplementary sections are explicitly enumerated in **Table 6-3** and **Figure 6.1**.

Table 6-3: - Different sections used in EWM and DSM comparison study.

Type		ID	Dimensions (mm)				
			H	B	D	t	r
C - Sections	Stiffened	12CS4×105	304.80	101.60	22.48	2.67	4.76
		12CS4×085	304.80	101.60	21.23	2.16	4.76
		9CS2.5×105	228.60	63.50	22.48	2.67	4.76
		9CS2.5×085	228.60	63.50	21.23	2.16	4.76
		6CS2.5×059	228.60	63.50	19.63	1.50	4.75
	Unstiffened	800T200-68	209.55	50.80	-	1.81	2.72
		1200T200-97	313.84	50.80	-	2.58	3.87
		362T200-68	98.43	50.80	-	1.81	2.72
		800T200-97	212.24	50.80	-	2.58	3.87
		362T200-33	95.78	50.80	-	0.88	1.94
Z - Sections	Stiffened	Z100×50×20×2	100.00	50.00	20.00	2.00	8.00
		Z150×60×20×2	150.00	60.00	20.00	2.00	8.00
		Z150×60×20×2.5	150.00	60.00	20.00	2.50	8.00
		Z200×60×20×2	200.00	60.00	20.00	2.00	8.00
		Z200×60×20×2.5	200.00	60.00	20.00	2.50	8.00
	Unstiffened	Z250×70×2	250.00	70.00	-	2.00	8.00
		Z300×70×2.5	300.00	70.00	-	2.50	8.00
		Z215×60×3	215.00	60.00	-	3.00	8.00
		Z180×75×4	180.00	75.00	-	4.00	8.00
		Z250×70×20×2.5	100.00	40.00	-	3.00	8.00

Figures 6.7 and 6.8 present a comparative analysis of the expected strength of CFS members using the EWM and DSM. The analysis is based on the comparison of the predicted strengths of CFS channel and Z-profiles using the aforementioned design codes against the results obtained from the FEM. These figures represent a relationship between the critical member slenderness ratio (λ) and the ratio between expected capacities for each code and verified FEM. **Appendix A** shows details about this comparative analysis.

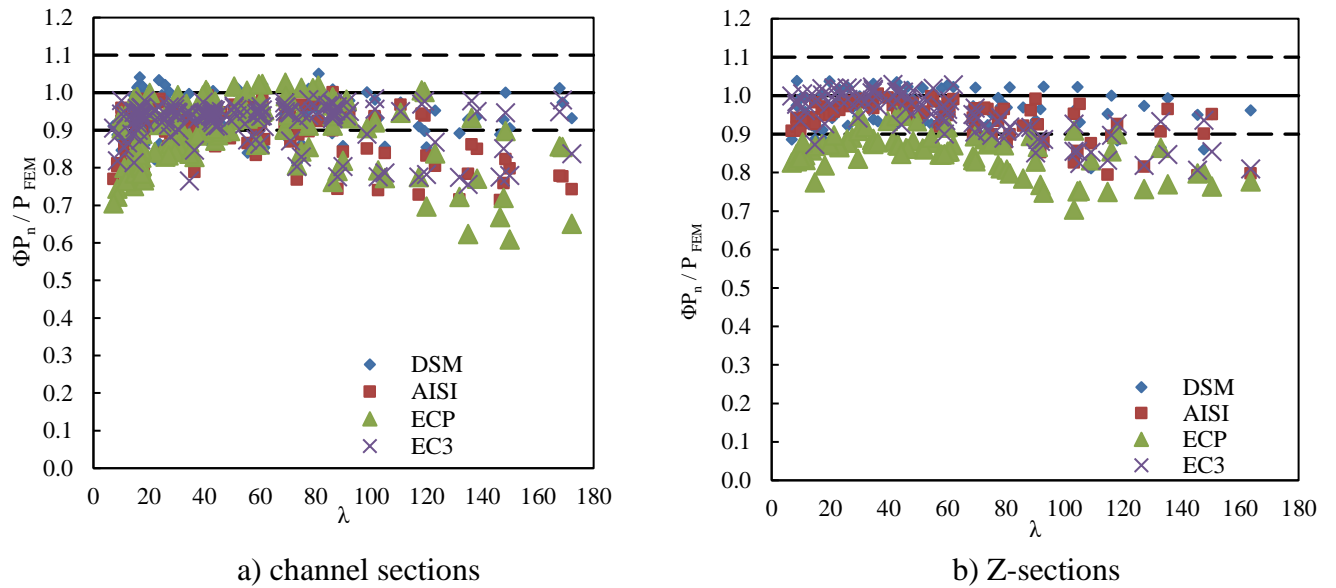


Figure 6.7: - Comparison between EWM and DSM for CFS compression members.

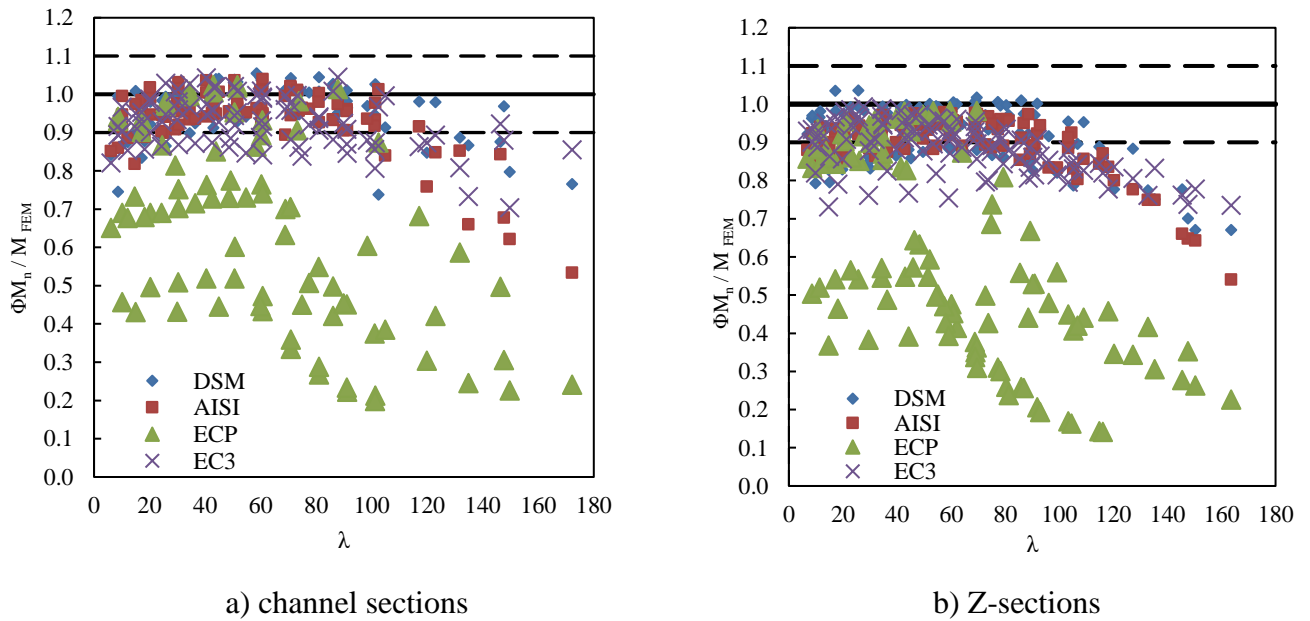


Figure 6.8: - Comparison between EWM and DSM for CFS Flexure members.

Table 6-4 to **Table 6-7** also provide a comparison between the capacities obtained from the FEM, AISI [21] (using the DSM as per Appendix 1), AISI [21] (using the EWM), ECP [20], and EC3 [22] for compression and flexure loading cases in both analyzed profiles.

Table 6-4: - Comparison between EWM and DSM for CFS compression channel sections.

	$P_{\text{AISI (DSM)}} / P_{\text{FEM}}$	$P_{\text{AISI}} / P_{\text{FEM}}$	$P_{\text{ECP}} / P_{\text{FEM}}$	$P_{\text{EC3}} / P_{\text{FEM}}$
Mean	0.94	0.9	0.89	0.92
COV	0.06	0.07	0.1	0.06

Table 6-5: - Comparison between EWM and DSM for CFS compression Z-sections.

	$P_{\text{AISI (DSM)}} / P_{\text{FEM}}$	$P_{\text{AISI}} / P_{\text{FEM}}$	$P_{\text{ECP}} / P_{\text{FEM}}$	$P_{\text{EC3}} / P_{\text{FEM}}$
Mean	0.96	0.94	0.85	0.95
COV	0.05	0.05	0.06	0.06

Table 6-6: - Comparison between EWM and DSM for CFS flexure channel sections.

	$M_{\text{AISI (DSM)}} / M_{\text{FEM}}$	$M_{\text{AISI}} / M_{\text{FEM}}$	$M_{\text{ECP}} / M_{\text{FEM}}$	$M_{\text{EC3}} / M_{\text{FEM}}$
Mean	0.96	0.93	0.61	0.93
COV	0.07	0.09	0.42	0.07

Table 6-7: - Comparison between EWM and DSM for CFS flexure Z-sections.

	$M_{\text{AISI (DSM)}} / M_{\text{FEM}}$	$M_{\text{AISI}} / M_{\text{FEM}}$	$M_{\text{ECP}} / M_{\text{FEM}}$	$M_{\text{EC3}} / M_{\text{FEM}}$
Mean	0.92	0.9	0.58	0.89
COV	0.09	0.09	0.44	0.08

Table 6-4 to **Table 6-7** demonstrate that the DSM and EWM whether using AISI [21], ECP [20], or EC3 [22] generally yield reasonable predictions of the bending moment and axial load capacities for the CFS members analyzed in this study.

Table 6-4 to **Table 6-7** indicate that the predicted CFS capacity based on the AISI (DSM) [21] is more accurate and closely aligned with the FEM capacity than the EWM. This difference can be attributed to the EWM's neglect of inter-element compatibility and equilibrium, particularly regarding the interaction between the web-flange junction and the flange stiffener junction. On the

other hand, the DSM is based on elastic buckling solutions for the entire cross-section, including the interaction between different elements, thus overcoming the disadvantages of the EWM [17].

From **Table 6-4** to **Table 6-5**, it can be observed that when the EWM is applied, EC3 [22] yields an axial load capacity that is more accurate and closer to FEM than those provided by AISI (EWM) [21] and ECP [20], and this can be explained that EC3 [22] is the only code that takes into account the effect of distortional buckling and the interaction between local and distortion buckling modes in determining the resistance and stiffness of CFS members. Furthermore, it is worth noting that ECP [20] displays the most conservative compressive capacity due to its usage of more conservative load factors for compressive loads as compared to other design codes.

From **Table 6-6** to **Table 6-7**, it can be observed that when the EWM is applied, EC3 [22] yields a flexural capacity similar to those provided by AISI (EWM) [21] and that is more accurate and closer to the FEM than those provided by ECP [20] and this can be explained that ECP [20] does not take into account the sectional degree of symmetry, and boundary conditions and does not include more detailed equations for calculating the flexural capacity of CFS sections. As an example, the values of flexural constants used in ECP [20] are given only for rolled, built-up, and welded sections. The ECP [20] did not mention any values for these constants while using CFS sections. So, the values of these constants were taken in this study as if sections were rolled. This suggests that the ECP [20] may require revision to improve the accuracy of its predictions for CFS flexural member bending moment capacity.

The high value of covariance observed in the ratios between the predicted axial load and bending moment capacity of CFS flexural members using various methods and FEM indicates a deficiency in the precision and reliability of the predictions. The inaccurate prediction for EC3 [22] and AISI (DSM) [21] is because both of them do not take into account distortion buckling and its interaction with other buckling modes in determining the resistance of CFS sections unless the section has a lip (stiffened section). Unlike AISI (EWM) [21] and ECP [20], which also disregard this interaction, regardless of whether the section has a lip or not. Consequently, it is suggested that a revision of these methods may be necessary to enhance the accuracy of their predictions for CFS axial load and bending moment capacities.

6.4 MEMBER UNDER COMBINED BENDING AND AXIAL FORCES

Parametric studies on the CFS combined bending and axial capacities were conducted for the channel and Z-section profiles using the verified FEM, as discussed in the previous section. The channel and Z-section profiles were studied with the same dimensions to determine the effect of the cross-section profile on the combined bending and axial capacity. This parametric study included 28 different CFS cross-sections. **Table 6-8 and Figure 6.1** provide the details of the cross-sectional dimensions used in the parametric studies. **Table A-25 in appendix A** shows details about the FEM results for this parametric study.

Five values of steel yielding strength (F_y) were used in this study; 240, 280, 320, 360 and 400 MPa, as mentioned before. The material defined in Abaqus during the study of different parameters, except for yielding stress (F_y) parameter, has yield strength (F_y) and ultimate strength (F_u) of 360 MPa and 400 MPa, respectively. The Young's modulus (E_0) and Poisson's ratio (ν) are 210 GPa and 0.3, respectively.

Various parameters were considered for analysis. These parameters include the length-to-web plate depth ratio (L/h), which ranges from 1 to 10. Additionally, the web plate slenderness ratio (h/t) was examined at 50, 100, 150, 200, 250 and 300. Similarly, the web-to-flange plate length ratio (h/b) was analyzed across a range of values including 2, 3, 4, 5, 6, and 7. Furthermore, the lip-to-flange plate length ratio (d/b) varied at 0.3, 0.4, 0.5, and 0.6. Lastly, the yielding stress (F_y) was studied using recommended values by European codes for cold-rolled flat products 240, 280, 320, 360, and 400 MPa. The studied members are subject to pin-pin boundary conditions.

Table 6-8: - Different sections with combined bending and compression forces used in this study.

H	B	D	t	r	L (mm)
mm	mm	mm	mm	mm	
100	50	20	2	8	100
100	50	20	2	8	200
100	50	20	2	8	300
100	50	20	2	8	400
100	50	20	2	8	500
100	50	20	2	8	600
100	50	20	2	8	700
100	50	20	2	8	800
100	50	20	2	8	900
100	50	20	2	8	1000
100	100	40	2	3	200
100	50	20	2	3	200
100	25	10	2	3	200
100	20	8	2	3	200
100	16.7	6.7	2	3	200
100	14.3	5.7	2	3	200
100	50	20	2	8	200
200	100	40	2	8	400
300	150	60	2	8	600
400	200	80	2	8	800
500	250	100	2	8	1000
600	300	120	2	8	1200
100	50	20	2	8	200
100	50	20	2	8	200
100	50	20	2	8	200
100	50	20	2	8	200
100	50	20	2	8	200

6.4.1. Effect of Length-to-Web Plate Depth Ratio (L/h) Parameter

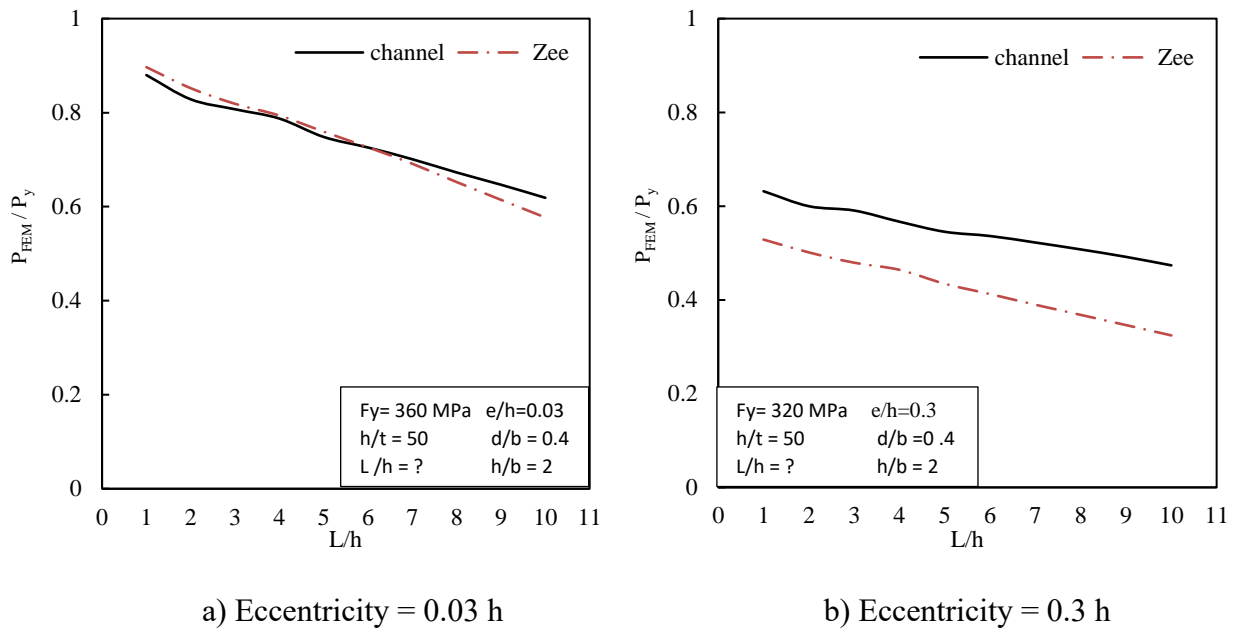


Figure 6.9: - Effect of length-to-web plate depth ratio (L/h) on CFS member under compression loads with eccentricity.

Figure 6.9 presents evidence of an inverse relationship between the combined bending and compression capacity of the CFS sections and the length-to-web plate depth ratio (L/h). This trend is attributed to the heightened frequency of global buckling as L/h increases.

Figure 6.9 (a) presents evidence that, with increasing length, the combined bending and compression capacity of both the channel and Z-sections becomes more similar. This convergence is primarily due to the heightened impact of flexural buckling, which is exclusively dependent on length, given the constant nature of the cross-sectional dimensions and moment of inertia about the minor axis. Consequently, the effects of torsion and distortional buckling diminish, leading to a reduced reliance on shape and symmetry.

From the observation of **Figure 6.9 (b)**, it is apparent that an inverse correlation exists between the combined bending and compression capacity of the CFS sections and the length-to-web plate depth ratio (L/h) owing to the amplified occurrence of lateral torsional buckling. Furthermore, it was demonstrated that as the length increased, the distinction between the

combined bending and compression capacity values of each channel and the Z- section remained relatively invariable. This phenomenon occurs because lateral torsional buckling is solely dependent on the shape and symmetry of the cross-section at a specific length, and the constant value of the cross-sectional dimensions ensures that the shape and symmetry remain constant during the L/h parameter evaluation.

6.4.2 Effect of Web Plate Slenderness Ratio (h/t) Parameter

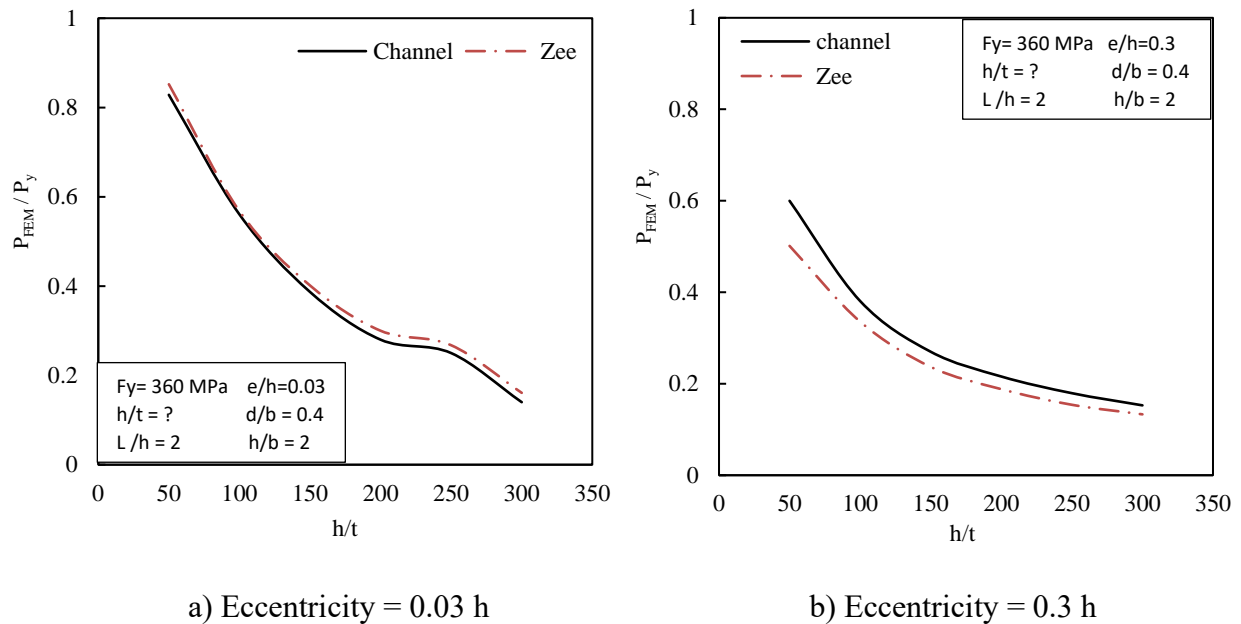


Figure 6.10: - Effect of web plate slenderness ratio (h/t) on CFS member under compression loads with eccentricity.

The increase of web plate slenderness ratio (h/t) ratio resulted in a decrease in the CFS combined bending and compression capacity, as illustrated in **Figure 6.10**. This is because an increase in h/t leads to a higher incidence of web local buckling, which in turn causes weakness and a decline in the CFS capacity. Furthermore, it was observed that the channel and Z-cross-section profiles of the same dimensions exhibited similar combined bending and compression capacities, coinciding with the increase in h/t resulting from the amplified effect of local buckling.

6.4.3 Effect of Lip-To-Flange Plates Length Ratio (d/b) Parameter

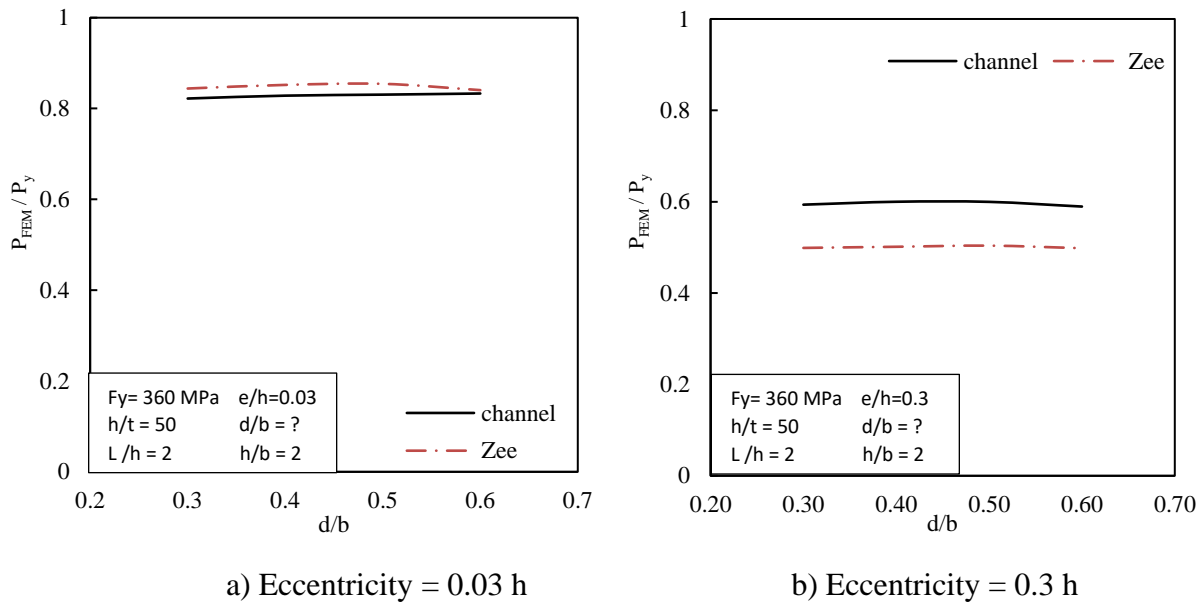


Figure 6.11: - Effect of lip-to-flange plates length (d/b) on CFS member under compression loads with eccentricity.

There is a slight change in the combined bending and compression strength of the CFS sections when changing the lip-to-flange plate length ratio (d/b). This is because the studied members are exposed to local buckling, which critically occurs in the web due to its higher slenderness ratio in comparison to the lip and flange. Furthermore, all the studied members in this parameter have a constant web plate slenderness ratio (h/t). Additionally, increasing the lip-to-flange plate length ratio causes the flange stiffness to increase; however, this does not affect the web local buckling, as shown in **Figure 6.11**.

6.4.4 Effect of Web-to-Flange Plate Length Ratio (h/b) Parameter

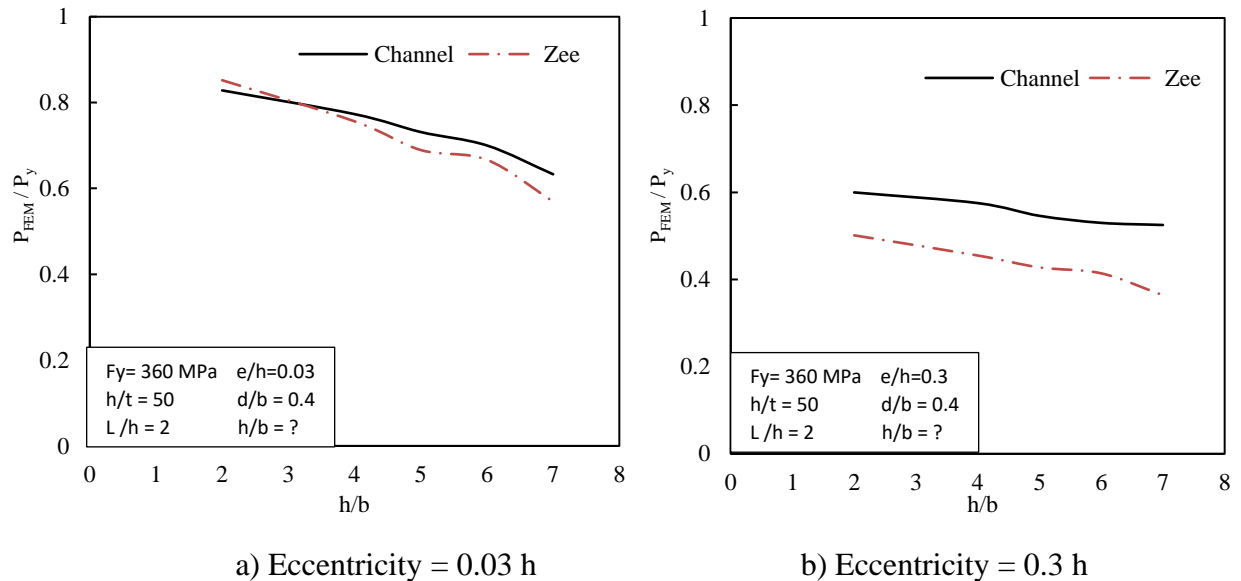


Figure 6.12: - Effect of web-to-flange plate length ratio (h/b) on CFS member under compression loads with eccentricity.

Observing **Figure 6.12**, it can be noted that an inverse correlation exists between the combined bending and compression capacity of the CFS sections and the web-to-flange plate length ratio (h/b). This is because an increase in h/b leads to a weaker connection between the flange and the web, consequently increasing the likelihood of distortional buckling.

The cross-sectional profiles of Channel and Z, of identical dimensions, exhibit similar combined bending and compression capacities at loading condition of small eccentricity ($e = 0.03h$). In addition, their respective capacities align with the increase in h/b due to the increased influence of the web local buckling; this is indicated in **Figure 6.12 (a)**.

The difference between the values of the combined bending and compression capacities of each channel and Z-section increases with increasing (h/b) at loading condition of big eccentricity ($e = 0.3h$) because the greater the value of h/b , the more twisting and bending occur, the more the difference between the Z and channel warping constants happens, and the more we get the difference between their lateral torsional resistance, as illustrated in **Figure 6.12 (b)**.

6.4.5 Effect of Yielding Stress (F_y) Parameter

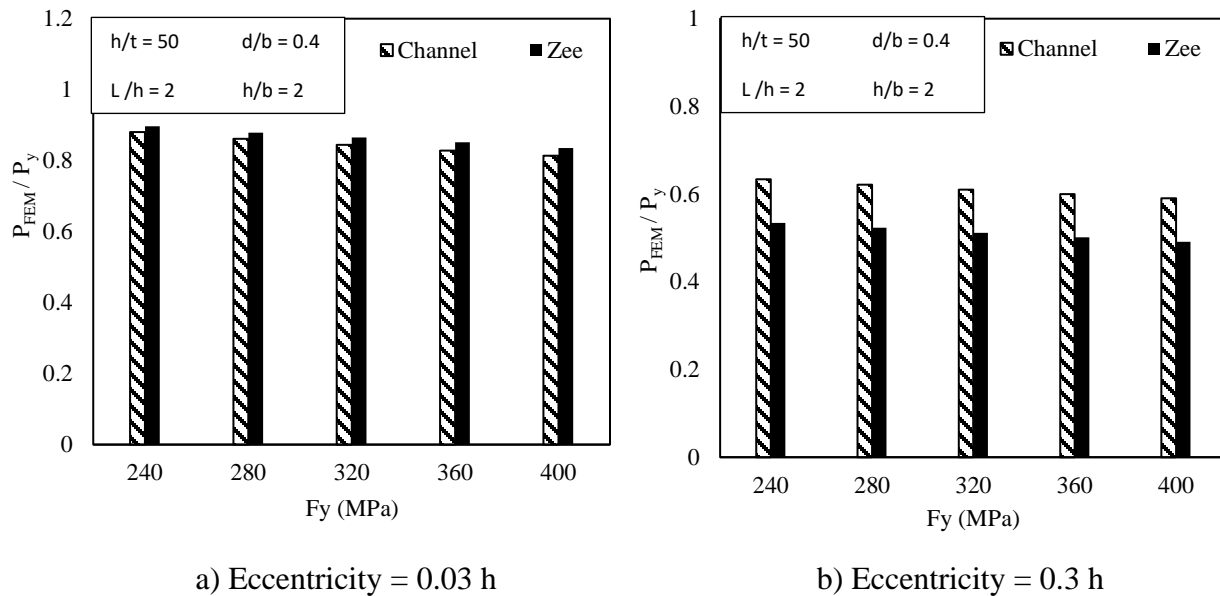


Figure 6.13: - Effect of yielding stress (F_y) on CFS member under compression loads with eccentricity.

As expected, there exists a positive correlation between steel yield stress (F_y) and the combined bending and compression capacities of CFS members, owing to material enhancements, as shown in **Figure 6.13**.

Figures 6.9 to 6.13 indicate that the channel provides lower combined bending and compression capacities than Z-sections of the same dimensions and loading conditions of small eccentricity ($e = 0.03h$) because the channel section provides lower compressive capacities than Z-sections of the same dimensions and loading conditions, as previously explained in 6.2 paragraph of this chapter.

Additionally, **Figures 6.9 to 6.13** also indicate that when considering the same dimensions and loading conditions of big eccentricity ($e = 0.3h$), channel sections exhibit greater combined bending and compression capacities than Z-sections. This is because the channel sections exhibit greater flexural capacities than Z-sections, as previously explained in 6.2 paragraph of this chapter.

Figures A.8 to A.12 in appendix (A) illustrate the relationship between pure bending moment and compression capacities obtained from EEM and the capacities of the same identical members subjected to combined bending moment and compression forces. M_c represents the ultimate moment, and P_c is the ultimate compression capacities obtained from the FEM while the members are subjected to combined bending moment and compression forces. M_u represents the ultimate moment capacities obtained from the FEM while the members are subjected to pure bending moment. P_u is the ultimate compression capacities obtained from the FEM while the members are subjected to pure compression forces. As expected, there exists an indirect correlation between the (P_c/P_u) ratio and the (M_c/M_u) ratio.

6.4.6 Comparison between Effective Width and Direct Strength Methods

The sectional maximum combined bending and compression capacities were found using the verified FEM, as discussed in the previous section, and then they were used to apply the interaction equations in the various codes to find out which of these codes is closest to accuracy (closest to the unity). To accomplish this, a total of 28 sections were included. These supplementary sections are explicitly enumerated in Table 6-8, mentioned previously. The sectional material has a yield strength (F_y) of 360 MPa. The Young's modulus (E_0) and Poisson's ratio (ν) are 210 GPa and 0.3, respectively.

Table 6-9 and Table 6-10 provide a comparison between the combined bending and axial capacities obtained from the FEM, AISI [21] (using the DSM as per Appendix 1), AISI [21] (using the EWM), ECP [20], and EC3 [22] for channel and Z-profiles. Tables contain the mean and covariance of the values produced from different aforementioned codes.

Table 6-9: - Comparison between interaction equations results for CFS channel sections.

	EC3	ECP	AISI _{EWM}	AISI _{DSM}
Mean	1.05	1.74	1.05	1.03
COV	0.05	0.17	0.09	0.07

Table 6-10: - Comparison between interaction equations results for CFS Z-sections.

	EC3	ECP	AISI _{EWM}	AISI _{DSM}
Mean	1.08	1.99	1.08	1.00
COV	0.08	0.43	0.07	0.1

Table 6-9 and **Table 6-10** demonstrate that the DSM and EWM whether using AISI [21], or EC3 [22] generally yield reasonable predictions of the combined bending and compression capacities for the CFS members analyzed in this study since the previously mentioned codes gave a value to the interaction equations that is slightly larger than the unity, therefore these sections are unsafe subjected to the applied straining actions, and this is consistent with the FEM. On the hand, The ECP [20] code yield a significantly safe predictions of the combined bending and compression capacities for the CFS members analyzed in this study since it gave a value to the interaction equation that is much higher than the unity, and this does not consistent with the FEM. This can be explained that ECP [20] does not take into account the sectional degree of symmetry, and boundary conditions and does not include more detailed equations for calculating the flexural capacity of CFS sections, as mentioned before. This suggests that the ECP [20] may require revision to improve the accuracy of its predictions for CFS combined bending and compression capacity.

Table 6-9 and **Table 6-10** indicate that the predicted CFS combined flexural and compression capacity based on the AISI(DSM) [21] is more accurate and closely aligned with the FEM capacity than the EWM. This difference can be attributed to the EWM's neglect of inter-element compatibility and equilibrium, particularly regarding the interaction between the web-flange junction and the flange stiffener junction. On the other hand, the DSM is based on elastic buckling solutions for the entire cross-section, including the interaction between different elements, thus overcoming the disadvantages of the EWM.

From **Table 6-9** and **Table 6-10**, it can be observed that when the EWM is applied, EC3 [22] yields a CFS combined flexural and compression capacity similar to those provided by AISI (EWM) [21] and that is more accurate and closer to the FEM than those provided by ECP [20].

The high value of covariance observed in the ratios between the predicted combined flexural and compression capacity of CFS sections using ECP [20] and FEM indicates a deficiency in the precision and reliability of the predictions. Consequently, it is suggested that a revision of this code may be necessary to enhance the accuracy of its predictions for CFS combined flexural and compression capacities.

CHAPTER (7)

SUMMARY AND CONCLUSIONS

7.1 SUMMARY

This study presents detailed investigations of the behavior of CFS members with channel and Z-profiles using validated finite-element (FE) models. The study entails a comprehensive parametric analysis of these profiles, particularly emphasizing their axial and flexural capacities. Moreover, the study compares the codified Effective Width Method (EWM) and the newly progressed Direct Strength Method (DSM) regarding the calculation procedures and predicted strengths. Besides, a graphical user interface (GUI) that processes EWM and DSM calculation procedures is developed. As an example of the EWM, the North American Specification (AISI) [21], Eurocode-3_part1.3 (EC3) [22], and the Egyptian Code of Practice (ECP-205) [20] have been utilized. On the other hand, Appendix 1 in the North American Specification (AISI) [21] is utilized as an example of the DSM.

7.2 CONCLUSIONS

Based on the results obtained from an extensive parametric study, the study draws several conclusions as follows: -

1. Channel and Z-profiles of the same dimensions and loading conditions exhibit lower axial capacities for members comprising channel sections than those of Z-sections. In contrast, channel sections provide higher bending moment capacities when compared to Z-sections.

2. As is consistent with existing codified member buckling curves, the CFS members exhibit lower buckling strengths with increasing the member length-to-depth ratio (L/h), the depth-to-width ratio (h/b), and the plate slenderness ratio, whether for web and flange (i.e., h/t or b/t).
3. The lip-to-flange width ratio (d/b) has a negligible effect on the axial load-bearing capacity of CFS compression members. Conversely, it is directly proportional to the flexural capacity of CFS beams.
4. The DSM produces more reliable predictions of CFS capacities than the EWM, whether for axial or bending moment capacity.
5. EC3 provides less conservative axial capacities than those provided by AISI and ECP. The AISI and EC3, however, yield almost identical bending moment strength for CFS sections.
6. ECP provides a more conservative compressive capacity and significantly compressive flexural capacity than the experimental results, indicating that the ECP needs to be revised.
7. There is a shift from a stable to an indirect relationship between the nominal flexural capacity and torsional slenderness ratio (L/rt) in AISI_{DSM}, AISI_{EWM}, and ECP at L/h ratios of 12, 11, and 8, respectively. Conversely, an indirect correlation was observed between the nominal flexural capacity in the EC3 code and the L/rt ratio.
8. A slight variation in the flexural capacities in different design codes was observed with a change in web slenderness ratio (h/t) until the ratio reached 100. However, after this ratio, the relationship between them became indirect.
9. The CFS compressive capacities using the EWM have an indirect relationship with the flange slenderness ratio (b/t). Conversely, using the DSM, it shows a positive correlation with a b/t ratio less than 35 but a negative correlation beyond that.
10. The flange slenderness (b/t) ratio indirectly affects the CFS flexural capacities in the EWM. Conversely, it does not affect on the DSM's nominal flexural capacity when the b/t ratio is less than 45, however, it affects directly beyond that

11. CFS capacities using DSM differ slightly owing to the change in the lip-to-flange width (d/b) ratio. In contrast, in the EWM, a direct relationship exists between them.

7.3 FUTURE RECOMMENDATIONS

For future studies, the following topics are recommended:

1. Study the effect of residual stress on different cold formed frame members.
2. Use the developed program to provide a design chart for different cold-formed members.
3. Study the ways to improve different cold formed frame members resistance.
4. Study the difference between design code in the designing of composite cold formed beams and columns.
5. The design of cold formed beam-columns connections under different loading conditions.

REFERENCES

- [1] Chen, J., M.-T. Chen, and B. Young, Compression tests of cold-formed steel C-and Z-sections with different stiffeners. *Journal of Structural Engineering*, 2019. 145(5): p. 04019022.
- [2] Veljkovic, M. and B. Johansson, Thin-walled steel columns with partially closed cross-section: Tests and computer simulations. *Journal of Constructional Steel Research*, 2008. 64(7-8): p. 816-821.
- [3] Yu, C., *Recent trends in cold-formed steel construction*. 2016: Woodhead Publishing.
- [4] Davies, J., Recent research advances in cold-formed steel structures. *Journal of constructional steel research*, 2000. 55(1-3): p. 267-288.
- [5] Meza, F., J. Becque, and I. Hajirasouliha. Experimental investigation of cold-formed steel built-up stub columns. in *8th International Conference on Advances in Steel Structures*, Lisbon, Portugal, Paper. 2015.
- [6] Ghannam, M., Axial load capacity of cold-formed steel built-up stub columns. *International Journal of Steel Structures*, 2017. 17(4): p. 1273-1283.
- [7] Young, B. and J. Yan, *Finite element analysis of cold-formed channel columns*. 2000.
- [8] Qureshi, L.A., et al., Comparison of energy efficient cold rolls steel construction with the prevailing conventional construction. 2012.
- [9] Satpute, R. and V. Varghese, Building design using cold formed steel section. *International Refereed Journal of Engineering and Science*, 2012. 1(2): p. 01-16.
- [10] Doctolero, L. and M. Batikha. Using cold-formed steel section in buildings-comparative study. in *104th IASTEM International Conference 2018*. 2018.
- [11] Craveiro, H.D., J.P.C. Rodrigues, and L. Laím, Buckling resistance of axially loaded cold-formed steel columns. *Thin-Walled Structures*, 2016. 106: p. 358-375.
- [12] Lue, D.M., et al., The compressive strength of slender C-shaped cold-formed steel members with web openings. *International Journal of Steel Structures*, 2009. 9: p. 231-240.
- [13] Plaut, R.H. and C.D. Moen. Lateral-torsional deformations of C-section and Z-section beams with continuous bracing. in *Proc., 2020 SSRC Annual Stability Conference*, Atlanta: Structural Stability Research Council, Chicago. 2020.

REFERENCES

- [14] Von Kármán, T., E.E. Sechler, and L. Donnell, The strength of thin plates in compression. Transactions of the American Society of Mechanical Engineers, 1932. 54(2): p. 53-56.
- [15] Winter, G., Strength of thin steel compression flanges. Transactions of the American Society of Civil Engineers, 1947. 112(1): p. 527-554.
- [16] Schafer, B.W., The direct strength method of cold-formed steel member design. Journal of constructional steel research, 2008. 64(7-8): p. 766-778.
- [17] Schafer, B.W., Designing cold-formed steel using the direct strength method. 2006.
- [18] AISI, Supplement 2004 to the North American specification for the design of cold-formed steel structural members. 2004, AISI Washington, DC.
- [19] Kalavagunta, S., S. Naganathan, and K.N.B. Mustapha, Theoretical study of axially compressed Cold Formed Steel Sections. International Journal of Advanced Studies in Computers, Science and Engineering, 2013. 2(1): p. 67.
- [20] ECP-205, Egyptian code of practice for steel construction (load and resistance factor design (LRFD)). 2008, Cairo, Egypt: Ministry of Housing, Utilities and Urban Communities, Housing and Building National Research Centre.
- [21] Iron, A. and S. Institute, North American Specification for Design of Cold-Formed Steel. 2016: American Iron & Steel Institute, Committee of Steel Plate Producers
- [22] CEN, E., 1-3 Eurocode 3: Design of steel structures-Part 1-3: General rules-Supplementary rules for cold-formed members and sheeting. European Committee for Standardization, Brussels, 2006.
- [23] Abaqus, I., Abaqus 6.13-1. 2004, Abaqus, Inc. Providence, RI.
- [24] Yu, W.-W., R.A. LaBoube, and H. Chen, Cold-formed steel design. 2019: John Wiley & Sons.
- [25] Dubina, D., V. Ungureanu, and R. Landolfo, Design of Cold Formed Steel Structures. ECCS–European Convention for Constructional Steelwork. 2012, Ernst & Sohn.
- [26] Kirkland, W.G., Cold roll forming practice in the United States. 1966: American Iron and Steel Institute.
- [27] Winter, G. Light Gage (Thin-Walled) Steel Structures for Buildings in the United States of America. in International Association for Bridge and Structural Engineering, 4th Congress, Preliminary Publication. 1952.

REFERENCES

- [28] Winter, G., Cold-formed light-gage steel construction. *Journal of the Structural Division*, 1959. 85(9): p. 151-173.
- [29] Scharff, R., *Residential steel framing handbook*. 1996: McGraw-Hill Education.
- [30] Grubb, P.J. and R.M. Lawson, *Building design using cold formed steel sections: construction detailing and practice*. 1997: Steel Construction Institute.
- [31] Sangave, P., et al., Comparative study of analysis and design of RC and steel structures. *Int J Sci Eng Res*, 2015. 6(2): p. 256.
- [32] Kalavagunta, S., S. Naganathan, and K.N.B. Mustapha, Experimental study of axially compressed cold formed steel channel columns. *Indian journal of science and technology*, 2013. 6(4): p. 4251-4254.
- [33] Lawrence, K.L., *ANSYS tutorial*. Schroff Development Corporation, 2002.
- [34] Stolarski, T., Y. Nakasone, and S. Yoshimoto, *Engineering Analysis with ANSYS Software* 2011. Elsevier Science.
- [35] Wilson, E.L., et al., SAP—A structural analysis program for linear systems. *Nuclear Engineering and Design*, 1973. 25(2): p. 257-274.
- [36] Abdelrahman, A., et al., Simulation of thin-walled members with arbitrary-shaped cross-sections for static and dynamic analyses. *International Journal of Structural Stability and Dynamics*, 2020. 20(12): p. 2050128.
- [37] Li, Z. and B.W. Schafer, Buckling analysis of cold-formed steel members with general boundary conditions using CUFSM conventional and constrained finite strip methods. 2010.
- [38] Iron, A. and S.I.C.o.S.f.t.D.o.C.-F.S.S. Members, *Direct strength method (DSM) design guide*. 2006: American Iron and Steel Institute.
- [39] Zhang, J.-H. and B. Young, Compression tests of cold-formed steel I-shaped open sections with edge and web stiffeners. *Thin-Walled Structures*, 2012. 52: p. 1-11.
- [40] Wang, L. and B. Young, Behavior of cold-formed steel built-up sections with intermediate stiffeners under bending. I: Tests and numerical validation. *Journal of Structural Engineering*, 2016. 142(3): p. 04015150.
- [41] Ghannam, M., Axial load capacity of cold-formed steel built-up stub columns. *International Journal of Steel Structures*, 2017. 17: p. 1273-1283.
- [42] Ghannam, M., Bending moment capacity of cold-formed steel built-up beams. *International Journal of Steel Structures*, 2019. 19(2): p. 660-671.
-

REFERENCES

- [43] Manikandan, P., S. Sukumar, and T. Balaji, Effective shaping of cold-formed thin-walled built-up beams in pure bending. *Arabian Journal for Science and Engineering*, 2014. 39: p. 6043-6054.
- [44] Roy, K., et al., Nonlinear behaviour of back-to-back gapped built-up cold-formed steel channel sections under compression. *Journal of Constructional Steel Research*, 2018. 147: p. 257-276.
- [45] Roy, K., et al. Effect of thickness on the behaviour of axially loaded back-to-back cold-formed steel built-up channel sections-Experimental and numerical investigation. in *Structures*. 2018. Elsevier.
- [46] Ting, T.C.H., et al., Effect of screw spacing on behavior of axially loaded back-to-back cold-formed steel built-up channel sections. *Advances in Structural Engineering*, 2018. 21(3): p. 474-487.
- [47] Keerthan, P. and M. Mahendran, Experimental studies on the shear behaviour and strength of LiteSteel beams. *Engineering structures*, 2010. 32(10): p. 3235-3247.
- [48] Shu, G., B. Zheng, and X. Shen, Experimental and theoretical study on the behavior of cold-formed stainless steel stub columns. *International Journal of Steel Structures*, 2013. 13: p. 141-153.
- [49] Roy, K., et al., Experimental and numerical investigations on the axial capacity of cold-formed steel built-up box sections. *Journal of Constructional Steel Research*, 2019. 160: p. 411-427.
- [50] Roy, K., C. Mohammadjani, and J.B. Lim, Experimental and numerical investigation into the behaviour of face-to-face built-up cold-formed steel channel sections under compression. *Thin-Walled Structures*, 2019. 134: p. 291-309.
- [51] Rahnavard, R., et al., Numerical investigation on the composite action of cold-formed steel built-up battened columns. *Thin-Walled Structures*, 2021. 162: p. 107553.
- [52] Lian, Y., et al., Effect of web holes on web crippling strength of cold-formed steel channel sections under end-one-flange loading condition–Part I: Tests and finite element analysis. *Thin-Walled Structures*, 2016. 107: p. 443-452.
- [53] Lian, Y., et al., Effect of web holes on web crippling strength of cold-formed steel channel sections under end-one-flange loading condition-Part II: Parametric study and proposed design equations. *Thin-Walled Structures*, 2016. 107: p. 489-501.
-

REFERENCES

- [54] Chen, B., et al., Effects of edge-stiffened web openings on the behaviour of cold-formed steel channel sections under compression. *Thin-Walled Structures*, 2019. 144: p. 106307.
- [55] Yener, M. and T. Peköz, Limit design in cold-formed steel. *Journal of Structural Engineering*, 1983. 109(9): p. 2033-2047.
- [56] Yener, M. and T. Pekoz, Partial stress redistribution in cold-formed steel. *Journal of structural Engineering*, 1985. 111(6): p. 1169-1186.
- [57] Maduliat, S., M.R. Bambach, and X.L. Zhao, Inelastic behaviour and design of cold-formed channel sections in bending. *Thin-walled structures*, 2012. 51: p. 158-166.
- [58] De Miranda, S., et al. Design of thin-walled members undergoing distortional buckling: a simple EC3-compliant approach based on the GBT. in *European conference on steel and composite structures*, Eurosteel. 2014.
- [59] He, Z. and X. Zhou, Strength design curves and an effective width formula for cold-formed steel columns with distortional buckling. *Thin-walled structures*, 2014. 79: p. 62-70.
- [60] He, Z., et al., Post-buckling behaviour and DSM design of web-stiffened lipped channel columns with distortional and local mode interaction. *Thin-Walled Structures*, 2014. 84: p. 189-203.
- [61] Landesmann, A. and D. Camotim, On the Direct Strength Method (DSM) design of cold-formed steel columns against distortional failure. *Thin-Walled Structures*, 2013. 67: p. 168-187.
- [62] Young, B., N. Silvestre, and D. Camotim, Cold-formed steel lipped channel columns influenced by local-distortional interaction: strength and DSM design. *Journal of structural Engineering*, 2013. 139(6): p. 1059-1074.
- [63] Geleji, B., et al., Understanding the global buckling behavior of thin-walled members with slotted web. 2014.
- [64] Georgescu, M. and V. Ungureanu, Stabilisation of continuous Z-purlins by sandwich panels: Full scale experimental approach. *Thin-Walled Structures*, 2014. 81: p. 242-249.
- [65] Ye, W., et al., Load-deflection behaviour of sleeved joints in modified Z purlin system. *Thin-Walled Structures*, 2013. 73: p. 318-328.
- [66] Kujawa, M. and C. Szymczak, Numerical and experimental investigation of rotational stiffness of zed-purlins connection with sandwich panels. *Thin-walled structures*, 2014. 75: p. 43-52.
-

REFERENCES

- [67] Loureiro, A. and R. Calvo. Experimental results of a completed Z_purlings system. in European conference on steel and composite structures, Eurosteel. 2014.
- [68] Moen, C.D., A. Schudlich, and A. von der Heyden, Experiments on cold-formed steel C-section joists with unstiffened web holes. *Journal of Structural Engineering*, 2013. 139(5): p. 695-704.
- [69] Pham, C., L. Bruneau, and Y. Chin. New developments in the direct strength method of design for coldformed sections subject to shear. in European conference on steel and composite structures, Eurosteel. 2014.
- [70] Cheng, S.-s., B. Kim, and L.-y. Li, Lateral–torsional buckling of cold-formed channel sections subject to combined compression and bending. *Journal of Constructional Steel Research*, 2013. 80: p. 174-180.
- [71] Yao, X. and Y. Guo, Inelastic Test and Design Method of Cold-formed Steel Lipped Channel Members in Bending. *The Open Civil Engineering Journal*, 2016. 10(1).
- [72] Haidarali, M.R. and D.A. Nethercot, Local and distortional buckling of cold-formed steel beams with edge-stiffened flanges. *Journal of Constructional Steel Research*, 2012. 73: p. 31-42.
- [73] Yu, C. and B.W. Schafer, Local buckling tests on cold-formed steel beams. *Journal of structural engineering*, 2003. 129(12): p. 1596-1606.
- [74] Yu, C. and B.W. Schafer, Distortional buckling tests on cold-formed steel beams. *Journal of structural engineering*, 2006. 132(4): p. 515-528.
- [75] Lee, J. and S.-E. Kim, Lateral buckling analysis of thin-walled laminated channel-section beams. *Composite Structures*, 2002. 56(4): p. 391-399.
- [76] Seah, L. and P. Khong, Lateral-torsional buckling of channel beams. *Journal of Constructional Steel Research*, 1990. 17(4): p. 265-282.
- [77] Li, L.-y., Lateral–torsional buckling of cold-formed zed-purlins partial-laterally restrained by metal sheeting. *Thin-walled structures*, 2004. 42(7): p. 995-1011.
- [78] Schardt, R., Lateral torsional and distortional buckling of channel-and hat-sections. *Journal of Constructional Steel Research*, 1994. 31(2-3): p. 243-265.
- [79] Wu, J.-R., et al., Buckling Resistance of Axially Loaded Cold-Formed Steel Compound Sections: Numerical Simulation and Assessment of Codified Design Approach. *International Journal of Steel Structures*, 2022. 22(6): p. 1695-1709.
-

REFERENCES

- [80] Rasmussen, K. and G. Hancock, Design of thin-walled plain channel section columns against flexural buckling. *Thin-walled structures*, 1994. 20(1-4): p. 219-240.
- [81] Young, B. and K.J. Rasmussen, Tests of fixed-ended plain channel columns. *Journal of Structural Engineering*, 1998. 124(2): p. 131-139.
- [82] Young, B. and K.J. Rasmussen, Design of lipped channel columns. *Journal of Structural Engineering*, 1998. 124(2): p. 140-148.
- [83] Becque, J. and K.J. Rasmussen, Experimental investigation of local-overall interaction buckling of stainless steel lipped channel columns. *Journal of Constructional Steel Research*, 2009. 65(8-9): p. 1677-1684.
- [84] Kesti, J. and J.M. Davies, Local and distortional buckling of thin-walled short columns. *Thin-walled structures*, 1999. 34(2): p. 115-134.
- [85] Yan, J. and B. Young, Column tests of cold-formed steel channels with complex stiffeners. *Journal of Structural Engineering*, 2002. 128(6): p. 737-745.
- [86] Yang, D. and G.J. Hancock, Compression tests of high strength steel channel columns with interaction between local and distortional buckling. *Journal of Structural Engineering*, 2004. 130(12): p. 1954-1963.
- [87] Kwon, Y.B., B.S. Kim, and G.J. Hancock, Compression tests of high strength cold-formed steel channels with buckling interaction. *Journal of Constructional Steel Research*, 2009. 65(2): p. 278-289.
- [88] Schafer, B.W. and T. Peköz, Laterally braced cold-formed steel flexural members with edge stiffened flanges. *Journal of Structural Engineering*, 1999. 125(2): p. 118-127.
- [89] Zhao, X. and B.W. Schafer, Laser scanning to develop three-dimensional fields for the precise geometry of cold-formed steel members. 2014.
- [90] Young, B., P. Dinis, and D. Camotim, CFS lipped channel columns affected by LDG interaction. Part I: Experimental investigation. *Computers & Structures*, 2018. 207: p. 219-232.
- [91] Chen, J., Y. He, and W.-L. Jin, Stub column tests of thin-walled complex section with intermediate stiffeners. *Thin-walled structures*, 2010. 48(6): p. 423-429.
- [92] Bhatti, A.A., Z. Barsoum, and M. Khurshid, Development of a finite element simulation framework for the prediction of residual stresses in large welded structures. *Computers & Structures*, 2014. 133: p. 1-11.
-

REFERENCES

- [93] Dinis, P.B., B. Young, and D. Camotim, Local–distortional interaction in cold-formed steel rack-section columns. *Thin-Walled Structures*, 2014. 81: p. 185-194.
- [94] Dinis, P.B., B. Young, and D. Camotim, Strength, interactive failure and design of web-stiffened lipped channel columns exhibiting distortional buckling. *Thin-Walled Structures*, 2014. 81: p. 195-209.
- [95] Kumar, M.A. and V. Kalyanaraman, Distortional buckling of CFS stiffened lipped channel compression members. *Journal of Structural Engineering*, 2014. 140(12): p. 04014099.
- [96] Martins, A.D., et al. Local–distortional interaction in cold-formed steel columns: Mechanics, testing, numerical simulation and design. in *Structures*. 2015. Elsevier.
- [97] Miller, T.H. and T. Pekoz, Load-eccentricity effects on cold-formed steel lipped-channel columns. *Journal of Structural Engineering*, 1994. 120(3): p. 805-823.
- [98] Polyzois, D. and P. Charnvarnichborikarn, Web-flange interaction in cold-formed steel Z-section columns. *Journal of Structural Engineering*, 1993. 119(9): p. 2607-2628.
- [99] Wang, C., et al., Compression tests and numerical analysis of web-stiffened channels with complex edge stiffeners. *Journal of constructional steel research*, 2016. 116: p. 29-39.
- [100] Yan, J. and B. Young, Numerical investigation of channel columns with complex stiffeners—part I: test verification. *Thin-walled structures*, 2004. 42(6): p. 883-893.
- [101] Young, B., Design of channel columns with inclined edge stiffeners. *Journal of Constructional Steel Research*, 2004. 60(2): p. 183-197.
- [102] Young, B. and G.J. Hancock, Cold-formed steel channels subjected to concentrated bearing load. *Journal of Structural Engineering*, 2003. 129(8): p. 1003-1010.
- [103] Bambach, M.R. and K.J. Rasmussen, Design provisions for sections containing unstiffened elements with stress gradient. *Journal of structural Engineering*, 2004. 130(10): p. 1620-1628.
- [104] Yu, C., Cold-formed steel flexural member with edge stiffened holes: Behavior, optimization, and design. *Journal of Constructional Steel Research*, 2012. 71: p. 210-218.
- [105] Dinis, P., et al., CFS lipped channel columns affected by LDG interaction. Part II: Numerical simulations and design considerations. *Computers & Structures*, 2018. 207: p. 200-218.
- [106] Kankanamge, N.D. and M. Mahendran, Behaviour and design of cold-formed steel beams subject to lateral–torsional buckling. *Thin-walled structures*, 2012. 51: p. 25-38.

REFERENCES

- [107] Keerthan, P. and M. Mahendran, Numerical modeling of littesteel beams subject to shear. *Journal of Structural Engineering*, 2011. 137(12): p. 1428-1439.
- [108] Ananthi, G.B.G., A study on cold-formed steel compound angle section subjected to axial compression. *KSCE Journal of Civil Engineering*, 2018. 22: p. 1803-1815.
- [109] Dangi, A., Nonlinear finite element bending analysis of Cold-Formed Steel of Z'section beams. 2017.
- [110] Roy, K., et al. Improved design rules on the buckling behaviour of axially loaded back-to-back cold-formed steel built-up channel sections. in *9th International Conference on Steel and Aluminium Structures (ICSAS19)*. 2019.
- [111] Garifullin, M. and U. Nackenhorst, Computational analysis of cold-formed steel columns with initial imperfections. *Procedia engineering*, 2015. 117: p. 1073-1079.
- [112] Ananthi, G., G. Palani, and N.R. Iyer, Numerical and theoretical studies on cold-formed steel unlippped channels subjected to axial compression. *Latin American Journal of Solids and Structures*, 2015. 12: p. 1-17.
- [113] Adeli, H. and A. Karim, Neural network model for optimization of cold-formed steel beams. *Journal of Structural Engineering*, 1997. 123(11): p. 1535-1543.
- [114] Lee, J., et al., Optimum design of cold-formed steel channel beams using micro Genetic Algorithm. *Engineering Structures*, 2005. 27(1): p. 17-24.
- [115] Lee, J., S.-M. Kim, and H.S. Park, Optimum design of cold-formed steel columns by using micro genetic algorithms. *Thin-Walled Structures*, 2006. 44(9): p. 952-960.
- [116] Tian, Y. and T. Lu, Minimum weight of cold-formed steel sections under compression. *Thin-Walled Structures*, 2004. 42(4): p. 515-532.
- [117] Leng, J., J.K. Guest, and B.W. Schafer, Shape optimization of cold-formed steel columns. *Thin-walled structures*, 2011. 49(12): p. 1492-1503.
- [118] Madeira, J., J. Dias, and N. Silvestre, Multiobjective optimization of cold-formed steel columns. *Thin-walled structures*, 2015. 96: p. 29-38.
- [119] Uzzaman, A., et al., Effects of edge-stiffened circular holes on the web crippling strength of cold-formed steel channel sections under one-flange loading conditions. *Engineering Structures*, 2017. 139: p. 96-107.
- [120] Ye, J., et al., Optimum design of cold-formed steel beams using Particle Swarm Optimisation method. *Journal of constructional steel research*, 2016. 122: p. 80-93.
-

REFERENCES

- [121] Dundu, M., Design approach of cold-formed steel portal frames. *International Journal of Steel Structures*, 2011. 11: p. 259-273.
- [122] Shifferaw, Y. and B. Schafer, Inelastic bending capacity of cold-formed steel members. *Journal of Structural Engineering*, 2012. 138(4): p. 468-480.
- [123] EN, C., 1-5: Eurocode 3—Design of steel structures—Part 1-5: Plated Structural Elements. CEN: Brussels, Belgium, 2006.
- [124] Gulvanessian, H., P. Formichi, and J.-A. Calgaro, *Designers' Guide to Eurocode 1: Actions on Buildings: EN1991-1-1 and-1-3 TO-1-7*. 2009: Thomas Telford Ltd.
- [125] Baehre, R., The testing of profiled metal sheets:(ECCS Publication No. 20 (1978),£ 3). *Thin-Walled Structures*, 1986. 4(1): p. 79-80.
- [126] PEKOZ, T. 40 TESTING OF THIN-WALLED STRUCTURES. in *Testing of Metals for Structures: Proceedings of the International Workshop "Needs in Testing Metals"*. 1992. Taylor & Francis.
- [127] Van Vuuren, J., *A Comparison Investigation into Analysis Methods to Determine the Buckling Capacity of South African Cold-Formed Steel Lipped Channel Sections*. 2020: University of Johannesburg (South Africa).
- [128] Hancock, G.J., *Design of Cold-formed steel structures: to Australian/New Zealand standard AS/NZS 4600: 2005*. 2007: Australian steel institute.
- [129] Hancock, G.J., T. Murray, and D.S. Ellifrit, *Cold-formed steel structures to the AISI specification*. 2001: CRC Press.
- [130] Dessouki, A., *Steel Structures Design*, Ain-Shams University. Dar ElMarfah Press.
- [131] Torabian, S., B. Zheng, and B. Schafer. Experimental study and modeling of cold-formed steel lipped channel stub beam-columns. in *Proceedings of the Annual Stability Conference Structural Stability Research Council*. 2014.
- [132] Iron, A. and S. Institute, *North American specification for the design of cold-formed steel structural members*. 2007: American Iron & Steel Institute, Committee of Steel Plate Producers
....
- [133] Abdel-Rahman, N. and K. Sivakumaran, Material properties models for analysis of cold-formed steel members. *Journal of Structural Engineering*, 1997. 123(9): p. 1135-1143.
- [134] Ellobody, E. and B. Young, Structural performance of cold-formed high strength stainless steel columns. *Journal of Constructional Steel Research*, 2005. 61(12): p. 1631-1649.
-

REFERENCES

- [135] Schafer, B.W. and T. Peköz, Computational modeling of cold-formed steel: characterizing geometric imperfections and residual stresses. *Journal of constructional steel research*, 1998. 47(3): p. 193-210.
- [136] Zeinoddini, V. and B. Schafer. Simulation of geometric imperfections in cold-formed steel members. in *Proceedings of the Annual Stability Conference, Structural Stability Research Council, SSRC*. 2012.
- [137] Galambos, T.V., *Guide to stability design criteria for metal structures*. 1998: John Wiley & Sons.
- [138] Chou, S., G. Chai, and L. Ling, Finite element technique for design of stub columns. *Thin-walled structures*, 2000. 37(2): p. 97-112.
- [139] Gardner, L. and D. Nethercot, Numerical modeling of stainless steel structural components—a consistent approach. *Journal of structural Engineering*, 2004. 130(10): p. 1586-1601.
- [140] Camotim, D., N. Silvestre, and P.B. Dinis, Numerical analysis of cold-formed steel members. *International Journal of Steel Structures*, 2005. 5(1): p. 63-78.
- [141] Ashraf, M., L. Gardner, and D.A. Nethercot, Finite element modelling of structural stainless steel cross-sections. *Thin-walled structures*, 2006. 44(10): p. 1048-1062.
- [142] Dinis, P.B., D. Camotim, and N. Silvestre, FEM-based analysis of the local-plate/distortional mode interaction in cold-formed steel lipped channel columns. *Computers & Structures*, 2007. 85(19-20): p. 1461-1474.
- [143] Schafer, B.W., Z. Li, and C.D. Moen, Computational modeling of cold-formed steel. *Thin-walled structures*, 2010. 48(10-11): p. 752-762.
- [144] Pham, C.H. and G.J. Hancock, Numerical simulation of high strength cold-formed purlins in combined bending and shear. *Journal of Constructional Steel Research*, 2010. 66(10): p. 1205-1217.
- [145] Schafer, B.W. and S. Adany. Buckling analysis of cold-formed steel members using CUFSM: conventional and constrained finite strip methods. in *Eighteenth international specialty conference on cold-formed steel structures*. 2006. Citeseer.
- [146] Haidarali, M.R. and D.A. Nethercot, Finite element modelling of cold-formed steel beams under local buckling or combined local/distortional buckling. *Thin-Walled Structures*, 2011. 49(12): p. 1554-1562.
-

APPENDIX (A)

A.1 Elastic Straining Actions

It simply became easy to get the elastic buckling straining actions of any cold-formed steel cross-section by freely, available, open source software, such as CUFSM, CFS and THIN-WALL or by manual elastic buckling calculation.

A.1.1 Software solution of elastic straining actions

There are three software, which depend on the finite strip method, and are known to determine elastic buckling such as CUFSM, CFS and THIN-WALL. The analyses used in this research deal with CUFSM [29] program. The main steps for performing CUFSM [29] analysis are:-

➤ Define the cross-section geometry.

In this step, the engineer enters the description of the cross section in terms of materials, dimensions, thickness, shape (c or z) and location of different nodes or he can also select and choose one of the standards and well-known sections within the program, as shown in **Figures A.1, A.2 & A.3.**

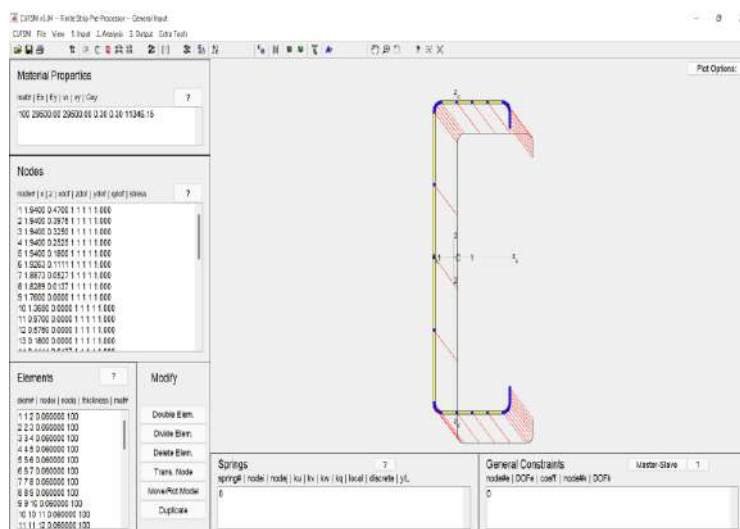


Figure A.1: - Interface of CUFSM program.

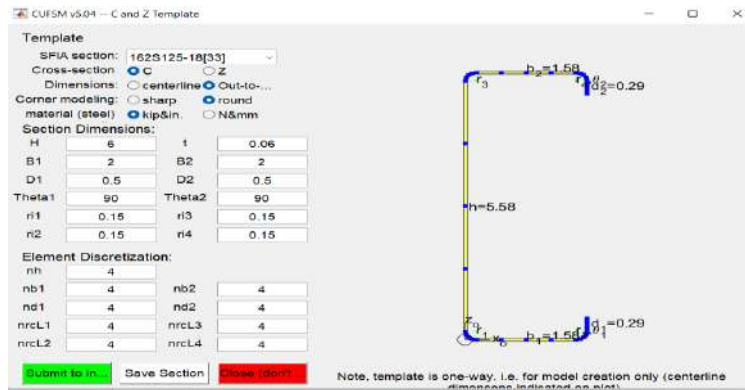


Figure A.2: - Insert a desire CFS dimensions.

Standard cross sections

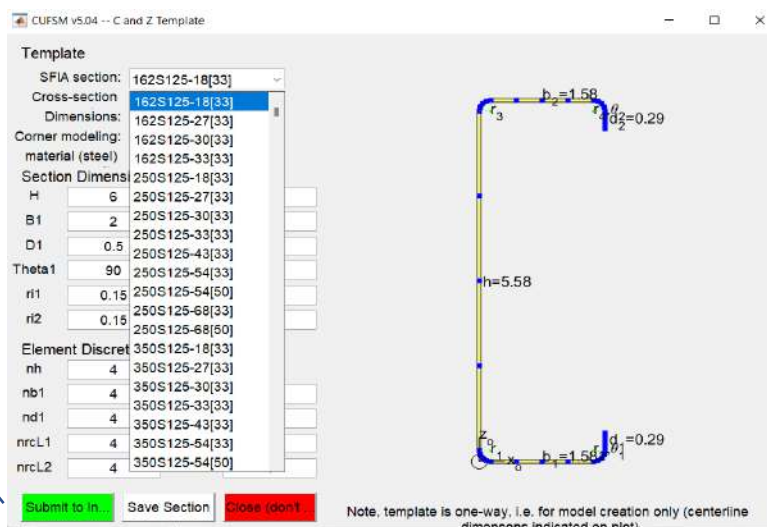


Figure A.3: - Choose a specific known dimension of standard AISI section.

➤ Define the applied (reference) stress.

In this step, the engineer enters loads and stresses for the studied cold formed section. If the cross section is due to applied load in the center of gravity (C_g), use the first yield calculator list (inputs on the right side). When using the first yield calculator list, just enter the yield stress (F_y) and click on P_y button for compression member and M_{xxy} (use geometric axes) or M_{11y} (use principles axes) buttons for flexural member so that the stress is directly inputted. If the cross section is due to more than moments in different directions or there is eccentricity during loading, deal with the reference applied loads list (inputs on the left side) , as shown in Figures A.4 & A.5.

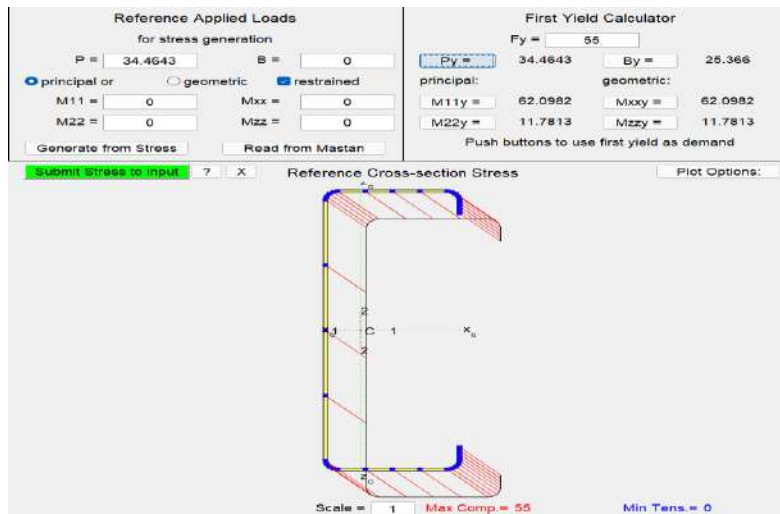


Figure A.4: - Define the applied compressive stress.

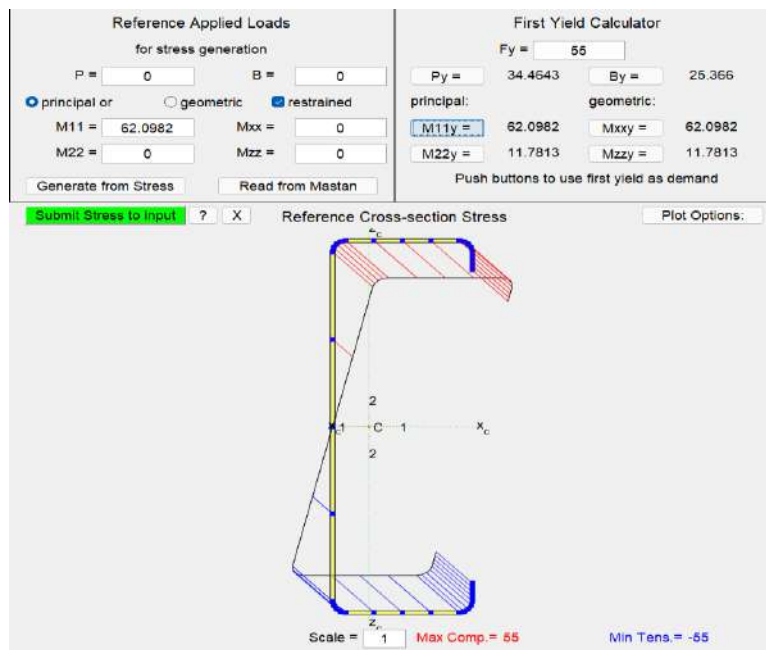


Figure A.5: - Define the applied flexural stress.

➤ **Define the half-wavelengths to be investigated.**

In this step, the engineer defines half-wavelength, number of eigenvalues and boundary conditions of the studied section, as shown in **Figure A.6**.

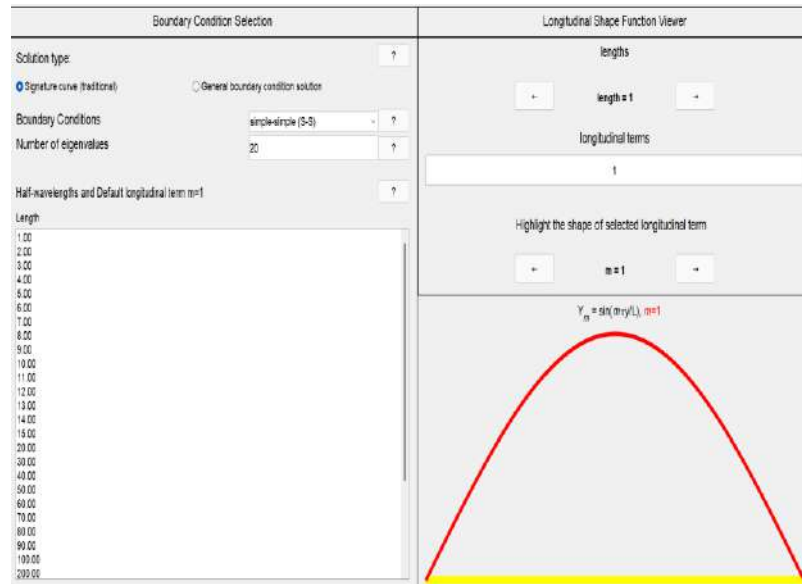


Figure A.6: - Define the half-wavelength of CFS.

➤ Perform an elastic buckling analysis

In this step, the engineer gets the curve between the load (or moment) factor (P_{cr}/P_y) vs. half-wavelength, so he can simply determine the minimum load-factors for each mode shape and define buckling straining actions (moment or load), i.e. local (M_{crL} or P_{crL}), distortional (M_{crd} or P_{crd}), global buckling (M_{cre} or P_{cre}), as shown in **Figure A.7**.

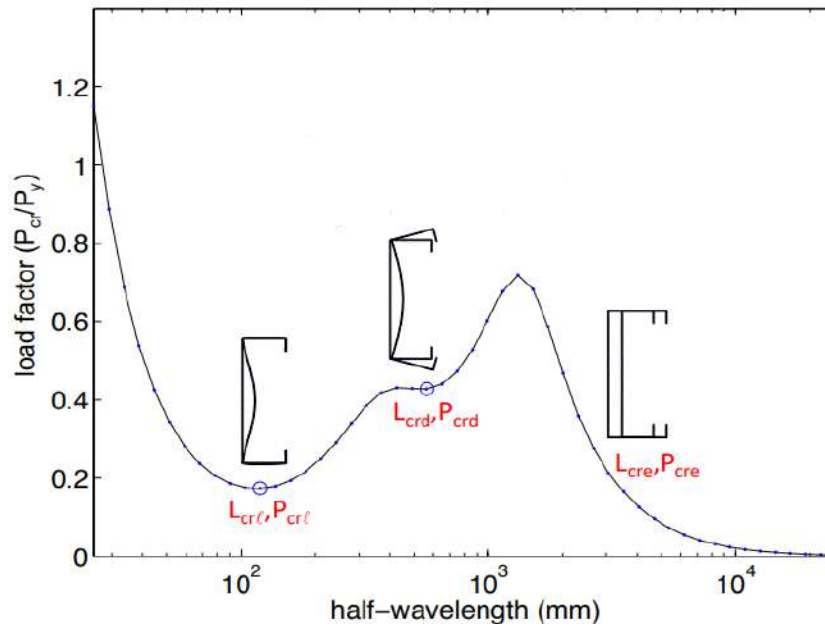
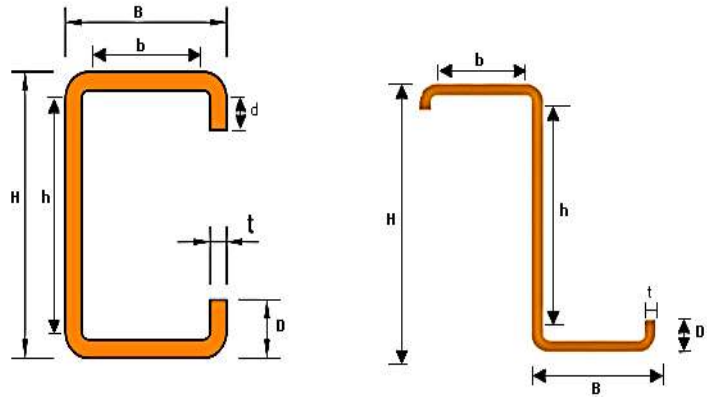


Figure A.7: - The load factor and half-wavelength curve.

A.1.2 Numerical solution of elastic straining actions

Note: - $b' = B - t$
 $a' = H - t$
 $c' = D - t/2$



A.1.2.1 Compression Member

• **Local Buckling (P_{cr1})**

➤ For unstiffened channel (Use element method)

Flange local buckling

$$K_{flange} = .43 \tag{A-1}$$

$$F_{cr_flange} = K_{flange} * \frac{\pi^2 * E}{12 * (1 - \nu^2)} * \left(\frac{t}{b'} \right)^2 \tag{A-2}$$

Web local buckling

$$K_{web} = 4 \tag{A-3}$$

$$F_{cr_web} = K_{web} * \frac{\pi^2 * E}{12 * (1 - \nu^2)} * \left(\frac{t}{a'} \right)^2 \tag{A-4}$$

$$F_{cr1} = \min \text{ of } (F_{cr_flange} , F_{cr_web}) \tag{A-5}$$

$$A_g = (a' + 2b') * t \tag{A-6}$$

$$P_{cr1} = A_g * F_{cr1} \tag{A-7}$$

➤ For lipped (stiffened) channel

- If $\frac{c'}{b'} < .6$ use Interaction method

Flange / lip local buckling

$$K_{flange_lip} = - 11.07 * \left(\frac{c'}{b'} \right)^2 + 3.95 * \left(\frac{c'}{b'} \right) + 4 \tag{A-8}$$

$$F_{cr_flange_lip} = K_{flange_lip} * \frac{\pi^2 * E}{12 * (1 - \nu^2)} * \left(\frac{t}{b'} \right)^2 \tag{A-9}$$

Flange / Web local buckling

$$K_{flange_web} = \begin{cases} \left[2 - \left(\frac{b'}{a'} \right)^4 \right] * 4 * \left(\frac{b'}{a'} \right)^2 & \text{if } \frac{a'}{b'} \geq 1 \\ \left[2 - \left(\frac{a'}{b'} \right)^2 \right] * 4 & \text{if } \frac{a'}{b'} < 1 \end{cases} \tag{A-10}$$

$$F_{cr_flange_web} = K_{flange_web} * \frac{\pi^2 * E}{12 * (1 - \nu^2)} * \left(\frac{t}{b'} \right)^2 \quad (A-11)$$

$$F_{cr1} = \min \text{ of } (F_{cr_flange_lip} , F_{cr_flange_web}) \quad (A-12)$$

$$A_g = (a' + 2b' + 2C') * t \quad (A-13)$$

$$P_{cr1} = A_g * F_{cr1} \quad (A-14)$$

- If $\frac{c'}{b'} \geq .6$ use element method

Flange local buckling

$$K_{flange} = 4 \quad (A-15)$$

$$F_{cr_flange} = K_{flange} * \frac{\pi^2 * E}{12 * (1 - \nu^2)} * \left(\frac{t}{b'} \right)^2 \quad (A-16)$$

Web local buckling

$$K_{web} = 4 \quad (A-17)$$

$$F_{cr_web} = K_{web} * \frac{\pi^2 * E}{12 * (1 - \nu^2)} * \left(\frac{t}{a'} \right)^2 \quad (A-18)$$

Lip local buckling

$$K_{lip} = .43 \quad (A-19)$$

$$F_{cr_lip} = K_{lip} * \frac{\pi^2 * E}{12 * (1 - \nu^2)} * \left(\frac{t}{c'} \right)^2 \quad (A-20)$$

$$F_{cr1} = \min \text{ of } (F_{cr_flange} , F_{cr_web} , F_{cr_lip}) \quad (A-21)$$

$$A_g = (a' + 2b' + 2C') * t \quad (A-22)$$

$$P_{cr1} = A_g * F_{cr1} \quad (A-23)$$

• **Distortional Buckling (P_{crd})**

Properties of flange only :-

$$A_f = (b' + c') * t \quad (A-24)$$

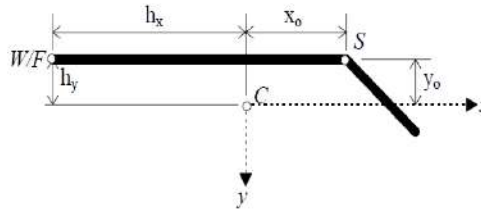
$$J_f = \frac{1}{3} * b' * t^3 + \frac{1}{3} * c' * t^3 \quad (A-25)$$

$$I_{xf} = \frac{t * [t^2 * (b')^2 + 4 * b' * (c')^3 + t^2 * b' * c' + (c')^4]}{12 * (b' + c')} \quad (A-26)$$

$$I_{yf} = \frac{t * [(b')^4 + 4 * c' * (b')^3]}{12 * (b' + c')} \quad (A-27)$$

$$I_{xyf} = \frac{t * (b')^2 * (c')^2}{4 * (b' + c')} \quad (A-28)$$

$$I_{of} = \frac{t * (b')^3}{3} + \frac{b' * t^3}{12} + \frac{t * (c')^3}{3} \quad (A-29)$$



$$X_{of} = \frac{(b')^2}{2*(b'+c')} \quad (A-30)$$

$$Y_{of} = \frac{-(c')^2}{2*(b'+c')} \quad (A-31)$$

$$h_{xf} = \frac{-[(b')^2+2*b'*c']}{2*(b'+c')} \quad (A-32)$$

$$h_{yf} = \frac{-(c')^2}{2*(b'+c')} \quad (A-33)$$

$$C_{wf} = \text{zero} \quad (A-34)$$

$$L_{cr} = \left[\frac{6*\pi^4*a'*(1-\nu^2)}{t^3} * \left[I_{xf} * (x_{of} - h_{xf})^2 + c_{wf} - \frac{I_{xyf}^2}{I_{yf}} * (x_{of} - h_{xf})^2 \right] \right]^{\frac{1}{4}} \leq L_u \quad (A-35)$$

Determine the elastic and “geometric” rotational spring stiffness of the flange :-

$$k_{\phi fe} = \left(\frac{\pi}{L_{cr}} \right)^4 * \left[E * I_{xf} * (x_{of} - h_{xf})^2 + E * c_{wf} - E * \frac{I_{xyf}^2}{I_{yf}} * (x_{of} - h_{xf})^2 \right] + \left(\frac{\pi}{L_{cr}} \right)^2 * G * J_f \quad (A-36)$$

$$k_{\phi fg} = \left(\frac{\pi}{L_{cr}} \right)^2 * \left[A_f * \left[(x_{of} - h_{xf})^2 * \left(\frac{I_{xyf}}{I_{yf}} \right) - 2 * y_{of} * (x_{of} - h_{xf}) * \left(\frac{I_{xyf}}{I_{yf}} \right) + h_{xf}^2 + y_{of}^2 \right] + I_{xf} + I_{yf} \right] \quad (A-37)$$

Determine the elastic and “geometric” rotational spring stiffness of the web :

$$k_{\phi we} = \frac{t^3 * E}{6 * a' * (1-\nu^2)} \quad (A-38)$$

$$k_{\phi wg} = \left(\frac{\pi}{L_{cr}} \right)^2 * \frac{t * (a')^3}{60} \quad (A-39)$$

Determine the distortional buckling stress:

$$F_{crd} = \frac{k_{\phi fe} + k_{\phi we}}{k_{\phi fg} + k_{\phi wg}} \quad (A-40)$$

$$P_{crd} = A_g * F_{crd} \quad (A-41)$$

- **Global Buckling (P_{cre})**

Individual buckling modes

$$\sigma_{ex} = \frac{\pi^2 * E}{\left(\frac{K_x * L_x}{r_x} \right)^2} \quad (A-42)$$

$$\sigma_{ey} = \frac{\pi^2 * E}{\left(\frac{K_y * L_y}{r_y}\right)^2} \quad (\text{A-43})$$

$$F_{e1} = \min \text{ of } (\sigma_{ex} , \sigma_{ey}) \quad (\text{A-44})$$

$$r_0 = \sqrt{r_x^2 + r_y^2 + x_0^2} \quad (\text{A-45})$$

$$\sigma_t = \frac{1}{A * (r_0)^2} * \left[G * J + \frac{\pi^2 * E * C_w}{(K_t * L_t)^2} \right] \quad (\text{A-46})$$

Torsional flexural buckling

$$\beta = 1 - \left(\frac{x_0}{r_0}\right)^2 \quad (\text{A-47})$$

$$F_{e2} = \frac{1}{2 * \beta} * \left[(\sigma_{ex} + \sigma_t) - \sqrt{(\sigma_{ex} + \sigma_t)^2 - 4 * \beta * \sigma_{ex} * \sigma_t} \right] \quad (\text{A-48})$$

$$F_{cre} = \min \text{ of } (F_{e1} , F_{e2}) \quad (\text{A-49})$$

$$P_{cre} = A * F_{cre} \quad (\text{A-50})$$

A.2.2 Flexural Member

• Local Buckling (M_{crl})

➤ For unstiffened channel (Use element method)

Flange local buckling

$$K_{flange} = .43 \quad (\text{A-51})$$

$$F_{cr_flange} = K_{flange} * \frac{\pi^2 * E}{12 * (1 - \nu^2)} * \left(\frac{t}{b'}\right)^2 \quad (\text{A-52})$$

Web local buckling

$$K_{web} = 24 \quad (\text{A-53})$$

$$F_{cr_web} = K_{web} * \frac{\pi^2 * E}{12 * (1 - \nu^2)} * \left(\frac{t}{a'}\right)^2 \quad (\text{A-54})$$

$$F_{crl} = \min \text{ of } (F_{cr_flange} , F_{cr_web}) \quad (\text{A-55})$$

$$S_g = I_x / (H/2) \quad (\text{A-56})$$

$$M_{crl} = S_g * F_{crl} \quad (\text{A-57})$$

➤ For lipped (stiffened) channel

$$\text{Stress at extreme fiber } f_1 = 1 \quad \& \quad \text{stress at lip end } f_2 = \frac{.5 * H - C'}{.5 * H}$$

$$\varepsilon = (f_1 - f_2) / f_1 \quad (\text{A-58})$$

▪ If $\frac{C'}{b'} < .6$ & $\varepsilon < 1$ use Interaction method

Flange / lip local buckling

$$K_{\text{flange_lip}} = (8.55 * \varepsilon - 11.07) * \left(\frac{c'}{b'}\right)^2 + (3.95 - 1.59 * \varepsilon) * \left(\frac{c'}{b'}\right) + 4 \quad (\text{A-59})$$

$$F_{\text{cr_flange_lip}} = K_{\text{flange_lip}} * \frac{\pi^2 * E}{12 * (1 - \nu^2)} * \left(\frac{t}{b'}\right)^2 \quad (\text{A-60})$$

Flange / Web local buckling

Stress gradient on the web $f_1 = 1$ & $f_2 = -1$, so $\varepsilon = (f_1 - f_2) / f_1$

$$K_{\text{flange_web}} = 1.125 * \min \text{ of } \left\{ \begin{array}{l} [.5 * \varepsilon^3 + 4 * \varepsilon^2 + 4] * \left(\frac{b'}{a'}\right)^2 \\ 4 \end{array} \right. \quad (\text{A-61})$$

$$F_{\text{cr_flange_web}} = K_{\text{flange_web}} * \frac{\pi^2 * E}{12 * (1 - \nu^2)} * \left(\frac{t}{b'}\right)^2 \quad (\text{A-62})$$

$$F_{\text{crl}} = \min \text{ of } (F_{\text{cr_flange_lip}}, F_{\text{cr_flange_web}}) \quad (\text{A-63})$$

$$S_g = I_X / (H/2) \quad (\text{A-64})$$

$$M_{\text{crl}} = S_g * F_{\text{crl}} \quad (\text{A-65})$$

- If $\frac{c'}{b'} \geq .6$ & $\varepsilon > 1$ use element method

Flange local buckling

$$K_{\text{flange}} = 4 \quad (\text{A-66})$$

$$F_{\text{cr_flange}} = K_{\text{flange}} * \frac{\pi^2 * E}{12 * (1 - \nu^2)} * \left(\frac{t}{b'}\right)^2 \quad (\text{A-67})$$

Web local buckling

$$K_{\text{web}} = 24 \quad (\text{A-68})$$

$$F_{\text{cr_web}} = K_{\text{web}} * \frac{\pi^2 * E}{12 * (1 - \nu^2)} * \left(\frac{t}{a'}\right)^2 \quad (\text{A-69})$$

Lip local buckling

Stress at extreme fiber $f_1 = 1$ & stress at lip end $f_2 = \frac{.5 * H - c'}{.5 * H}$

$$\varepsilon = (f_1 - f_2) / f_1 \quad (\text{A-70})$$

$$K_{\text{lip}} = 1.4 * \varepsilon^2 - .25 * \varepsilon + .425 \quad (\text{A-71})$$

$$F_{\text{cr_lip}} = K_{\text{lip}} * \frac{\pi^2 * E}{12 * (1 - \nu^2)} * \left(\frac{t}{c'}\right)^2 \quad (\text{A-72})$$

$$F_{\text{crl}} = \min \text{ of } (F_{\text{cr_flange}}, F_{\text{cr_web}}, F_{\text{cr_lip}}) \quad (\text{A-73})$$

$$M_{\text{crl}} = S_g * F_{\text{crl}} \quad (\text{A-74})$$

- **Distortional Buckling (M_{crd})**

$$L_{cr} = \left[\frac{4\pi^4 a' (1-\nu^2)}{t^3} * \left[I_{xf} * (X_{of} - h_{xf})^2 + C_{wf} - \frac{I_{xyf}^2}{I_{yf}} * (X_{of} - h_{xf})^2 \right] + \frac{\pi^4 (a')^4}{720} \right]^{\frac{1}{4}} \leq L_u \quad (A-75)$$

$$K_{\emptyset fe} = \left(\frac{\pi}{L_{cr}} \right)^4 * \left[E * I_{xf} * (X_{of} - h_{xf})^2 + E * C_{wf} - E * \frac{I_{xyf}^2}{I_{yf}} * (X_{of} - h_{xf})^2 \right] + \left(\frac{\pi}{L_{cr}} \right)^2 * G * J_f \quad (A-76)$$

$$K_{\emptyset fg} = \left(\frac{\pi}{L_{cr}} \right)^2 * \left[A_f * \left[\left(\frac{I_{xyf}}{I_{yf}} \right)^2 * (X_{of} - h_{xf})^2 - 2 * y_{of} * (X_{of} - h_{xf}) * \left(\frac{I_{xyf}}{I_{yf}} \right) + h_{xf}^2 + y_{of}^2 \right] + I_{xf} + I_{yf} \right] \quad (A-77)$$

$$K_{\emptyset we} = \frac{E * t^3}{12 * (1-\nu^2)} * \left[\frac{3}{a'} + \left(\frac{\pi}{L_{cr}} \right)^2 * \frac{19 * a'}{60} + \left(\frac{\pi}{L_{cr}} \right)^4 * \frac{(a')^3}{240} \right] \quad (A-78)$$

Earlier Stress gradient on web $\psi = -1$

$$K_{\emptyset wg} = \frac{a' * t * \pi^2}{13440} * \frac{(45360 * \psi + 62160) * \left(\frac{L_{cr}}{a'} \right)^2 + 448 * \pi^2 + \left(\frac{a'}{L_{cr}} \right)^2 * (53 + 3\psi) * \pi^4}{\pi^4 + 28 * \pi^2 * \left(\frac{L_{cr}}{a'} \right)^2 + 420 * \left(\frac{L_{cr}}{a'} \right)^4} \quad (A-79)$$

$$f_{crd} = \frac{K_{\emptyset fe} + K_{\emptyset we}}{K_{\emptyset fg} + K_{\emptyset wg}} \quad (A-80)$$

$$M_{crd} = S_g * f_{crd} \quad (A-81)$$

- **Global Buckling (M_{cre})**

$$\sigma_{ey} = \frac{\pi^2 * E}{\left(\frac{K_y * l_y}{r_y} \right)^2} \quad (A-82)$$

$$\sigma_t = \frac{1}{A * (r_0)^2} * \left[G * J + \frac{\pi^2 * E * C_w}{(K_t * L_t)^2} \right] \quad (A-83)$$

$$F_e = \frac{C_b * r_0 * A}{S_g} * \sqrt{\sigma_{ey} * \sigma_t} \quad (A-84)$$

$$f_{cre} = F_e \quad (A-85)$$

$$M_{cre} = S_g * f_{cre} \quad (A-86)$$

A.2. FEM Failure Mode Used in Parametric Study

A.2.1 Length-to-Web Plate Depth Ratio (L/h) Parameter

A.2.1.1 Flexural channel section

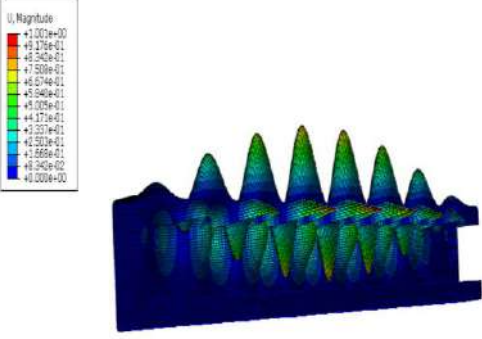
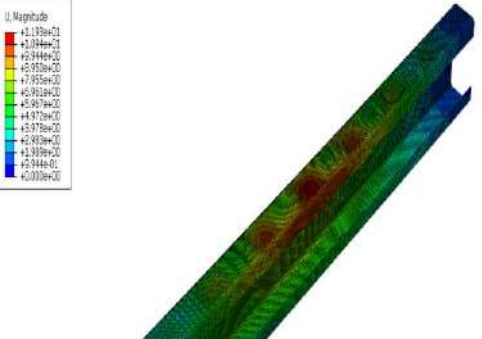
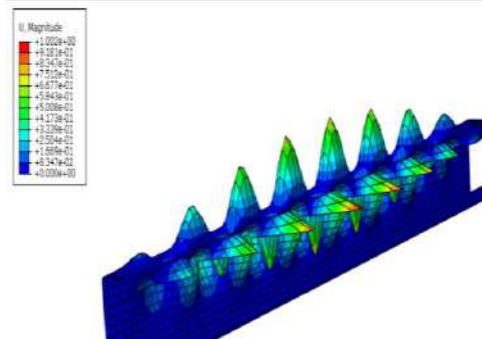
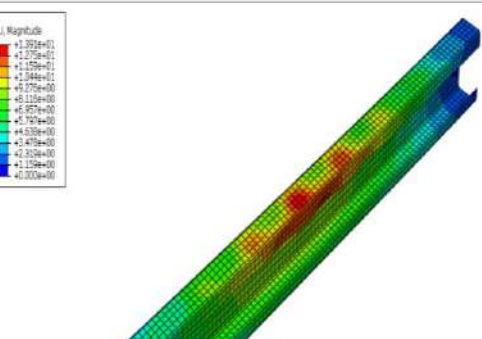
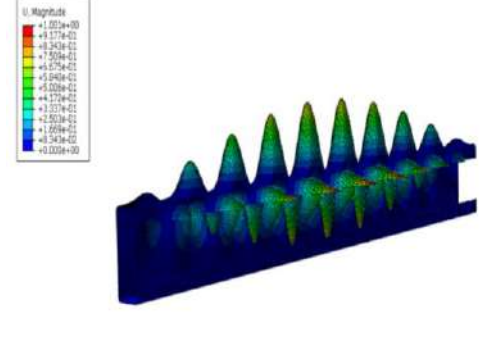
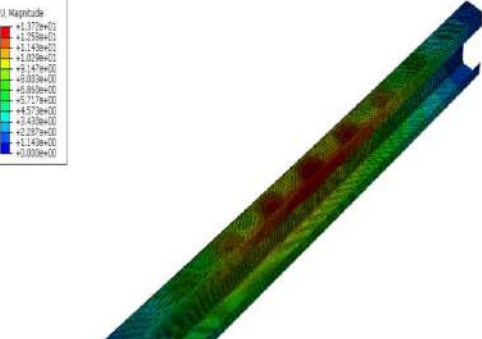
In **Table A-1**, we see that the channel section collapses due to combination of local and distortion buckling until a length-to-web plate depth ratio (L/h) equals 4. After this ratio, the channel section collapses due to combination of local, distortion and global buckling.

Table A-1: - Various FEM modes for flexural channel with different L/h ratios.

Flexural channel FEM modes				
L/h	Buckling mode	Failure mode		
1	<p>U, Magnitude +1.000e+00 +0.800e-01 +0.600e-01 +0.400e-01 +0.200e-01 +0.000e+00 -0.200e-01 -0.400e-01 -0.600e-01 -0.800e-01 -1.000e+00</p> <p>Step: Step-1 Mode: 1; EigenValue = 2.89490E+07 Primary Var: U, Magnitude Deformed Var: U, Deformation Scale Factor: +2.000e+02</p>	<p>U, Magnitude +2.200e+00 +2.000e+00 +1.800e+00 +1.600e+00 +1.400e+00 +1.200e+00 +1.000e+00 +0.800e+00 +0.600e+00 +0.400e+00 +0.200e+00 +0.000e+00</p> <p>Step: Step-1 Increment: 27; Arc Length = 7.5751E+04 Primary Var: U, Magnitude Deformed Var: U, Deformation Scale Factor: +1.000e+02</p>		
2	<p>U, Magnitude +1.001e+00 +0.801e-01 +0.601e-01 +0.401e-01 +0.201e-01 +0.001e+00 -0.201e-01 -0.401e-01 -0.601e-01 -0.801e-01 -1.001e+00</p> <p>Step: Step-1 Mode: 1; EigenValue = 2.51430E+07 Primary Var: U, Magnitude Deformed Var: U, Deformation Scale Factor: +4.000e+01</p>	<p>U, Magnitude +4.455e+00 +4.000e+00 +3.500e+00 +3.000e+00 +2.500e+00 +2.000e+00 +1.500e+00 +1.000e+00 +0.500e+00 +0.000e+00</p> <p>Step: Step-1 Increment: 26; Arc Length = 5.0501E+04 Primary Var: U, Magnitude Deformed Var: U, Deformation Scale Factor: +1.000e+00</p>		

Flexural channel FEM modes		
L/h	Buckling mode	Failure mode
3	<p>U, Magnitude +1.000e+02 +1.178e+01 +1.344e+01 +1.509e+01 +1.675e+01 +1.841e+01 +2.007e+01 +2.172e+01 +2.338e+01 +2.504e+01 +2.669e+01 +2.835e+01 +3.000e+01</p> <p>OOB: nonbuckling... Step: Step-1 Mode: 1, Eigenvalue = 1.000e+02 Primary Var: U, Magnitude Deformed Var: U, Deformation Scale Factor: +1.000e+02</p>	<p>U, Magnitude +1.590e+00 +1.490e+00 +1.390e+00 +1.290e+00 +1.190e+00 +1.090e+00 +9.90e-01 +8.90e-01 +7.90e-01 +6.90e-01 +5.90e-01 +4.90e-01 +3.90e-01 +2.90e-01 +1.90e-01 +9.00e-02 +0.000e+00</p> <p>OOB: non20043JOB... Step: Step-1 Increment: 20, Air Length = 1.000e+00 Primary Var: U, Magnitude Deformed Var: U, Deformation Scale Factor: +1.000e+00</p>
4	<p>U, Magnitude +1.000e+00 +9.178e-01 +8.344e-01 +7.509e-01 +6.675e-01 +5.841e-01 +5.007e-01 +4.172e-01 +3.338e-01 +2.504e-01 +1.669e-01 +8.35e-02 +0.000e+00</p> <p>OOB: nonbuckling... Step: Step-1 Mode: 1, Eigenvalue = 1.000e+00 Primary Var: U, Magnitude Deformed Var: U, Deformation Scale Factor: +1.000e+00</p>	<p>U, Magnitude +4.500e+00 +4.190e+00 +3.870e+00 +3.550e+00 +3.230e+00 +2.910e+00 +2.590e+00 +2.270e+00 +1.950e+00 +1.630e+00 +1.310e+00 +9.90e-01 +6.70e-01 +3.50e-01 +0.000e+00</p> <p>OOB: non2004H... Step: Step-1 Increment: 20, Air Length = 1.000e+00 Primary Var: U, Magnitude Deformed Var: U, Deformation Scale Factor: +1.000e+00</p>
5	<p>U, Magnitude +1.000e+00 +9.178e-01 +8.344e-01 +7.509e-01 +6.675e-01 +5.841e-01 +5.007e-01 +4.172e-01 +3.338e-01 +2.504e-01 +1.669e-01 +8.35e-02 +0.000e+00</p> <p>OOB: nonbuckling... Step: Step-1 Mode: 1, Eigenvalue = 1.000e+01 Primary Var: U, Magnitude Deformed Var: U, Deformation Scale Factor: +1.000e+02</p>	<p>U, Magnitude +5.200e+00 +4.800e+00 +4.400e+00 +4.000e+00 +3.600e+00 +3.200e+00 +2.800e+00 +2.400e+00 +2.000e+00 +1.600e+00 +1.200e+00 +8.00e-01 +4.00e-01 +0.000e+00</p> <p>OOB: non200... Step: Step-1 Increment: 27, Air Length = 1.000e+00 Primary Var: U, Magnitude Deformed Var: U, Deformation Scale Factor: +1.000e+00</p>

Flexural channel FEM modes			
L/h	Buckling mode	Failure mode	
6	<p>U Magnitude +1.001e+00 +9.178e-01 +8.344e-01 +7.509e-01 +6.675e-01 +5.841e-01 +5.006e-01 +4.172e-01 +3.337e-01 +2.503e-01 +1.669e-01 +8.344e-02 +0.000e+00</p> <p>Step: Step-1 Mode: 1 Eigenvalue = 2.4322E+07 Primary Var: U Magnitude Deformed Var: U Deformation Scale Factor: +1.000e+00</p>	<p>U Magnitude +8.265e+00 +7.431e+00 +6.596e+00 +5.762e+00 +4.928e+00 +4.094e+00 +3.259e+00 +2.425e+00 +1.591e+00 +7.566e-01 +0.000e+00</p> <p>Step: Step-1 Increment: 1 Mode: 1 Eigenvalue = 2.4639E+04 Primary Var: U Magnitude Deformed Var: U Deformation Scale Factor: +1.000e+00</p>	
7	<p>U Magnitude +1.001e+00 +9.178e-01 +8.344e-01 +7.509e-01 +6.675e-01 +5.841e-01 +5.006e-01 +4.172e-01 +3.337e-01 +2.503e-01 +1.669e-01 +8.344e-02 +0.000e+00</p> <p>Step: Step-1 Mode: 1 Eigenvalue = 2.3992E+07 Primary Var: U Magnitude Deformed Var: U Deformation Scale Factor: +1.000e+00</p>	<p>U Magnitude +7.606e+00 +6.772e+00 +5.938e+00 +5.104e+00 +4.270e+00 +3.436e+00 +2.602e+00 +1.768e+00 +9.34e-01 +0.000e+00</p> <p>Step: Step-1 Increment: 1 Mode: 1 Eigenvalue = 2.2444E+04 Primary Var: U Magnitude Deformed Var: U Deformation Scale Factor: +1.000e+00</p>	
8	<p>U Magnitude +1.001e+00 +9.178e-01 +8.344e-01 +7.509e-01 +6.675e-01 +5.841e-01 +5.006e-01 +4.172e-01 +3.337e-01 +2.503e-01 +1.669e-01 +8.344e-02 +0.000e+00</p> <p>Step: Step-2 Mode: 1 Eigenvalue = 2.3972E+07 Primary Var: U Magnitude Deformed Var: U Deformation Scale Factor: +1.000e+00</p>	<p>U Magnitude +6.467e+00 +5.633e+00 +4.799e+00 +3.965e+00 +3.131e+00 +2.297e+00 +1.463e+00 +6.29e-01 +0.000e+00</p> <p>Step: Step-1 Increment: 1 Mode: 1 Eigenvalue = 2.2444E+04 Primary Var: U Magnitude Deformed Var: U Deformation Scale Factor: +1.000e+00</p>	

Flexural channel FEM modes		
L/h	Buckling mode	Failure mode
9	 <p>U, Magnitude</p> <ul style="list-style-type: none"> +1.002e+00 +9.176e-01 +6.542e-01 +7.503e-01 +6.674e-01 +5.546e-01 +6.029e-01 +4.171e-01 +3.207e-01 +1.201e-01 +1.566e-01 +6.245e-02 +0.000e+00 <p>Step: Step-1 Mode: 1 EigenValue = 0.39561e+07 Primary Var: U, Magnitude Deformed Var: U Deformation Scale Factor: +1.000e+02</p>	 <p>U, Magnitude</p> <ul style="list-style-type: none"> +1.138e+01 +1.044e+01 +9.949e+00 +6.950e+00 +7.955e+00 +6.903e+00 +5.949e+00 +4.977e+00 +5.978e+00 +2.939e+00 +1.939e+00 +9.944e-01 +0.000e+00 <p>Step: Step-1 Increment: 1 Length = 2.2108e+04 Primary Var: U, Magnitude Deformed Var: U Deformation Scale Factor: +1.000e+02</p>
10	 <p>U, Magnitude</p> <ul style="list-style-type: none"> +1.002e+00 +8.123e-01 +6.411e-01 +7.503e-01 +6.674e-01 +5.546e-01 +4.170e-01 +3.207e-01 +1.201e-01 +1.566e-01 +6.245e-02 +0.000e+00 <p>Step: Step-1 Mode: 1 EigenValue = 2.61630e+07 Primary Var: U, Magnitude Deformed Var: U Deformation Scale Factor: +2.000e+02</p>	 <p>U, Magnitude</p> <ul style="list-style-type: none"> +1.395e+01 +1.275e+01 +1.255e+01 +1.044e+01 +6.975e+00 +6.116e+00 +4.957e+00 +5.767e+00 +4.630e+00 +3.405e+00 +2.204e+00 +1.126e+00 +0.000e+00 <p>Step: Step-1 Increment: 1 Length = 2.2446e+04 Primary Var: U, Magnitude Deformed Var: U Deformation Scale Factor: +1.000e+02</p>
11	 <p>U, Magnitude</p> <ul style="list-style-type: none"> +1.002e+00 +9.177e-01 +6.343e-01 +7.503e-01 +6.578e-01 +5.040e-01 +5.038e-01 +4.170e-01 +3.207e-01 +1.201e-01 +1.566e-01 +6.243e-02 +0.000e+00 <p>Step: Step-1 Mode: 1 EigenValue = 2.59250e+07 Primary Var: U, Magnitude Deformed Var: U Deformation Scale Factor: +2.000e+02</p>	 <p>U, Magnitude</p> <ul style="list-style-type: none"> +1.377e+01 +1.258e+01 +1.438e+01 +1.029e+01 +1.147e+01 +1.033e+01 +6.892e+00 +5.713e+00 +4.573e+00 +3.430e+00 +2.207e+00 +1.438e+00 +0.000e+00 <p>Step: Step-1 Increment: 1 Length = 1.99250e+04 Primary Var: U, Magnitude Deformed Var: U Deformation Scale Factor: +1.000e+02</p>

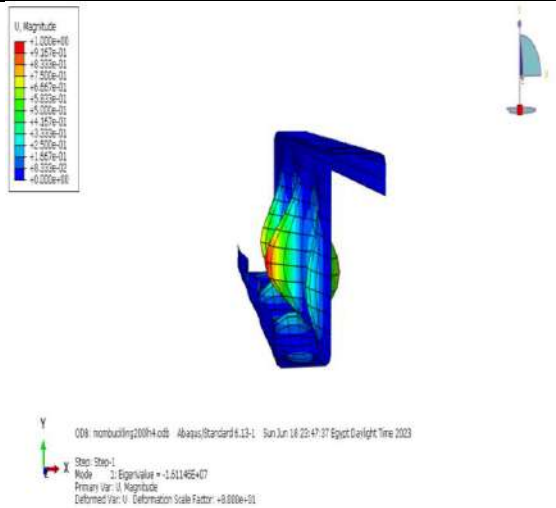
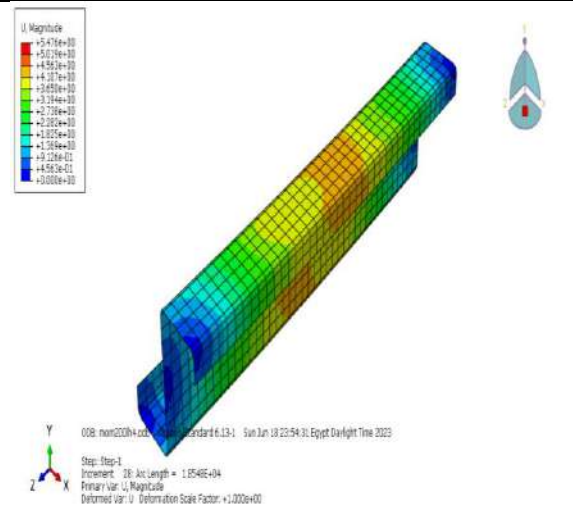
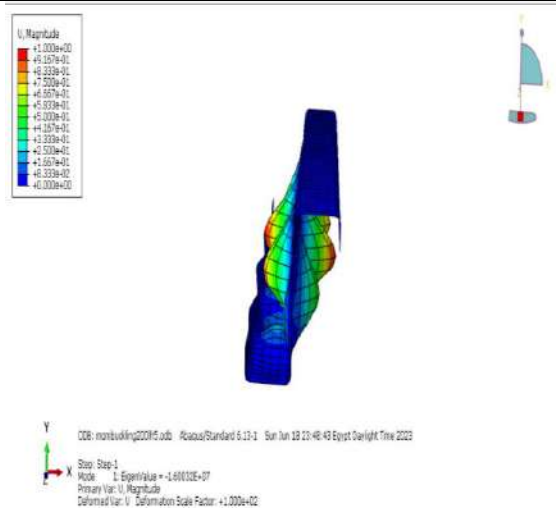
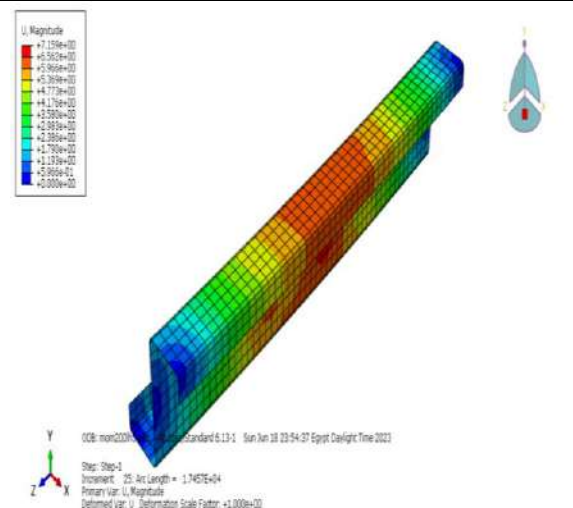
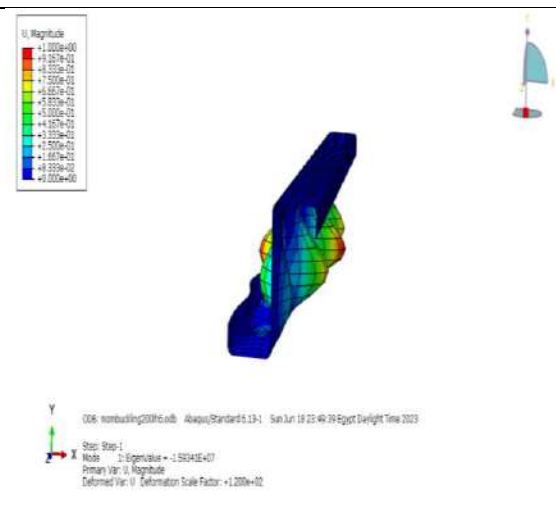
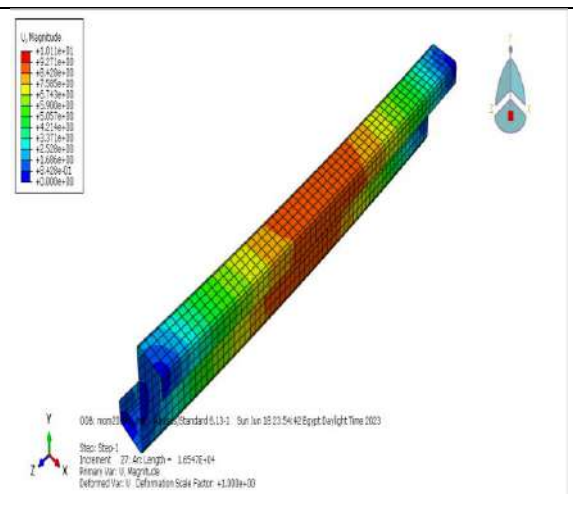
Flexural channel FEM modes		
L/h	Buckling mode	Failure mode
12		

A.2.1.2 Flexural Z-section moment

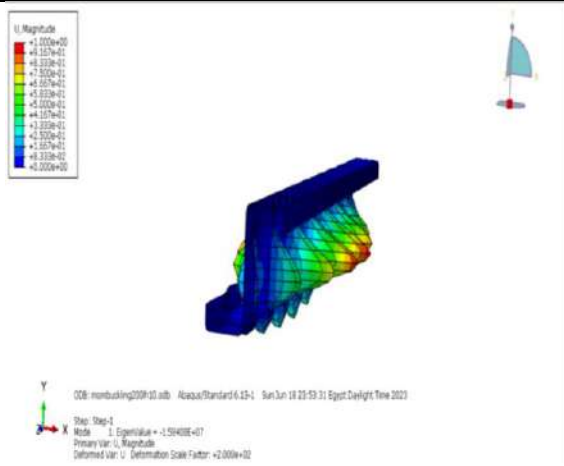
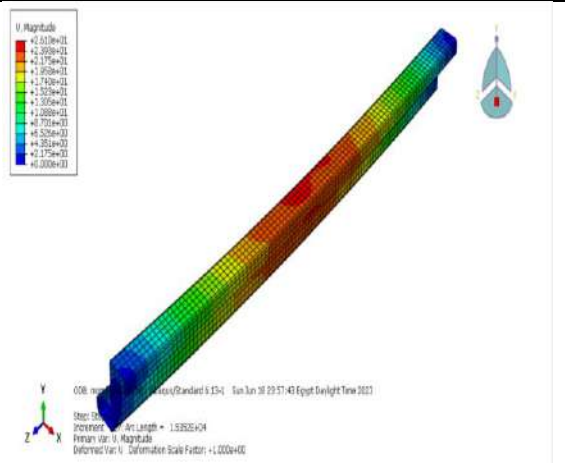
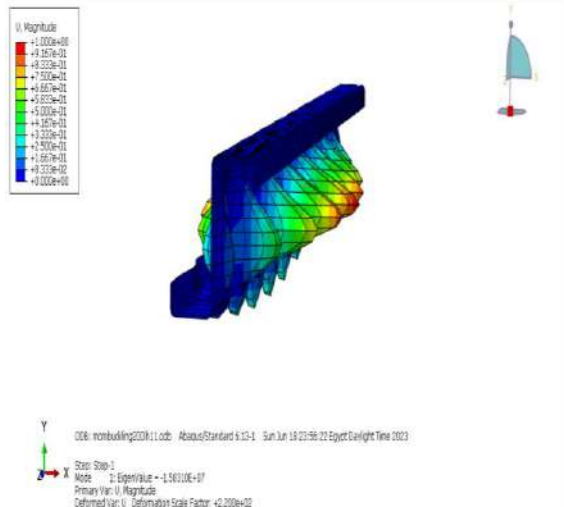
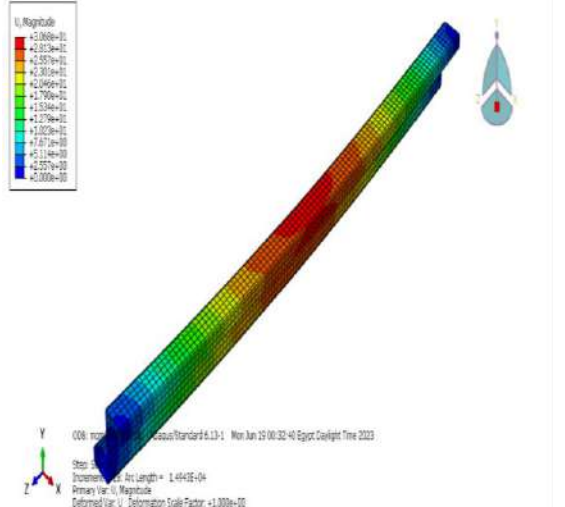
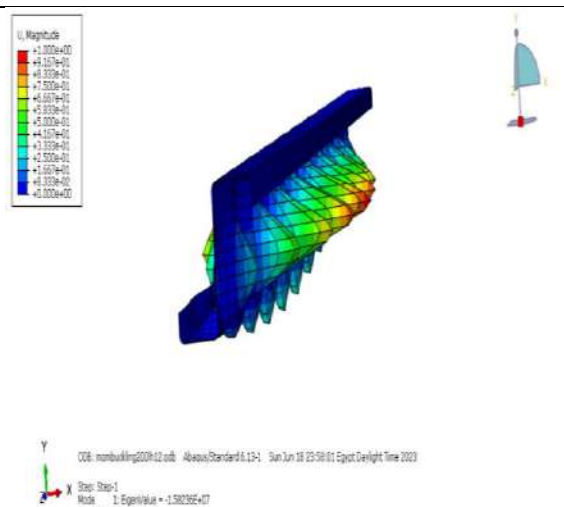
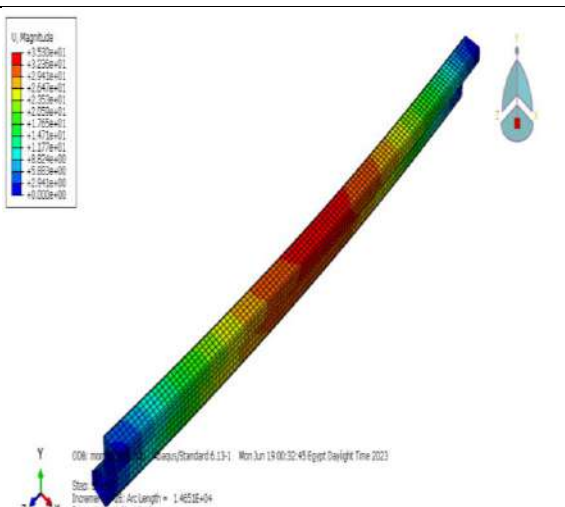
From **Table A-2**, the Z-section collapses due to local buckling until a length-to-web plate depth ratio (L/h) equals 4. After this ratio, the channel section collapses due to combination of local and lateral torsional buckling.

Table A-2: - Various FEM modes for flexural Z-sections with different L/h ratios.

Flexural Z-section FEM modes		
L/h	Buckling mode	Failure mode
1	<p>U Magnitude +1.000e+00 +0.750e+00 +0.500e+00 +0.250e+00 0.000e+00 -0.250e+00 -0.500e+00 -0.750e+00 -1.000e+00</p> <p>ODB: membuckling0091.odb Abaqus/Standard 6.13-1 Sun Jun 18 23:45:58 Egypt Daylight Time 2023 Step: Step-1 Mode: 1 Eigenvalue = -2.1490E+07 Primary Var: U, Magnitude Deformed Var: U, Deformation Scale Factor: +2.000e+01</p>	<p>U Magnitude +4.000e+00 +3.000e+00 +2.000e+00 +1.000e+00 0.000e+00 -1.000e+00 -2.000e+00 -3.000e+00 -4.000e+00</p> <p>ODB: mem0091.odb Abaqus/Standard 6.13-1 Sun Jun 18 23:54:09 Egypt Daylight Time 2023 Step: Step-1 Increment: 27 Arc Length = 4.0214E+04 Primary Var: U, Magnitude Deformed Var: U, Deformation Scale Factor: +1.000e+00</p>
2	<p>U Magnitude +1.000e+00 +0.750e+00 +0.500e+00 +0.250e+00 0.000e+00 -0.250e+00 -0.500e+00 -0.750e+00 -1.000e+00</p> <p>ODB: membuckling200494.odb Abaqus/Standard 6.13-1 Sun Jun 18 12:20:36 Egypt Daylight Time 2023 Step: Step-1 Mode: 1 Eigenvalue = -1.70219E+07 Primary Var: U, Magnitude Deformed Var: U, Deformation Scale Factor: +4.000e+01</p>	<p>U Magnitude +2.000e+00 +1.500e+00 +1.000e+00 +0.500e+00 0.000e+00 -0.500e+00 -1.000e+00 -1.500e+00 -2.000e+00</p> <p>ODB: mem020494.odb Abaqus/Standard 6.13-1 Sun Jun 18 12:25:19 Egypt Daylight Time 2023 Step: Step-1 Increment: 28 Arc Length = 3.1797E+04 Primary Var: U, Magnitude Deformed Var: U, Deformation Scale Factor: +1.000e+00</p>
3	<p>U Magnitude +1.000e+00 +0.750e+00 +0.500e+00 +0.250e+00 0.000e+00 -0.250e+00 -0.500e+00 -0.750e+00 -1.000e+00</p> <p>ODB: membuckling300849.odb Abaqus/Standard 6.13-1 Sun Jun 18 23:46:48 Egypt Daylight Time 2023 Step: Step-1 Mode: 1 Eigenvalue = -1.84039E+07 Primary Var: U, Magnitude Deformed Var: U, Deformation Scale Factor: +6.000e+01</p>	<p>U Magnitude +4.000e+00 +3.000e+00 +2.000e+00 +1.000e+00 0.000e+00 -1.000e+00 -2.000e+00 -3.000e+00 -4.000e+00</p> <p>ODB: mem030849.odb Abaqus/Standard 6.13-1 Mon Jun 19 00:02:01 Egypt Daylight Time 2023 Step: Step-1 Increment: 25 Arc Length = 1.8704E+04 Primary Var: U, Magnitude Deformed Var: U, Deformation Scale Factor: +1.000e+00</p>

Flexural Z-section FEM modes		
L/h	Buckling mode	Failure mode
4	 <p>ODB: nonbuckling2004.odb Abaqus/Standard 6.13-1 Sun Jun 18 22:47:37 Egypt Daylight Time 2023 Step: Step-1 Mode: 1; EigenValue = -1.61146E+07 Primary Var: U, Magnitude Deformed Var: U, Deformation Scale Factor: +8.000e+01</p>	 <p>ODB: non2004.odb Abaqus/Standard 6.13-1 Sun Jun 18 23:54:31 Egypt Daylight Time 2023 Step: Step-1 Increment: 28; Arc Length = 1.9548E+04 Primary Var: U, Magnitude Deformed Var: U, Deformation Scale Factor: +1.000e+00</p>
5	 <p>ODB: nonbuckling2005.odb Abaqus/Standard 6.13-1 Sun Jun 18 23:46:42 Egypt Daylight Time 2023 Step: Step-1 Mode: 2; EigenValue = -1.60032E+07 Primary Var: U, Magnitude Deformed Var: U, Deformation Scale Factor: +1.000e+02</p>	 <p>ODB: non2005.odb Abaqus/Standard 6.13-1 Sun Jun 18 23:54:27 Egypt Daylight Time 2023 Step: Step-1 Increment: 25; Arc Length = 1.7467E+04 Primary Var: U, Magnitude Deformed Var: U, Deformation Scale Factor: +1.000e+00</p>
6	 <p>ODB: nonbuckling2006.odb Abaqus/Standard 6.13-1 Sun Jun 18 23:49:39 Egypt Daylight Time 2023 Step: Step-1 Mode: 1; EigenValue = -1.5834E+07 Primary Var: U, Magnitude Deformed Var: U, Deformation Scale Factor: +1.000e+02</p>	 <p>ODB: non2006.odb Abaqus/Standard 6.13-1 Sun Jun 18 23:54:42 Egypt Daylight Time 2023 Step: Step-1 Increment: 27; Arc Length = 1.6547E+04 Primary Var: U, Magnitude Deformed Var: U, Deformation Scale Factor: +1.000e+00</p>

Flexural Z-section FEM modes		
L/h	Buckling mode	Failure mode
7	<p>U Magnitude</p> <ul style="list-style-type: none"> -1.000E+00 +9.267E-02 +8.233E-02 +7.200E-02 +6.167E-02 +5.133E-02 +4.100E-02 +3.067E-02 +2.033E-02 +1.000E-02 +0.000E+00 <p>OC6: mombulking200H7.odb Abaqus/Standard 6.13-1 Sun Jun 18 22:50:41 Egypt Daylight Time 2023</p> <p>Step: Step-1 Mode: 1 Eigenvalue = -1.58951E+07 Primary Var: U Magnitude Deformed Var: U Deformation Scale Factor: +1.400E+02</p>	<p>U Magnitude</p> <ul style="list-style-type: none"> +1.266E+01 +1.161E+01 +1.056E+01 +9.516E+00 +8.476E+00 +7.436E+00 +6.396E+00 +5.356E+00 +4.316E+00 +3.276E+00 +2.236E+00 +1.196E+00 +0.000E+00 <p>OC6: mombulking200H7.odb Abaqus/Standard 6.13-1 Sun Jun 18 22:54:50 Egypt Daylight Time 2023</p> <p>Step: Step-1 Increment: 26 Arc Length = 1.594E+04 Primary Var: U Magnitude Deformed Var: U Deformation Scale Factor: +1.000E+00</p>
8	<p>U Magnitude</p> <ul style="list-style-type: none"> +1.300E+00 +1.17E-01 +1.03E-01 +9.0E-02 +7.7E-02 +6.4E-02 +5.1E-02 +3.8E-02 +2.5E-02 +1.2E-02 +0.300E+00 <p>OC6: mombulking200H8.odb Abaqus/Standard 6.13-1 Sun Jun 18 22:51:32 Egypt Daylight Time 2023</p> <p>Step: Step-1 Mode: 1 Eigenvalue = -1.58712E+07 Primary Var: U Magnitude Deformed Var: U Deformation Scale Factor: +3.00E+02</p>	<p>U Magnitude</p> <ul style="list-style-type: none"> +1.812E+01 +1.602E+01 +1.392E+01 +1.182E+01 +9.72E+00 +7.62E+00 +5.52E+00 +3.42E+00 +1.32E+00 +0.000E+00 <p>OC6: mombulking200H8.odb Abaqus/Standard 6.13-1 Sun Jun 18 22:54:56 Egypt Daylight Time 2023</p> <p>Step: Step-1 Increment: 2 Arc Length = 1.6021E+04 Primary Var: U Magnitude Deformed Var: U Deformation Scale Factor: +1.000E+00</p>
9	<p>U Magnitude</p> <ul style="list-style-type: none"> +1.000E+00 +8.93E-01 +7.86E-01 +6.79E-01 +5.72E-01 +4.65E-01 +3.58E-01 +2.51E-01 +1.44E-01 +3.00E-02 +0.300E+00 <p>OC6: mombulking200H9.odb Abaqus/Standard 6.13-1 Sun Jun 18 22:52:38 Egypt Daylight Time 2023</p> <p>Step: Step-1 Mode: 1 Eigenvalue = -1.59254E+07 Primary Var: U Magnitude Deformed Var: U Deformation Scale Factor: +1.800E+02</p>	<p>U Magnitude</p> <ul style="list-style-type: none"> +2.395E+01 +2.181E+01 +1.967E+01 +1.753E+01 +1.539E+01 +1.325E+01 +1.111E+01 +8.97E+00 +6.83E+00 +4.69E+00 +0.300E+00 <p>OC6: mombulking200H9.odb Abaqus/Standard 6.13-1 Sun Jun 18 22:55:08 Egypt Daylight Time 2023</p> <p>Step: Step-1 Increment: 4 Arc Length = 1.5781E+04 Primary Var: U Magnitude Deformed Var: U Deformation Scale Factor: +1.000E+00</p>

Flexural Z-section FEM modes		
L/h	Buckling mode	Failure mode
10	 <p>ODB: mombuckling2008-10.odb Abaqus/Standard 6.13-1 Sun Jun 18 23:53:31 Egypt Daylight Time 2023 Step: Step-1 Mode: 1: EigenValue = -1.59408E+07 Primary Var: U, Magnitude Deformed Var: U, Deformation Scale Factor: +2.000e+02</p>	 <p>ODB: mombuckling2008-10.odb Abaqus/Standard 6.13-1 Sun Jun 18 23:57:43 Egypt Daylight Time 2023 Step: Step-1 Increment: 1: Arc Length = 1.53625e+04 Primary Var: U, Magnitude Deformed Var: U, Deformation Scale Factor: +1.000e+00</p>
11	 <p>ODB: mombuckling2008-11.odb Abaqus/Standard 6.13-1 Sun Jun 18 23:58:22 Egypt Daylight Time 2023 Step: Step-1 Mode: 2: EigenValue = -1.58110E+07 Primary Var: U, Magnitude Deformed Var: U, Deformation Scale Factor: +2.000e+02</p>	 <p>ODB: mombuckling2008-11.odb Abaqus/Standard 6.13-1 Mon Jun 19 00:32:40 Egypt Daylight Time 2023 Step: Step-1 Increment: 1: Arc Length = 1.49416e+04 Primary Var: U, Magnitude Deformed Var: U, Deformation Scale Factor: +1.000e+00</p>
12	 <p>ODB: mombuckling2008-12.odb Abaqus/Standard 6.13-1 Sun Jun 18 23:58:01 Egypt Daylight Time 2023 Step: Step-1 Mode: 1: EigenValue = -1.58239E+07 Primary Var: U, Magnitude Deformed Var: U, Deformation Scale Factor: +2.400e+02</p>	 <p>ODB: mombuckling2008-12.odb Abaqus/Standard 6.13-1 Mon Jun 19 00:32:45 Egypt Daylight Time 2023 Step: Step-1 Increment: 1: Arc Length = 1.46516e+04 Primary Var: U, Magnitude Deformed Var: U, Deformation Scale Factor: +1.000e+00</p>

A.2.1.3 Compressive channel section

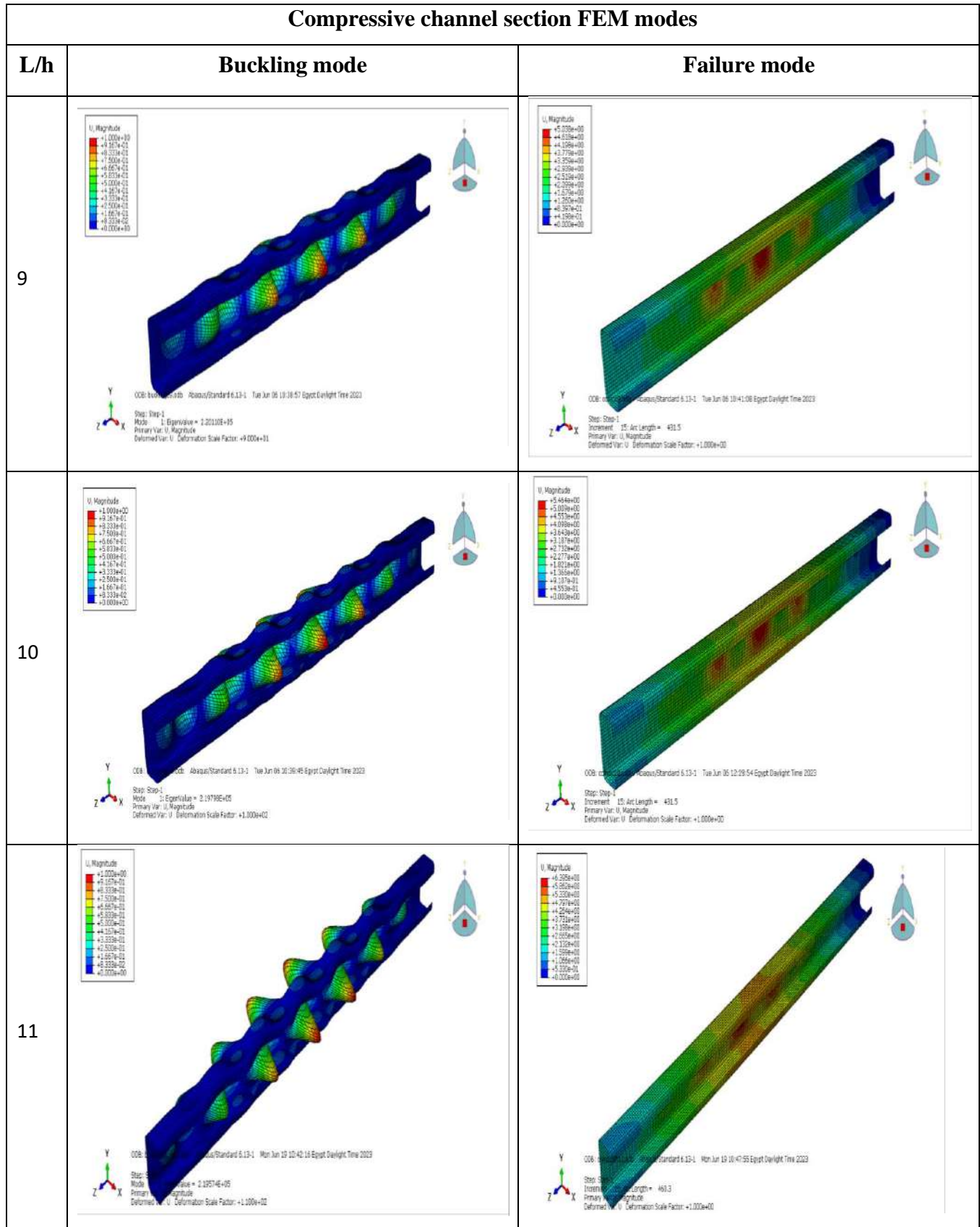
From Table A-3, it can be observed that the channel section collapses due to local buckling until a length-to-web plate depth ratio $L/h = 2$. After that, it collapses due to a combination of local and flexural buckling until $L/h = 11$. Finally, after this ratio, it collapses due to flexural buckling.

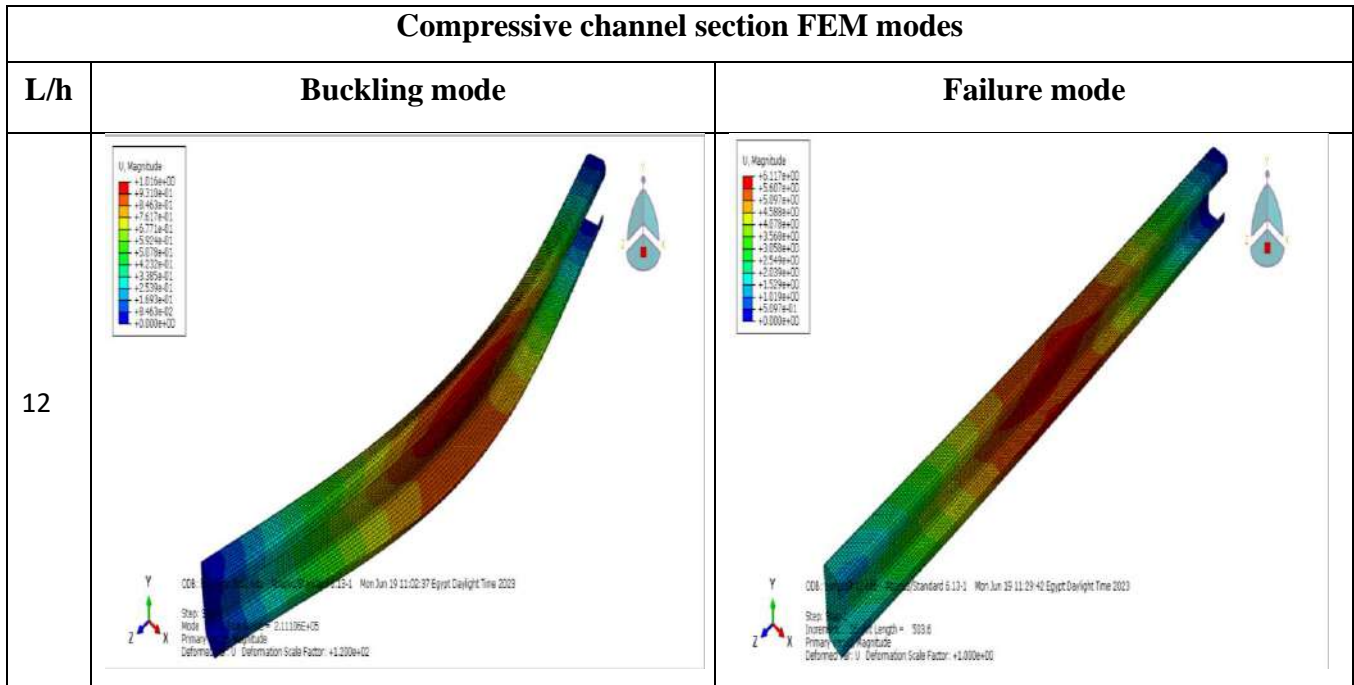
Table A-3: - Various FEM modes for Compressive channel sections with different L/h ratios.

Compressive channel section FEM modes				
L/h	Buckling mode	Failure mode		
1	<p>U, Magnitude +1.000e+00 +9.127e-01 +8.222e-01 +7.500e-01 +6.867e-01 +6.323e-01 +5.000e-01 +4.167e-01 +3.333e-01 +2.500e-01 +1.667e-01 +8.333e-02 +0.000e+00</p> <p>008: buckling1.odb - Abaqus/Standard... Egypt, Daylight Time 2023 Step: Step-1 Mode: 1; Eigenvalue = 3.02310E+05 Primary Var: U, Magnitude Deformed Var: U; Deformation Scale Factor: +1.000e+00</p>	<p>U, Magnitude +1.123e+00 +1.000e+00 +9.432e-01 +8.490e-01 +7.547e-01 +6.603e-01 +5.660e-01 +4.717e-01 +3.773e-01 +2.829e-01 +1.887e-01 +9.432e-02 +0.000e+00</p> <p>008: comp1.odb - Abaqus/Standard... Egypt, Daylight Time 2023 Step: Step-1 Increment: 15; Arc Length = 538.0 Primary Var: U, Magnitude Deformed Var: U; Deformation Scale Factor: +1.000e+00</p>		
2	<p>U, Magnitude +1.000e+00 +9.127e-01 +8.222e-01 +7.500e-01 +6.867e-01 +6.323e-01 +5.000e-01 +4.167e-01 +3.333e-01 +2.500e-01 +1.667e-01 +8.333e-02 +0.000e+00</p> <p>008: buckling2.odb - Abaqus/Standard... Jun 06 10:28:05 Egypt, Daylight Time 2023 Step: Step-1 Mode: 1; Eigenvalue = 3.46205E+05 Primary Var: U, Magnitude Deformed Var: U; Deformation Scale Factor: +2.000e+01</p>	<p>U, Magnitude +1.413e+00 +1.300e+00 +1.181e+00 +1.063e+00 +9.452e-01 +8.270e-01 +7.089e-01 +5.907e-01 +4.726e-01 +3.544e-01 +2.362e-01 +1.181e-01 +0.000e+00</p> <p>008: comp2.odb - Abaqus/Standard... Jun 06 10:40:02 Egypt, Daylight Time 2023 Step: Step-1 Increment: 14; Arc Length = 345.0 Primary Var: U, Magnitude Deformed Var: U; Deformation Scale Factor: +1.000e+00</p>		

Compressive channel section FEM modes		
L/h	Buckling mode	Failure mode
3	<p>U, Magnitude +1.000e+00 +9.357e-01 +8.323e-01 +7.500e-01 +6.667e-01 +5.523e-01 +4.389e-01 +3.256e-01 +2.122e-01 +1.000e-01 +0.000e+00</p> <p>Step: Step-1 Mode: 1; EigenValue = 2.3121E+05 Primary Var: U, Magnitude Deformed Var: U, Deformation Scale Factor: +3.000e+01</p>	<p>U, Magnitude +1.372e+00 +1.250e+00 +1.144e+00 +1.029e+00 +9.146e-01 +8.029e-01 +6.851e-01 +5.719e-01 +4.576e-01 +3.421e-01 +2.257e-01 +1.144e-01 +0.000e+00</p> <p>Step: Step-1 Increment: 14; Arc Length = 226.1 Primary Var: U, Magnitude Deformed Var: U, Deformation Scale Factor: +1.000e+00</p>
4	<p>U, Magnitude +1.000e+00 +9.167e-01 +8.333e-01 +7.500e-01 +6.667e-01 +5.833e-01 +5.000e-01 +4.167e-01 +3.333e-01 +2.500e-01 +1.667e-01 +8.333e-02 +0.000e+00</p> <p>Step: Step-1 Mode: 1; EigenValue = 2.2556E+05 Primary Var: U, Magnitude Deformed Var: U, Deformation Scale Factor: +4.000e+01</p>	<p>S, Max (MEQ, fraction = -1.0) (Avg: 75%) +3.446e+02 +3.220e+02 +3.110e+02 +3.007e+02 +2.897e+02 +2.795e+02 +2.679e+02 +2.559e+02 +2.455e+02 +2.345e+02 +2.214e+02</p> <p>Step: Step-1 Increment: 33; Arc Length = 225.7 Primary Var: S, Max Deformed Var: U, Deformation Scale Factor: +1.000e+00</p>
5	<p>U, Magnitude +1.000e+00 +9.357e-01 +8.323e-01 +7.500e-01 +6.667e-01 +5.523e-01 +4.389e-01 +3.256e-01 +2.122e-01 +1.000e-01 +0.000e+00</p> <p>Step: Step-1 Mode: 1; EigenValue = 2.2319E+05 Primary Var: U, Magnitude Deformed Var: U, Deformation Scale Factor: +5.000e+01</p>	<p>U, Magnitude +2.332e+00 +2.138e+00 +1.945e+00 +1.749e+00 +1.555e+00 +1.360e+00 +1.166e+00 +9.217e-01 +6.810e-01 +4.389e-01 +1.945e-01 +0.000e+00</p> <p>Step: Step-1 Increment: 14; Arc Length = 297.3 Primary Var: U, Magnitude Deformed Var: U, Deformation Scale Factor: +1.000e+00</p>

Compressive channel section FEM modes		
L/h	Buckling mode	Failure mode
6	<p>U Magnitude +1.000e+00 +6.223e-01 +3.500e-01 +1.500e-01 +8.667e-02 +5.000e-02 +3.000e-02 +1.875e-02 +1.125e-02 +6.750e-03 +4.125e-03 +2.500e-03 +1.500e-03 +9.375e-04 +5.625e-04 +3.375e-04 +2.062e-04 +1.275e-04 +7.875e-05 +4.837e-05 +2.962e-05 +1.837e-05 +1.125e-05 +6.937e-06 +4.237e-06 +2.625e-06 +1.612e-06 +9.937e-07 +6.125e-07 +3.787e-07 +2.362e-07 +1.462e-07 +9.125e-08 +5.687e-08 +3.537e-08 +2.187e-08 +1.362e-08 +8.437e-09 +5.237e-09 +3.237e-09 +2.012e-09 +1.262e-09 +7.837e-10 +4.837e-10 +2.987e-10 +1.837e-10 +1.125e-10 +6.937e-11 +4.237e-11 +2.625e-11 +1.612e-11 +9.937e-12 +6.125e-12 +3.787e-12 +2.362e-12 +1.462e-12 +9.125e-13 +5.687e-13 +3.537e-13 +2.187e-13 +1.362e-13 +8.437e-14 +5.237e-14 +3.237e-14 +2.012e-14 +1.262e-14 +7.837e-15 +4.837e-15 +2.987e-15 +1.837e-15 +1.125e-15 +6.937e-16 +4.237e-16 +2.625e-16 +1.612e-16 +9.937e-17 +6.125e-17 +3.787e-17 +2.362e-17 +1.462e-17 +9.125e-18 +5.687e-18 +3.537e-18 +2.187e-18 +1.362e-18 +8.437e-19 +5.237e-19 +3.237e-19 +2.012e-19 +1.262e-19 +7.837e-20 +4.837e-20 +2.987e-20 +1.837e-20 +1.125e-20 +6.937e-21 +4.237e-21 +2.625e-21 +1.612e-21 +9.937e-22 +6.125e-22 +3.787e-22 +2.362e-22 +1.462e-22 +9.125e-23 +5.687e-23 +3.537e-23 +2.187e-23 +1.362e-23 +8.437e-24 +5.237e-24 +3.237e-24 +2.012e-24 +1.262e-24 +7.837e-25 +4.837e-25 +2.987e-25 +1.837e-25 +1.125e-25 +6.937e-26 +4.237e-26 +2.625e-26 +1.612e-26 +9.937e-27 +6.125e-27 +3.787e-27 +2.362e-27 +1.462e-27 +9.125e-28 +5.687e-28 +3.537e-28 +2.187e-28 +1.362e-28 +8.437e-29 +5.237e-29 +3.237e-29 +2.012e-29 +1.262e-29 +7.837e-30 +4.837e-30 +2.987e-30 +1.837e-30 +1.125e-30 +6.937e-31 +4.237e-31 +2.625e-31 +1.612e-31 +9.937e-32 +6.125e-32 +3.787e-32 +2.362e-32 +1.462e-32 +9.125e-33 +5.687e-33 +3.537e-33 +2.187e-33 +1.362e-33 +8.437e-34 +5.237e-34 +3.237e-34 +2.012e-34 +1.262e-34 +7.837e-35 +4.837e-35 +2.987e-35 +1.837e-35 +1.125e-35 +6.937e-36 +4.237e-36 +2.625e-36 +1.612e-36 +9.937e-37 +6.125e-37 +3.787e-37 +2.362e-37 +1.462e-37 +9.125e-38 +5.687e-38 +3.537e-38 +2.187e-38 +1.362e-38 +8.437e-39 +5.237e-39 +3.237e-39 +2.012e-39 +1.262e-39 +7.837e-40 +4.837e-40 +2.987e-40 +1.837e-40 +1.125e-40 +6.937e-41 +4.237e-41 +2.625e-41 +1.612e-41 +9.937e-42 +6.125e-42 +3.787e-42 +2.362e-42 +1.462e-42 +9.125e-43 +5.687e-43 +3.537e-43 +2.187e-43 +1.362e-43 +8.437e-44 +5.237e-44 +3.237e-44 +2.012e-44 +1.262e-44 +7.837e-45 +4.837e-45 +2.987e-45 +1.837e-45 +1.125e-45 +6.937e-46 +4.237e-46 +2.625e-46 +1.612e-46 +9.937e-47 +6.125e-47 +3.787e-47 +2.362e-47 +1.462e-47 +9.125e-48 +5.687e-48 +3.537e-48 +2.187e-48 +1.362e-48 +8.437e-49 +5.237e-49 +3.237e-49 +2.012e-49 +1.262e-49 +7.837e-50 +4.837e-50 +2.987e-50 +1.837e-50 +1.125e-50 +6.937e-51 +4.237e-51 +2.625e-51 +1.612e-51 +9.937e-52 +6.125e-52 +3.787e-52 +2.362e-52 +1.462e-52 +9.125e-53 +5.687e-53 +3.537e-53 +2.187e-53 +1.362e-53 +8.437e-54 +5.237e-54 +3.237e-54 +2.012e-54 +1.262e-54 +7.837e-55 +4.837e-55 +2.987e-55 +1.837e-55 +1.125e-55 +6.937e-56 +4.237e-56 +2.625e-56 +1.612e-56 +9.937e-57 +6.125e-57 +3.787e-57 +2.362e-57 +1.462e-57 +9.125e-58 +5.687e-58 +3.537e-58 +2.187e-58 +1.362e-58 +8.437e-59 +5.237e-59 +3.237e-59 +2.012e-59 +1.262e-59 +7.837e-60 +4.837e-60 +2.987e-60 +1.837e-60 +1.125e-60 +6.937e-61 +4.237e-61 +2.625e-61 +1.612e-61 +9.937e-62 +6.125e-62 +3.787e-62 +2.362e-62 +1.462e-62 +9.125e-63 +5.687e-63 +3.537e-63 +2.187e-63 +1.362e-63 +8.437e-64 +5.237e-64 +3.237e-64 +2.012e-64 +1.262e-64 +7.837e-65 +4.837e-65 +2.987e-65 +1.837e-65 +1.125e-65 +6.937e-66 +4.237e-66 +2.625e-66 +1.612e-66 +9.937e-67 +6.125e-67 +3.787e-67 +2.362e-67 +1.462e-67 +9.125e-68 +5.687e-68 +3.537e-68 +2.187e-68 +1.362e-68 +8.437e-69 +5.237e-69 +3.237e-69 +2.012e-69 +1.262e-69 +7.837e-70 +4.837e-70 +2.987e-70 +1.837e-70 +1.125e-70 +6.937e-71 +4.237e-71 +2.625e-71 +1.612e-71 +9.937e-72 +6.125e-72 +3.787e-72 +2.362e-72 +1.462e-72 +9.125e-73 +5.687e-73 +3.537e-73 +2.187e-73 +1.362e-73 +8.437e-74 +5.237e-74 +3.237e-74 +2.012e-74 +1.262e-74 +7.837e-75 +4.837e-75 +2.987e-75 +1.837e-75 +1.125e-75 +6.937e-76 +4.237e-76 +2.625e-76 +1.612e-76 +9.937e-77 +6.125e-77 +3.787e-77 +2.362e-77 +1.462e-77 +9.125e-78 +5.687e-78 +3.537e-78 +2.187e-78 +1.362e-78 +8.437e-79 +5.237e-79 +3.237e-79 +2.012e-79 +1.262e-79 +7.837e-80 +4.837e-80 +2.987e-80 +1.837e-80 +1.125e-80 +6.937e-81 +4.237e-81 +2.625e-81 +1.612e-81 +9.937e-82 +6.125e-82 +3.787e-82 +2.362e-82 +1.462e-82 +9.125e-83 +5.687e-83 +3.537e-83 +2.187e-83 +1.362e-83 +8.437e-84 +5.237e-84 +3.237e-84 +2.012e-84 +1.262e-84 +7.837e-85 +4.837e-85 +2.987e-85 +1.837e-85 +1.125e-85 +6.937e-86 +4.237e-86 +2.625e-86 +1.612e-86 +9.937e-87 +6.125e-87 +3.787e-87 +2.362e-87 +1.462e-87 +9.125e-88 +5.687e-88 +3.537e-88 +2.187e-88 +1.362e-88 +8.437e-89 +5.237e-89 +3.237e-89 +2.012e-89 +1.262e-89 +7.837e-90 +4.837e-90 +2.987e-90 +1.837e-90 +1.125e-90 +6.937e-91 +4.237e-91 +2.625e-91 +1.612e-91 +9.937e-92 +6.125e-92 +3.787e-92 +2.362e-92 +1.462e-92 +9.125e-93 +5.687e-93 +3.537e-93 +2.187e-93 +1.362e-93 +8.437e-94 +5.237e-94 +3.237e-94 +2.012e-94 +1.262e-94 +7.837e-95 +4.837e-95 +2.987e-95 +1.837e-95 +1.125e-95 +6.937e-96 +4.237e-96 +2.625e-96 +1.612e-96 +9.937e-97 +6.125e-97 +3.787e-97 +2.362e-97 +1.462e-97 +9.125e-98 +5.687e-98 +3.537e-98 +2.187e-98 +1.362e-98 +8.437e-99 +5.237e-99 +3.237e-99 +2.012e-99 +1.262e-99 +7.837e-100 +4.837e-100 +2.987e-100 +1.837e-100 +1.125e-100 +6.937e-101 +4.237e-101 +2.625e-101 +1.612e-101 +9.937e-102 +6.125e-102 +3.787e-102 +2.362e-102 +1.462e-102 +9.125e-103 +5.687e-103 +3.537e-103 +2.187e-103 +1.362e-103 +8.437e-104 +5.237e-104 +3.237e-104 +2.012e-104 +1.262e-104 +7.837e-105 +4.837e-105 +2.987e-105 +1.837e-105 +1.125e-105 +6.937e-106 +4.237e-106 +2.625e-106 +1.612e-106 +9.937e-107 +6.125e-107 +3.787e-107 +2.362e-107 +1.462e-107 +9.125e-108 +5.687e-108 +3.537e-108 +2.187e-108 +1.362e-108 +8.437e-109 +5.237e-109 +3.237e-109 +2.012e-109 +1.262e-109 +7.837e-110 +4.837e-110 +2.987e-110 +1.837e-110 +1.125e-110 +6.937e-111 +4.237e-111 +2.625e-111 +1.612e-111 +9.937e-112 +6.125e-112 +3.787e-112 +2.362e-112 +1.462e-112 +9.125e-113 +5.687e-113 +3.537e-113 +2.187e-113 +1.362e-113 +8.437e-114 +5.237e-114 +3.237e-114 +2.012e-114 +1.262e-114 +7.837e-115 +4.837e-115 +2.987e-115 +1.837e-115 +1.125e-115 +6.937e-116 +4.237e-116 +2.625e-116 +1.612e-116 +9.937e-117 +6.125e-117 +3.787e-117 +2.362e-117 +1.462e-117 +9.125e-118 +5.687e-118 +3.537e-118 +2.187e-118 +1.362e-118 +8.437e-119 +5.237e-119 +3.237e-119 +2.012e-119 +1.262e-119 +7.837e-120 +4.837e-120 +2.987e-120 +1.837e-120 +1.125e-120 +6.937e-121 +4.237e-121 +2.625e-121 +1.612e-121 +9.937e-122 +6.125e-122 +3.787e-122 +2.362e-122 +1.462e-122 +9.125e-123 +5.687e-123 +3.537e-123 +2.187e-123 +1.362e-123 +8.437e-124 +5.237e-124 +3.237e-124 +2.012e-124 +1.262e-124 +7.837e-125 +4.837e-125 +2.987e-125 +1.837e-125 +1.125e-125 +6.937e-126 +4.237e-126 +2.625e-126 +1.612e-126 +9.937e-127 +6.125e-127 +3.787e-127 +2.362e-127 +1.462e-127 +9.125e-128 +5.687e-128 +3.537e-128 +2.187e-128 +1.362e-128 +8.437e-129 +5.237e-129 +3.237e-129 +2.012e-129 +1.262e-129 +7.837e-130 +4.837e-130 +2.987e-130 +1.837e-130 +1.125e-130 +6.937e-131 +4.237e-131 +2.625e-131 +1.612e-131 +9.937e-132 +6.125e-132 +3.787e-132 +2.362e-132 +1.462e-132 +9.125e-133 +5.687e-133 +3.537e-133 +2.187e-133 +1.362e-133 +8.437e-134 +5.237e-134 +3.237e-134 +2.012e-134 +1.262e-134 +7.837e-135 +4.837e-135 +2.987e-135 +1.837e-135 +1.125e-135 +6.937e-136 +4.237e-136 +2.625e-136 +1.612e-136 +9.937e-137 +6.125e-137 +3.787e-137 +2.362e-137 +1.462e-137 +9.125e-138 +5.687e-138 +3.537e-138 +2.187e-138 +1.362e-138 +8.437e-139 +5.237e-139 +3.237e-139 +2.012e-139 +1.262e-139 +7.837e-140 +4.837e-140 +2.987e-140 +1.837e-140 +1.125e-140 +6.937e-141 +4.237e-141 +2.625e-141 +1.612e-141 +9.937e-142 +6.125e-142 +3.787e-142 +2.362e-142 +1.462e-142 +9.125e-143 +5.687e-143 +3.537e-143 +2.187e-143 +1.362e-143 +8.437e-144 +5.237e-144 +3.237e-144 +2.012e-144 +1.262e-144 +7.837e-145 +4.837e-145 +2.987e-145 +1.837e-145 +1.125e-145 +6.937e-146 +4.237e-146 +2.625e-146 +1.612e-146 +9.937e-147 +6.125e-147 +3.787e-147 +2.362e-147 +1.462e-147 +9.125e-148 +5.687e-148 +3.537e-148 +2.187e-148 +1.362e-148 +8.437e-149 +5.237e-149 +3.237e-149 +2.012e-149 +1.262e-149 +7.837e-150 +4.837e-150 +2.987e-150 +1.837e-150 +1.125e-150 +6.937e-151 +4.237e-151 +2.625e-151 +1.612e-151 +9.937e-152 +6.125e-152 +3.787e-152 +2.362e-152 +1.462e-152 +9.125e-153 +5.687e-153 +3.537e-153 +2.187e-153 +1.362e-153 +8.437e-154 +5.237e-154 +3.237e-154 +2.012e-154 +1.262e-154 +7.837e-155 +4.837e-155 +2.987e-155 +1.837e-155 +1.125e-155 +6.937e-156 +4.237e-156 +2.625e-156 +1.612e-156 +9.937e-157 +6.125e-157 +3.787e-157 +2.362e-157 +1.462e-157 +9.125e-158 +5.687e-158 +3.537e-158 +2.187e-158 +1.362e-158 +8.437e-159 +5.237e-159 +3.237e-159 +2.012e-159 +1.262e-159 +7.837e-160 +4.837e-160 +2.987e-160 +1.837e-160 +1.125e-160 +6.937e-161 +4.237e-161 +2.625e-161 +1.612e-161 +9.937e-162 +6.125e-162 +3.787e-162 +2.362e-162 +1.462e-162 +9.125e-163 +5.687e-163 +3.537e-163 +2.187e-163 +1.362e-163 +8.437e-164 +5.237e-164 +3.237e-164 +2.012e-164 +1.262e-164 +7.837e-165 +4.837e-165 +2.987e-165 +1.837e-165 +1.125e-165 +6.937e-166 +4.237e-166 +2.625e-166 +1.612e-166 +9.937e-167 +6.125e-167 +3.787e-167 +2.362e-167 +1.462e-167 +9.125e-168 +5.687e-168 +3.537e-168 +2.187e-168 +1.362e-168 +8.437e-169 +5.237e-169 +3.237e-169 +2.012e-169 +1.262e-169 +7.837e-170 +4.837e-170 +2.987e-170 +1.837e-170 +1.125e-170 +6.937e-171 +4.237e-171 +2.625e-171 +1.612e-171 +9.937e-172 +6.125e-172 +3.787e-172 +2.362e-172 +1.462e-172 +9.125e-173 +5.687e-173 +3.537e-173 +2.187e-173 +1.362e-173 +8.437e-174 +5.237e-174 +3.237e-174 +2.012e-174 +1.262e-174 +7.837e-175 +4.837e-175 +2.987e-175 +1.837e-175 +1.125e-175 +6.937e-176 +4.237e-176 +2.625e-176 +1.612e-176 +9.937e-177 +6.125e-177 +3.787e-177 +2.362e-177 +1.462e-177 +9.125e-178 +5.687e-178 +3.537e-178 +2.187e-178 +1.362e-178 +8.437e-179 +5.237e-179 +3.237e-179 +2.012e-179 +1.262e-179 +7.837e-180 +4.837e-180 +2.987e-180 +1.837e-180 +1.125e-180 +6.937e-181 +4.237e-181 +2.625e-181 +1.612e-181 +9.937e-182 +6.125e-182 +3.787e-182 +2.362e-182 +1.462e-182 +9.125e-183 +5.687e-183 +3.537e-183 +2.187e-183 +1.362e-183 +8.437e-184 +5.237e-184 +3.237e-184 +2.012e-184 +1.262e-184 +7.837e-185 +4.837e-185 +2.987e-185 +1.837e-185 +1.125e-185 +6.937e-186 +4.237e-186 +2.625e-186 +1.612e-186 +9.937e-187 +6.125e-187 +3.787e-187 +2.362e-187 +1.462e-187 +9.125e-188 +5.687e-188 +3.537e-188 +2.187e-188 +1.362e-188 +8.437e-189 +5.237e-189 +3.237e-189 +2.012e-189 +1.262e-189 +7.837e-190 +4.837e-190 +2.987e-190 +1.837e-190 +1.125e-190 +6.937e-191 +4.237e-191 +2.625e-191 +1.612e-191 +9.937e-192 +6.125e-192 +3.787e-192 +2.362e-192 +1.462e-192 +9.125e-193 +5.687e-193 +3.537e-193 +2.187e-193 +1.362e-193 +8.437e-194 +5.237e-194 +3.237e-194 +2.012e-194 +1.262e-194 +7.837e-195 +4.837e-195 +2.987e-195 +1.837e-195 +1.125e-195 +6.937e-196 +4.237e-196 +2.625e-196 +1.612e-196 +9.937e-197 +6.125e-197 +3.787e-197 +2.362e-197 +1.462e-197 +9.125e-198 +5.687e-198 +3.537e-198 +2.187e-198 +1.362e-198 +8.437e-199 +5.237e-199 +3.237e-199 +2.012e-199 +1.262e-199 +7.837e-200 +4.837e-200 +2.987e-200 +1.837e-200 +1.125e-200 +6.937e-201 +4.237e-201 +2.625e-201 +1.612e-201 +9.937e-202 +6.125e-202 +3.787e-202 +2.362e-202 +1.462e-202 +9.125e</p>	

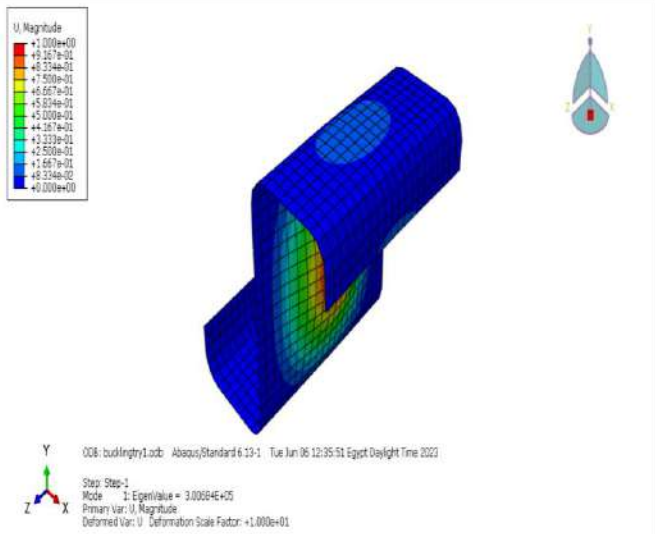
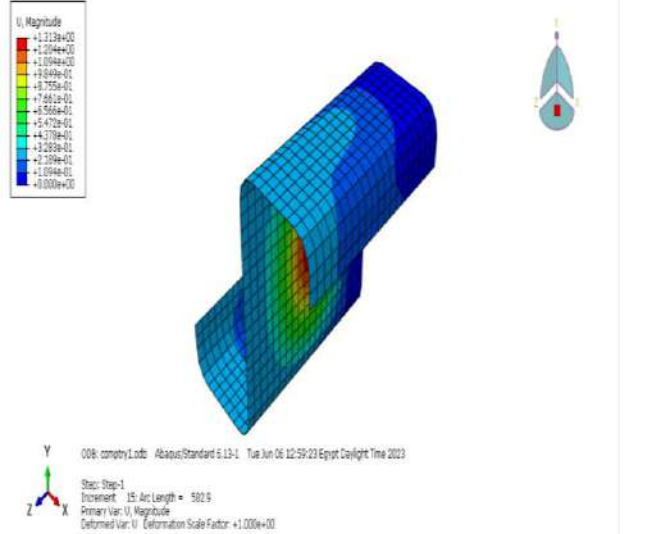
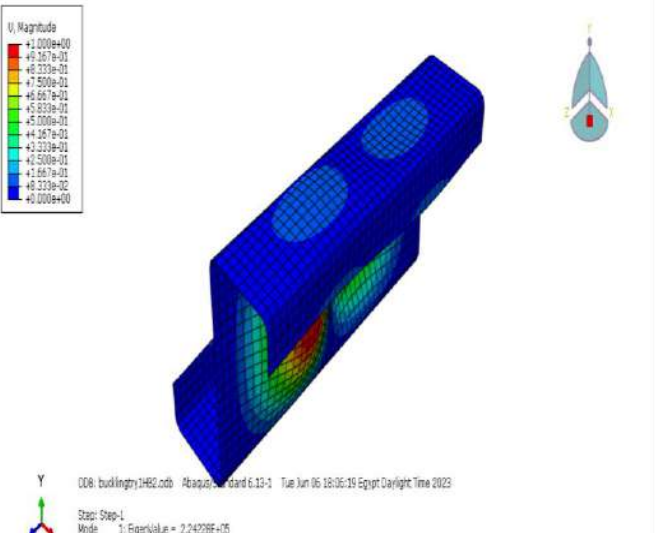
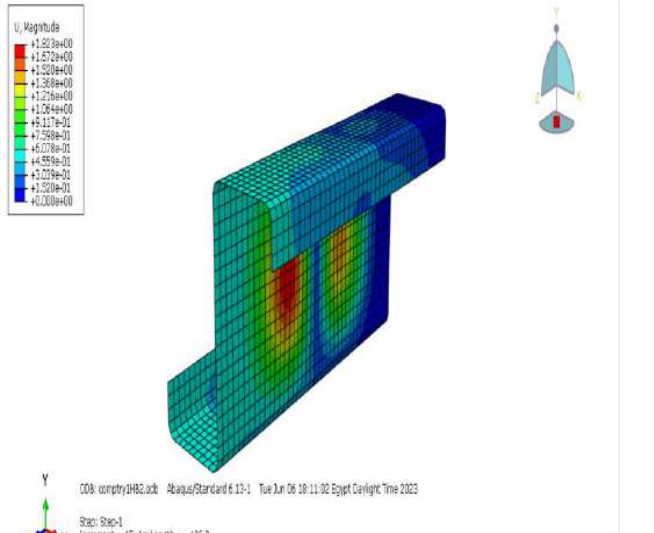


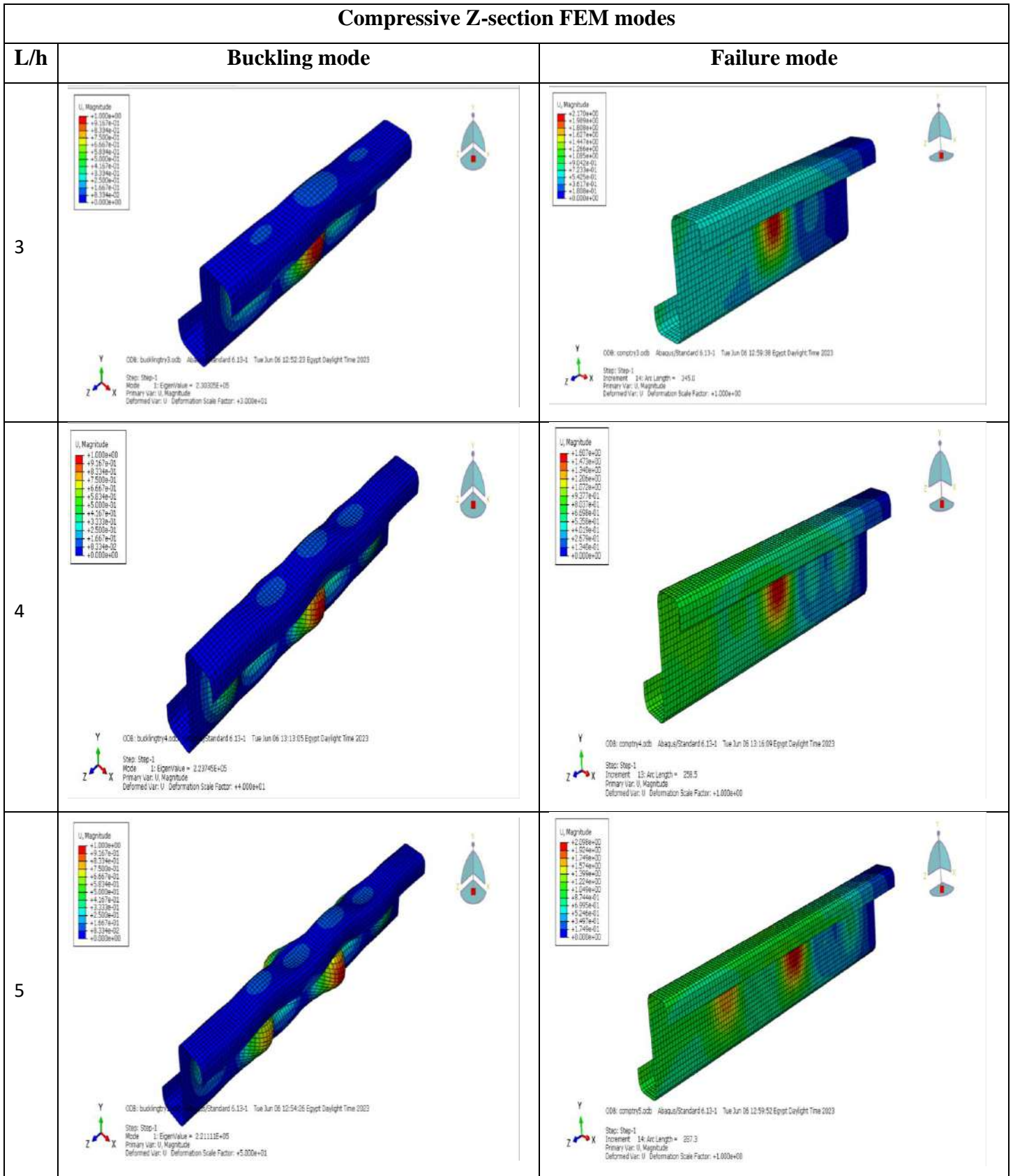


A.2.1.4 Compressive Z-section

From **Table A-4**, it is clear to us that the Z-section collapses due to web-local buckling until a length-to-web plate depth ratio (L/h) equals 2. After this ratio and until it equals 9, the Z-section collapses due to combination of local and flexural buckling. Finally, after this ratio, the Z-section collapses due to flexural buckling.

Table A-4: - Various FEM modes for Compressive Z-sections with different L/h ratios.

Compressive Z-section FEM modes				
L/h	Buckling mode	Failure mode		
1	 <p>U, Magnitude +9.167e-01 +8.374e-01 +7.500e-01 +6.667e-01 +5.834e-01 +5.000e-01 +4.167e-01 +3.333e-01 +2.500e-01 +1.667e-01 +8.334e-02 +0.000e+00</p> <p>Y X Z</p> <p>ODB: buckling1.odb Abaqus/Standard 6.13-1 Tue Jun 06 12:35:51 Egypt Daylight Time 2023</p> <p>Step: Step-1 Mode 1: Eigenvalue = 3.000E+05 Primary Var: U, Magnitude Deformed Var: U, Deformation Scale Factor: +1.000e+01</p>	 <p>U, Magnitude +1.212e+02 +1.074e+02 +1.036e+02 +9.694e+01 +8.755e+01 +7.662e+01 +6.568e+01 +5.474e+01 +4.379e+01 +3.285e+01 +2.191e+01 +1.096e+01 +0.000e+00</p> <p>Y X Z</p> <p>ODB: comp1y1.odb Abaqus/Standard 6.13-1 Tue Jun 06 12:59:23 Egypt Daylight Time 2023</p> <p>Step: Step-1 Increment 15: Arc Length = 502.9 Primary Var: U, Magnitude Deformed Var: U, Deformation Scale Factor: +1.000e+00</p>		
2	 <p>U, Magnitude +2.000e+00 +1.667e+01 +8.333e+01 +7.500e+01 +6.667e+01 +5.833e+01 +5.000e+01 +4.167e+01 +3.333e+01 +2.500e+01 +1.667e+01 +8.333e+00 +0.000e+00</p> <p>Y X Z</p> <p>ODB: buckling1482.odb Abaqus/Standard 6.13-1 Tue Jun 06 18:06:19 Egypt Daylight Time 2023</p> <p>Step: Step-1 Mode 1: Eigenvalue = 2.24206E+05 Primary Var: U, Magnitude Deformed Var: U, Deformation Scale Factor: +2.000e+01</p>	 <p>U, Magnitude +1.923e+00 +1.672e+00 +1.520e+00 +1.368e+00 +1.216e+00 +1.064e+00 +9.117e+01 +7.569e+01 +6.078e+01 +4.588e+01 +3.079e+01 +1.589e+01 +0.000e+00</p> <p>Y X Z</p> <p>ODB: comp1y1482.odb Abaqus/Standard 6.13-1 Tue Jun 06 18:11:02 Egypt Daylight Time 2023</p> <p>Step: Step-1 Increment 15: Arc Length = 436.9 Primary Var: U, Magnitude Deformed Var: U, Deformation Scale Factor: +1.000e+00</p>		



Compressive Z-section FEM modes		
L/h	Buckling mode	Failure mode
6	<p>ODB: buckling6.odb Abaqus/Standard 6.13-1 Tue Jun 06 12:55:29 Egypt Daylight Time 2023 Step: Step-1 Mode 1: EigenValue = 2.13889E+05 Primary Var: U, Magnitude Deformed Var: U, Deformation Scale Factor: 1.000E+01</p>	<p>ODB: comph7.odb Abaqus/Standard 6.13-1 Tue Jun 06 13:00:09 Egypt Daylight Time 2023 Step: Step-1 Increment 15: Arc Length = 373.8 Primary Var: U, Magnitude Deformed Var: U, Deformation Scale Factor: 1.000E+00</p>
7	<p>ODB: buckling7.odb Abaqus/Standard 6.13-1 Tue Jun 06 12:56:24 Egypt Daylight Time 2023 Step: Step-1 Mode 2: EigenValue = 2.19155E+05 Primary Var: U, Magnitude Deformed Var: U, Deformation Scale Factor: 1.000E+01</p>	<p>ODB: comph7.odb Abaqus/Standard 6.13-1 Tue Jun 06 13:00:12 Egypt Daylight Time 2023 Step: Step-1 Increment 15: Arc Length = 373.8 Primary Var: U, Magnitude Deformed Var: U, Deformation Scale Factor: 1.000E+00</p>
8	<p>ODB: buckling8.odb Abaqus/Standard 6.13-1 Tue Jun 06 12:57:18 Egypt Daylight Time 2023 Step: Step-1 Mode 2: EigenValue = 2.16510E+05 Primary Var: U, Magnitude Deformed Var: U, Deformation Scale Factor: 1.000E+01</p>	<p>ODB: comph8.odb Abaqus/Standard 6.13-1 Tue Jun 06 13:00:25 Egypt Daylight Time 2023 Step: Step-1 Increment 16: Arc Length = 480.3 Primary Var: U, Magnitude Deformed Var: U, Deformation Scale Factor: 1.000E+00</p>

Compressive Z-section FEM modes		
L/h	Buckling mode	Failure mode
9	<p>U, Magnitude +1.000e+00 +6.157e-01 +3.334e-01 +7.551e-01 +5.557e-01 +3.334e-01 +8.000e-01 +4.151e-01 +3.334e-01 +2.550e-01 +1.557e-01 +6.334e-02 +1.000e+00</p> <p>008: buckingr9.cdb Abaqus/Standard 6.13-1 Tue Jun 06 12:58:15 Egypt Daylight Time 2023</p> <p>Step: Step-1 Mode: 1, Eigenvalue = 2.18141E+05 Primary Var: U, Magnitude Deformed Var: U, Deformation Scale Factor: +9.000e+01</p>	<p>U, Magnitude +4.412e+00 +3.414e+00 +3.478e+00 +3.309e+00 +2.241e+00 +2.373e+00 +2.709e+00 +1.838e+00 +1.471e+00 +1.409e+00 +7.353e-01 +3.478e-01 +9.000e+00</p> <p>008: comptr9.cdb Abaqus/Standard 6.13-1 Tue Jun 06 13:00:34 Egypt Daylight Time 2023</p> <p>Step: Step-1 Increment: 10, Arc Length = 453.1 Primary Var: U, Magnitude Deformed Var: U, Deformation Scale Factor: +1.000e+00</p>
10	<p>U, Magnitude +1.130e+00 +1.036e+00 +9.401e-01 +9.470e-01 +7.536e-01 +5.544e-01 +2.551e-01 +4.710e-01 +2.559e-01 +2.559e-01 +1.384e-01 +4.420e-02 +1.000e+00</p> <p>008: buckr10.cdb Abaqus/Standard 6.13-1 Tue Jun 06 12:59:16 Egypt Daylight Time 2023</p> <p>Step: Step-1 Mode: 1, Eigenvalue = 1.98322E+05 Primary Var: U, Magnitude Deformed Var: U, Deformation Scale Factor: +1.000e+02</p>	<p>U, Magnitude +5.220e+00 +4.791e+00 +4.331e+00 +3.025e+00 +3.620e+00 +3.025e+00 +2.617e+00 +2.103e+00 +1.744e+00 +1.330e+00 +8.722e-01 +4.321e-01 +1.000e+00</p> <p>008: comptr10.cdb Abaqus/Standard 6.13-1 Tue Jun 06 13:11:46 Egypt Daylight Time 2023</p> <p>Step: Step-1 Increment: 10, Arc Length = 451.5 Primary Var: U, Magnitude Deformed Var: U, Deformation Scale Factor: +1.000e+00</p>
11	<p>U, Magnitude +1.147e+00 +1.248e+00 +9.528e-02 +8.573e-01 +7.459e-01 +6.670e-02 +5.717e-01 +4.784e-01 +3.811e-01 +2.859e-01 +1.910e-01 +9.528e-02 +1.000e+00</p> <p>008: buckr11.cdb Abaqus/Standard 6.13-1 Mon Jun 19 10:42:03 Egypt Daylight Time 2023</p> <p>Step: Step-1 Mode: 1, Eigenvalue = 1.35600E+05 Primary Var: U, Magnitude Deformed Var: U, Deformation Scale Factor: +1.100e+02</p>	<p>U, Magnitude +5.420e+00 +4.999e+00 +4.617e+00 +4.060e+00 +3.613e+00 +3.263e+00 +2.710e+00 +2.258e+00 +1.601e+00 +1.355e+00 +9.624e-01 +4.517e-01 +1.000e+00</p> <p>008: comptr11.cdb Abaqus/Standard 6.13-1 Mon Jun 19 10:45:25 Egypt Daylight Time 2023</p> <p>Step: Step-1 Increment: 15, Arc Length = 273.8 Primary Var: U, Magnitude Deformed Var: U, Deformation Scale Factor: +1.000e+00</p>

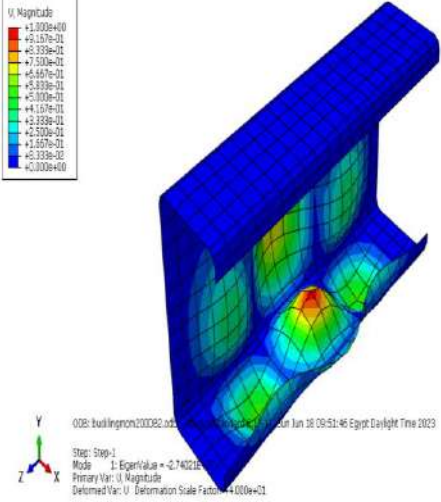
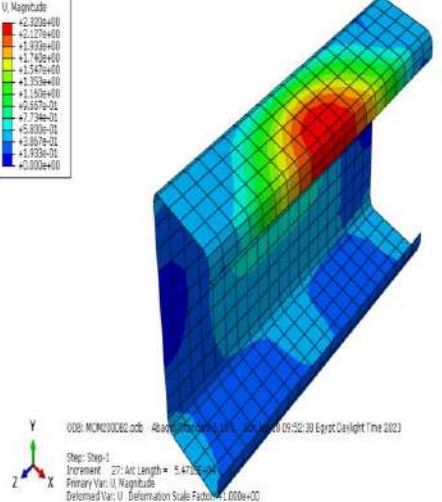
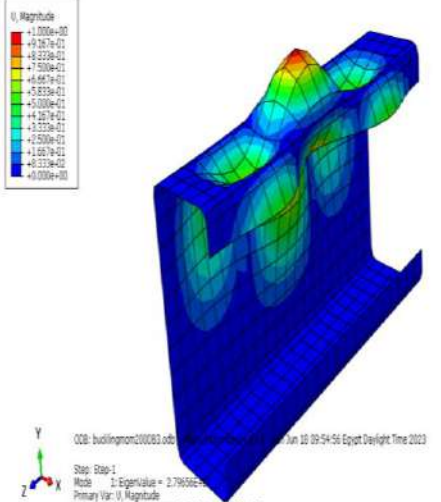
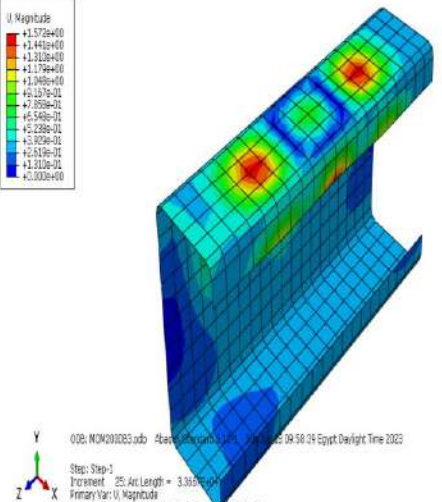
Compressive Z-section FEM modes		
L/h	Buckling mode	Failure mode
12		

A.2.2 Lip-to-Flange Plates Length Ratio (d/b) Parameter

A.2.2.1 Flexural channel section

From **Table A-5**, it is clear to us that the channel section collapses due to combination of local and distortional buckling until a lip-to-flange plates length ratio (d/b) equals 0.5. After this ratio and until it equals 0.8, the channel section collapses due to distortion buckling.

Table A-5: - Various FEM modes for Flexural channel section with different d/b ratios.

Flexural channel section FEM modes			
d/b	Buckling mode	Failure mode	
.2	 <p>U, Magnitude +1.000e+00 +6.167e-01 +5.335e-01 +7.500e-01 +6.667e-01 +5.833e-01 +5.000e-01 +4.167e-01 +3.333e-01 +2.500e-01 +1.667e-01 +8.333e-02 +0.000e+00</p> <p>Step: Step-1 Mode: 1; EigenValue = -2.74021e+01 Primary Var: U, Magnitude Deformed Var: U, Deformation Scale Factor: 4.000e+01</p>	 <p>U, Magnitude +2.220e+00 +2.127e+00 +1.930e+00 +1.740e+00 +1.540e+00 +1.350e+00 +1.150e+00 +9.507e-01 +7.794e-01 +5.800e-01 +3.807e-01 +1.930e-01 +0.000e+00</p> <p>Step: Step-1 Increment: 27; Arc Length = 5.4735e-01 Primary Var: U, Magnitude Deformed Var: U, Deformation Scale Factor: 1.000e+00</p>	
.3	 <p>U, Magnitude +1.000e+00 +9.167e-01 +8.335e-01 +7.500e-01 +6.667e-01 +5.833e-01 +5.000e-01 +4.167e-01 +3.333e-01 +2.500e-01 +1.667e-01 +8.333e-02 +0.000e+00</p> <p>Step: Step-1 Mode: 1; EigenValue = 2.78956e+01 Primary Var: U, Magnitude Deformed Var: U, Deformation Scale Factor: 4.000e+01</p>	 <p>U, Magnitude +1.572e+00 +1.448e+00 +1.312e+00 +1.179e+00 +1.046e+00 +9.137e-01 +7.858e-01 +6.548e-01 +5.288e-01 +3.929e-01 +2.619e-01 +1.312e-01 +0.000e+00</p> <p>Step: Step-1 Increment: 25; Arc Length = 3.3187e-01 Primary Var: U, Magnitude Deformed Var: U, Deformation Scale Factor: 1.000e+00</p>	

Flexural channel section FEM modes		
d/b	Buckling mode	Failure mode
.4		
.5		
.6		

Flexural channel section FEM modes		
d/b	Buckling mode	Failure mode
.7	<p>DOB: bucklingm000067.odb Step: Step-1 Mode: 1; EigenValue = -2.15002e+07 Primary Var: U, Magnitude Deformed Var: U, Deformation Scale Factor: +1.000e+00</p>	<p>DOB: MOM000067.odb Step: Step-1 Increment: 35; Arc Length = 4.664e+00 Primary Var: U, Magnitude Deformed Var: U, Deformation Scale Factor: +1.000e+00</p>
.8	<p>DOB: bucklingm000068.odb Step: Step-1 Mode: 1; EigenValue = 2.00236e+07 Primary Var: U, Magnitude Deformed Var: U, Deformation Scale Factor: +4.000e+00</p>	<p>DOB: MOM000068.odb Step: Step-1 Increment: 26; Arc Length = 5.050e+00 Primary Var: U, Magnitude Deformed Var: U, Deformation Scale Factor: +1.000e+00</p>

A.2.2.2 Flexural Z-section

Table A-6 shows that the Z-section collapses due to web-local buckling until a lip-to-flange plates length ratio (d/b) equals 0.5. After this ratio and until it equals 0.8, the Z-section collapses due to distortion buckling.

Table A-6: - Various FEM modes for Flexural Z-section with different d/b ratios.

Flexural channel section FEM modes		
d/b	Buckling mode	Failure mode
.2	<p>U Magnitude +1.000e+00 +9.157e+01 +8.330e+01 +7.500e+01 +6.674e+01 +5.839e+01 +5.000e+01 +4.167e+01 +3.330e+01 +2.500e+01 +1.667e+01 +8.330e+00 +0.000e+00</p> <p>008: monbuckling200d02.cdb: Abaqus/Standard 6.13-1 Sun Jun 18 12:17:22 Egypt Daylight Time 2023 Step: Step-1 Mode: 1: EigenValue = -1.57643E-07 Primary Var: U, Magnitude Deformed Var: U, Deformation Scale Factor: +4.000e+01</p>	<p>U Magnitude +2.144e+00 +1.881e+00 +1.667e+00 +1.444e+00 +1.222e+00 +1.000e+00 +7.778e+00 +5.556e+00 +3.333e+00 +1.111e+00 +0.000e+00</p> <p>008: mon200d02.cdb: Abaqus/Standard 6.13-1 Sun Jun 18 12:25:07 Egypt Daylight Time 2023 Step: Step-1 Increment: 24: Arc Length = 1.99515e+04 Primary Var: U, Magnitude Deformed Var: U, Deformation Scale Factor: +1.000e+00</p>
.3	<p>U Magnitude +1.000e+00 +9.157e+01 +8.330e+01 +7.500e+01 +6.674e+01 +5.839e+01 +5.000e+01 +4.167e+01 +3.330e+01 +2.500e+01 +1.667e+01 +8.330e+00 +0.000e+00</p> <p>008: monbuckling200d03.cdb: Abaqus/Standard 6.13-1 Sun Jun 18 12:19:52 Egypt Daylight Time 2023 Step: Step-1 Mode: 1: EigenValue = -1.63291E-07 Primary Var: U, Magnitude Deformed Var: U, Deformation Scale Factor: +4.000e+01</p>	<p>U Magnitude +2.063e+00 +1.881e+00 +1.719e+00 +1.547e+00 +1.375e+00 +1.203e+00 +1.031e+00 +8.594e+00 +6.879e+00 +5.156e+00 +3.438e+00 +1.719e+00 +0.000e+00</p> <p>008: mon200d03.cdb: Abaqus/Standard 6.13-1 Sun Jun 18 12:25:14 Egypt Daylight Time 2023 Step: Step-1 Increment: 25: Arc Length = 1.8704e+04 Primary Var: U, Magnitude Deformed Var: U, Deformation Scale Factor: +1.000e+00</p>

Flexural channel section FEM modes		
d/b	Buckling mode	Failure mode
.4	<p>U, Magnitude +1.000e+00 +8.167e-01 +6.333e-01 +4.500e-01 +2.667e-01 +0.833e-01 -0.000e+00 -0.833e-01 -2.667e-01 -4.500e-01 -6.333e-01 -8.167e-01 -1.000e+00</p> <p>008: nonbuckling200d04.job Abaqus/Standard 6.13-1 Sun Jun 19 12:20:36 Egypt Daylight Time 2023 Step: Step-1 Mode: 1; EigenValue = -1.70219E+07 Primary Var: U, Magnitude Deformed Var: U, Deformation Scale Factor: +4.000e+01</p>	<p>U, Magnitude +2.200e+00 +2.050e+00 +1.900e+00 +1.750e+00 +1.600e+00 +1.450e+00 +1.300e+00 +1.150e+00 +1.000e+00 +0.850e+00 +0.700e+00 +0.550e+00 +0.400e+00 +0.250e+00 +0.100e+00 -0.050e+00 -0.200e+00 -0.350e+00 -0.500e+00 -0.650e+00 -0.800e+00 -0.950e+00 -1.100e+00 -1.250e+00 -1.400e+00 -1.550e+00 -1.700e+00 -1.850e+00 -2.000e+00 -2.150e+00 -2.300e+00</p> <p>008: non200d04.job Abaqus/Standard 6.13-1 Sun Jun 19 12:25:19 Egypt Daylight Time 2023 Step: Step-1 Increment: 29; Arc Length = 3.1797E+04 Primary Var: U, Magnitude Deformed Var: U, Deformation Scale Factor: +1.000e+00</p>
.5	<p>U, Magnitude +1.000e+00 +8.167e-01 +6.333e-01 +4.500e-01 +2.667e-01 +0.833e-01 -0.000e+00 -0.833e-01 -2.667e-01 -4.500e-01 -6.333e-01 -8.167e-01 -1.000e+00</p> <p>008: nonbuckling200d05.job Abaqus/Standard 6.13-1 Sun Jun 19 12:21:27 Egypt Daylight Time 2023 Step: Step-1 Mode: 1; EigenValue = -1.77769E+07 Primary Var: U, Magnitude Deformed Var: U, Deformation Scale Factor: +4.000e+01</p>	<p>U, Magnitude +1.390e+00 +1.270e+00 +1.150e+00 +1.040e+00 +0.930e+00 +0.820e+00 +0.710e+00 +0.600e+00 +0.490e+00 +0.380e+00 +0.270e+00 +0.160e+00 +0.050e+00 -0.060e+00 -0.170e+00 -0.280e+00 -0.390e+00 -0.500e+00 -0.610e+00 -0.720e+00 -0.830e+00 -0.940e+00 -1.050e+00 -1.160e+00 -1.270e+00 -1.380e+00</p> <p>008: non200d05.job Abaqus/Standard 6.13-1 Sun Jun 19 12:25:22 Egypt Daylight Time 2023 Step: Step-1 Increment: 24; Arc Length = 2.2444E+04 Primary Var: U, Magnitude Deformed Var: U, Deformation Scale Factor: +1.000e+00</p>
.6	<p>U, Magnitude +1.000e+00 +8.167e-01 +6.333e-01 +4.500e-01 +2.667e-01 +0.833e-01 -0.000e+00 -0.833e-01 -2.667e-01 -4.500e-01 -6.333e-01 -8.167e-01 -1.000e+00</p> <p>008: nonbuckling200d06.job Abaqus/Standard 6.13-1 Sun Jun 19 12:22:10 Egypt Daylight Time 2023 Step: Step-1 Mode: 1; EigenValue = -1.49572E+07 Primary Var: U, Magnitude Deformed Var: U, Deformation Scale Factor: +4.000e+01</p>	<p>U, Magnitude +8.134e+00 +7.550e+00 +6.967e+00 +6.383e+00 +5.799e+00 +5.215e+00 +4.631e+00 +4.047e+00 +3.463e+00 +2.879e+00 +2.295e+00 +1.711e+00 +1.127e+00 +0.543e+00 -0.041e+00 -0.625e+00 -1.209e+00 -1.793e+00 -2.377e+00 -2.961e+00 -3.545e+00 -4.129e+00 -4.713e+00 -5.297e+00 -5.881e+00 -6.465e+00 -7.049e+00 -7.633e+00 -8.217e+00</p> <p>008: non200d06.job Abaqus/Standard 6.13-1 Sun Jun 19 12:25:29 Egypt Daylight Time 2023 Step: Step-1 Increment: 28; Arc Length = 3.2667E+04 Primary Var: U, Magnitude Deformed Var: U, Deformation Scale Factor: +1.000e+00</p>

Flexural channel section FEM modes		
d/b	Buckling mode	Failure mode
.7	<p>Step: Step-1 Mode: 1; Eigenvalue = 1.15725E+07 Primary Var: U, Magnitude Deformed Var: U Deformation Scale Factor: +1.000E+01</p>	<p>Step: Step-1 Increment: 40; Arc Length = 5.9422E+04 Primary Var: U, Magnitude Deformed Var: U Deformation Scale Factor: +1.000E+00</p>
.8	<p>Step: Step-1 Mode: 1; Eigenvalue = 0.99422E+06 Primary Var: U, Magnitude Deformed Var: U Deformation Scale Factor: +1.000E+01</p>	<p>Step: Step-1 Increment: 30; Arc Length = 4.0769E+04 Primary Var: U, Magnitude Deformed Var: U Deformation Scale Factor: +1.000E+00</p>

A.2.2.3 Compressive channel section

From **Table A-7**, it can be observed that the channel section collapses due to web-local buckling until a lip-to-flange plates length ratio (d/b) equals 0.5. After this ratio and until it equals 0.8, the channel section collapses due to combination of local and distortion buckling.

Table A-7: - Various FEM modes for Compressive channel section with different d/b ratios.

Compressive channel section FEM modes		
d/b	Buckling mode	Failure mode
.2		
.3		

Compressive channel section FEM modes		
d/b	Buckling mode	Failure mode
.4	<p>U, Magnitude +1.000e+00 +9.157e-01 +8.333e-01 +7.500e-01 +6.667e-01 +5.833e-01 +5.000e-01 +4.167e-01 +3.333e-01 +2.500e-01 +1.667e-01 +8.333e-02 +0.000e+00</p> <p>006: buckling1b2.cdb: Abaqus/Explicit, Job: buckling1b2, 06/17/2023 17:48:14 Egypt Daylight Time 2023 Step: Step-1 Mode: 1; EigenValue = 2.268015e+05 Primary Var: U, Magnitude Deformed Var: U, Deformation Scale Factor: +0.000e+01</p>	<p>U, Magnitude +1.698e+00 +1.529e+00 +1.359e+00 +1.229e+00 +1.099e+00 +9.552e-01 +8.196e-01 +6.839e-01 +5.484e-01 +4.095e-01 +2.732e-01 +1.369e-01 +0.000e+00</p> <p>006: compc1b2.cdb: Abaqus/Explicit, Job: compc1b2, 06/17/2023 17:47:35 Egypt Daylight Time 2023 Step: Step-1 Increment: 14; Arc Length = 388.2 Primary Var: U, Magnitude Deformed Var: U, Deformation Scale Factor: +1.000e+00</p>
.5	<p>U, Magnitude +1.000e+00 +9.167e-01 +8.333e-01 +7.500e-01 +6.667e-01 +5.833e-01 +5.000e-01 +4.167e-01 +3.333e-01 +2.500e-01 +1.667e-01 +8.333e-02 +0.000e+00</p> <p>006: buckling1b5.cdb: Abaqus/Explicit, Job: buckling1b5, 06/17/2023 15:21:26 Egypt Daylight Time 2023 Step: Step-1 Mode: 1; EigenValue = 2.56718E+05 Primary Var: U, Magnitude Deformed Var: U, Deformation Scale Factor: +2.000e+01</p>	<p>U, Magnitude +1.345e+00 +1.233e+00 +1.122e+00 +1.009e+00 +8.94e-01 +7.843e-01 +6.723e-01 +5.602e-01 +4.485e-01 +3.351e-01 +2.241e-01 +1.120e-01 +0.000e+00</p> <p>006: compc1b5.cdb: Abaqus/Explicit, Job: compc1b5, 06/17/2023 15:36:19 Egypt Daylight Time 2023 Step: Step-1 Increment: 14; Arc Length = 345.0 Primary Var: U, Magnitude Deformed Var: U, Deformation Scale Factor: +1.000e+00</p>
.6	<p>U, Magnitude +1.000e+00 +9.167e-01 +8.333e-01 +7.500e-01 +6.667e-01 +5.833e-01 +5.000e-01 +4.167e-01 +3.333e-01 +2.500e-01 +1.667e-01 +8.333e-02 +0.000e+00</p> <p>006: buckling1b6.cdb: Abaqus/Explicit, Job: buckling1b6, 06/17/2023 15:32:42 Egypt Daylight Time 2023 Step: Step-1 Mode: 1; EigenValue = 2.67433E+05 Primary Var: U, Magnitude Deformed Var: U, Deformation Scale Factor: +2.000e+01</p>	<p>U, Magnitude +1.456e+00 +1.322e+00 +1.193e+00 +1.057e+00 +9.259e-01 +7.931e-01 +6.629e-01 +5.327e-01 +4.044e-01 +2.741e-01 +1.422e-01 +0.000e+00</p> <p>006: compc1b6.cdb: Abaqus/Explicit, Job: compc1b6, 06/17/2023 15:36:25 Egypt Daylight Time 2023 Step: Step-1 Increment: 14; Arc Length = 388.2 Primary Var: U, Magnitude Deformed Var: U, Deformation Scale Factor: +1.000e+00</p>

Compressive channel section FEM modes			
d/b	Buckling mode	Failure mode	
.7	<p>OOB: buckling1d7.odb Abaqus/Standard 6.13-1 Tue Jun 06 15:24:40 Egypt Daylight Time 2023</p> <p>Step: Step-1 Mode 1: Eigenvalue = 2.76798E+05 Primary var: U, Magnitude Deformed var: U, Deformation Scale Factor: +2.000e+01</p>	<p>OOB: compr1d7.odb Abaqus/Standard 6.13-1 Tue Jun 06 15:26:30 Egypt Daylight Time 2023</p> <p>Step: Step-1 Increment: 14, Arc Length = 388.2 Primary var: U, Magnitude Deformed var: U, Deformation Scale Factor: +1.000e+00</p>	
.8	<p>OOB: buckling1d8.odb Abaqus/Standard 6.13-1 Tue Jun 06 15:25:12 Egypt Daylight Time 2023</p> <p>Step: Step-1 Mode 1: Eigenvalue = 2.78600E+05 Primary var: U, Magnitude Deformed var: U, Deformation Scale Factor: +2.000e+01</p>	<p>OOB: compr1d8.odb Abaqus/Standard 6.13-1 Tue Jun 06 15:26:56 Egypt Daylight Time 2023</p> <p>Step: Step-1 Increment: 18, Arc Length = 399.2 Primary var: U, Magnitude Deformed var: U, Deformation Scale Factor: +1.000e+00</p>	

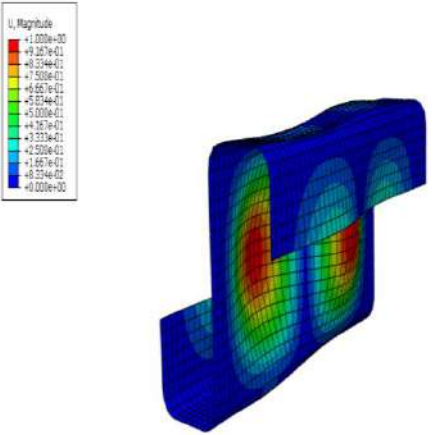
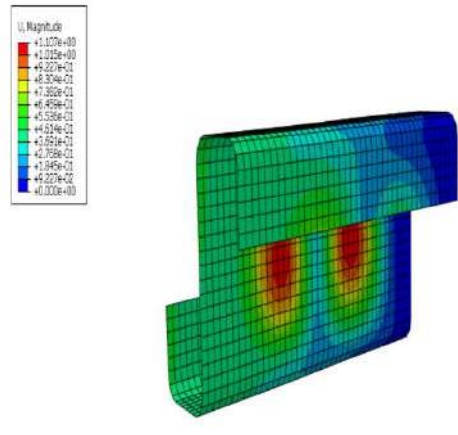
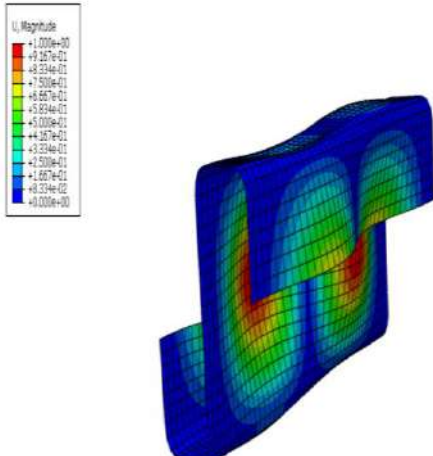
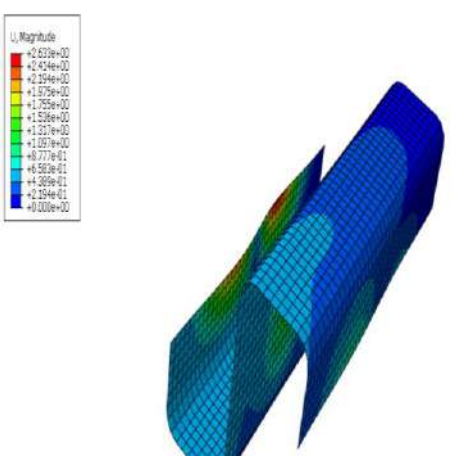
A.2.2.4 Compressive Z-section

According to **Table A-8**, the Z-section collapses due to web-local buckling until a lip-to-flange plates length ratio (d/b) equals 0.5. After this ratio and until it equals 0.8, the Z-section collapses due to combination of local and distortion buckling.

Table A-8: - Various FEM modes for Compressive Z-section with different d/b ratios.

Compressive Z-section FEM modes		
d/b	Buckling mode	Failure mode
.2		
.3		

Compressive Z-section FEM modes			
d/b	Buckling mode	Failure mode	
.4	<p>ODB: bucklingr1482.odb Abaqus/Standard 6.13-1 Tue Jun 06 16:06:15 Egypt Daylight Time 2023</p> <p>Step: Step-1 Mode: 1, Eigenvalue = 2.24209E+05 Primary Var: U, Magnitude Deformed Var: U, Deformation Scale Factor: +2.000e+01</p>	<p>ODB: comphy1482.odb Abaqus/Standard 6.13-1 Tue Jun 06 16:11:02 Egypt Daylight Time 2023</p> <p>Step: Step-1 Increment: 15, Arc Length = 436.9 Primary Var: U, Magnitude Deformed Var: U, Deformation Scale Factor: +1.000e+00</p>	
.5	<p>ODB: bucklingr1485.odb Abaqus/Standard 6.13-1 Tue Jun 06 16:07:10 Egypt Daylight Time 2023</p> <p>Step: Step-1 Mode: 1, Eigenvalue = 2.54167E+05 Primary Var: U, Magnitude Deformed Var: U, Deformation Scale Factor: +2.000e+01</p>	<p>ODB: comphy1485.odb Abaqus/Standard 6.13-1 Tue Jun 06 16:10:14 Egypt Daylight Time 2023</p> <p>Step: Step-1 Increment: 24, Arc Length = 389.2 Primary Var: U, Magnitude Deformed Var: U, Deformation Scale Factor: +1.000e+00</p>	
.6	<p>ODB: bucklingr1486.odb Abaqus/Standard 6.13-1 Tue Jun 06 16:08:16 Egypt Daylight Time 2023</p> <p>Step: Step-1 Mode: 1, Eigenvalue = 2.64457E+05 Primary Var: U, Magnitude Deformed Var: U, Deformation Scale Factor: +2.000e+01</p>	<p>ODB: comphy1486.odb Abaqus/Standard 6.13-1 Tue Jun 06 16:10:18 Egypt Daylight Time 2023</p> <p>Step: Step-1 Increment: 14, Arc Length = 389.2 Primary Var: U, Magnitude Deformed Var: U, Deformation Scale Factor: +1.000e+00</p>	

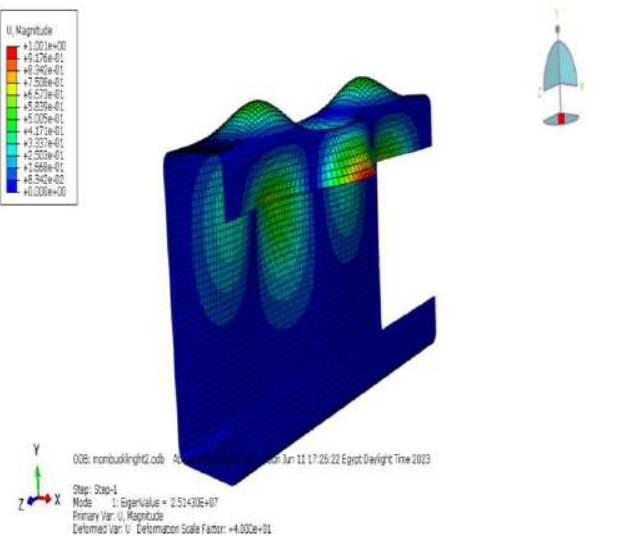
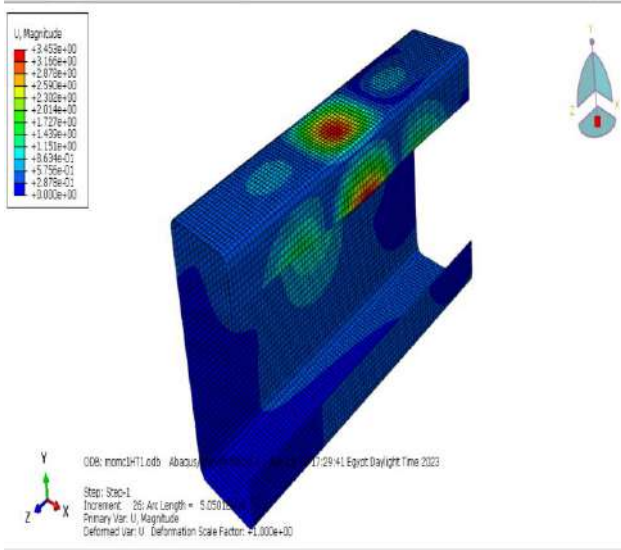
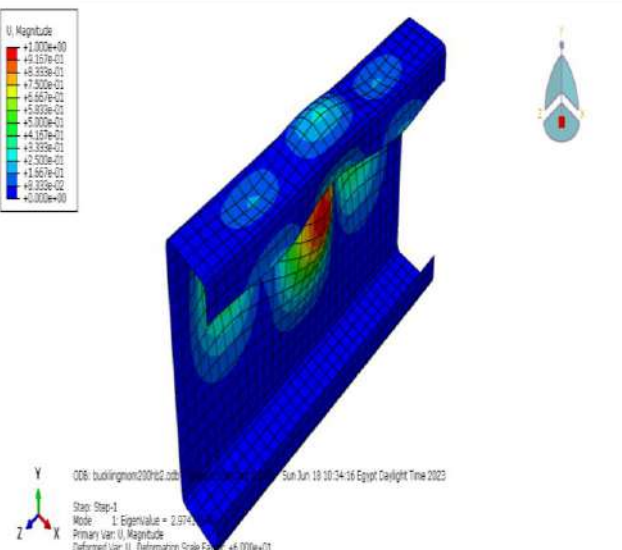
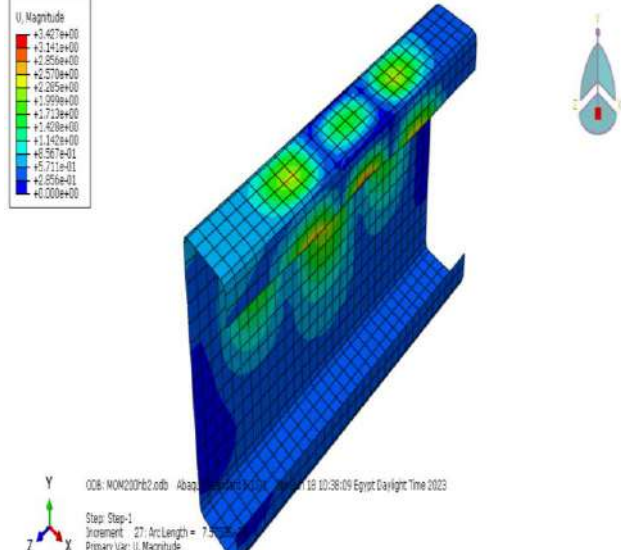
Compressive Z-section FEM modes			
d/b	Buckling mode	Failure mode	
.7	 <p> <small> U, Magnitude +1.000e+00 +9.367e-01 +6.534e-01 +7.500e-01 +6.667e-01 +5.674e-01 +5.000e-01 +4.367e-01 +3.333e-01 +2.500e-01 +1.667e-01 +0.534e-01 +0.000e+00 </small> </p> <p> <small> ODB: bucklingny1db7.odb Abaqus/Standard 6.13-1 Tue Jun 06 16:09:09 Egypt Daylight Time 2023 Step: Step-1 Mode: 1, Eigenvalue = 2.73827E+05 Primary Var: U, Magnitude Deformed Var: U, Deformation Scale Factor: +2.000e+01 </small> </p>	 <p> <small> U, Magnitude +1.070e+00 +1.015e+00 +9.227e-01 +8.384e-01 +7.350e-01 +6.459e-01 +5.526e-01 +4.624e-01 +3.691e-01 +2.758e-01 +1.845e-01 +9.227e-02 +0.000e+00 </small> </p> <p> <small> ODB: comrny1db7.odb Abaqus/Standard 6.13-1 Tue Jun 06 16:10:23 Egypt Daylight Time 2023 Step: Step-1 Increment: 14, Arc Length = 388.2 Primary Var: U, Magnitude Deformed Var: U, Deformation Scale Factor: +1.000e+00 </small> </p>	
.8	 <p> <small> U, Magnitude +1.000e+00 +9.367e-01 +6.534e-01 +7.500e-01 +6.667e-01 +5.674e-01 +5.000e-01 +4.367e-01 +3.333e-01 +2.500e-01 +1.667e-01 +0.534e-01 +0.000e+00 </small> </p> <p> <small> ODB: bucklingny1db8.odb Abaqus/Standard 6.13-1 Tue Jun 06 16:09:59 Egypt Daylight Time 2023 Step: Step-1 Mode: 1, Eigenvalue = 2.77215E+05 Primary Var: U, Magnitude Deformed Var: U, Deformation Scale Factor: +2.000e+01 </small> </p>	 <p> <small> U, Magnitude +2.620e+00 +2.494e+00 +2.354e+00 +1.975e+00 +1.755e+00 +1.556e+00 +1.317e+00 +1.097e+00 +8.777e-01 +6.569e-01 +4.369e-01 +2.504e-01 +0.000e+00 </small> </p> <p> <small> ODB: comrny1db8.odb Abaqus/Standard 6.13-1 Tue Jun 06 17:00:09 Egypt Daylight Time 2023 Step: Step-1 Increment: 15, Arc Length = 582.9 Primary Var: U, Magnitude Deformed Var: U, Deformation Scale Factor: +1.000e+00 </small> </p>	

A.2.3 Web-to-Flange Plate Length Ratio (h/b) Parameter

A.2.3.1 Flexural channel section

According to **Table A-9**, the channel section collapses due to combination of local and distortional buckling until a web-to-flange plate length ratio (h/b) equals 3. After this ratio and until it equals 6, the channel section collapses due to web local buckling.

Table A-9: - Various FEM modes for flexural channel section with different h/b ratios.

Flexural channel section FEM modes			
h/b	Buckling mode	Failure mode	
2	 <p>U, Magnitude +1.001e+00 +6.176e-01 +6.592e-01 +7.339e-01 +6.573e-01 +5.239e-01 +5.035e-01 +4.271e-01 +3.537e-01 +2.503e-01 +1.266e-01 +8.562e-02 +0.000e+00</p> <p>008: mombuckling2.odb Abaqus/Viewer Job: mombuckling2 Date: Sun Jun 11 17:25:22 Egypt Daylight Time 2023 Step: Step-1 Mode: 1, EigenValue = 2.514305e+07 Primary Var: U, Magnitude Deformed Var: U, Deformation Scale Factor: +4.000e+01</p>	 <p>U, Magnitude +3.455e+00 +3.166e+00 +2.875e+00 +2.582e+00 +2.302e+00 +2.014e+00 +1.727e+00 +1.439e+00 +1.151e+00 +8.634e-01 +5.759e-01 +2.875e-01 +0.000e+00</p> <p>008: momf11.odb Abaqus/Viewer Job: momf11 Date: Sun Jun 11 17:29:41 Egypt Daylight Time 2023 Step: Step-1 Increment: 25, ArcLength = 5.05019e+00 Primary Var: U, Magnitude Deformed Var: U, Deformation Scale Factor: +1.000e+00</p>	
3	 <p>U, Magnitude +1.000e+00 +6.337e-01 +8.355e-01 +7.300e-01 +6.667e-01 +5.039e-01 +3.000e-01 +4.167e-01 +3.355e-01 +2.300e-01 +1.667e-01 +9.339e-02 +0.000e+00</p> <p>008: buckling3000h2.odb Abaqus/Viewer Job: buckling3000h2 Date: Sun Jun 18 10:34:16 Egypt Daylight Time 2023 Step: Step-1 Mode: 1, EigenValue = 2.674e+07 Primary Var: U, Magnitude Deformed Var: U, Deformation Scale Factor: +4.000e+01</p>	 <p>U, Magnitude +3.427e+00 +3.143e+00 +2.859e+00 +2.570e+00 +2.285e+00 +1.999e+00 +1.713e+00 +1.428e+00 +1.143e+00 +8.567e-01 +5.711e-01 +2.859e-01 +0.000e+00</p> <p>008: MOM2000h2.odb Abaqus/Viewer Job: MOM2000h2 Date: Sun Jun 18 10:38:09 Egypt Daylight Time 2023 Step: Step-1 Increment: 27, ArcLength = 7.50000e+00 Primary Var: U, Magnitude Deformed Var: U, Deformation Scale Factor: +1.000e+00</p>	

Flexural channel section FEM modes		
h/b	Buckling mode	Failure mode
4		
5		
6		

A.2.3.2 Flexural Z-section

According to **Table A-10**, the Z-section collapses due to web-local buckling until a web-to-flange plate length ratio (h/b) is less than 6.

Table A-10: - Various FEM modes for flexural Z-section with different h/b ratios.

Flexural Z-section FEM modes			
h/b	Buckling mode	Failure mode	
2			
3			

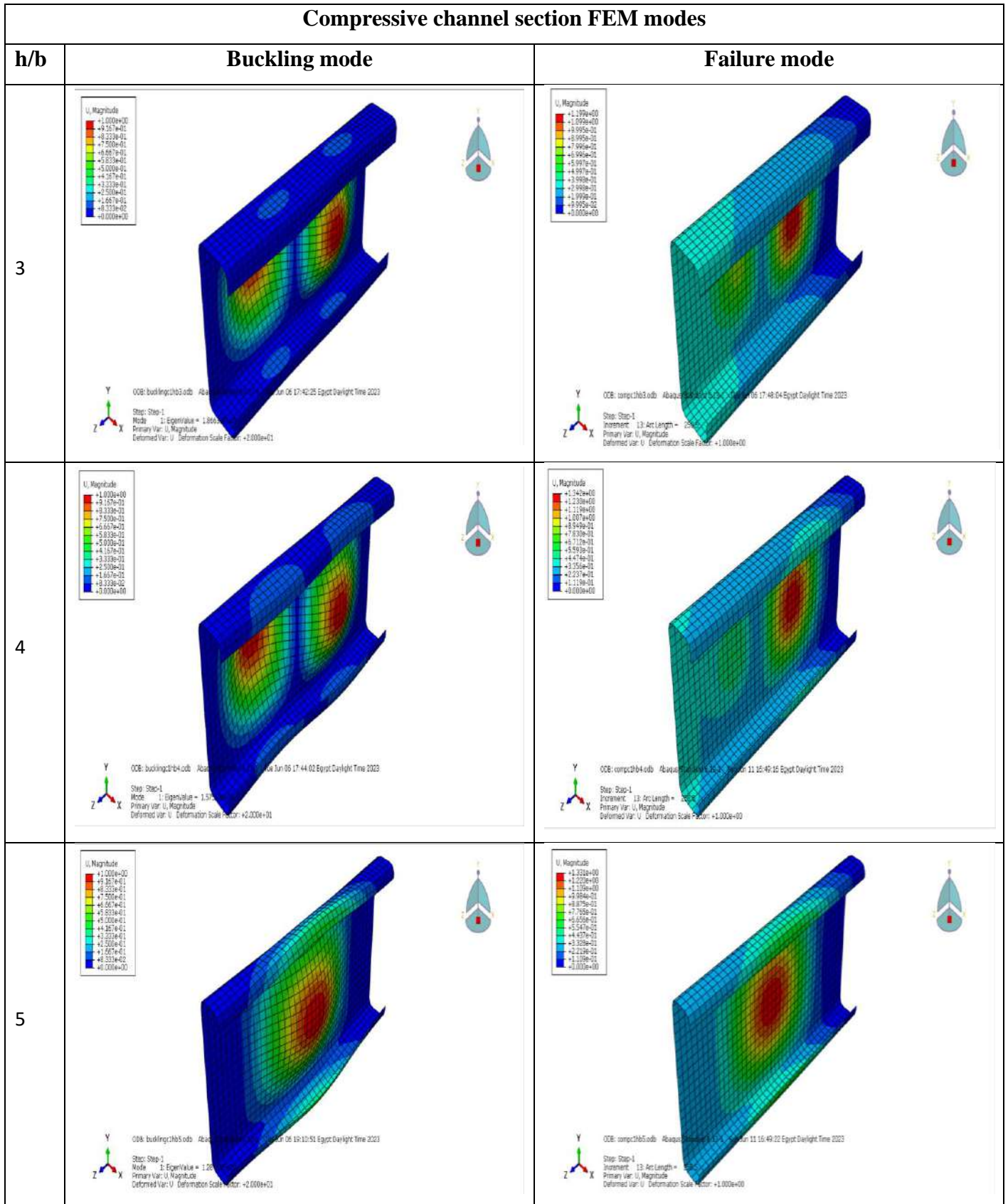
Flexural Z-section FEM modes		
h/b	Buckling mode	Failure mode
4		
5		
6		

A.2.3.3 Compressive channel section

According to **Table A-11**, the channel section collapses due to combination of local and distortional buckling until a web-to-flange plate length ratio (h/b) equals 1. After this ratio and until it equals 3, the channel section collapses due to web-local buckling. Finally, after this ratio and until it equals 5, the channel section collapses due to combination of distortional and web-local buckling.

Table A-11: - Various FEM modes for Compressive channel section with different h/b ratios.

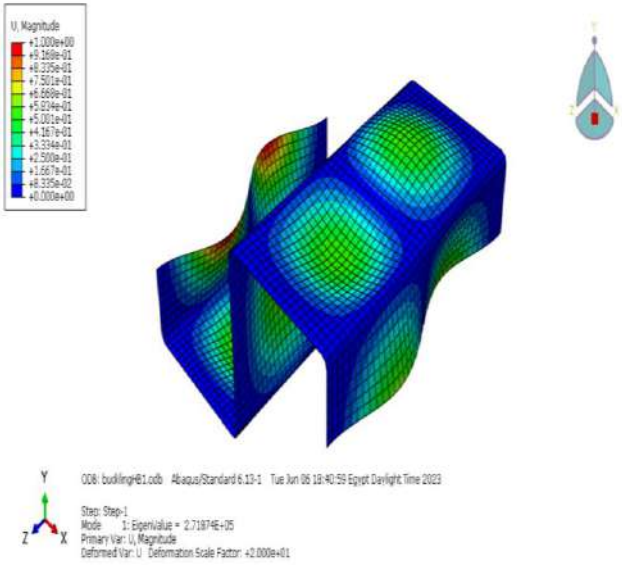
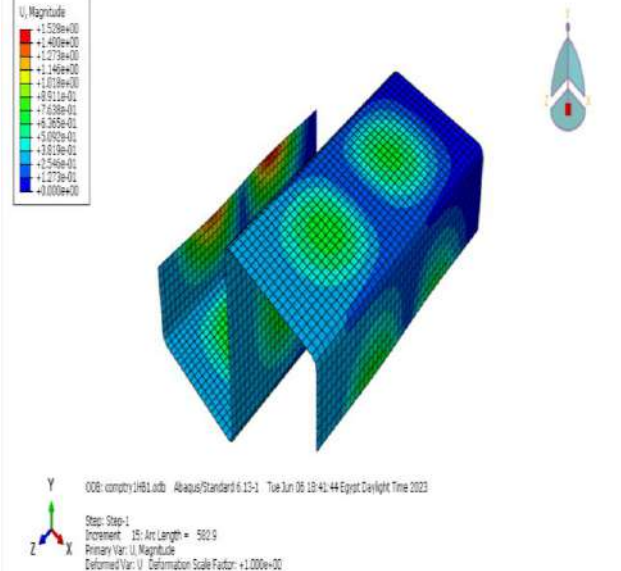
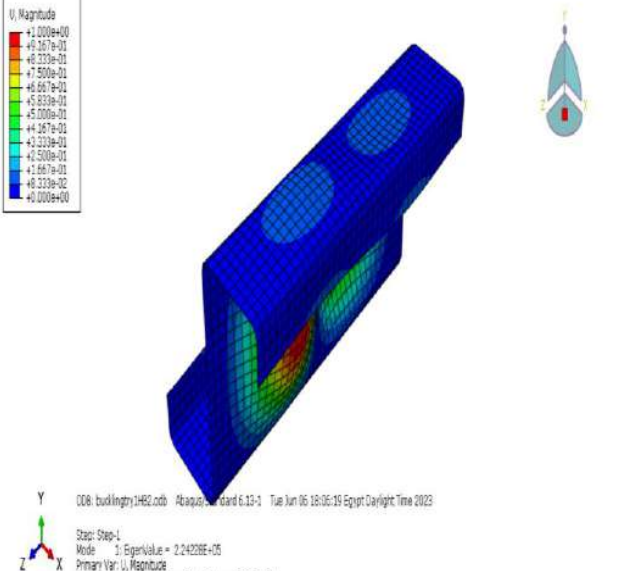
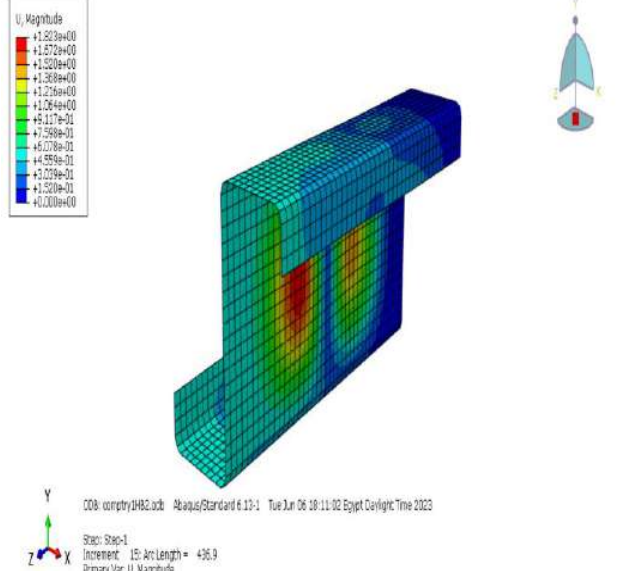
Compressive channel section FEM modes				
h/b	Buckling mode	Failure mode		
1	<p>U, Magnitude +1.000e+00 +6.171e-01 +6.337e-01 +7.552e-01 +6.670e-01 +5.036e-01 +3.000e-01 +4.458e-01 +1.285e-01 +2.331e-01 +1.887e-01 +0.000e+00 +0.000e+00</p> <p>Step: Step-1 Mode: 1: Eigenvalue = 0.76860E+05 Primary Var: U, Magnitude Deformed Var: U, Deformation Scale Factor: +2.000e+01</p>	<p>U, Magnitude +2.251e+00 +2.063e+00 +1.875e+00 +1.689e+00 +1.501e+00 +1.313e+00 +1.125e+00 +9.375e-01 +7.500e-01 +5.625e-01 +3.750e-01 +1.875e-01 +0.000e+00</p> <p>Step: Step-1 Increment: 17: Arc Length = 364.3 Primary Var: U, Magnitude Deformed Var: U, Deformation Scale Factor: +1.000e+00</p>		
2	<p>U, Magnitude +1.000e+00 +9.157e-01 +8.332e-01 +7.500e-01 +6.667e-01 +5.833e-01 +5.000e-01 +4.167e-01 +3.332e-01 +2.500e-01 +1.667e-01 +8.333e-02 +0.000e+00</p> <p>Step: Step-1 Mode: 1: Eigenvalue = 2.26601E+05 Primary Var: U, Magnitude Deformed Var: U, Deformation Scale Factor: +3.000e+01</p>	<p>U, Magnitude +1.029e+00 +1.502e+00 +1.366e+00 +1.029e+00 +1.093e+00 +9.582e-01 +8.196e-01 +6.800e-01 +5.404e-01 +4.009e-01 +2.732e-01 +1.366e-01 +0.000e+00</p> <p>Step: Step-1 Increment: 14: Arc Length = 388.2 Primary Var: U, Magnitude Deformed Var: U, Deformation Scale Factor: +1.000e+00</p>		



A.2.3.4 Compressive Z-section

As shown in **Table A-12**, the Z- section collapses due to combination of local and distortional buckling until a web-to-flange plate length ratio (h/b) equals 5.

Table A-12: - Various FEM modes for Compressive Z-section with different h/b ratios.

Compressive Z-section FEM modes		
h/b	Buckling mode	Failure mode
1	 <p>ODB: buckling1H1.odb Abaqus/Standard 6.13-1 Tue Jun 06 18:40:59 Egypt Daylight Time 2023</p> <p>Step: Step-1 Mode: 1; Eigenvalue = 2.71874E+05 Primary Var: U, Magnitude Deformed Var: U, Deformation Scale Factor: +2.000e+01</p>	 <p>ODB: comp1y1H1.odb Abaqus/Standard 6.13-1 Tue Jun 06 18:41:44 Egypt Daylight Time 2023</p> <p>Step: Step-1 Increment: 15; Arc Length = 582.9 Primary Var: U, Magnitude Deformed Var: U, Deformation Scale Factor: +1.000e+00</p>
2	 <p>ODB: buckling1H2.odb Abaqus/Standard 6.13-1 Tue Jun 06 18:06:19 Egypt Daylight Time 2023</p> <p>Step: Step-1 Mode: 3; Eigenvalue = 2.24228E+05 Primary Var: U, Magnitude Deformed Var: U, Deformation Scale Factor: +2.000e+01</p>	 <p>ODB: comp1y1H2.odb Abaqus/Standard 6.13-1 Tue Jun 06 18:11:02 Egypt Daylight Time 2023</p> <p>Step: Step-1 Increment: 15; Arc Length = 436.9 Primary Var: U, Magnitude Deformed Var: U, Deformation Scale Factor: +1.000e+00</p>

Compressive Z-section FEM modes		
h/b	Buckling mode	Failure mode
3	<p>ODB: buckling12483.odb; Abaqus/Standard 6.13-1; Tue Jun 06 18:07:11 Egypt Daylight Time 2023</p> <p>Step: Step-1 Mode: 2; Eigenvalue = 1.69430E+05 Primary Var: U, Magnitude Deformed Var: U; Deformation Scale Factor: +2.000e+01</p>	<p>ODB: comrty12483.odb; Abaqus/Standard 6.13-1; Tue Jun 06 18:11:06 Egypt Daylight Time 2023</p> <p>Step: Step-1 Increment: 14; Arc Length = 388.0 Primary Var: U, Magnitude Deformed Var: U; Deformation Scale Factor: +1.000e+00</p>
4	<p>ODB: buckling12484.odb; Abaqus/Standard 6.13-1; Tue Jun 06 18:08:10 Egypt Daylight Time 2023</p> <p>Step: Step-1 Mode: 1; Eigenvalue = 1.60312E+05 Primary Var: U, Magnitude Deformed Var: U; Deformation Scale Factor: +2.000e+01</p>	<p>ODB: comrty12484.odb; Abaqus/Standard 6.13-1; Tue Jun 06 18:11:11 Egypt Daylight Time 2023</p> <p>Step: Step-1 Increment: 13; Arc Length = 259.5 Primary Var: U, Magnitude Deformed Var: U; Deformation Scale Factor: +1.000e+00</p>
5	<p>ODB: buckling12485.odb; Abaqus/Standard 6.13-1; Tue Jun 06 18:04:09 Egypt Daylight Time 2023</p> <p>Step: Step-1 Mode: 1; Eigenvalue = 1.31011E+05 Primary Var: U, Magnitude Deformed Var: U; Deformation Scale Factor: +2.000e+01</p>	<p>ODB: comrty12485.odb; Abaqus/Standard 6.13-1; Tue Jun 06 18:05:06 Egypt Daylight Time 2023</p> <p>Step: Step-1 Increment: 14; Arc Length = 358.2 Primary Var: U, Magnitude Deformed Var: U; Deformation Scale Factor: +1.000e+00</p>

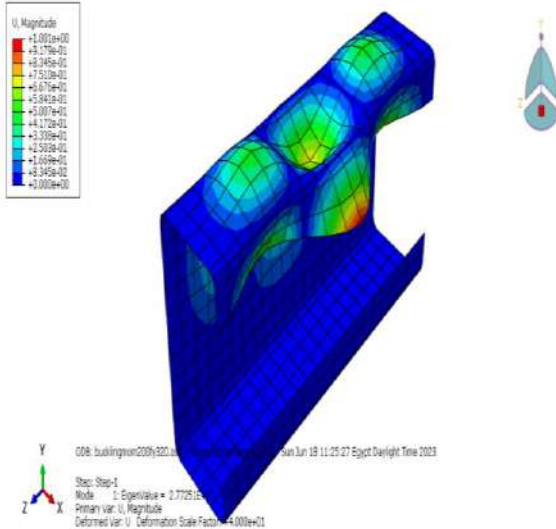
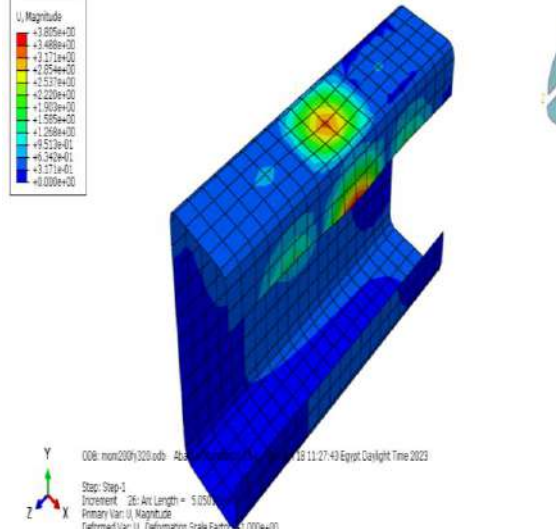
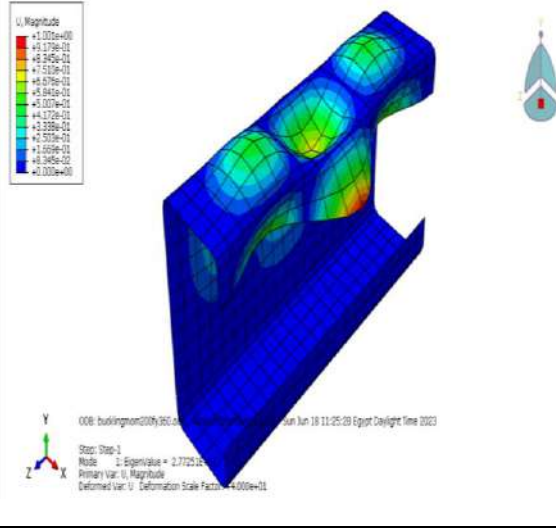
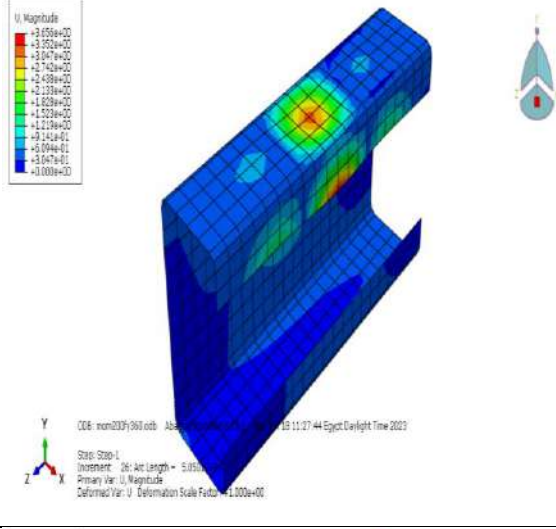
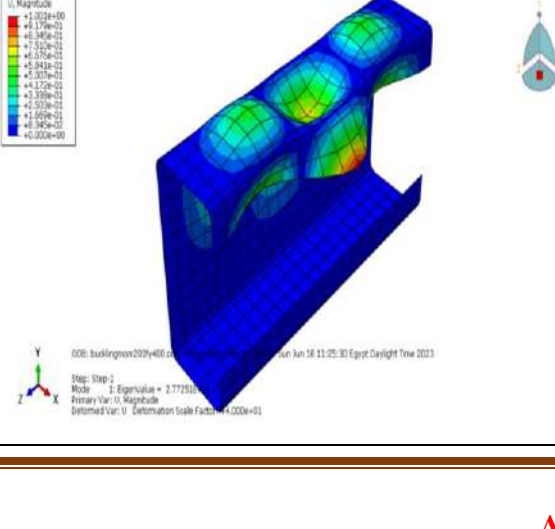
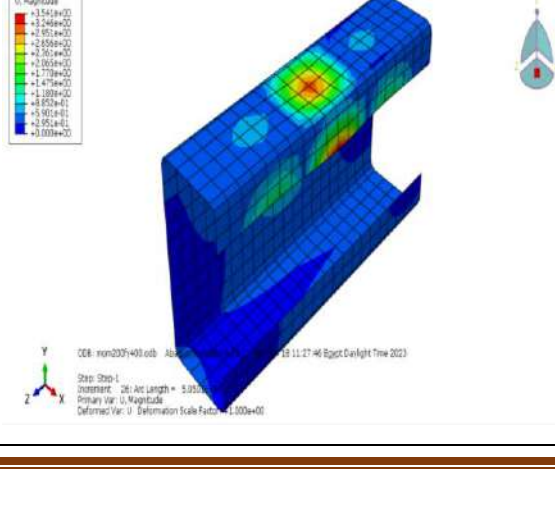
A.2.4 Yielding Strength (F_y) Parameter

A.2.4.1 Flexural channel section

As shown in **Table A-13**, all-flexural channel section collapses due to a combination of local and distortional buckling in all different steel yield strengths (F_y) parameters.

Table A-13: - Various FEM modes for flexural channel section with different yielding strengths.

Flexural channel section FEM modes		
F_y	Buckling mode	Failure mode
240	<p>008: bucklingmon200(240).ebs Sun Jun 18 11:25:23 Egypt Daylight Time 2023 Step: Step-1 Mode: 1: Eigenvalue = 2.77251E-01 Primary Var: U, Magnitude Deformed Var: U, Deformation Scale Factor = 4.000e+01</p>	<p>008: max200(240).ebs Abu-El-Khawas@iut.ac.eg Sun Jun 18 11:27:40 Egypt Daylight Time 2023 Step: Step-1 Increment: 25: Arc Length = 3.365e+00 Primary Var: U, Magnitude Deformed Var: U, Deformation Scale Factor = 1.000e+00</p>
280	<p>008: bucklingmon200(280).ebs Sun Jun 18 11:25:25 Egypt Daylight Time 2023 Step: Step-1 Mode: 1: Eigenvalue = 2.77251E-01 Primary Var: U, Magnitude Deformed Var: U, Deformation Scale Factor = 4.000e+01</p>	<p>008: mon200(280).ebs Abu-El-Khawas@iut.ac.eg Sun Jun 18 11:27:41 Egypt Daylight Time 2023 Step: Step-1 Increment: 25: Arc Length = 3.365e+00 Primary Var: U, Magnitude Deformed Var: U, Deformation Scale Factor = 1.000e+00</p>

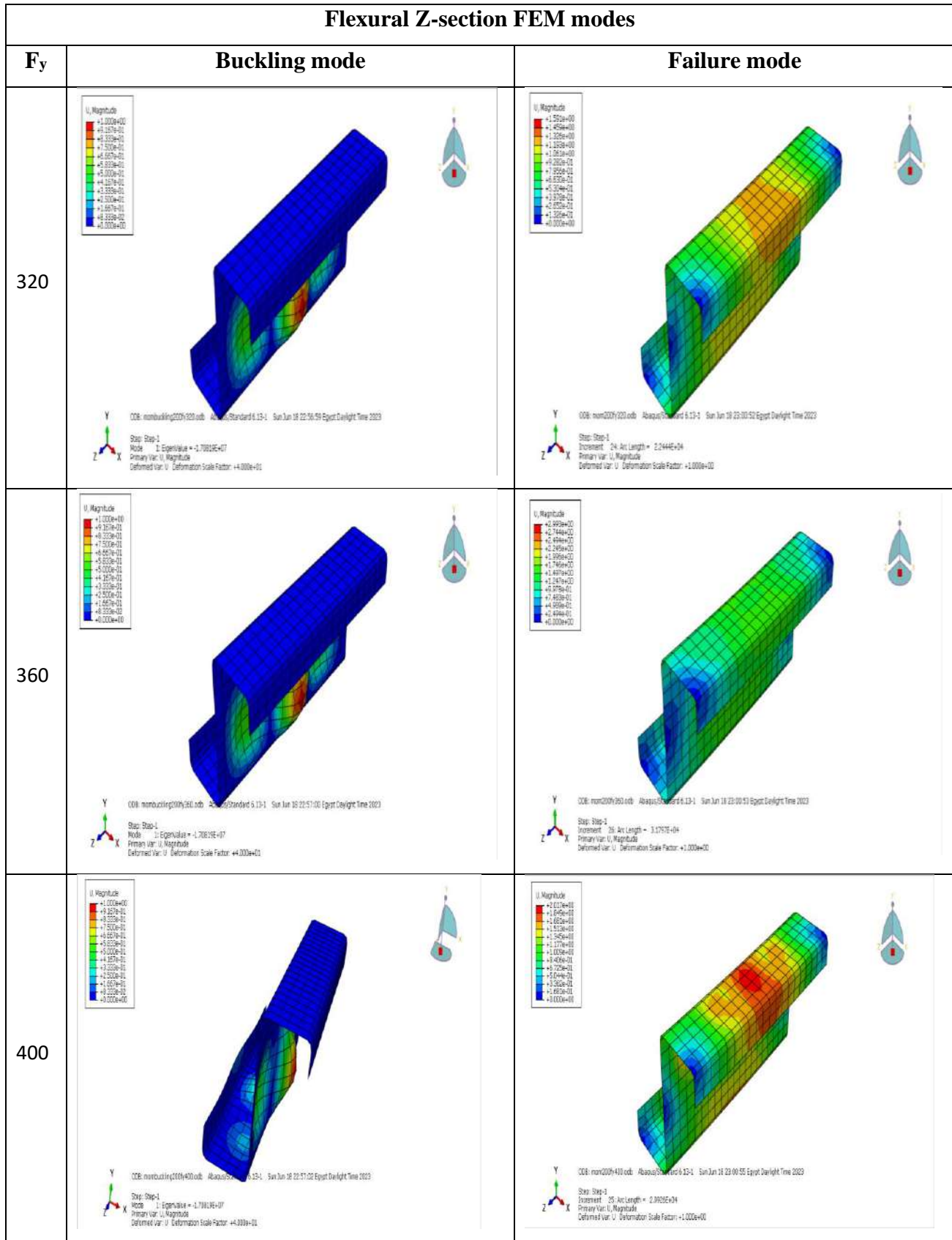
Flexural channel section FEM modes		
Fy	Buckling mode	Failure mode
320	 <p>U, Magnitude +1.000e+00 +8.179e-01 +6.349e-01 +4.519e-01 +2.689e-01 +8.590e-02 +6.760e-02 +4.930e-02 +3.100e-02 +1.270e-02 -5.559e-03 -7.389e-03 -9.219e-03 -1.105e-02 -1.289e-02 -1.473e-02 -1.657e-02 -1.841e-02 -2.025e-02 -2.209e-02 -2.393e-02 -2.577e-02 -2.761e-02 -2.945e-02 -3.129e-02 -3.313e-02 -3.497e-02 -3.681e-02 -3.865e-02 -4.049e-02 -4.233e-02 -4.417e-02 -4.601e-02 -4.785e-02 -4.969e-02 -5.153e-02 -5.337e-02 -5.521e-02 -5.705e-02 -5.889e-02 -6.073e-02 -6.257e-02 -6.441e-02 -6.625e-02 -6.809e-02 -6.993e-02 -7.177e-02 -7.361e-02 -7.545e-02 -7.729e-02 -7.913e-02 -8.097e-02 -8.281e-02 -8.465e-02 -8.649e-02 -8.833e-02 -9.017e-02 -9.201e-02 -9.385e-02 -9.569e-02 -9.753e-02 -9.937e-02 -1.012e+00</p> <p>COE: bucklingmon2009\320... Step: Step-1 Mode: 1; Eigenvalue = 2.77251e+01 Primary Var: U, Magnitude Deformed Var: U, Deformation Scale Factor = 4.000e+01</p>	 <p>U, Magnitude +3.000e+00 +2.488e+00 +1.976e+00 +1.464e+00 +9.52e+00 +4.376e+00 -2.200e+00 -7.056e+00 -1.200e+00 -6.144e+00 -1.100e+00 -5.232e+00 -1.000e+00 -4.512e+00 -9.000e+00 -1.500e+00 -3.408e+00 -6.816e+00 -1.000e+00 -2.208e+00 -4.416e+00 -6.624e+00 -8.832e+00 -1.104e+01 -1.324e+01 -1.544e+01 -1.764e+01 -1.984e+01 -2.204e+01 -2.424e+01 -2.644e+01 -2.864e+01 -3.084e+01 -3.304e+01 -3.524e+01 -3.744e+01 -3.964e+01 -4.184e+01 -4.404e+01 -4.624e+01 -4.844e+01 -5.064e+01 -5.284e+01 -5.504e+01 -5.724e+01 -5.944e+01 -6.164e+01 -6.384e+01 -6.604e+01 -6.824e+01 -7.044e+01 -7.264e+01 -7.484e+01 -7.704e+01 -7.924e+01 -8.144e+01 -8.364e+01 -8.584e+01 -8.804e+01 -9.024e+01 -9.244e+01 -9.464e+01 -9.684e+01 -9.904e+01 -1.012e+02</p> <p>COE: mon2009\320\ob... Step: Step-1 Increment: 26; Arc Length = 5.020e+00 Primary Var: U, Magnitude Deformed Var: U, Deformation Scale Factor = 1.000e+00</p>
360	 <p>U, Magnitude +1.000e+00 +8.179e-01 +6.349e-01 +4.519e-01 +2.689e-01 +8.590e-02 +6.760e-02 +4.930e-02 +3.100e-02 +1.270e-02 -5.559e-03 -7.389e-03 -9.219e-03 -1.105e-02 -1.289e-02 -1.473e-02 -1.657e-02 -1.841e-02 -2.025e-02 -2.209e-02 -2.393e-02 -2.577e-02 -2.761e-02 -2.945e-02 -3.129e-02 -3.313e-02 -3.497e-02 -3.681e-02 -3.865e-02 -4.049e-02 -4.233e-02 -4.417e-02 -4.601e-02 -4.785e-02 -4.969e-02 -5.153e-02 -5.337e-02 -5.521e-02 -5.705e-02 -5.889e-02 -6.073e-02 -6.257e-02 -6.441e-02 -6.625e-02 -6.809e-02 -6.993e-02 -7.177e-02 -7.361e-02 -7.545e-02 -7.729e-02 -7.913e-02 -8.097e-02 -8.281e-02 -8.465e-02 -8.649e-02 -8.833e-02 -9.017e-02 -9.201e-02 -9.385e-02 -9.569e-02 -9.753e-02 -9.937e-02 -1.012e+00</p> <p>COE: bucklingmon2009\360... Step: Step-1 Mode: 1; Eigenvalue = 2.77251e+01 Primary Var: U, Magnitude Deformed Var: U, Deformation Scale Factor = 4.000e+01</p>	 <p>U, Magnitude +3.000e+00 +2.488e+00 +1.976e+00 +1.464e+00 +9.52e+00 +4.376e+00 -2.200e+00 -7.056e+00 -1.200e+00 -6.144e+00 -1.100e+00 -5.232e+00 -1.000e+00 -4.512e+00 -9.000e+00 -1.500e+00 -3.408e+00 -6.816e+00 -1.000e+00 -2.208e+00 -4.416e+00 -6.624e+00 -8.832e+00 -1.104e+01 -1.324e+01 -1.544e+01 -1.764e+01 -1.984e+01 -2.204e+01 -2.424e+01 -2.644e+01 -2.864e+01 -3.084e+01 -3.304e+01 -3.524e+01 -3.744e+01 -3.964e+01 -4.184e+01 -4.404e+01 -4.624e+01 -4.844e+01 -5.064e+01 -5.284e+01 -5.504e+01 -5.724e+01 -5.944e+01 -6.164e+01 -6.384e+01 -6.604e+01 -6.824e+01 -7.044e+01 -7.264e+01 -7.484e+01 -7.704e+01 -7.924e+01 -8.144e+01 -8.364e+01 -8.584e+01 -8.804e+01 -9.024e+01 -9.244e+01 -9.464e+01 -9.684e+01 -9.904e+01 -1.012e+02</p> <p>COE: mon2009\360\ob... Step: Step-1 Increment: 26; Arc Length = 5.020e+00 Primary Var: U, Magnitude Deformed Var: U, Deformation Scale Factor = 1.000e+00</p>
400	 <p>U, Magnitude +1.000e+00 +8.179e-01 +6.349e-01 +4.519e-01 +2.689e-01 +8.590e-02 +6.760e-02 +4.930e-02 +3.100e-02 +1.270e-02 -5.559e-03 -7.389e-03 -9.219e-03 -1.105e-02 -1.289e-02 -1.473e-02 -1.657e-02 -1.841e-02 -2.025e-02 -2.209e-02 -2.393e-02 -2.577e-02 -2.761e-02 -2.945e-02 -3.129e-02 -3.313e-02 -3.497e-02 -3.681e-02 -3.865e-02 -4.049e-02 -4.233e-02 -4.417e-02 -4.601e-02 -4.785e-02 -4.969e-02 -5.153e-02 -5.337e-02 -5.521e-02 -5.705e-02 -5.889e-02 -6.073e-02 -6.257e-02 -6.441e-02 -6.625e-02 -6.809e-02 -6.993e-02 -7.177e-02 -7.361e-02 -7.545e-02 -7.729e-02 -7.913e-02 -8.097e-02 -8.281e-02 -8.465e-02 -8.649e-02 -8.833e-02 -9.017e-02 -9.201e-02 -9.385e-02 -9.569e-02 -9.753e-02 -9.937e-02 -1.012e+00</p> <p>COE: bucklingmon2009\400... Step: Step-1 Mode: 1; Eigenvalue = 2.77251e+01 Primary Var: U, Magnitude Deformed Var: U, Deformation Scale Factor = 4.000e+01</p>	 <p>U, Magnitude +3.000e+00 +2.488e+00 +1.976e+00 +1.464e+00 +9.52e+00 +4.376e+00 -2.200e+00 -7.056e+00 -1.200e+00 -6.144e+00 -1.100e+00 -5.232e+00 -1.000e+00 -4.512e+00 -9.000e+00 -1.500e+00 -3.408e+00 -6.816e+00 -1.000e+00 -2.208e+00 -4.416e+00 -6.624e+00 -8.832e+00 -1.104e+01 -1.324e+01 -1.544e+01 -1.764e+01 -1.984e+01 -2.204e+01 -2.424e+01 -2.644e+01 -2.864e+01 -3.084e+01 -3.304e+01 -3.524e+01 -3.744e+01 -3.964e+01 -4.184e+01 -4.404e+01 -4.624e+01 -4.844e+01 -5.064e+01 -5.284e+01 -5.504e+01 -5.724e+01 -5.944e+01 -6.164e+01 -6.384e+01 -6.604e+01 -6.824e+01 -7.044e+01 -7.264e+01 -7.484e+01 -7.704e+01 -7.924e+01 -8.144e+01 -8.364e+01 -8.584e+01 -8.804e+01 -9.024e+01 -9.244e+01 -9.464e+01 -9.684e+01 -9.904e+01 -1.012e+02</p> <p>COE: mon2009\400\ob... Step: Step-1 Increment: 26; Arc Length = 5.020e+00 Primary Var: U, Magnitude Deformed Var: U, Deformation Scale Factor = 1.000e+00</p>

A.2.4.2 Flexural Z-section

According to **Table A-14**, all-flexural Z-section collapses due to combination of local and distortional buckling in all different steel yield strengths (F_y) parameters.

Table A-14: - Various FEM modes for flexural Z-section with different yielding strengths.

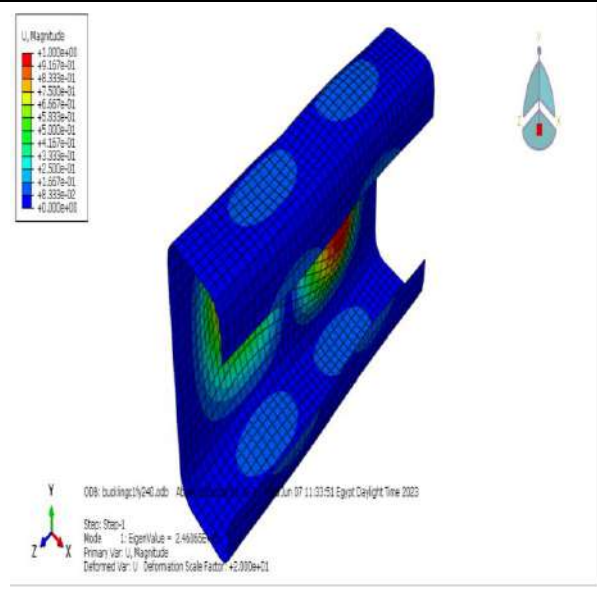
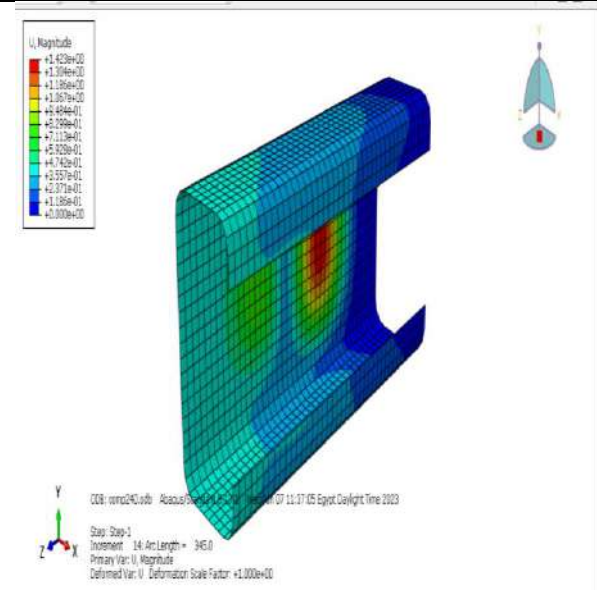
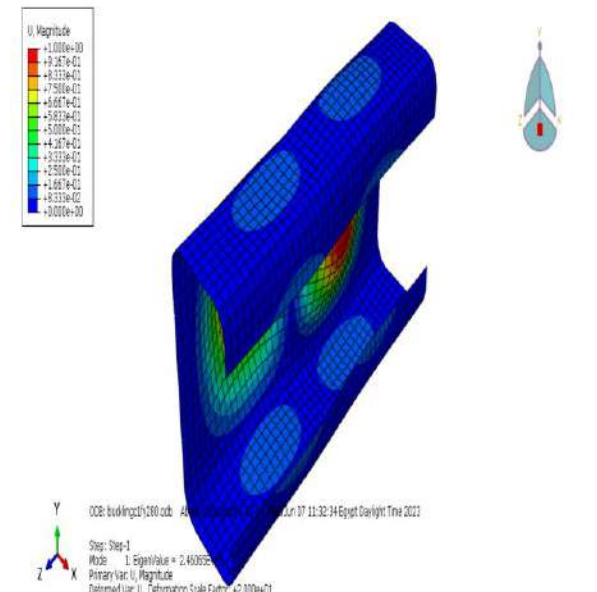
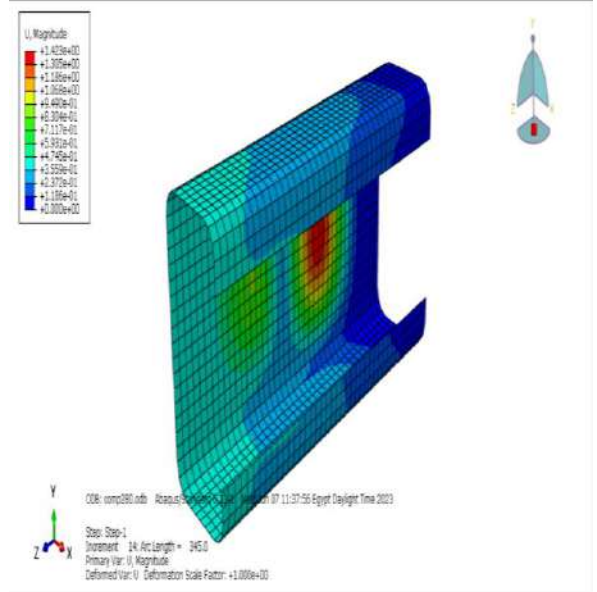
Flexural Z-section FEM modes		
F_y	Buckling mode	Failure mode
240		
280		

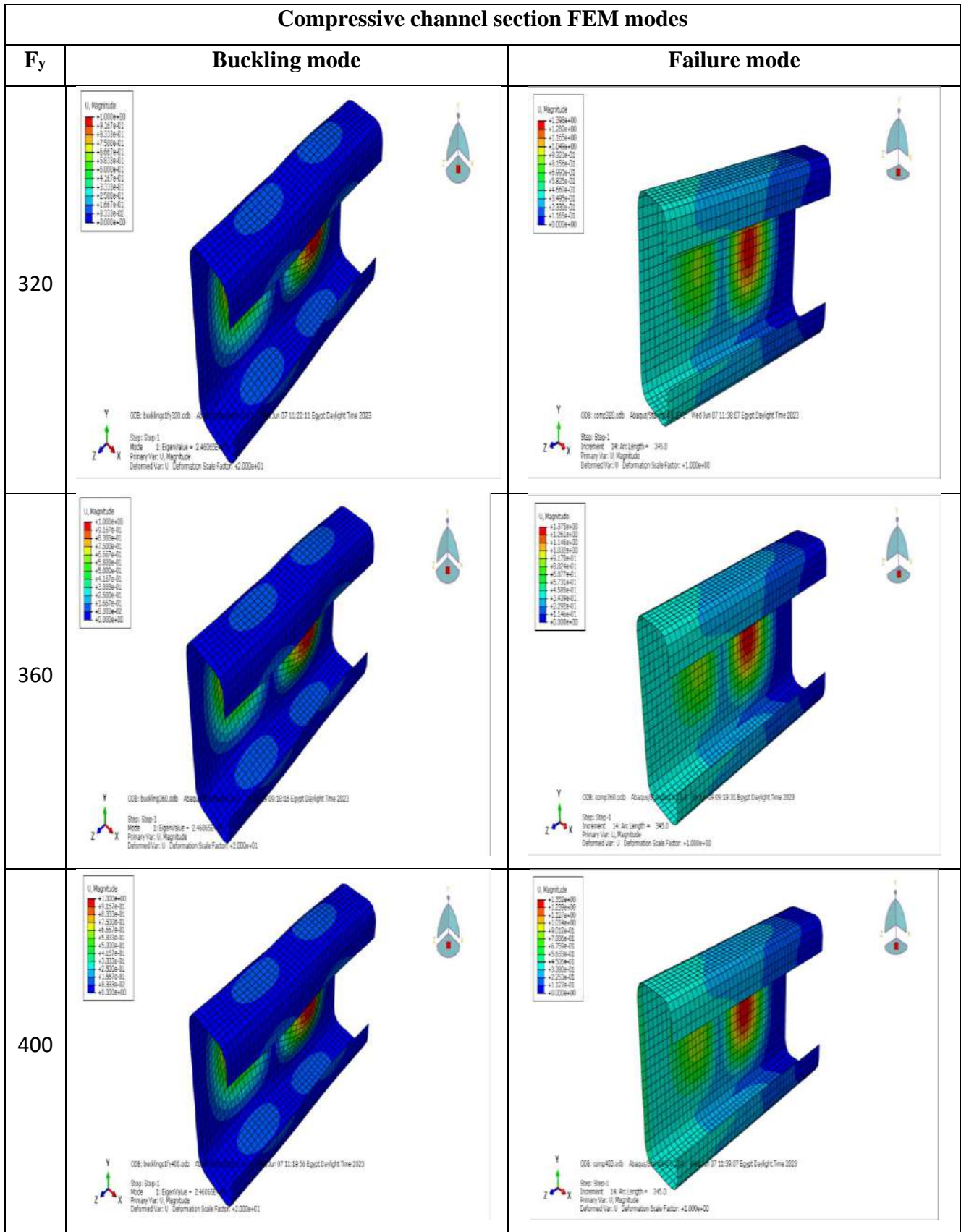


A.2.4.3 Compressive channel section

As shown in **Table A-15**, all-Compressive channel section collapses due to local buckling in all different steel yield strengths (F_y) parameters.

Table A-15: - Various FEM modes for Compressive channel section with different yielding strengths.

Compressive channel section FEM modes		
F_y	Buckling mode	Failure mode
240	 <p>U, Magnitude +1.000e+01 +6.167e-01 +6.335e-01 +7.503e-01 +6.167e-01 +5.000e-01 +4.167e-01 +3.335e-01 +3.503e-01 +1.667e-01 +6.335e-02 +0.000e+00</p> <p>008: bucking1\240.job: Abacus/Exec/Pre/PreProc/PreProc - Sun 07 11:33:53 Egypt Daylight Time 2023 Step: Step-1 Mode: 1, EigenValue = 2.46065e+01 Primary Var: U, Magnitude Deformed Var: U, Deformation Scale Factor: +3.000e+01</p>	 <p>U, Magnitude +1.432e+00 +1.336e+00 +1.186e+00 +1.167e+00 +6.484e-01 +5.199e-01 +7.113e-01 +5.329e-01 +4.742e-01 +3.337e-01 +2.371e-01 +1.186e-01 +0.000e+00</p> <p>008: vomo240.job: Abacus/Exec/Pre/PreProc/PreProc - Sun 07 11:37:05 Egypt Daylight Time 2023 Step: Step-1 Increment: 14, Arc Length = 34E-01 Primary Var: U, Magnitude Deformed Var: U, Deformation Scale Factor: +1.000e+00</p>
280	 <p>U, Magnitude +1.000e+00 +9.267e-01 +8.337e-01 +7.500e-01 +6.667e-01 +5.667e-01 +3.000e-01 +4.337e-01 +2.500e-01 +1.667e-01 +8.336e-02 +0.000e+00</p> <p>008: bucking1\280.job: Abacus/Exec/Pre/PreProc/PreProc - Sun 07 11:32:34 Egypt Daylight Time 2023 Step: Step-1 Mode: 1, EigenValue = 2.46065e+01 Primary Var: U, Magnitude Deformed Var: U, Deformation Scale Factor: +2.000e+01</p>	 <p>U, Magnitude +1.432e+00 +1.336e+00 +1.186e+00 +1.167e+00 +6.484e-01 +5.199e-01 +7.113e-01 +5.329e-01 +4.742e-01 +3.337e-01 +2.371e-01 +1.186e-01 +0.000e+00</p> <p>008: vomo280.job: Abacus/Exec/Pre/PreProc/PreProc - Sun 07 11:37:56 Egypt Daylight Time 2023 Step: Step-1 Increment: 14, Arc Length = 34E-01 Primary Var: U, Magnitude Deformed Var: U, Deformation Scale Factor: +1.000e+00</p>



A.2.4.4 Compressive channel section

According to **Table A-16**, all-Compressive Z-section collapses due to local buckling in all different steel yield strengths (F_y) parameters.

Table A-16: - Various FEM modes for Compressive channel section with different yielding strengths.

Compressive Z-section FEM modes			
F_y	Buckling mode	Failure mode	
240			
280			

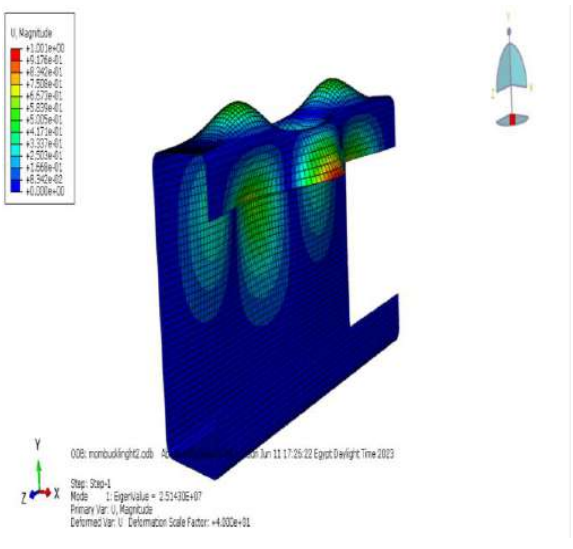
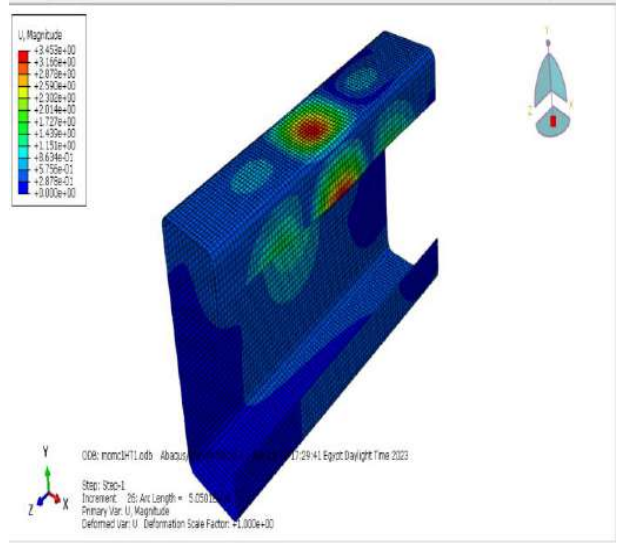
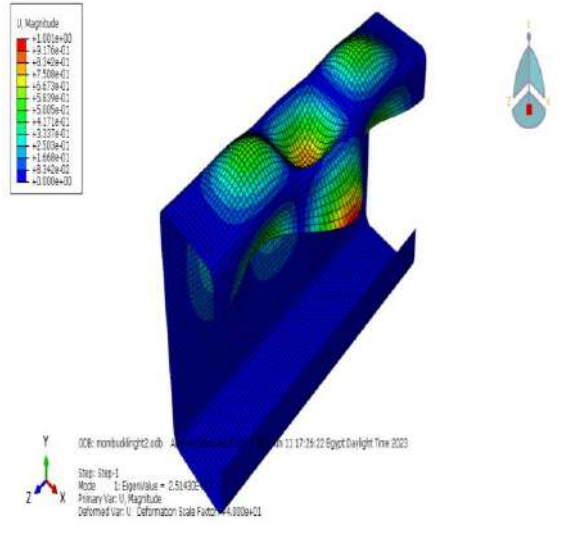
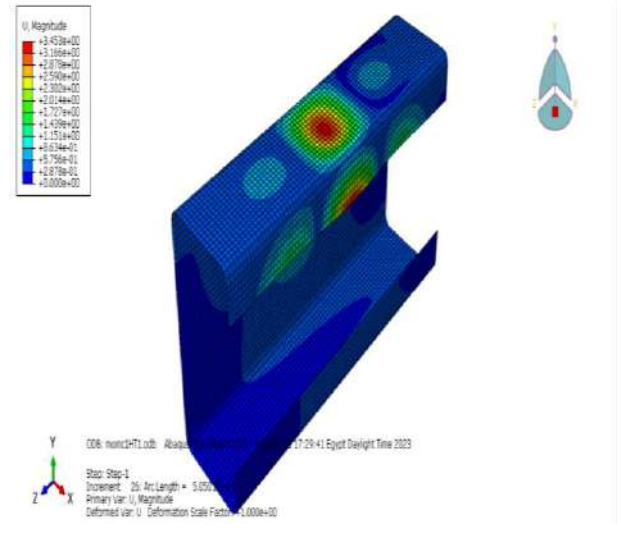
Compressive Z-section FEM modes		
F_y	Buckling mode	Failure mode
320		
360		
400		

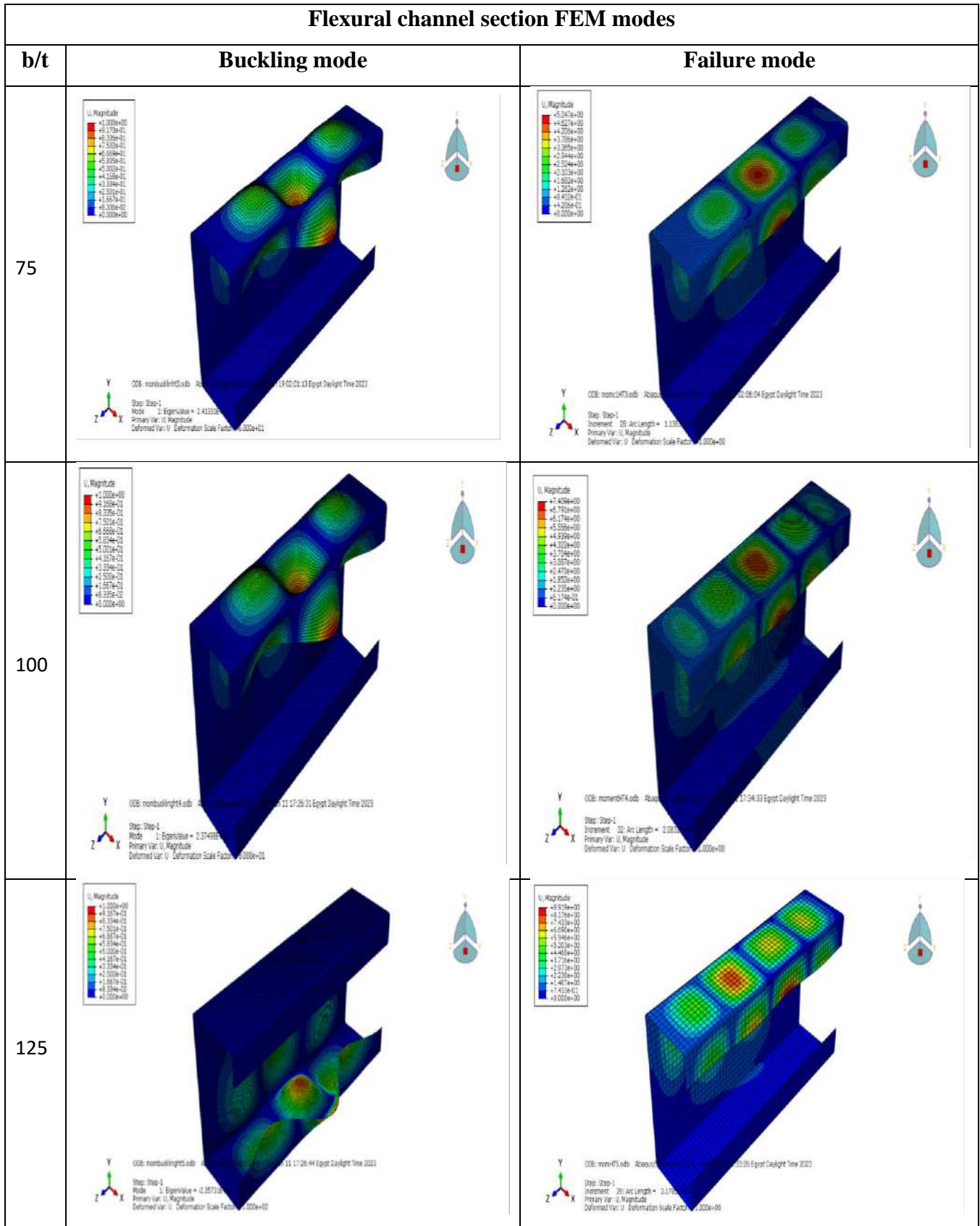
A.2.5 Plate Slenderness Ratio Parameter

A.2.5.1 Flexural channel section

As shown in **Table A-17**, all-flexural channel section collapses due to combination of local and distortional buckling in all different studied flange slenderness ratios (b/t).

Table A-17: - Various FEM modes for flexural channel section with different b/t ratios.

Flexural channel section FEM modes			
b/t	Buckling mode	Failure mode	
25	 <p>U, Magnitude +1.001e+00 +5.176e-01 +6.396e-01 +7.599e-01 +8.879e-01 +5.859e-01 +5.035e-01 +4.171e-01 +3.327e-01 +2.503e-01 +1.680e-01 +8.542e-02 +3.000e-02</p> <p>Step: Step-1 Mode: 1: EigenValue = 2.51430E+07 Primary Var: U, Magnitude Deformed Var: U, Deformation Scale Factor: +1.000e+01</p>	 <p>U, Magnitude +3.452e+00 +3.166e+00 +2.875e+00 +2.542e+00 +2.202e+00 +2.014e+00 +1.727e+00 +1.439e+00 +1.151e+00 +8.634e-01 +5.756e-01 +2.875e-01 +3.000e+00</p> <p>Step: Step-1 Increment: 25: Arc Length = 5.0501e-01 Primary Var: U, Magnitude Deformed Var: U, Deformation Scale Factor: +1.000e+00</p>	
50	 <p>U, Magnitude +1.001e+00 +9.176e-01 +8.342e-01 +7.509e-01 +6.679e-01 +5.859e-01 +5.035e-01 +4.171e-01 +3.327e-01 +2.503e-01 +1.680e-01 +8.542e-02 +3.000e-02</p> <p>Step: Step-1 Mode: 1: EigenValue = 2.51430E+07 Primary Var: U, Magnitude Deformed Var: U, Deformation Scale Factor: +1.000e+01</p>	 <p>U, Magnitude +3.452e+00 +3.166e+00 +2.875e+00 +2.542e+00 +2.202e+00 +2.014e+00 +1.727e+00 +1.439e+00 +1.151e+00 +8.634e-01 +5.756e-01 +2.875e-01 +3.000e+00</p> <p>Step: Step-1 Increment: 25: Arc Length = 5.0501e-01 Primary Var: U, Magnitude Deformed Var: U, Deformation Scale Factor: +1.000e+00</p>	



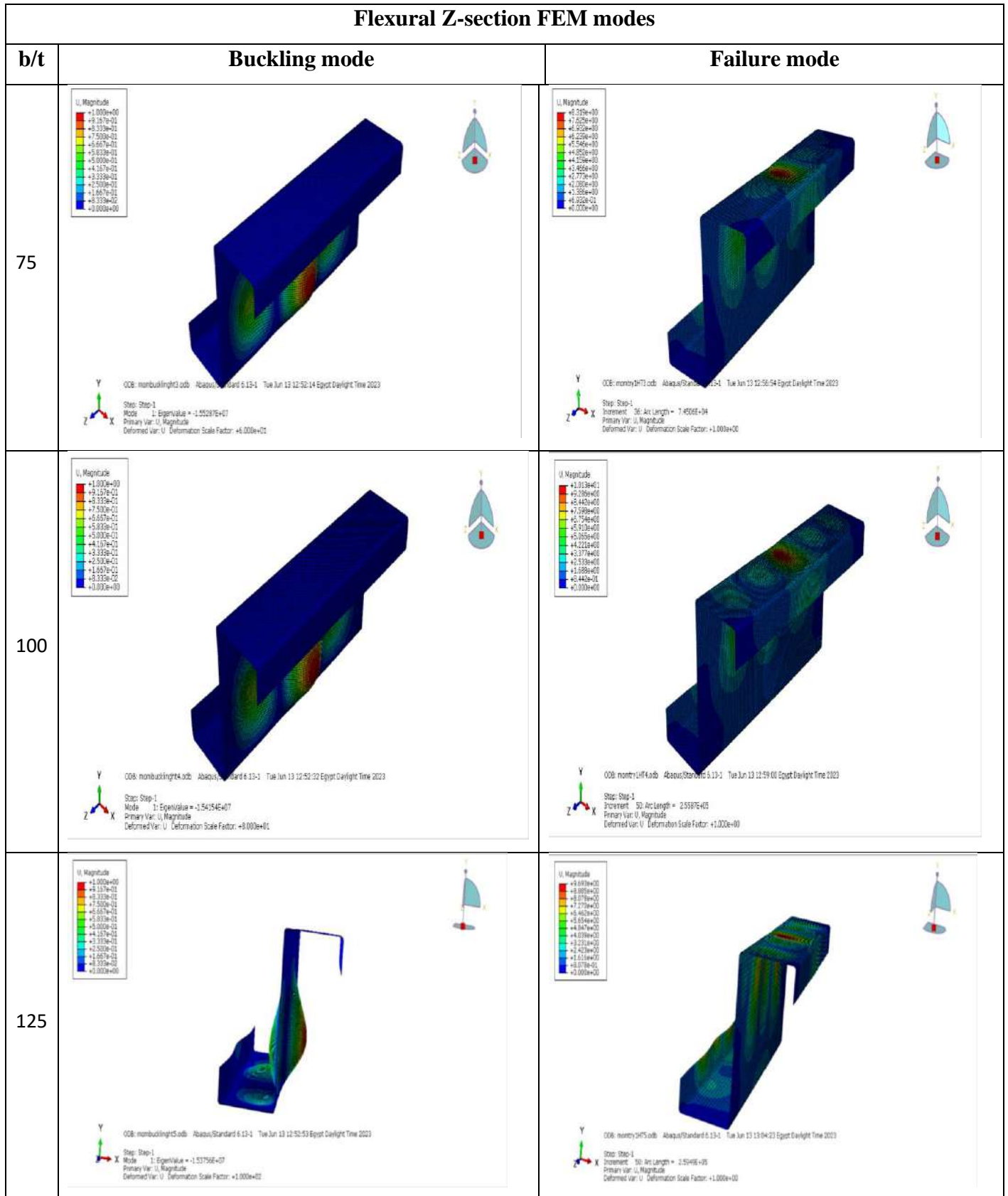
Flexural channel section FEM modes		
b/t	Buckling mode	Failure mode
150	<p>U, Magnitude</p> <ul style="list-style-type: none"> +1.303e+02 +1.127e+01 +0.974e+01 +7.503e+01 +5.657e+01 +5.854e+01 +0.803e+01 +4.157e+01 +3.374e+01 +2.503e+01 +1.657e+01 +0.334e+02 +0.000e+00 <p>008: inombuckling161.odb 11:17:27:00 Egsst Daylight Time 2023</p> <p>Step: Step-1 Mode: U, Eigenvalue = 2.346102e+02 Primary Var: U, Magnitude Deformed Var: U, Deformation Scale Factor = 1.200e+02</p>	<p>U, Magnitude</p> <ul style="list-style-type: none"> +4.174e+02 +3.825e+02 +1.670e+02 +1.110e+02 +2.710e+02 +2.470e+02 +2.087e+02 +1.770e+02 +1.391e+02 +1.044e+02 +0.977e+01 +0.679e+01 +0.000e+00 <p>008: inombuck161.odb 11:17:33:00 Egsst Daylight Time 2023</p> <p>Step: Step-1 Increment: 38: Arc Length = 1.2048 Primary Var: U, Magnitude Deformed Var: U, Deformation Scale Factor = 1.000e+00</p>

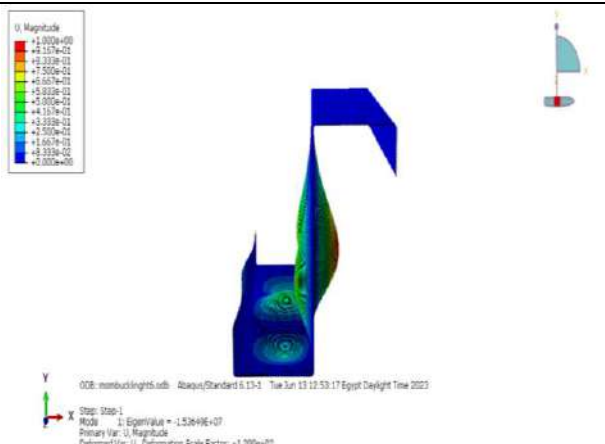
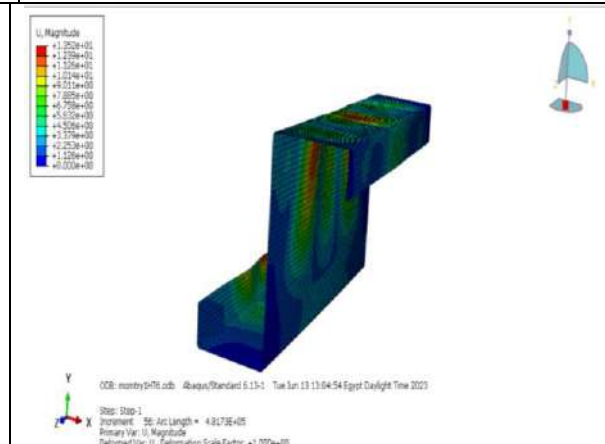
A.2.5.2 Flexural Z-section

Flexural Z-section collapses due to local buckling when flange slenderness ratio (b/t) is less than 100 and greater than this ratio it collapses due to combination of local and distortional buckling, as shown in **Table A-18**.

Table A-18: - Various FEM modes for flexural Z-section with different b/t ratios.

Flexural Z-section FEM modes		
b/t	Buckling mode	Failure mode
25		
50		

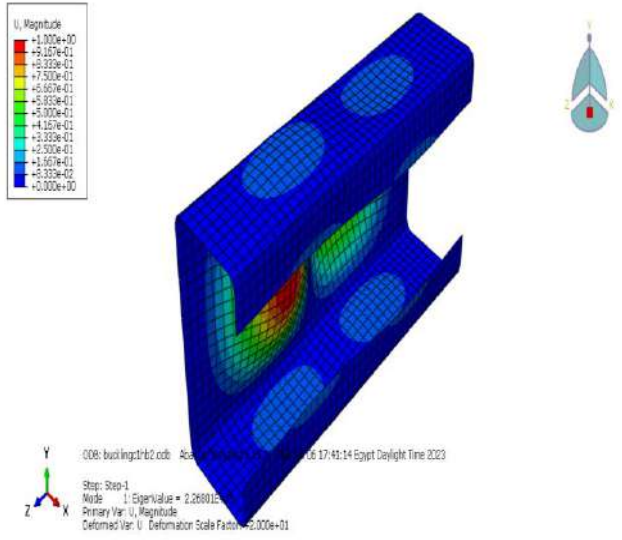
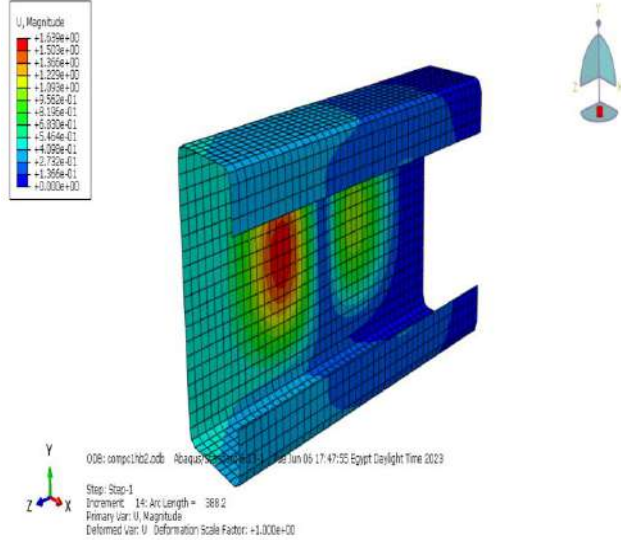
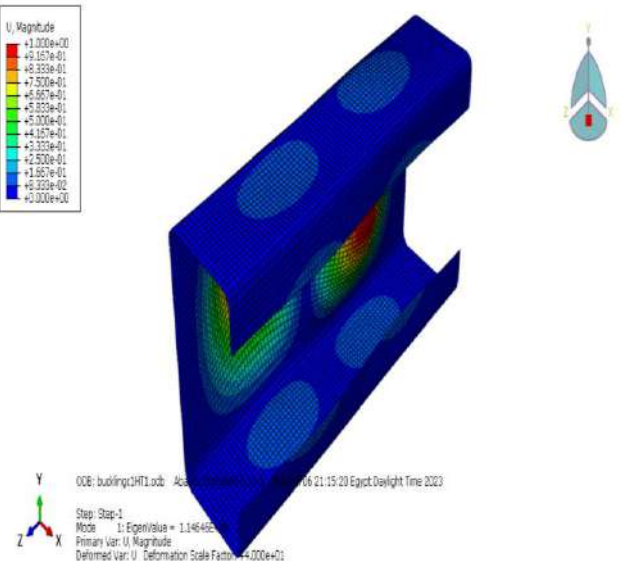
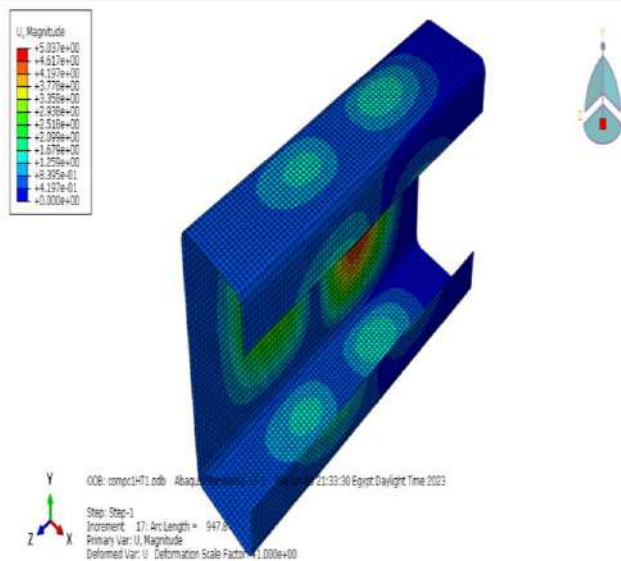


Flexural Z-section FEM modes		
b/t	Buckling mode	Failure mode
150	 <p> <small> U, Magnitude 1.000e+02 5.57e+01 3.33e+01 7.50e+00 6.67e+00 5.00e+00 3.33e+00 1.67e+00 6.67e-01 3.33e-01 1.000e+00 </small> </p> <p> <small> ODB: membuck1right5.odb - Abaqus/Standard 6.13-1 Tue Jun 13 12:53:17 Egypt Daylight Time 2023 Step: Step-1 Mode 1: EigenValue = -1.52649E+07 Primary Var: U, Magnitude Deformed Var: U, Deformation Scale Factor = 1.000e+02 </small> </p>	 <p> <small> U, Magnitude 1.250e+01 1.000e+01 7.50e+00 5.00e+00 2.50e+00 1.25e+00 6.25e-01 3.12e-01 1.56e-01 7.81e-02 3.91e-02 </small> </p> <p> <small> ODB: memtyp9r6.odb - Abaqus/Standard 6.13-1 Tue Jun 13 13:04:54 Egypt Daylight Time 2023 Step: Step-1 Element: 50; Set Length = 4.8173E+05 Primary Var: U, Magnitude Deformed Var: U, Deformation Scale Factor = 1.000e+00 </small> </p>

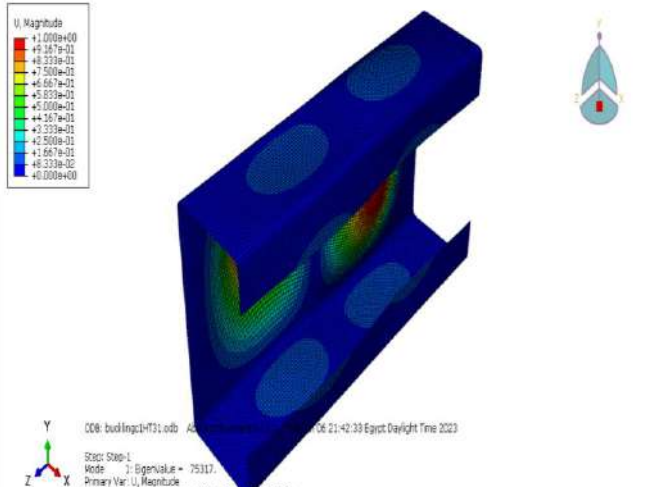
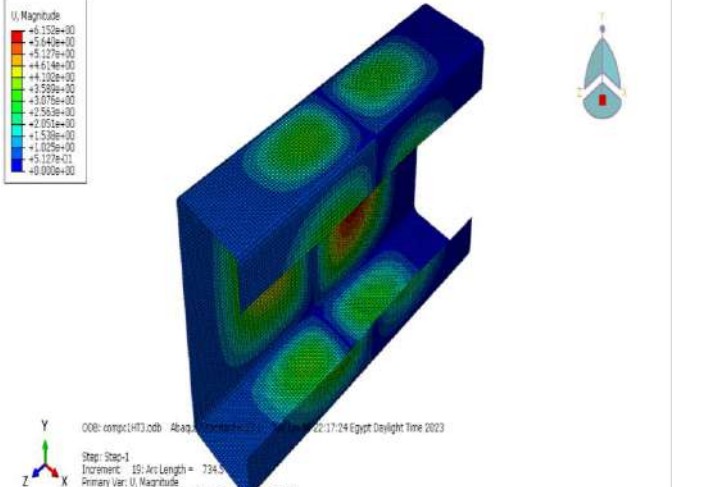
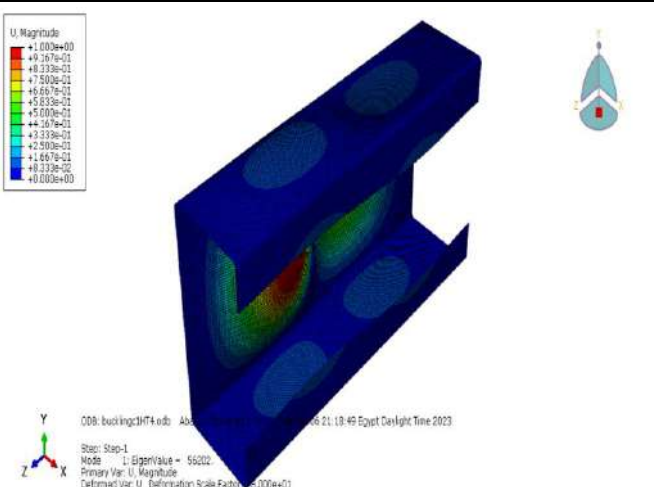
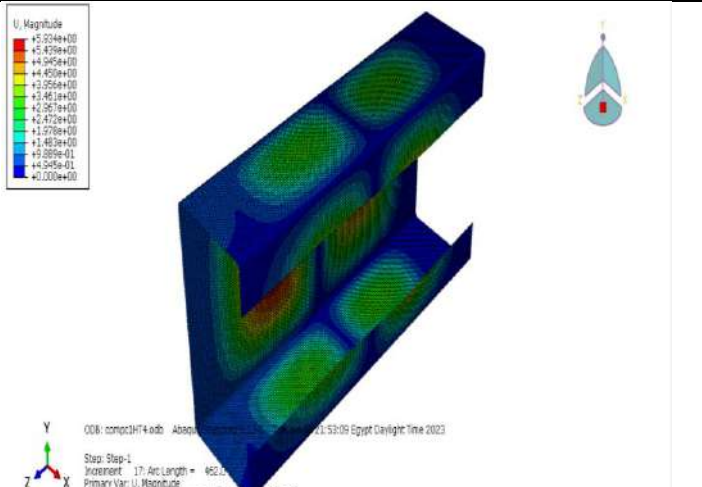
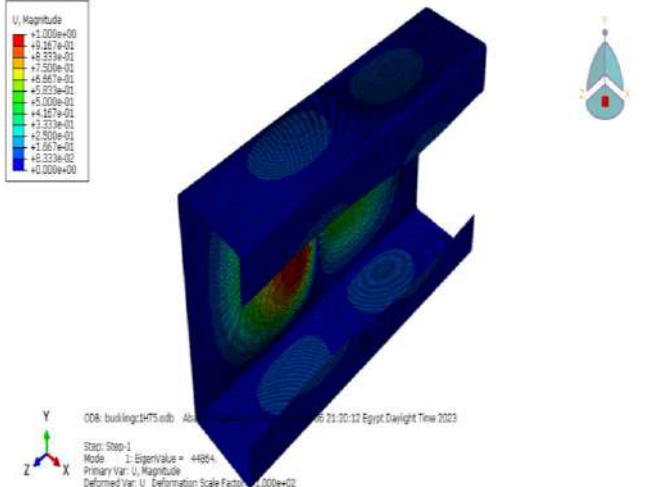
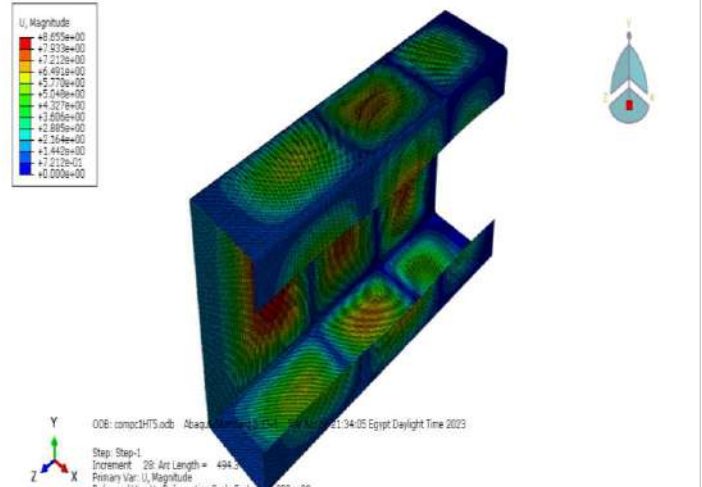
A.2.5.3 Compressive channel section

According to **Table A-19**, all-compressive channel section collapses due to local buckling in all different studied web slenderness ratios (h/t).

Table A-19: - Various FEM modes for compressive channel with different h/t ratios.

Compressive channel section FEM modes			
h/t	Buckling mode	Failure mode	
50	 <p>008: buckling1b2.cdb Abaqus/Standard 2023/06/06 17:49:14 Egypt Daylight Time 2023 Step: Step-1 Mode: 1: Eigenvalue = 2.268012 Primary Var: U, Magnitude Deformed Var: U, Deformation Scale Factor = 2.000e+01</p>	 <p>008: comp11b2.cdb Abaqus/Standard 2023/06/06 17:47:55 Egypt Daylight Time 2023 Step: Step-1 Increment: 14: Arc Length = 388.2 Primary Var: U, Magnitude Deformed Var: U, Deformation Scale Factor = 1.000e+00</p>	
100	 <p>008: buckling1HT1.cdb Abaqus/Standard 2023/06/06 21:15:20 Egypt Daylight Time 2023 Step: Step-1 Mode: 1: Eigenvalue = 1.146465 Primary Var: U, Magnitude Deformed Var: U, Deformation Scale Factor = 4.000e+01</p>	 <p>008: comp11HT1.cdb Abaqus/Standard 2023/06/06 23:53:30 Egypt Daylight Time 2023 Step: Step-1 Increment: 17: Arc Length = 947.8 Primary Var: U, Magnitude Deformed Var: U, Deformation Scale Factor = 1.000e+00</p>	

Compressive channel section FEM modes

h/t	Buckling mode	Failure mode
150	 <p>U, Magnitude +1.009e+00 +9.267e-01 +8.233e-01 +7.500e-01 +6.667e-01 +5.553e-01 +5.000e-01 +4.367e-01 +3.333e-01 +2.500e-01 +1.667e-01 +8.233e-02 +0.000e+00</p> <p>Step: Step-1 Mode 1: EigenValue = 75317. Primary Var: U, Magnitude Deformed Var: U, Deformation Scale Factor = 1.000e+01</p>	 <p>U, Magnitude +6.152e+00 +5.649e+00 +5.127e+00 +4.614e+00 +4.100e+00 +3.589e+00 +3.075e+00 +2.559e+00 +2.051e+00 +1.539e+00 +1.026e+00 +5.127e-01 +0.000e+00</p> <p>Step: Step-1 Increment: 10; Arc Length = 734.5 Primary Var: U, Magnitude Deformed Var: U, Deformation Scale Factor = 1.000e+00</p>
200	 <p>U, Magnitude +1.000e+00 +9.267e-01 +8.233e-01 +7.500e-01 +6.667e-01 +5.553e-01 +5.000e-01 +4.367e-01 +3.333e-01 +2.500e-01 +1.667e-01 +8.233e-02 +0.000e+00</p> <p>Step: Step-1 Mode 1: EigenValue = 56202. Primary Var: U, Magnitude Deformed Var: U, Deformation Scale Factor = 1.000e+01</p>	 <p>U, Magnitude +5.224e+00 +4.695e+00 +4.045e+00 +3.355e+00 +2.641e+00 +2.067e+00 +1.472e+00 +1.078e+00 +6.899e-01 +4.945e-01 +0.000e+00</p> <p>Step: Step-1 Increment: 17; Arc Length = 452.1 Primary Var: U, Magnitude Deformed Var: U, Deformation Scale Factor = 1.000e+00</p>
250	 <p>U, Magnitude +1.000e+00 +9.267e-01 +8.233e-01 +7.500e-01 +6.667e-01 +5.553e-01 +5.000e-01 +4.367e-01 +3.333e-01 +2.500e-01 +1.667e-01 +8.233e-02 +0.000e+00</p> <p>Step: Step-1 Mode 1: EigenValue = 44864. Primary Var: U, Magnitude Deformed Var: U, Deformation Scale Factor = 1.000e+02</p>	 <p>U, Magnitude +8.055e+00 +7.533e+00 +7.212e+00 +6.492e+00 +5.770e+00 +5.048e+00 +4.327e+00 +3.606e+00 +2.885e+00 +2.164e+00 +1.442e+00 +7.212e-01 +0.000e+00</p> <p>Step: Step-1 Increment: 28; Arc Length = 494.3 Primary Var: U, Magnitude Deformed Var: U, Deformation Scale Factor = 1.000e+00</p>

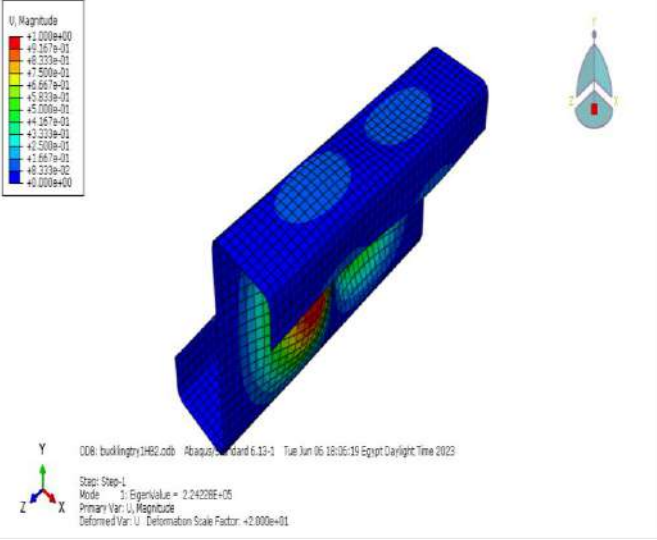
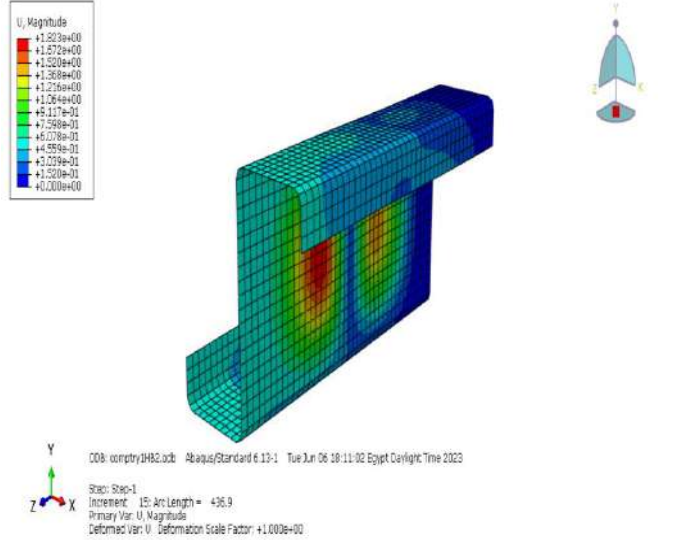
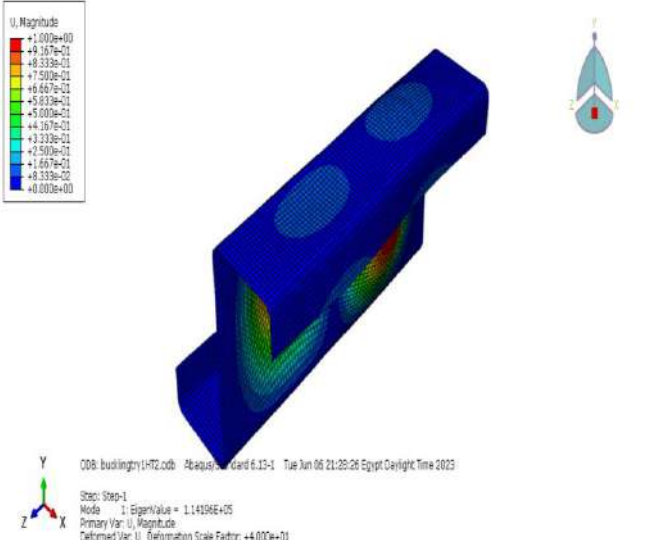
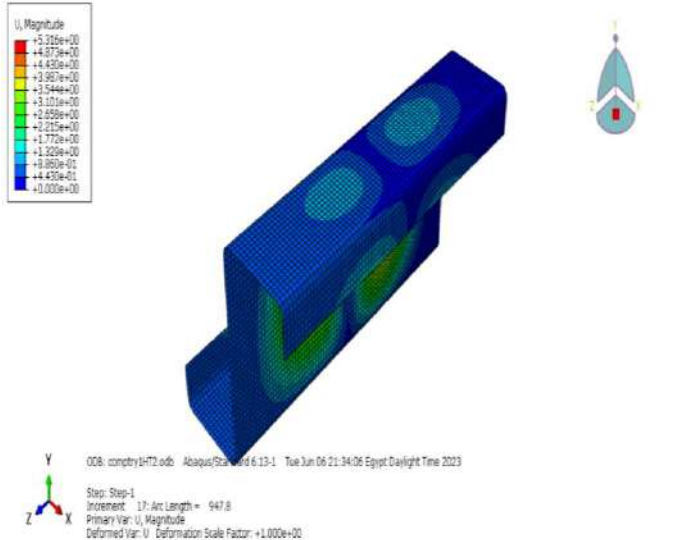
Compressive channel section FEM modes

h/t	Buckling mode	Failure mode
300		

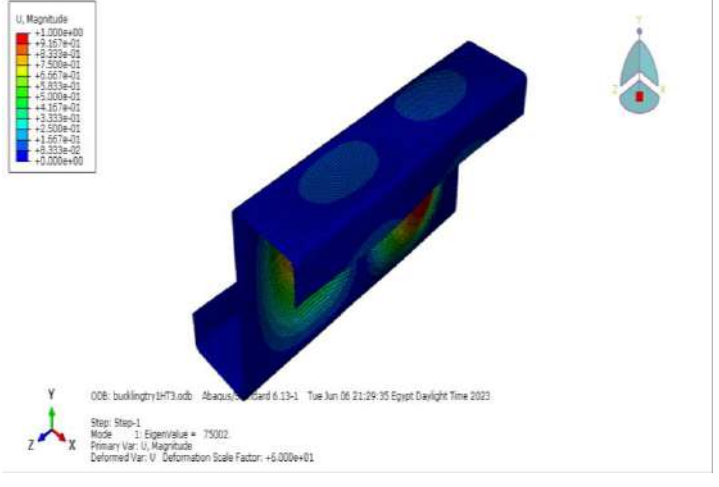
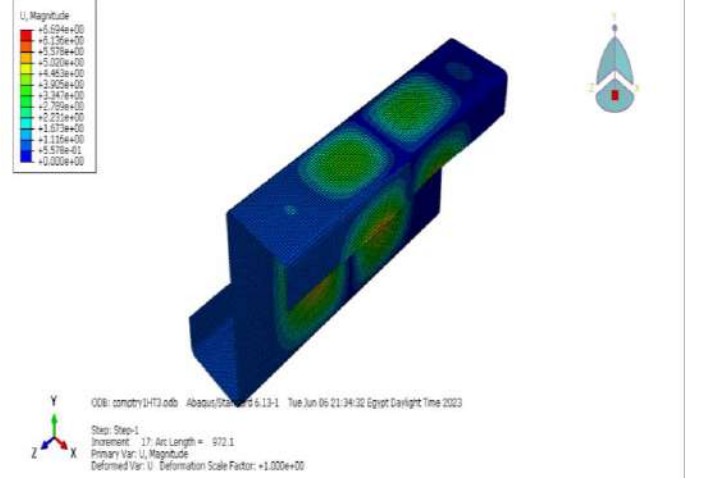
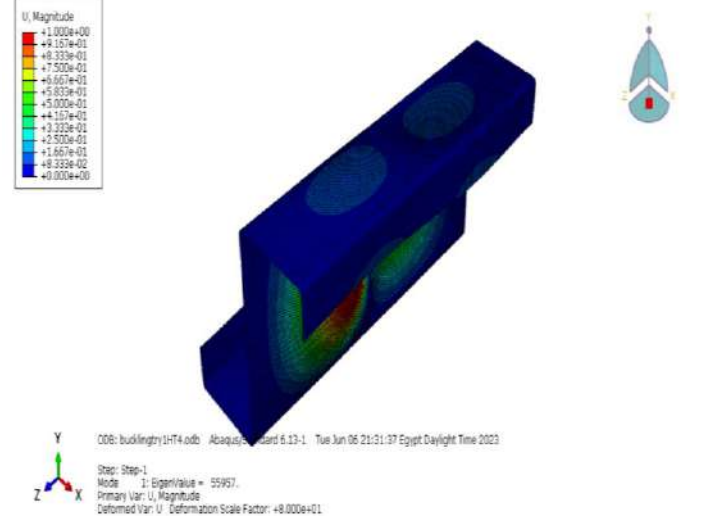
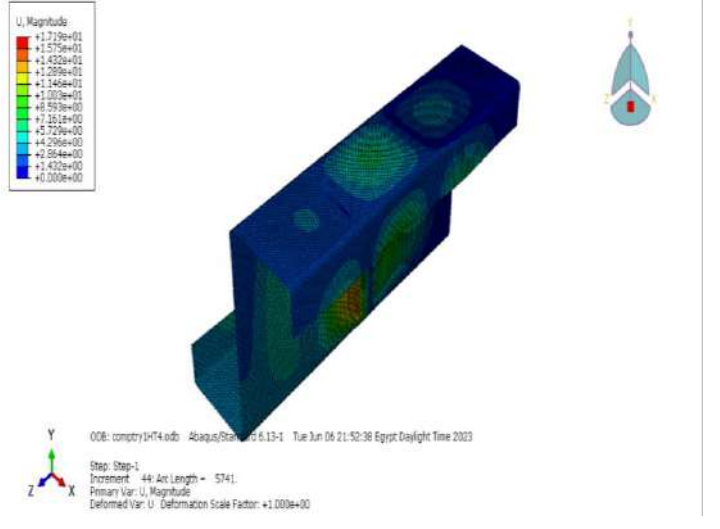
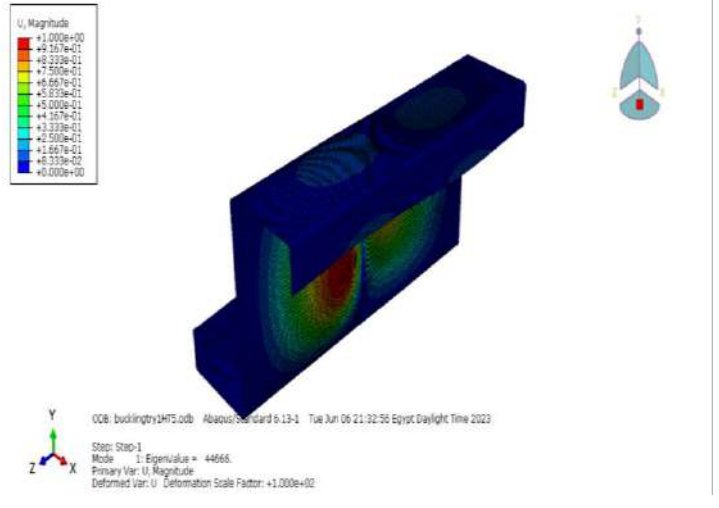
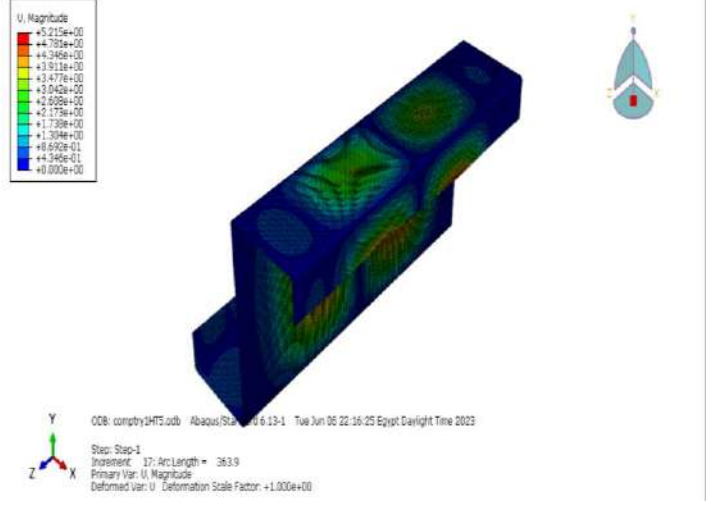
A.2.5.4 Compressive Z-section

According to **Table A-20**, all-compressive Z-section collapses due to local buckling in all different studied web slenderness ratios (h/t).

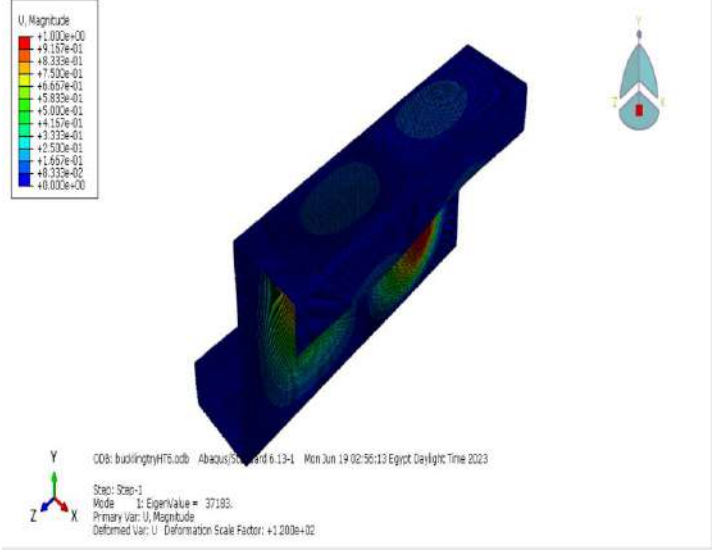
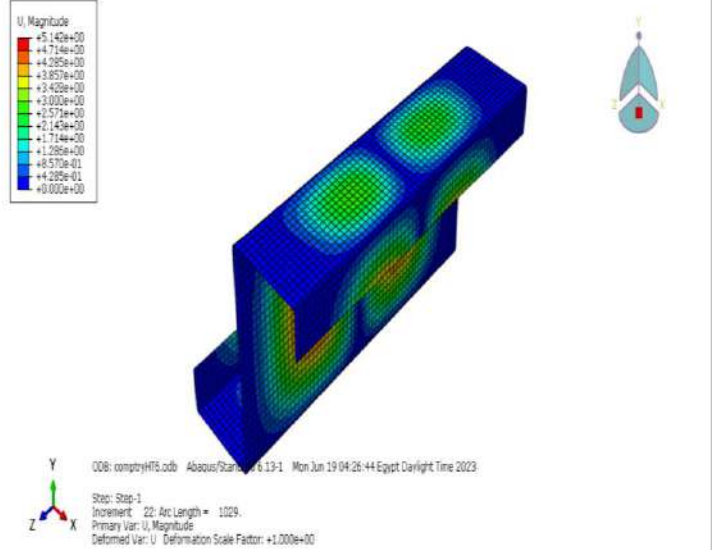
Table A-20: - Various FEM modes for compressive Z-sections with different h/t ratios.

Compressive Z-section FEM modes			
h/t	Buckling mode	Failure mode	
50	 <p>U, Magnitude +1.000e+00 +5.167e-01 +3.333e-01 +7.500e-01 +6.667e-01 +5.833e-01 +5.000e-01 +4.167e-01 +3.333e-01 +2.500e-01 +1.667e-01 +8.333e-02 +0.000e+00</p> <p>ODB: buckling1482.odb Abaqus/Standard 6.13-1 Tue Jun 06 18:05:19 Egypt Daylight Time 2023</p> <p>Step: Step-1 Mode 1: EigenValue = 2.24296E+05 Primary Var: U, Magnitude Deformed Var: U, Deformation Scale Factor: +2.900e+01</p>	 <p>U, Magnitude +1.823e+00 +1.572e+00 +1.320e+00 +1.068e+00 +1.216e+00 +9.117e-01 +7.599e-01 +6.078e-01 +4.559e-01 +3.039e-01 +1.520e-01 +0.000e+00</p> <p>ODB: comptry1482.odb Abaqus/Standard 6.13-1 Tue Jun 06 18:11:02 Egypt Daylight Time 2023</p> <p>Step: Step-1 Increment 15: Arc Length = 436.9 Primary Var: U, Magnitude Deformed Var: U, Deformation Scale Factor: +1.000e+00</p>	
100	 <p>U, Magnitude +1.000e+00 +8.333e-01 +6.667e-01 +5.000e-01 +3.333e-01 +1.667e-01 +0.000e+00</p> <p>ODB: buckling1472.odb Abaqus/Standard 6.13-1 Tue Jun 06 21:28:26 Egypt Daylight Time 2023</p> <p>Step: Step-1 Mode 1: EigenValue = 1.14196E+05 Primary Var: U, Magnitude Deformed Var: U, Deformation Scale Factor: +4.000e+01</p>	 <p>U, Magnitude +5.215e+00 +4.377e+00 +4.455e+00 +3.957e+00 +3.544e+00 +3.103e+00 +2.659e+00 +2.215e+00 +1.772e+00 +1.329e+00 +8.859e-01 +4.429e-01 +0.000e+00</p> <p>ODB: comptry1472.odb Abaqus/Standard 6.13-1 Tue Jun 06 21:34:06 Egypt Daylight Time 2023</p> <p>Step: Step-1 Increment 17: Arc Length = 947.8 Primary Var: U, Magnitude Deformed Var: U, Deformation Scale Factor: +1.000e+00</p>	

Flexural Z-section FEM modes

h/t	Buckling mode	Failure mode
150	 <p>U, Magnitude</p> <ul style="list-style-type: none"> +1.000e+00 +9.167e-01 +8.333e-01 +7.500e-01 +6.667e-01 +5.833e-01 +5.000e-01 +4.167e-01 +3.333e-01 +2.500e-01 +1.667e-01 +8.333e-02 +0.000e+00 <p>008: bucklingry1H3.odb Abaqus/Standard 6.13-1 Tue Jun 06 21:29:35 Egypt Daylight Time 2023</p> <p>Step: Step-1 Mode 1: EigenValue = 75002 Primary Var: U, Magnitude Deformed Var: U, Deformation Scale Factor: +6.000e+01</p>	 <p>U, Magnitude</p> <ul style="list-style-type: none"> +5.529e+00 +5.126e+00 +4.723e+00 +4.320e+00 +3.917e+00 +3.514e+00 +3.111e+00 +2.708e+00 +2.305e+00 +1.902e+00 +1.499e+00 +1.096e+00 +0.693e+00 +0.290e+00 +0.000e+00 <p>008: comdry1H3.odb Abaqus/Standard 6.13-1 Tue Jun 06 21:34:32 Egypt Daylight Time 2023</p> <p>Step: Step-1 Increment 17: Arc Length = 972.1 Primary Var: U, Magnitude Deformed Var: U, Deformation Scale Factor: +1.000e+00</p>
200	 <p>U, Magnitude</p> <ul style="list-style-type: none"> +1.000e+00 +9.167e-01 +8.333e-01 +7.500e-01 +6.667e-01 +5.833e-01 +5.000e-01 +4.167e-01 +3.333e-01 +2.500e-01 +1.667e-01 +8.333e-02 +0.000e+00 <p>008: bucklingry1H4.odb Abaqus/Standard 6.13-1 Tue Jun 06 21:31:37 Egypt Daylight Time 2023</p> <p>Step: Step-1 Mode 1: EigenValue = 55957. Primary Var: U, Magnitude Deformed Var: U, Deformation Scale Factor: +8.000e+01</p>	 <p>U, Magnitude</p> <ul style="list-style-type: none"> +1.719e+01 +1.575e+01 +1.432e+01 +1.289e+01 +1.146e+01 +1.003e+01 +8.599e+00 +7.195e+00 +5.791e+00 +4.387e+00 +2.983e+00 +1.579e+00 +0.175e+00 +0.000e+00 <p>008: comdry1H4.odb Abaqus/Standard 6.13-1 Tue Jun 06 21:32:38 Egypt Daylight Time 2023</p> <p>Step: Step-1 Increment 44: Arc Length = 5741. Primary Var: U, Magnitude Deformed Var: U, Deformation Scale Factor: +1.000e+00</p>
250	 <p>U, Magnitude</p> <ul style="list-style-type: none"> +1.000e+00 +9.167e-01 +8.333e-01 +7.500e-01 +6.667e-01 +5.833e-01 +5.000e-01 +4.167e-01 +3.333e-01 +2.500e-01 +1.667e-01 +8.333e-02 +0.000e+00 <p>008: bucklingry1H5.odb Abaqus/Standard 6.13-1 Tue Jun 06 21:32:56 Egypt Daylight Time 2023</p> <p>Step: Step-1 Mode 1: EigenValue = 44668. Primary Var: U, Magnitude Deformed var: U, Deformation Scale Factor: +1.000e+02</p>	 <p>U, Magnitude</p> <ul style="list-style-type: none"> +5.215e+00 +4.781e+00 +4.346e+00 +3.911e+00 +3.477e+00 +3.042e+00 +2.607e+00 +2.172e+00 +1.738e+00 +1.304e+00 +8.699e-01 +4.346e-01 +0.000e+00 <p>008: comdry1H5.odb Abaqus/Standard 6.13-1 Tue Jun 06 22:16:25 Egypt Daylight Time 2023</p> <p>Step: Step-1 Increment 17: Arc Length = 383.9 Primary Var: U, Magnitude Deformed Var: U, Deformation Scale Factor: +1.000e+00</p>

Flexural Z-section FEM modes

h/t	Buckling mode	Failure mode
300	 <p>COB: buckingtryHT6.cdb Abaqus/Standard 6.13-1 Mon Jun 19 02:56:13 Egypt Daylight Time 2023</p> <p>Step: Step-1 Mode 1: EigenValue = 37183. Primary Var: U, Magnitude Deformed Var: U Deformation Scale Factor: +1.200e+02</p>	 <p>COB: comptryHT6.cdb Abaqus/Standard 6.13-1 Mon Jun 19 04:26:44 Egypt Daylight Time 2023</p> <p>Step: Step-1 Increment 22: Arc Length = 1029. Primary Var: U, Magnitude Deformed Var: U Deformation Scale Factor: +1.000e+00</p>

A.3 Compression Between Effective Width and Direct Strength Methods

Table A-21: - Comparison between EWM and DSM for CFS compression channel sections.

Dimension (mm)					length (mm)	P _{FEM} (Kn)	DSM ($\phi=0.85$)		AISI ($\phi=0.85$)		EGY ($\phi=0.8$)		EURO	
h	b	d	t	r			ϕP_n	$\phi P_n/P_{FEM}$	ϕP_n	$\phi P_n/P_{FEM}$	ϕP_n	$\phi P_n/P_{FEM}$	P _n	P _n /P _{FEM}
304.80	101.60	22.48	2.67	4.76	304.80	276.04	254.20	0.92	224.20	0.81	205.66	0.75	244.89	0.89
304.80	101.60	22.48	2.67	4.76	609.60	255.31	251.50	0.99	222.00	0.87	205.66	0.81	244.89	0.96
304.80	101.60	22.48	2.67	4.76	914.40	241.97	247.07	1.02	217.85	0.90	205.66	0.85	228.52	0.94
304.80	101.60	22.48	2.67	4.76	1219.20	233.39	209.55	0.90	212.88	0.91	205.66	0.88	221.33	0.95
304.80	101.60	22.48	2.67	4.76	1524.00	223.88	203.04	0.91	206.92	0.92	205.66	0.92	209.65	0.94
304.80	101.60	22.48	2.67	4.76	1828.80	212.68	195.36	0.92	199.95	0.94	205.66	0.97	199.74	0.94
304.80	101.60	22.48	2.67	4.76	2133.60	200.71	186.71	0.93	192.13	0.96	190.32	0.95	188.10	0.94
304.80	101.60	22.48	2.67	4.76	2438.40	188.12	177.28	0.94	183.63	0.98	170.21	0.90	180.50	0.96
304.80	101.60	22.48	2.67	4.76	2743.20	175.53	167.25	0.95	157.48	0.90	160.21	0.91	164.83	0.94
304.80	101.60	22.48	2.67	4.76	3048.00	162.05	156.82	0.97	145.85	0.90	123.61	0.76	150.93	0.93
304.80	101.60	21.23	2.16	4.76	304.80	197.82	175.64	0.89	159.21	0.80	143.20	0.72	162.04	0.82
304.80	101.60	21.23	2.16	4.76	609.60	172.97	173.78	1.00	157.50	0.91	143.20	0.83	162.04	0.94
304.80	101.60	21.23	2.16	4.76	914.40	172.54	170.72	0.99	154.77	0.90	143.20	0.83	160.42	0.93
304.80	101.60	21.23	2.16	4.76	1219.20	167.02	166.54	1.00	151.04	0.90	143.20	0.86	155.99	0.93
304.80	101.60	21.23	2.16	4.76	1524.00	160.53	161.34	1.00	146.37	0.91	143.20	0.89	151.36	0.94
304.80	101.60	21.23	2.16	4.76	1828.80	153.32	155.21	1.01	140.87	0.92	143.20	0.93	146.43	0.96
304.80	101.60	21.23	2.16	4.76	2133.60	146.49	148.30	1.01	134.64	0.92	143.20	0.98	141.09	0.96
304.80	101.60	21.23	2.16	4.76	2438.40	138.99	140.74	1.01	127.80	0.92	125.36	0.90	135.27	0.97
304.80	101.60	21.23	2.16	4.76	2743.20	131.26	132.69	1.01	120.47	0.92	112.35	0.86	128.91	0.98
304.80	101.60	21.23	2.16	4.76	3048.00	123.11	124.28	1.01	113.18	0.92	112.36	0.91	114.81	0.93
228.60	63.50	22.48	2.67	4.76	228.60	223.56	197.92	0.89	207.15	0.93	202.28	0.90	218.98	0.98
228.60	63.50	22.48	2.67	4.76	457.20	208.85	195.22	0.93	203.49	0.97	199.37	0.95	196.60	0.94
228.60	63.50	22.48	2.67	4.76	685.80	195.71	190.71	0.97	189.50	0.97	194.51	0.99	185.55	0.95

Dimension (mm)					length (mm)	P _{FEM} (Kn)	DSM ($\phi=.85$)		AISI ($\phi=.85$)		EGY ($\phi=.8$)		EURO	
h	b	d	t	r			ϕP_n	$\phi P_n/P_{FEM}$	ϕP_n	$\phi P_n/P_{FEM}$	ϕP_n	$\phi P_n/P_{FEM}$	P _n	P _n /P _{FEM}
228.60	63.50	22.48	2.67	4.76	914.40	186.39	184.60	0.99	179.80	0.96	187.72	1.01	176.39	0.95
228.60	63.50	22.48	2.67	4.76	1143.00	176.01	177.02	1.01	170.42	0.97	178.98	1.02	169.74	0.96
228.60	63.50	22.48	2.67	4.76	1371.60	164.47	168.15	1.02	161.94	0.98	168.31	1.02	156.97	0.95
228.60	63.50	22.48	2.67	4.76	1600.20	152.71	150.00	0.98	132.87	0.87	142.35	0.93	133.20	0.87
228.60	63.50	22.48	2.67	4.76	1828.80	140.27	147.43	1.05	136.15	0.97	141.13	1.01	133.20	0.95
228.60	63.50	22.48	2.67	4.76	2057.40	127.36	121.75	0.96	121.56	0.95	124.63	0.98	124.14	0.97
228.60	63.50	22.48	2.67	4.76	2286.00	114.64	112.57	0.98	107.01	0.93	105.91	0.92	109.59	0.96
228.60	63.50	21.23	2.16	4.76	228.60	161.85	137.14	0.85	155.35	0.96	151.87	0.94	152.64	0.94
228.60	63.50	21.23	2.16	4.76	457.20	149.87	135.28	0.90	145.86	0.97	149.84	1.00	140.95	0.94
228.60	63.50	21.23	2.16	4.76	685.80	141.37	132.22	0.94	126.30	0.89	130.25	0.92	133.64	0.95
228.60	63.50	21.23	2.16	4.76	914.40	135.82	128.05	0.94	121.58	0.90	125.36	0.92	127.84	0.94
228.60	63.50	21.23	2.16	4.76	1143.00	128.72	122.87	0.95	121.56	0.94	119.35	0.93	123.69	0.96
228.60	63.50	21.23	2.16	4.76	1371.60	121.51	116.81	0.96	118.65	0.98	115.36	0.95	114.15	0.94
228.60	63.50	21.23	2.16	4.76	1600.20	114.68	110.02	0.96	109.83	0.96	112.36	0.98	108.54	0.95
228.60	63.50	21.23	2.16	4.76	1828.80	107.37	102.65	0.96	99.29	0.92	109.40	1.02	105.33	0.98
228.60	63.50	21.23	2.16	4.76	2057.40	99.76	94.87	0.95	96.84	0.97	97.94	0.98	93.64	0.94
228.60	63.50	21.23	2.16	4.76	2286.00	92.36	86.82	0.94	86.59	0.94	85.13	0.92	90.89	0.98
209.55	50.80	-	1.81	2.72	209.55	92.68	74.78	0.81	69.81	0.75	69.67	0.75	75.44	0.81
209.55	50.80	-	1.81	2.72	419.10	77.08	72.69	0.94	67.97	0.88	68.34	0.89	73.75	0.96
209.55	50.80	-	1.81	2.72	628.65	75.79	69.34	0.91	65.00	0.86	66.13	0.87	69.04	0.91
209.55	50.80	-	1.81	2.72	838.20	73.15	64.90	0.89	61.04	0.83	63.03	0.86	64.10	0.88
209.55	50.80	-	1.81	2.72	1047.75	73.20	59.58	0.81	56.29	0.77	59.05	0.81	58.81	0.80
209.55	50.80	-	1.81	2.72	1257.30	68.46	64.38	0.94	50.94	0.74	54.19	0.79	53.18	0.78
209.55	50.80	-	1.81	2.72	1466.85	61.04	56.85	0.93	45.22	0.74	48.44	0.79	47.41	0.78
209.55	50.80	-	1.81	2.72	1676.40	53.91	49.14	0.91	39.30	0.73	41.81	0.78	41.81	0.78
209.55	50.80	-	1.81	2.72	1885.95	47.26	42.16	0.89	33.83	0.72	34.14	0.72	36.63	0.78
209.55	50.80	-	1.81	2.72	2095.50	41.32	36.73	0.89	29.50	0.71	27.66	0.67	32.03	0.78
313.84	50.80	-	2.58	3.87	313.84	162.53	161.53	0.99	136.39	0.84	136.78	0.84	149.71	0.92

Dimension (mm)					length (mm)	P _{FEM} (Kn)	DSM ($\phi=.85$)		AISI ($\phi=.85$)		EGY ($\phi=.8$)		EURO	
h	b	d	t	r			ϕP_n	$\phi P_n/P_{FEM}$	ϕP_n	$\phi P_n/P_{FEM}$	ϕP_n	$\phi P_n/P_{FEM}$	P _n	P _n /P _{FEM}
313.84	50.80	-	2.58	3.87	627.68	143.55	130.54	0.91	126.18	0.88	128.99	0.90	133.42	0.93
313.84	50.80	-	2.58	3.87	941.53	124.59	115.69	0.93	110.71	0.89	116.01	0.93	115.71	0.93
313.84	50.80	-	2.58	3.87	1255.37	107.94	108.07	1.00	91.90	0.85	97.83	0.91	96.02	0.89
313.84	50.80	-	2.58	3.87	1569.21	88.74	84.59	0.95	71.50	0.81	74.45	0.84	77.07	0.87
313.84	50.80	-	2.58	3.87	1883.05	71.83	66.68	0.93	54.54	0.76	51.70	0.72	61.18	0.85
313.84	50.80	-	2.58	3.87	2196.90	58.34	54.39	0.93	43.34	0.74	37.99	0.65	48.87	0.84
212.24	50.80	-	2.58	3.87	212.24	161.44	137.55	0.85	134.60	0.83	134.83	0.84	146.59	0.91
212.24	50.80	-	2.58	3.87	424.48	147.40	133.46	0.91	130.67	0.89	131.16	0.89	139.78	0.95
212.24	50.80	-	2.58	3.87	636.73	140.92	126.91	0.90	124.36	0.88	125.04	0.89	128.63	0.91
212.24	50.80	-	2.58	3.87	848.97	135.03	118.24	0.88	115.97	0.86	116.47	0.86	116.61	0.86
212.24	50.80	-	2.58	3.87	1061.21	124.94	107.92	0.86	105.92	0.85	105.46	0.84	103.63	0.83
212.24	50.80	-	2.58	3.87	1273.45	112.33	96.46	0.86	94.65	0.84	92.00	0.82	90.26	0.80
212.24	50.80	-	2.58	3.87	1485.70	98.48	84.39	0.86	82.66	0.84	76.10	0.77	77.46	0.79
212.24	50.80	-	2.58	3.87	1697.94	84.36	72.12	0.85	70.27	0.83	58.82	0.70	66.03	0.78
212.24	50.80	-	2.58	3.87	1910.18	74.46	69.16	0.93	58.39	0.78	46.47	0.62	56.30	0.76
212.24	50.80	-	2.58	3.87	2122.42	61.81	56.02	0.91	49.35	0.80	37.64	0.61	48.20	0.78
304.80	69.34	15.58	2.67	4.76	609.60	202.63	187.32	0.92	191.89	0.95	188.93	0.93	192.50	0.95
304.80	82.68	18.43	2.67	4.76	609.60	226.28	186.04	0.82	209.37	0.93	190.62	0.84	216.27	0.96
304.80	96.01	21.28	2.67	4.76	609.60	247.53	213.34	0.86	218.14	0.88	192.01	0.78	242.48	0.98
304.80	101.60	22.48	2.67	4.76	609.60	255.51	218.19	0.85	222.39	0.87	206.04	0.81	245.40	0.96
304.80	109.35	24.13	2.67	4.76	609.60	267.63	224.89	0.84	228.44	0.85	211.82	0.79	248.92	0.93
304.80	122.68	26.98	2.67	4.76	609.60	285.43	236.19	0.83	239.72	0.84	222.52	0.78	253.94	0.89
304.80	136.02	29.84	2.67	4.76	609.60	297.65	247.28	0.83	250.87	0.84	233.37	0.78	257.98	0.87
304.80	149.35	32.69	2.67	4.76	609.60	305.93	258.19	0.84	262.35	0.86	244.78	0.80	261.25	0.85
304.80	69.34	15.58	2.67	4.76	1524.00	161.80	155.82	0.96	156.51	0.97	166.23	1.03	153.71	0.95
304.80	82.68	18.43	2.67	4.76	1524.00	189.57	178.80	0.94	186.18	0.98	190.62	1.01	180.10	0.95
304.80	96.01	21.28	2.67	4.76	1524.00	214.41	196.57	0.92	203.17	0.95	192.01	0.90	203.69	0.95
304.80	101.60	22.48	2.67	4.76	1524.00	224.03	202.27	0.90	207.31	0.93	206.04	0.92	214.09	0.96

Dimension (mm)					length (mm)	P _{FEM} (Kn)	DSM ($\phi=.85$)		AISI ($\phi=.85$)		EGY ($\phi=.8$)		EURO	
h	b	d	t	r			ϕP_n	$\phi P_n/P_{FEM}$	ϕP_n	$\phi P_n/P_{FEM}$	ϕP_n	$\phi P_n/P_{FEM}$	P _n	P _n /P _{FEM}
304.80	109.35	24.13	2.67	4.76	1524.00	236.86	209.90	0.89	213.59	0.90	211.82	0.89	231.01	0.98
304.80	122.68	26.98	2.67	4.76	1524.00	256.34	222.35	0.87	226.24	0.88	222.52	0.87	238.82	0.93
304.80	136.02	29.84	2.67	4.76	1524.00	271.90	234.18	0.86	238.31	0.88	233.37	0.86	245.05	0.90
304.80	149.35	32.69	2.67	4.76	1524.00	282.86	245.58	0.87	250.40	0.89	244.78	0.87	250.08	0.88
304.80	69.34	15.58	2.67	4.76	3048.00	88.37	82.77	0.94	75.19	0.85	68.17	0.77	83.95	0.95
304.80	82.68	18.43	2.67	4.76	3048.00	120.36	117.24	0.97	116.49	0.97	114.00	0.95	114.34	0.95
304.80	96.01	21.28	2.67	4.76	3048.00	150.36	147.17	0.98	141.00	0.94	140.21	0.93	142.84	0.95
304.80	101.60	22.48	2.67	4.76	3048.00	162.19	155.43	0.96	149.01	0.92	152.31	0.94	154.08	0.95
304.80	109.35	24.13	2.67	4.76	3048.00	178.13	164.96	0.93	172.50	0.97	180.35	1.01	169.23	0.95
304.80	122.68	26.98	2.67	4.76	3048.00	203.56	179.82	0.88	184.12	0.90	201.81	0.99	196.09	0.96
304.80	136.02	29.84	2.67	4.76	3048.00	226.41	193.26	0.85	198.46	0.88	216.02	0.95	206.15	0.91
304.80	149.35	32.69	2.67	4.76	3048.00	244.83	205.69	0.84	212.04	0.87	228.05	0.93	214.14	0.87
136.02	101.60	22.48	2.67	4.76	272.03	273.70	249.56	0.91	210.77	0.77	193.11	0.71	248.07	0.91
216.03	101.60	22.48	2.67	4.76	432.05	263.22	229.07	0.87	218.78	0.83	201.54	0.77	248.39	0.94
269.37	101.60	22.48	2.67	4.76	538.73	259.98	221.69	0.85	220.96	0.85	204.34	0.79	246.75	0.95
304.80	101.60	22.48	2.67	4.76	609.60	255.51	218.30	0.85	222.39	0.87	206.04	0.81	245.40	0.96
402.72	101.60	22.48	2.67	4.76	805.43	225.26	194.65	0.86	221.62	0.98	208.09	0.92	211.54	0.94
482.73	101.60	22.48	2.67	4.76	965.45	228.23	217.92	0.95	219.75	0.96	209.34	0.92	214.52	0.94
136.02	101.60	22.48	2.67	4.76	680.09	251.81	228.36	0.91	202.61	0.80	193.11	0.77	233.32	0.93
216.03	101.60	22.48	2.67	4.76	1080.14	239.36	217.23	0.91	208.17	0.87	201.54	0.84	231.83	0.97
269.37	101.60	22.48	2.67	4.76	1346.84	230.62	207.65	0.90	208.01	0.90	204.34	0.89	214.61	0.93
304.80	101.60	22.48	2.67	4.76	1524.00	224.03	202.39	0.90	207.31	0.93	206.04	0.92	206.12	0.92
402.72	101.60	22.48	2.67	4.76	2013.59	203.42	184.79	0.91	196.88	0.97	208.09	1.02	192.54	0.95
136.02	101.60	22.48	2.67	4.76	1360.17	226.40	207.46	0.92	178.76	0.79	187.73	0.83	191.71	0.85
216.03	101.60	22.48	2.67	4.76	2160.27	197.84	180.48	0.91	177.45	0.90	185.26	0.94	186.82	0.94
269.37	101.60	22.48	2.67	4.76	2693.67	176.24	165.34	0.94	170.58	0.97	178.62	1.01	166.90	0.95
304.80	101.60	22.48	2.67	4.76	3048.00	162.19	155.58	0.96	147.79	0.91	160.21	0.99	152.54	0.94
402.72	101.60	22.48	2.67	4.76	4027.17	126.92	114.03	0.90	119.24	0.94	127.18	1.00	124.04	0.98

Dimension (mm)					length (mm)	P _{FEM} (Kn)	DSM ($\phi=.85$)		AISI ($\phi=.85$)		EGY ($\phi=.8$)		EURO	
h	b	d	t	r			ϕP_n	$\phi P_n/P_{FEM}$	ϕP_n	$\phi P_n/P_{FEM}$	ϕP_n	$\phi P_n/P_{FEM}$	P _n	P _n /P _{FEM}
482.73	101.60	22.48	2.67	4.76	4827.27	103.01	103.08	1.00	84.85	0.82	92.50	0.90	97.55	0.95
536.07	101.60	22.48	2.67	4.76	5360.67	89.73	87.44	0.97	69.76	0.78	76.78	0.86	88.02	0.98
304.80	101.60	22.48	2.67	4.76	609.60	255.51	254.01	0.99	222.39	0.87	206.04	0.81	245.40	0.96
304.80	101.60	26.07	2.67	4.76	609.60	259.79	265.48	1.02	230.41	0.89	215.66	0.83	244.12	0.94
304.80	101.60	31.01	2.67	4.76	609.60	265.43	270.47	1.02	245.09	0.92	233.00	0.88	249.54	0.94
304.80	101.60	35.96	2.67	4.76	609.60	270.98	275.45	1.02	266.54	0.98	258.23	0.95	256.83	0.95
304.80	101.60	40.91	2.67	4.76	609.60	276.55	280.42	1.01	268.06	0.97	272.60	0.99	253.98	0.92
304.80	101.60	22.48	2.67	4.76	1524.00	224.03	210.54	0.94	207.31	0.93	206.04	0.92	214.11	0.96
304.80	101.60	26.07	2.67	4.76	1524.00	227.89	222.18	0.97	215.78	0.95	215.66	0.95	214.10	0.94
304.80	101.60	31.01	2.67	4.76	1524.00	232.96	227.26	0.98	231.37	0.99	233.00	1.00	219.36	0.94
304.80	101.60	35.96	2.67	4.76	1524.00	237.50	232.30	0.98	228.09	0.96	235.67	0.99	223.76	0.94
304.80	101.60	40.91	2.67	4.76	1524.00	242.37	237.31	0.98	233.29	0.96	240.64	0.99	228.65	0.94
304.80	101.60	22.48	2.67	4.76	3048.00	162.19	154.64	0.95	162.41	1.00	152.31	0.94	152.93	0.94
304.80	101.60	26.07	2.67	4.76	3048.00	166.10	163.56	0.98	160.31	0.97	162.65	0.98	160.52	0.97
304.80	101.60	22.48	1.70	4.76	609.60	120.45	116.79	0.97	112.44	0.93	101.33	0.84	105.30	0.87
304.80	101.60	22.48	2.00	4.76	609.60	150.93	147.15	0.97	142.87	0.95	129.94	0.86	142.67	0.95
304.80	101.60	22.48	2.50	4.76	609.60	231.33	215.90	0.93	200.96	0.87	185.29	0.80	217.30	0.94
304.80	101.60	22.48	2.67	4.76	609.60	255.51	254.01	0.99	222.39	0.87	206.04	0.81	245.40	0.96
304.80	101.60	22.48	3.00	4.76	609.60	307.98	294.43	0.96	269.70	0.88	241.70	0.78	287.54	0.93
304.80	101.60	22.48	3.50	4.76	609.60	382.59	381.76	1.00	349.16	0.91	325.22	0.85	357.18	0.93
304.80	101.60	22.48	4.00	4.76	609.60	468.87	477.00	1.02	421.80	0.90	417.67	0.89	437.33	0.93
304.80	101.60	22.48	1.70	4.76	1524.00	108.02	97.29	0.90	104.67	0.97	101.33	0.94	99.96	0.93
304.80	101.60	22.48	2.00	4.76	1524.00	142.05	122.42	0.86	132.99	0.94	129.94	0.91	134.02	0.94
304.80	101.60	22.48	2.50	4.76	1524.00	202.51	179.17	0.88	186.44	0.92	185.29	0.91	191.28	0.94
304.80	101.60	22.48	2.67	4.76	1524.00	224.03	210.54	0.94	207.31	0.93	206.04	0.92	209.64	0.94
304.80	101.60	22.48	3.00	4.76	1524.00	267.32	243.76	0.91	252.07	0.94	241.70	0.90	252.58	0.94
304.80	101.60	22.48	3.50	4.76	1524.00	335.89	315.32	0.94	320.49	0.95	325.22	0.97	319.17	0.95
304.80	101.60	22.48	4.00	4.76	1524.00	409.27	393.12	0.96	385.82	0.94	399.86	0.98	389.83	0.95

Dimension (mm)					length (mm)	P _{FEM} (Kn)	DSM ($\phi=.85$)		AISI ($\phi=.85$)		EGY ($\phi=.8$)		EURO	
h	b	d	t	r			ϕP_n	$\phi P_n/P_{FEM}$	ϕP_n	$\phi P_n/P_{FEM}$	ϕP_n	$\phi P_n/P_{FEM}$	P _n	P _n /P _{FEM}
304.80	101.60	22.48	2.50	4.76	3048.00	147.58	131.72	0.89	141.00	0.96	142.68	0.97	143.15	0.97
304.80	101.60	22.48	2.67	4.76	3048.00	162.19	154.64	0.95	148.66	0.92	160.23	0.99	157.67	0.97
304.80	101.60	22.48	3.00	4.76	3048.00	192.12	178.92	0.93	183.68	0.96	180.35	0.94	181.14	0.94
304.80	101.60	22.48	3.50	4.76	3048.00	240.23	231.26	0.96	229.76	0.96	234.65	0.98	228.64	0.95
304.80	101.60	22.48	4.00	4.76	3048.00	291.58	286.50	0.98	278.73	0.96	276.58	0.95	280.89	0.96
304.80	95.00	43.88	2.67	4.76	609.60	260.61	271.47	1.04	249.63	0.96	251.02	0.96	247.92	0.95
304.80	110.00	38.88	2.67	4.76	609.60	281.70	279.74	0.99	262.24	0.93	277.17	0.98	266.92	0.95
304.80	108.88	30.00	2.67	4.76	609.60	270.25	268.98	1.00	244.31	0.90	230.50	0.85	252.07	0.93
304.80	101.60	40.64	2.67	4.76	609.60	275.49	274.25	1.00	260.30	0.94	272.44	0.99	263.80	0.96
304.80	108.88	30.00	2.67	4.76	1524.00	239.08	226.05	0.95	228.76	0.96	230.33	0.96	224.75	0.94
400.00	101.60	22.48	2.67	4.76	800.00	227.86	235.65	1.03	222.05	0.97	208.42	0.91	219.01	0.96
450.00	101.60	22.48	2.67	4.76	900.00	217.84	218.35	1.00	204.04	0.94	209.27	0.96	209.55	0.96
533.40	101.60	22.48	2.67	4.76	1066.80	216.35	200.89	0.93	204.04	0.94	209.93	0.97	204.89	0.95
400.00	101.60	22.48	2.67	4.76	2000.00	203.99	187.16	0.92	197.26	0.97	195.65	0.96	195.33	0.96
400.00	101.60	22.48	2.67	4.76	4000.00	127.88	126.01	0.99	120.77	0.94	128.69	1.01	124.08	0.97
450.00	101.60	22.48	2.67	4.76	4500.00	112.22	104.62	0.93	96.78	0.86	104.70	0.93	109.83	0.98
533.40	101.60	22.48	2.67	4.76	5334.00	90.36	91.46	1.01	70.41	0.78	77.47	0.86	85.79	0.95
183.20	152.40	32.48	2.67	4.76	916.00	283.54	270.66	0.95	246.83	0.87	236.92	0.84	255.27	0.90
247.80	125.10	27.48	2.67	4.76	1239.00	266.55	251.02	0.94	228.87	0.86	222.08	0.83	243.79	0.91
330.20	88.90	22.48	2.67	4.76	1651.00	198.94	187.92	0.94	186.60	0.94	190.67	0.96	182.41	0.92
355.60	76.20	22.48	2.67	4.76	1778.00	170.49	161.36	0.95	162.33	0.95	160.25	0.94	161.71	0.95
279.40	114.30	22.48	2.67	4.76	1397.00	246.01	227.74	0.93	211.52	0.86	206.05	0.84	188.22	0.77

Table A-22: - Comparison between EWM and DSM for CFS compression Z-sections.

Dimension (mm)					length (mm)	P _{FEM}	DSM ($\phi=0.85$)		AISI ($\phi=0.85$)		EGY ($\phi=0.8$)		EURO	
h	b	d	t	r			ϕP_n	$\phi P_n / P_{FEM}$	ϕP_n	$\phi P_n / P_{FEM}$	ϕP_n	$\phi P_n / P_{FEM}$	P_n	P_n / P_{FEM}
100.00	50.00	20.00	2.00	8.00	100.00	140.16	124.21	0.89	127.29	0.91	115.78	0.83	140.06	1.00
100.00	50.00	20.00	2.00	8.00	200.00	133.76	123.38	0.92	126.17	0.94	114.75	0.86	134.26	1.00
100.00	50.00	20.00	2.00	8.00	300.00	129.57	122.00	0.94	124.31	0.96	113.03	0.87	128.95	1.00
100.00	50.00	20.00	2.00	8.00	400.00	124.13	120.09	0.97	121.76	0.98	110.62	0.89	126.37	1.02
100.00	50.00	20.00	2.00	8.00	500.00	121.39	117.69	0.97	118.56	0.98	107.52	0.89	124.09	1.02
100.00	50.00	20.00	2.00	8.00	600.00	117.71	114.80	0.98	114.76	0.97	103.74	0.88	121.12	1.03
100.00	50.00	20.00	2.00	8.00	700.00	112.62	111.48	0.99	110.42	0.98	99.27	0.88	114.16	1.01
100.00	50.00	20.00	2.00	8.00	800.00	107.18	107.75	1.01	105.61	0.99	94.11	0.88	109.25	1.02
100.00	50.00	20.00	2.00	8.00	900.00	101.37	103.66	1.02	100.40	0.99	88.26	0.87	104.19	1.03
150.00	60.00	20.00	2.00	8.00	150.00	153.25	149.31	0.97	144.33	0.94	130.08	0.85	149.84	0.98
150.00	60.00	20.00	2.00	8.00	300.00	147.18	147.81	1.00	142.97	0.97	128.55	0.87	149.84	1.02
150.00	60.00	20.00	2.00	8.00	450.00	142.08	145.34	1.02	140.10	0.99	126.00	0.89	144.95	1.02
150.00	60.00	20.00	2.00	8.00	600.00	138.44	141.95	1.03	135.80	0.98	122.43	0.88	139.47	1.01
150.00	60.00	20.00	2.00	8.00	750.00	135.11	137.71	1.02	130.48	0.97	117.84	0.87	133.47	0.99
150.00	60.00	20.00	2.00	8.00	900.00	130.07	132.68	1.02	124.26	0.96	112.23	0.86	126.75	0.97
150.00	60.00	20.00	2.00	8.00	1050.00	123.56	126.96	1.03	117.30	0.95	105.61	0.85	119.16	0.96
150.00	60.00	20.00	2.00	8.00	1200.00	116.40	110.35	0.95	109.75	0.94	97.96	0.84	110.72	0.95
150.00	60.00	20.00	2.00	8.00	1350.00	108.97	108.35	0.99	101.79	0.93	89.29	0.82	101.63	0.93
150.00	60.00	20.00	2.00	8.00	1500.00	101.52	98.35	0.97	93.58	0.92	79.61	0.78	92.28	0.91
150.00	60.00	20.00	2.50	8.00	150.00	208.60	216.48	1.04	191.83	0.92	173.03	0.83	205.33	0.98
150.00	60.00	20.00	2.50	8.00	300.00	195.98	178.52	0.91	189.24	0.97	170.80	0.87	196.36	1.00
150.00	60.00	20.00	2.50	8.00	450.00	190.30	175.41	0.92	185.01	0.97	167.07	0.88	188.41	0.99
150.00	60.00	20.00	2.50	8.00	600.00	182.41	171.15	0.94	179.25	0.98	161.86	0.89	185.45	1.02

Dimension (mm)					length (mm)	P_{FEM}	DSM ($\phi=.85$)		AISI ($\phi=.85$)		EGY ($\phi=.8$)		EURO	
h	b	d	t	r			ϕP_n	$\phi P_n / P_{FEM}$	ϕP_n	$\phi P_n / P_{FEM}$	ϕP_n	$\phi P_n / P_{FEM}$	P_n	P_n / P_{FEM}
150.00	60.00	20.00	2.50	8.00	750.00	178.37	165.82	0.93	172.10	0.96	155.16	0.87	180.09	1.01
150.00	60.00	20.00	2.50	8.00	900.00	170.85	159.51	0.93	163.74	0.96	146.97	0.86	169.88	0.99
150.00	60.00	20.00	2.50	8.00	1050.00	160.49	152.33	0.95	154.39	0.96	137.29	0.86	158.31	0.99
150.00	60.00	20.00	2.50	8.00	1200.00	150.39	144.43	0.96	144.25	0.96	126.12	0.84	145.50	0.97
150.00	60.00	20.00	2.50	8.00	1350.00	139.88	135.93	0.97	133.55	0.95	113.46	0.81	131.98	0.94
200.00	60.00	20.00	2.00	8.00	200.00	155.55	148.96	0.96	146.53	0.94	131.49	0.85	149.50	0.96
200.00	60.00	20.00	2.00	8.00	400.00	148.31	146.34	0.99	143.83	0.97	129.10	0.87	147.44	0.99
200.00	60.00	20.00	2.00	8.00	600.00	142.53	142.09	1.00	138.34	0.97	125.13	0.88	140.87	0.99
200.00	60.00	20.00	2.00	8.00	800.00	138.42	136.33	0.98	131.01	0.95	119.58	0.86	133.64	0.97
200.00	60.00	20.00	2.00	8.00	1000.00	132.78	129.24	0.97	122.18	0.92	112.43	0.85	125.35	0.94
200.00	60.00	20.00	2.00	8.00	1200.00	124.53	121.06	0.97	112.22	0.90	103.69	0.83	115.75	0.93
200.00	60.00	20.00	2.00	8.00	1400.00	115.58	112.03	0.97	101.53	0.88	93.37	0.81	104.94	0.91
200.00	60.00	20.00	2.00	8.00	1600.00	106.10	102.40	0.97	90.48	0.85	81.46	0.77	93.51	0.88
200.00	60.00	20.00	2.00	8.00	1800.00	96.20	92.43	0.96	79.44	0.83	67.69	0.70	82.28	0.86
200.00	60.00	20.00	2.00	8.00	2000.00	86.47	82.36	0.95	68.72	0.79	64.83	0.75	71.94	0.83
200.00	60.00	20.00	2.50	8.00	200.00	211.32	210.23	0.99	196.22	0.93	175.93	0.83	206.88	0.98
200.00	60.00	20.00	2.50	8.00	400.00	199.17	202.28	1.02	191.65	0.96	172.41	0.87	202.81	1.02
200.00	60.00	20.00	2.50	8.00	600.00	190.39	196.17	1.03	184.27	0.97	166.54	0.87	192.98	1.01
200.00	60.00	20.00	2.50	8.00	800.00	183.66	187.91	1.02	174.42	0.95	158.32	0.86	181.97	0.99
200.00	60.00	20.00	2.50	8.00	1000.00	174.46	177.77	1.02	162.55	0.93	147.76	0.85	169.13	0.97
200.00	60.00	20.00	2.50	8.00	1200.00	162.64	166.08	1.02	149.15	0.92	134.84	0.83	154.22	0.95
200.00	60.00	20.00	2.50	8.00	1400.00	149.91	153.19	1.02	134.76	0.90	119.58	0.80	137.69	0.92
200.00	60.00	20.00	2.50	8.00	1600.00	136.32	139.48	1.02	119.88	0.88	101.97	0.75	120.80	0.89
200.00	60.00	20.00	2.50	8.00	1800.00	122.62	125.33	1.02	105.00	0.86	92.08	0.75	104.88	0.86
200.00	60.00	20.00	2.50	8.00	2000.00	101.17	101.16	1.00	90.53	0.89	86.49	0.85	90.75	0.90

Dimension (mm)					length (mm)	P_{FEM}	DSM ($\phi=.85$)		AISI ($\phi=.85$)		EGY ($\phi=.8$)		EURO	
h	b	d	t	r			ϕP_n	$\phi P_n / P_{FEM}$	ϕP_n	$\phi P_n / P_{FEM}$	ϕP_n	$\phi P_n / P_{FEM}$	P_n	P_n / P_{FEM}
250.00	70.00	-	2.00	8.00	250.00	111.43	98.81	0.89	103.22	0.93	86.32	0.77	97.20	0.87
250.00	70.00	-	2.00	8.00	500.00	101.47	96.01	0.95	100.30	0.99	84.81	0.84	95.53	0.94
250.00	70.00	-	2.00	8.00	750.00	97.00	91.52	0.94	95.61	0.99	82.30	0.85	89.74	0.93
250.00	70.00	-	2.00	8.00	1000.00	92.96	85.57	0.92	89.42	0.96	78.77	0.85	83.70	0.90
250.00	70.00	-	2.00	8.00	1250.00	85.00	78.46	0.92	82.03	0.97	74.24	0.87	77.25	0.91
250.00	70.00	-	2.00	8.00	1500.00	76.72	70.54	0.92	73.81	0.96	68.71	0.90	70.38	0.92
250.00	70.00	-	2.00	8.00	1750.00	68.35	62.17	0.91	65.11	0.95	62.16	0.91	63.28	0.93
250.00	70.00	-	2.00	8.00	2000.00	60.68	53.63	0.88	56.20	0.93	54.61	0.90	56.26	0.93
250.00	70.00	-	2.00	8.00	2250.00	53.22	46.04	0.87	48.25	0.91	46.01	0.86	49.64	0.93
250.00	70.00	-	2.00	8.00	2500.00	46.64	40.13	0.86	42.00	0.90	37.27	0.80	43.67	0.94
300.00	70.00	-	2.50	8.00	300.00	161.98	142.78	0.88	153.73	0.95	132.55	0.82	150.12	0.93
300.00	70.00	-	2.50	8.00	600.00	146.44	136.68	0.93	147.21	1.01	128.69	0.88	142.41	0.97
300.00	70.00	-	2.50	8.00	900.00	137.19	127.07	0.93	136.94	1.00	122.27	0.89	130.56	0.95
300.00	70.00	-	2.50	8.00	1200.00	127.77	114.70	0.90	123.71	0.97	113.27	0.89	117.72	0.92
300.00	70.00	-	2.50	8.00	1500.00	117.29	100.49	0.86	108.48	0.92	101.70	0.87	103.88	0.89
300.00	70.00	-	2.50	8.00	1800.00	105.28	85.40	0.81	92.23	0.88	87.56	0.83	89.77	0.85
300.00	70.00	-	2.50	8.00	2100.00	93.44	90.93	0.97	76.15	0.81	70.76	0.76	76.49	0.82
300.00	70.00	-	2.50	8.00	2400.00	80.42	76.37	0.95	63.73	0.79	64.18	0.80	64.83	0.81
300.00	70.00	-	2.50	8.00	2700.00	67.97	65.38	0.96	54.22	0.80	52.81	0.78	55.03	0.81
215.00	60.00	-	3.00	8.00	215.00	206.90	189.63	0.92	203.33	0.98	179.93	0.87	203.56	0.98
215.00	60.00	-	3.00	8.00	430.00	184.15	183.90	1.00	181.08	0.98	174.53	0.95	183.52	1.00
215.00	60.00	-	3.00	8.00	645.00	174.74	174.70	1.00	168.60	0.96	165.54	0.95	176.33	1.01
215.00	60.00	-	3.00	8.00	860.00	166.61	162.56	0.98	164.03	0.98	152.96	0.92	158.59	0.95
215.00	60.00	-	3.00	8.00	1075.00	155.49	148.11	0.95	139.80	0.90	136.77	0.88	139.48	0.90
215.00	60.00	-	3.00	8.00	1290.00	141.16	132.08	0.94	139.97	0.99	117.00	0.83	120.12	0.85

Dimension (mm)					length (mm)	P _{FEM}	DSM ($\phi=.85$)		AISI ($\phi=.85$)		EGY ($\phi=.8$)		EURO	
h	b	d	t	r			ϕP_n	$\phi P_n / P_{FEM}$	ϕP_n	$\phi P_n / P_{FEM}$	ϕP_n	$\phi P_n / P_{FEM}$	P _n	P _n / P _{FEM}
215.00	60.00	-	3.00	8.00	1505.00	123.83	115.23	0.93	121.19	0.98	93.27	0.75	102.03	0.82
215.00	60.00	-	3.00	8.00	1935.00	86.28	85.69	0.99	83.26	0.97	66.42	0.77	73.09	0.85
215.00	60.00	-	3.00	8.00	2150.00	72.95	69.41	0.95	69.40	0.95	55.70	0.76	62.31	0.85
180.00	75.00	-	4.00	8.00	180.00	360.88	358.14	0.99	327.92	0.91	302.42	0.84	337.53	0.94
180.00	75.00	-	4.00	8.00	360.00	340.53	353.30	1.04	323.20	0.95	297.37	0.87	332.83	0.98
180.00	75.00	-	4.00	8.00	540.00	318.05	316.25	0.99	315.46	0.99	288.96	0.91	313.27	0.98
180.00	75.00	-	4.00	8.00	720.00	296.70	274.22	0.92	295.29	1.00	277.17	0.93	292.98	0.99
180.00	75.00	-	4.00	8.00	900.00	280.65	263.19	0.94	262.92	0.94	262.02	0.93	271.37	0.97
180.00	75.00	-	4.00	8.00	1080.00	265.59	250.28	0.94	257.05	0.97	243.50	0.92	248.36	0.94
180.00	75.00	-	4.00	8.00	1260.00	247.91	235.77	0.95	239.61	0.97	221.62	0.89	224.42	0.91
180.00	75.00	-	4.00	8.00	1440.00	225.41	220.00	0.98	217.58	0.97	196.36	0.87	200.53	0.89
100.00	40.00	-	3.00	8.00	100.00	162.79	149.83	0.92	152.85	0.94	142.96	0.88	163.62	1.01
100.00	40.00	-	3.00	8.00	200.00	155.69	147.40	0.95	149.24	0.96	139.65	0.90	158.78	1.02
100.00	40.00	-	3.00	8.00	300.00	146.01	143.43	0.98	143.42	0.98	134.13	0.92	143.91	0.99
100.00	40.00	-	3.00	8.00	400.00	133.36	138.03	1.04	130.85	0.98	126.41	0.95	134.62	1.01

Table A-23: - Comparison between EWM and DSM for CFS flexure channel sections.

Dimension (mm)					length (mm)	M _{FEM} (Kn.m)	DSM($\phi=0.9$)		AISI($\phi=0.9$)		EGY($\phi=0.85$)		EURO	
h	b	d	t	r			ϕM_n	$\phi M_n/FEM$	ϕM_n	$\phi M_n/FEM$	ϕM_n	$\phi M_n/FEM$	M _n	M _{n/FEM}
304.80	101.60	22.48	2.67	4.76	304.80	40.47	30.16	0.75	34.83	0.86	37.66	0.93	37.09	0.92
304.80	101.60	22.48	2.67	4.76	609.60	36.16	30.16	0.83	34.83	0.96	33.83	0.94	33.38	0.92
304.80	101.60	22.48	2.67	4.76	914.40	34.84	30.16	0.87	31.35	0.90	33.83	0.97	33.02	0.95
304.80	101.60	22.48	2.67	4.76	1,219.20	33.55	30.16	0.90	31.35	0.93	33.83	1.01	32.38	0.97
304.80	101.60	22.48	2.67	4.76	1,524.00	33.05	30.16	0.91	31.35	0.95	33.83	1.02	31.68	0.96
304.80	101.60	22.48	2.67	4.76	1,828.80	32.44	30.16	0.93	31.35	0.97	33.22	1.02	30.90	0.95
304.80	101.60	22.48	2.67	4.76	2,133.60	32.19	30.16	0.94	30.99	0.96	24.63	0.77	29.99	0.93
304.80	101.60	22.48	2.67	4.76	2,438.40	30.10	30.16	1.00	29.96	1.00	19.05	0.63	28.91	0.96
304.80	101.60	22.48	2.67	4.76	2,743.20	30.02	30.16	1.00	28.88	0.96	15.22	0.51	27.64	0.92
304.80	101.60	22.48	2.67	4.76	3,048.00	29.65	30.16	1.02	27.71	0.93	12.48	0.42	26.15	0.88
304.80	101.60	21.23	2.16	4.76	304.80	27.99	27.87	1.00	25.85	0.92	26.34	0.94	25.02	0.89
304.80	101.60	21.23	2.16	4.76	609.60	26.25	25.27	0.96	25.85	0.98	23.69	0.90	25.02	0.95
304.80	101.60	21.23	2.16	4.76	914.40	24.17	24.03	0.99	22.75	0.94	23.69	0.98	24.87	1.03
304.80	101.60	21.23	2.16	4.76	1,219.20	23.79	24.03	1.01	22.75	0.96	23.69	1.00	24.44	1.03
304.80	101.60	21.23	2.16	4.76	1,524.00	23.55	24.03	1.02	22.75	0.97	23.69	1.01	23.98	1.02
304.80	101.60	21.23	2.16	4.76	1,828.80	23.27	24.03	1.03	22.75	0.98	23.69	1.02	23.47	1.01
304.80	101.60	21.23	2.16	4.76	2,133.60	22.68	23.54	1.04	21.02	0.93	20.28	0.89	22.90	1.01
304.80	101.60	21.23	2.16	4.76	2,438.40	22.30	22.58	1.01	19.94	0.89	15.63	0.70	22.23	1.00
304.80	101.60	21.23	2.16	4.76	3,048.00	20.39	20.94	1.03	19.02	0.93	10.16	0.50	20.55	1.01
228.60	63.50	22.48	2.67	4.76	228.60	23.45	20.34	0.87	22.20	0.95	16.19	0.69	21.18	0.90
228.60	63.50	22.48	2.67	4.76	457.20	23.45	21.62	0.92	22.20	0.95	16.19	0.69	21.14	0.90
228.60	63.50	22.48	2.67	4.76	685.80	21.52	21.42	1.00	22.20	1.03	16.19	0.75	20.64	0.96
228.60	63.50	22.48	2.67	4.76	914.40	21.21	21.42	1.01	19.98	0.94	16.19	0.76	20.09	0.95

Dimension (mm)					length (mm)	M _{FEM} (Kn.m)	DSM($\phi=.9$)		AISI($\phi=.9$)		EGY($\phi=.85$)		EURO	
h	b	d	t	r			ϕM_n	$\phi M_n/FEM$	ϕM_n	$\phi M_n/FEM$	ϕM_n	$\phi M_n/FEM$	Mn	Mn/FEM
228.60	63.50	22.48	2.67	4.76	1,143.00	21.15	21.42	1.01	19.98	0.94	12.74	0.60	19.45	0.92
228.60	63.50	22.48	2.67	4.76	1,371.60	20.97	21.42	1.02	19.94	0.95	9.09	0.43	20.75	0.99
228.60	63.50	22.48	2.67	4.76	1,600.20	20.55	21.42	1.04	19.43	0.95	6.88	0.33	19.70	0.96
228.60	63.50	22.48	2.67	4.76	1,828.80	20.31	20.45	1.01	18.83	0.93	5.44	0.27	18.41	0.91
228.60	63.50	22.48	2.67	4.76	2,057.40	19.98	19.28	0.96	18.10	0.91	4.45	0.22	16.91	0.85
228.60	63.50	22.48	2.67	4.76	2,286.00	17.53	17.99	1.03	17.14	0.98	3.74	0.21	15.31	0.87
228.60	63.50	21.23	2.16	4.76	228.60	18.13	17.17	0.95	16.55	0.91	8.29	0.46	16.37	0.90
228.60	63.50	21.23	2.16	4.76	457.20	16.70	16.37	0.98	16.55	0.99	8.29	0.50	16.35	0.98
228.60	63.50	21.23	2.16	4.76	685.80	16.30	15.96	0.98	16.55	1.02	8.29	0.51	15.98	0.98
228.60	63.50	21.23	2.16	4.76	914.40	15.97	15.96	1.00	16.55	1.04	8.29	0.52	15.56	0.97
228.60	63.50	21.23	2.16	4.76	1,143.00	15.97	15.96	1.00	16.55	1.04	8.29	0.52	15.09	0.94
228.60	63.50	21.23	2.16	4.76	1,371.60	15.85	15.96	1.01	16.48	1.04	7.50	0.47	14.51	0.92
228.60	63.50	21.23	2.16	4.76	1,600.20	15.65	15.96	1.02	15.93	1.02	5.62	0.36	13.80	0.88
228.60	63.50	21.23	2.16	4.76	1,828.80	15.27	15.96	1.05	15.32	1.00	4.40	0.29	14.38	0.94
228.60	63.50	21.23	2.16	4.76	2,057.40	15.23	15.39	1.01	14.64	0.96	3.56	0.23	13.25	0.87
228.60	63.50	21.23	2.16	4.76	2,286.00	14.90	14.53	0.97	13.92	0.93	2.96	0.20	12.02	0.81
228.60	63.50	19.63	1.50	4.75	228.60	10.21	9.42	0.92	10.16	1.00	1.57	0.15	9.86	0.97
228.60	63.50	19.63	1.50	4.75	457.20	9.98	9.42	0.94	10.16	1.02	1.60	0.16	9.86	0.99
228.60	63.50	19.63	1.50	4.75	685.80	9.57	9.42	0.98	9.15	0.96	1.67	0.17	9.70	1.01
228.60	63.50	19.63	1.50	4.75	914.40	9.10	9.42	1.03	9.15	1.00	1.76	0.19	9.49	1.04
228.60	63.50	19.63	1.50	4.75	1,143.00	9.07	9.42	1.04	9.15	1.01	8.65	0.95	9.26	1.02
228.60	63.50	19.63	1.50	4.75	1,371.60	9.04	9.38	1.04	9.15	1.01	8.43	0.93	8.98	0.99
228.60	63.50	19.63	1.50	4.75	1,600.20	8.87	9.11	1.03	9.06	1.02	6.26	0.71	8.66	0.98
228.60	63.50	19.63	1.50	4.75	1,828.80	8.83	8.80	1.00	8.66	0.98	4.84	0.55	8.27	0.94
228.60	63.50	19.63	1.50	4.75	2,057.40	8.59	8.43	0.98	8.21	0.96	3.87	0.45	7.80	0.91

Dimension (mm)					length (mm)	M _{FEM} (Kn.m)	DSM($\phi=.9$)		AISI($\phi=.9$)		EGY($\phi=.85$)		EURO	
h	b	d	t	r			ϕM_n	$\phi M_n/FEM$	ϕM_n	$\phi M_n/FEM$	ϕM_n	$\phi M_n/FEM$	M _n	M _{n/FEM}
228.60	63.50	19.63	1.50	4.75	2,286.00	8.48	8.03	0.95	7.78	0.92	3.18	0.38	7.26	0.86
209.55	50.80	-	1.81	2.72	209.55	8.24	7.39	0.90	6.75	0.82	6.04	0.73	7.56	0.92
209.55	50.80	-	1.81	2.72	419.10	7.42	7.39	1.00	6.75	0.91	6.04	0.81	7.47	1.01
209.55	50.80	-	1.81	2.72	628.65	7.10	7.39	1.04	6.75	0.95	6.04	0.85	7.24	1.02
209.55	50.80	-	1.81	2.72	838.20	7.00	7.39	1.06	6.75	0.96	6.04	0.86	6.98	1.00
209.55	50.80	-	1.81	2.72	1,047.75	6.67	6.32	0.95	6.75	1.01	6.04	0.91	6.65	1.00
209.55	50.80	-	1.81	2.72	1,257.30	5.96	5.67	0.95	5.81	0.97	6.04	1.01	6.23	1.04
209.55	50.80	-	1.81	2.72	1,466.85	5.89	4.35	0.74	5.97	1.01	5.15	0.87	5.70	0.97
209.55	50.80	-	1.81	2.72	1,676.40	5.89	5.78	0.98	5.40	0.92	4.02	0.68	5.09	0.86
209.55	50.80	-	1.81	2.72	1,885.95	5.52	4.90	0.89	4.71	0.85	3.24	0.59	4.46	0.81
209.55	50.80	-	1.81	2.72	2,095.50	5.40	4.73	0.88	4.55	0.84	2.68	0.50	4.98	0.92
313.84	50.80	-	2.58	3.87	313.84	23.88	23.49	0.98	22.60	0.95	20.70	0.87	22.16	0.93
313.84	50.80	-	2.58	3.87	627.68	23.76	22.76	0.96	22.60	0.95	18.42	0.78	21.03	0.89
313.84	50.80	-	2.58	3.87	941.53	23.62	22.40	0.95	22.60	0.96	23.20	0.98	20.36	0.86
313.84	50.80	-	2.58	3.87	1,255.37	22.28	21.60	0.97	20.86	0.94	13.46	0.60	19.62	0.88
313.84	50.80	-	2.58	3.87	1,569.21	21.22	20.79	0.98	18.00	0.85	8.93	0.42	18.96	0.89
313.84	50.80	-	2.58	3.87	1,883.05	21.17	20.52	0.97	14.35	0.68	6.47	0.31	18.63	0.88
313.84	50.80	-	2.58	3.87	2,196.90	20.62	15.79	0.77	11.01	0.53	4.97	0.24	17.63	0.86
98.43	50.80	-	1.81	2.72	98.43	3.32	2.79	0.84	2.83	0.85	2.16	0.65	2.72	0.82
98.43	50.80	-	1.81	2.72	196.85	3.19	2.79	0.87	2.83	0.89	2.16	0.68	2.72	0.85
98.43	50.80	-	1.81	2.72	295.28	3.18	2.79	0.88	2.83	0.89	2.16	0.68	2.72	0.86
98.43	50.80	-	1.81	2.72	393.70	3.13	2.79	0.89	2.83	0.90	2.16	0.69	2.70	0.86
98.43	50.80	-	1.81	2.72	492.13	3.07	2.79	0.91	2.83	0.92	2.16	0.70	2.67	0.87
98.43	50.80	-	1.81	2.72	590.55	3.02	2.79	0.92	2.83	0.94	2.16	0.72	2.63	0.87
98.43	50.80	-	1.81	2.72	688.98	2.97	2.79	0.94	2.83	0.95	2.16	0.73	2.59	0.87

Dimension (mm)					length (mm)	M_{FEM} (Kn.m)	DSM($\phi=.9$)		AISI($\phi=.9$)		EGY($\phi=.85$)		EURO	
h	b	d	t	r			ϕM_n	$\phi M_n/FEM$	ϕM_n	$\phi M_n/FEM$	ϕM_n	$\phi M_n/FEM$	Mn	M_n/FEM
98.43	50.80	-	1.81	2.72	787.40	2.96	2.79	0.94	2.83	0.96	2.16	0.73	2.55	0.86
98.43	50.80	-	1.81	2.72	885.83	2.96	2.78	0.94	2.82	0.95	2.16	0.73	2.50	0.85
98.43	50.80	-	1.81	2.72	984.25	2.91	2.96	1.02	2.76	0.95	2.16	0.74	2.45	0.84
212.24	50.80	-	2.58	3.87	212.24	14.19	14.32	1.01	13.84	0.98	6.12	0.43	13.50	0.95
212.24	50.80	-	2.58	3.87	424.48	14.18	14.32	1.01	13.84	0.98	6.12	0.43	13.24	0.93
212.24	50.80	-	2.58	3.87	636.73	13.75	14.32	1.04	13.84	1.01	6.12	0.45	12.76	0.93
212.24	50.80	-	2.58	3.87	848.97	13.71	14.31	1.04	13.84	1.01	6.12	0.45	12.17	0.89
212.24	50.80	-	2.58	3.87	1,061.21	13.60	13.72	1.01	13.12	0.97	6.12	0.45	11.40	0.84
212.24	50.80	-	2.58	3.87	1,273.45	13.49	13.01	0.96	12.22	0.91	6.12	0.45	12.48	0.92
212.24	50.80	-	2.58	3.87	1,485.70	13.30	12.15	0.91	11.17	0.84	5.12	0.39	13.25	1.00
212.24	50.80	-	2.58	3.87	1,697.94	13.16	11.15	0.85	9.98	0.76	4.00	0.30	11.49	0.87
212.24	50.80	-	2.58	3.87	1,910.18	13.10	11.36	0.87	8.64	0.66	3.22	0.25	9.60	0.73
212.24	50.80	-	2.58	3.87	2,122.42	11.77	9.39	0.80	7.32	0.62	2.67	0.23	8.28	0.70

Table A-24: - Comparison between EWM and DSM for CFS flexure Z-sections.

Dimension (mm)					length (mm)	M _{FEM} (Kn.m)	DSM($\phi=.9$)		AISI($\phi=.9$)		EGY($\phi=.85$)		EURO	
h	b	d	t	r			ϕM_n	$\phi M_n/FEM$	ϕM_n	$\phi M_n/FEM$	ϕM_n	$\phi M_n/FEM$	M _n	M _n /FEM
100.00	50.00	20.00	2.00	8.00	100.00	5.60	5.16	0.92	4.92	0.88	4.80	0.86	5.20	0.93
100.00	50.00	20.00	2.00	8.00	200.00	5.48	5.16	0.94	4.92	0.90	4.80	0.88	5.20	0.95
100.00	50.00	20.00	2.00	8.00	300.00	5.31	5.16	0.97	4.92	0.93	4.80	0.90	5.20	0.98
100.00	50.00	20.00	2.00	8.00	400.00	5.24	5.16	0.98	4.92	0.94	4.80	0.92	5.20	0.99
100.00	50.00	20.00	2.00	8.00	500.00	5.24	5.16	0.99	4.92	0.94	4.80	0.92	5.17	0.99
100.00	50.00	20.00	2.00	8.00	600.00	5.21	5.16	0.99	4.92	0.94	4.35	0.83	5.12	0.98
100.00	50.00	20.00	2.00	8.00	700.00	5.21	5.16	0.99	4.92	0.95	3.30	0.63	5.07	0.97
100.00	50.00	20.00	2.00	8.00	800.00	5.20	5.16	0.99	4.92	0.95	2.61	0.50	5.01	0.96
100.00	50.00	20.00	2.00	8.00	900.00	5.16	5.16	1.00	4.92	0.95	2.13	0.41	4.95	0.96
100.00	50.00	20.00	2.00	8.00	1000.00	5.12	5.16	1.01	4.92	0.96	1.79	0.35	4.89	0.96
150.00	60.00	20.00	2.00	8.00	150.00	10.57	10.18	0.96	9.06	0.86	5.32	0.50	9.51	0.90
150.00	60.00	20.00	2.00	8.00	300.00	9.84	10.18	1.03	9.06	0.92	5.32	0.54	9.51	0.97
150.00	60.00	20.00	2.00	8.00	450.00	9.83	10.18	1.04	9.06	0.92	5.32	0.54	9.51	0.97
150.00	60.00	20.00	2.00	8.00	600.00	9.76	9.51	0.97	9.06	0.93	5.32	0.55	9.44	0.97
150.00	60.00	20.00	2.00	8.00	750.00	9.72	9.51	0.98	9.06	0.93	5.32	0.55	9.32	0.96
150.00	60.00	20.00	2.00	8.00	900.00	9.71	9.51	0.98	9.06	0.93	5.32	0.55	9.18	0.95
150.00	60.00	20.00	2.00	8.00	1050.00	9.70	9.51	0.98	9.06	0.93	4.61	0.48	9.04	0.93
150.00	60.00	20.00	2.00	8.00	1200.00	9.59	9.51	0.99	9.06	0.95	3.61	0.38	8.89	0.93
150.00	60.00	20.00	2.00	8.00	1350.00	9.46	9.51	1.01	8.84	0.93	2.93	0.31	8.72	0.92
150.00	60.00	20.00	2.00	8.00	1500.00	9.42	9.51	1.01	8.59	0.91	2.44	0.26	8.54	0.91
150.00	60.00	20.00	2.50	8.00	150.00	12.90	12.50	0.97	11.91	0.92	10.75	0.83	12.05	0.93
150.00	60.00	20.00	2.50	8.00	300.00	12.73	12.50	0.98	11.91	0.94	10.75	0.84	12.05	0.95
150.00	60.00	20.00	2.50	8.00	450.00	12.62	12.50	0.99	11.91	0.94	10.75	0.85	12.05	0.95
150.00	60.00	20.00	2.50	8.00	600.00	12.58	12.50	0.99	11.91	0.95	10.75	0.85	11.94	0.95
150.00	60.00	20.00	2.50	8.00	750.00	12.53	12.50	1.00	11.91	0.95	10.37	0.83	11.78	0.94
150.00	60.00	20.00	2.50	8.00	900.00	12.50	12.50	1.00	11.91	0.95	7.41	0.59	11.61	0.93

Dimension (mm)					length (mm)	M _{FEM} (Kn.m)	DSM($\phi=.9$)		AISI($\phi=.9$)		EGY($\phi=.85$)		EURO	
h	b	d	t	r			ϕM_n	$\phi M_n/FEM$	ϕM_n	$\phi M_n/FEM$	ϕM_n	$\phi M_n/FEM$	M _n	M _n /FEM
150.00	60.00	20.00	2.50	8.00	1050.00	12.44	12.50	1.01	11.91	0.96	5.63	0.45	11.43	0.92
150.00	60.00	20.00	2.50	8.00	1200.00	12.29	12.50	1.02	11.89	0.97	4.46	0.36	11.23	0.91
150.00	60.00	20.00	2.50	8.00	1350.00	12.14	12.10	1.00	11.66	0.96	3.66	0.30	11.01	0.91
150.00	60.00	20.00	2.50	8.00	1500.00	11.99	11.68	0.97	11.39	0.95	3.08	0.26	10.76	0.90
200.00	60.00	20.00	2.00	8.00	200.00	15.22	14.69	0.97	13.46	0.88	7.90	0.52	13.79	0.91
200.00	60.00	20.00	2.00	8.00	400.00	13.99	13.88	0.99	13.46	0.96	7.90	0.56	13.79	0.99
200.00	60.00	20.00	2.00	8.00	600.00	13.86	13.32	0.96	13.46	0.97	7.90	0.57	13.67	0.99
200.00	60.00	20.00	2.00	8.00	800.00	13.81	13.32	0.96	13.46	0.98	7.90	0.57	13.41	0.97
200.00	60.00	20.00	2.00	8.00	1000.00	13.76	13.32	0.97	13.46	0.98	6.47	0.47	13.14	0.95
200.00	60.00	20.00	2.00	8.00	1200.00	13.64	13.32	0.98	13.32	0.98	4.60	0.34	12.83	0.94
200.00	60.00	20.00	2.00	8.00	1400.00	13.36	13.32	1.00	12.82	0.96	3.47	0.26	12.48	0.93
200.00	60.00	20.00	2.00	8.00	1600.00	13.30	13.32	1.00	12.27	0.92	2.73	0.21	12.07	0.91
200.00	60.00	20.00	2.00	8.00	1800.00	13.17	12.58	0.95	11.66	0.88	2.23	0.17	11.58	0.88
200.00	60.00	20.00	2.00	8.00	2000.00	13.05	11.59	0.89	11.01	0.84	1.86	0.14	11.01	0.84
200.00	60.00	20.00	2.50	8.00	200.00	18.96	18.61	0.98	17.83	0.94	16.00	0.84	17.54	0.93
200.00	60.00	20.00	2.50	8.00	400.00	18.60	18.03	0.97	17.83	0.96	16.00	0.86	17.54	0.94
200.00	60.00	20.00	2.50	8.00	600.00	18.37	17.82	0.97	17.83	0.97	16.00	0.87	17.36	0.95
200.00	60.00	20.00	2.50	8.00	800.00	18.33	17.82	0.97	17.83	0.97	11.79	0.64	17.03	0.93
200.00	60.00	20.00	2.50	8.00	1000.00	18.26	17.82	0.98	17.83	0.98	7.79	0.43	16.67	0.91
200.00	60.00	20.00	2.50	8.00	1200.00	18.15	17.82	0.98	17.67	0.97	5.61	0.31	16.26	0.90
200.00	60.00	20.00	2.50	8.00	1400.00	18.00	17.48	0.97	17.21	0.96	4.28	0.24	15.80	0.88
200.00	60.00	20.00	2.50	8.00	1600.00	17.65	16.50	0.93	16.67	0.94	3.42	0.19	15.25	0.86
200.00	60.00	20.00	2.50	8.00	1800.00	17.26	15.39	0.89	15.96	0.92	2.82	0.16	14.60	0.85
200.00	60.00	20.00	2.50	8.00	2000.00	16.91	14.15	0.84	14.73	0.87	2.39	0.14	13.85	0.82
250.00	70.00	-	2.00	8.00	250.00	15.51	12.84	0.83	13.96	0.90	5.70	0.37	11.33	0.73
250.00	70.00	-	2.00	8.00	500.00	14.90	12.84	0.86	13.96	0.94	5.70	0.38	11.33	0.76
250.00	70.00	-	2.00	8.00	750.00	14.59	12.84	0.88	13.96	0.96	5.70	0.39	11.19	0.77
250.00	70.00	-	2.00	8.00	1000.00	14.53	12.84	0.88	13.96	0.96	5.70	0.39	10.96	0.75

Dimension (mm)					length (mm)	M _{FEM} (Kn.m)	DSM($\phi=.9$)		AISI($\phi=.9$)		EGY($\phi=.85$)		EURO	
h	b	d	t	r			ϕM_n	$\phi M_n/FEM$	ϕM_n	$\phi M_n/FEM$	ϕM_n	$\phi M_n/FEM$	M _n	M _n /FEM
250.00	70.00	-	2.00	8.00	1250.00	13.39	12.50	0.93	12.95	0.97	5.70	0.43	10.71	0.80
250.00	70.00	-	2.00	8.00	1500.00	12.94	11.93	0.92	12.60	0.97	5.70	0.44	10.43	0.81
250.00	70.00	-	2.00	8.00	1750.00	12.70	11.24	0.88	11.60	0.91	5.70	0.45	10.10	0.80
250.00	70.00	-	2.00	8.00	2000.00	12.48	10.40	0.83	10.43	0.84	5.70	0.46	9.71	0.78
250.00	70.00	-	2.00	8.00	2250.00	12.15	9.41	0.77	9.09	0.75	5.06	0.42	9.24	0.76
250.00	70.00	-	2.00	8.00	2500.00	11.81	8.27	0.70	7.64	0.65	4.16	0.35	8.70	0.74
300.00	70.00	-	2.50	8.00	300.00	26.19	24.38	0.93	21.83	0.83	12.16	0.46	20.69	0.79
300.00	70.00	-	2.50	8.00	600.00	24.96	24.38	0.98	21.83	0.87	12.16	0.49	20.58	0.82
300.00	70.00	-	2.50	8.00	900.00	24.51	24.38	0.99	21.83	0.89	12.16	0.50	20.04	0.82
300.00	70.00	-	2.50	8.00	1200.00	24.41	23.71	0.97	21.83	0.89	12.16	0.50	19.43	0.80
300.00	70.00	-	2.50	8.00	1500.00	22.98	22.31	0.97	20.36	0.89	12.16	0.53	18.70	0.81
300.00	70.00	-	2.50	8.00	1800.00	21.54	20.53	0.95	18.45	0.86	9.49	0.44	17.80	0.83
300.00	70.00	-	2.50	8.00	2100.00	20.71	18.29	0.88	16.08	0.78	7.12	0.34	16.67	0.80
300.00	70.00	-	2.50	8.00	2400.00	20.09	15.60	0.78	13.26	0.66	5.57	0.28	15.30	0.76
300.00	70.00	-	2.50	8.00	2700.00	19.93	13.36	0.67	10.78	0.54	4.51	0.23	14.65	0.73
215.00	60.00	-	3.00	8.00	215.00	20.02	15.92	0.80	17.61	0.88	17.22	0.86	17.28	0.86
215.00	60.00	-	3.00	8.00	430.00	19.16	15.92	0.83	17.61	0.92	17.22	0.90	17.26	0.90
215.00	60.00	-	3.00	8.00	645.00	18.55	15.92	0.86	17.61	0.95	17.22	0.93	16.86	0.91
215.00	60.00	-	3.00	8.00	860.00	18.05	15.92	0.88	17.61	0.98	17.22	0.95	16.42	0.91
215.00	60.00	-	3.00	8.00	1075.00	17.85	15.46	0.87	16.93	0.95	13.16	0.74	15.92	0.89
215.00	60.00	-	3.00	8.00	1290.00	17.80	14.72	0.83	15.88	0.89	9.42	0.53	15.32	0.86
215.00	60.00	-	3.00	8.00	1505.00	17.57	13.82	0.79	14.61	0.83	7.15	0.41	14.59	0.83
215.00	60.00	-	3.00	8.00	1720.00	16.41	12.74	0.78	13.14	0.80	5.68	0.35	13.71	0.84
215.00	60.00	-	3.00	8.00	1935.00	15.25	11.45	0.75	11.43	0.75	4.66	0.31	12.69	0.83
215.00	60.00	-	3.00	8.00	2150.00	14.91	10.00	0.67	9.58	0.64	3.92	0.26	11.59	0.78
180.00	75.00	-	4.00	8.00	180.00	25.19	19.97	0.79	20.78	0.82	22.20	0.88	20.64	0.82
180.00	75.00	-	4.00	8.00	360.00	24.10	19.97	0.83	20.78	0.86	22.20	0.92	20.64	0.86
180.00	75.00	-	4.00	8.00	540.00	23.51	19.97	0.85	20.78	0.88	22.20	0.94	20.64	0.88

Dimension (mm)					length (mm)	M _{FEM} (Kn.m)	DSM($\phi=0.9$)		AISI($\phi=0.9$)		EGY($\phi=0.85$)		EURO	
h	b	d	t	r			ϕM_n	$\phi M_n/FEM$	ϕM_n	$\phi M_n/FEM$	ϕM_n	$\phi M_n/FEM$	M _n	M _{n/FEM}
180.00	75.00	-	4.00	8.00	720.00	23.08	19.97	0.86	20.78	0.90	22.20	0.96	20.35	0.88
180.00	75.00	-	4.00	8.00	900.00	22.84	19.97	0.87	20.78	0.91	22.20	0.97	20.04	0.88
180.00	75.00	-	4.00	8.00	1080.00	22.63	19.97	0.88	20.78	0.92	22.20	0.98	19.71	0.87
180.00	75.00	-	4.00	8.00	1260.00	22.60	19.88	0.88	20.67	0.91	22.20	0.98	19.36	0.86
180.00	75.00	-	4.00	8.00	1440.00	22.50	19.40	0.86	20.04	0.89	18.19	0.81	18.98	0.84
180.00	75.00	-	4.00	8.00	1620.00	22.22	18.85	0.85	19.32	0.87	14.84	0.67	18.55	0.83
180.00	75.00	-	4.00	8.00	1800.00	22.21	18.22	0.82	18.51	0.83	12.42	0.56	18.08	0.81
100.00	40.00	-	3.00	8.00	100.00	5.93	5.31	0.90	4.99	0.84	5.54	0.93	5.26	0.89
100.00	40.00	-	3.00	8.00	200.00	5.80	5.31	0.91	4.99	0.86	5.54	0.96	5.26	0.91
100.00	40.00	-	3.00	8.00	300.00	5.77	5.31	0.92	4.99	0.86	5.54	0.96	5.24	0.91
100.00	40.00	-	3.00	8.00	400.00	5.65	5.31	0.94	4.99	0.88	5.54	0.98	5.15	0.91
100.00	40.00	-	3.00	8.00	500.00	5.65	5.31	0.94	4.99	0.88	5.54	0.98	5.06	0.90
100.00	40.00	-	3.00	8.00	600.00	5.60	5.31	0.95	4.99	0.89	4.89	0.87	4.96	0.89
100.00	40.00	-	3.00	8.00	700.00	5.55	5.26	0.95	4.92	0.89	3.80	0.69	4.86	0.88
100.00	40.00	-	3.00	8.00	800.00	5.53	5.11	0.92	4.72	0.85	3.09	0.56	4.74	0.86
100.00	40.00	-	3.00	8.00	900.00	5.41	4.95	0.92	4.51	0.83	2.59	0.48	4.61	0.85
100.00	40.00	-	3.00	8.00	1000.00	5.31	4.75	0.90	4.27	0.80	2.23	0.42	4.47	0.84

A.4 Members Under Combined Bending And Axial Forces**Table A-25:** - Members under combined bending and axial forces.

Dimensions						L	F _y	Small eccentricity (e/h= 0.03)		Big eccentricity (e/h= 0.3)	
h	b	d	t	r	R			Channel	Zee	Channel	Zee
mm	mm	mm	mm	mm	mm			P _{FEM} (kN)	P _{FEM} (kN)	P _{FEM} (kN)	P _{FEM} (kN)
100	50	15	2	8	10	200	360	131.394	134.911	94.8628	79.7341
100	50	20	2	8	10	200	360	138.369	142.319	100.202	83.7446
100	50	25	2	8	10	200	360	144.72	148.871	104.475	87.7781
100	50	30	2	8	10	200	360	151.154	152.507	106.929	90.3893
100	50	20	2	8	10	100	360	146.975	149.793	105.525	88.3107
100	50	20	2	8	10	200	360	138.369	142.319	100.202	83.7446
100	50	20	2	8	10	300	360	134.83	136.772	98.6588	80.0707
100	50	20	2	8	10	400	360	131.528	132.607	94.6791	77.5303
100	50	20	2	8	10	500	360	124.994	126.872	91.0836	72.5571
100	50	20	2	8	10	600	360	121.246	121.315	89.5808	68.8895
100	50	20	2	8	10	700	360	117.077	115.46	87.259	65.0938
100	50	20	2	8	10	800	360	112.37	108.962	84.7937	61.4771
100	50	20	2	8	10	900	360	108.015	102.653	82.143	57.84
100	50	20	2	8	10	1000	360	103.372	96.3764	79.1251	54.1627
100	50	20	2	3	5	200	360	138.369	142.319	100.202	83.7446
100	25	10	2	3	5	200	360	90.1686	88.2189	67.1039	53.0799
100	20	8	2	3	5	200	360	77.9297	73.4715	58.1956	45.5804
100	16.66667	6.666667	2	3	5	200	360	69.9638	63.2539	53.9038	39.3046
100	14.28571	5.714286	2	3	5	200	360	57.0249	51.303	47.3069	32.8004
100	50	20	2	8	10	200	360	138.369	142.319	100.202	83.7446
200	100	40	2	8	10	400	360	190.493	193.022	129.406	114.113

Dimensions						L	F _y	Small eccentricity (e/h= 0.03)		Big eccentricity (e/h= 0.3)	
h	b	d	t	r	R			Channel	Zee	Channel	Zee
mm	mm	mm	mm	mm	mm			P _{FEM} (kN)	P _{FEM} (kN)	P _{FEM} (kN)	P _{FEM} (kN)
300	150	60	2	8	10	600	360	198.338	205.785	138.403	121.429
400	200	80	2	8	10	800	360	169.558	220.068	147.974	129.015
500	250	100	2	8	10	1000	360	137.932	229.654	153.99	132.234
600	300	120	2	8	10	1200	360	115.707	165.908	157.532	137.316
100	50	20	2	8	10	200	240	98.0611	99.8306	70.5886	59.4743
100	50	20	2	8	10	200	280	111.935	114.167	80.7478	67.994
100	50	20	2	8	10	200	320	125.342	128.517	90.6062	75.9761
100	50	20	2	8	10	200	360	138.369	142.319	100.202	83.7446
100	50	20	2	8	10	200	400	151.066	155.007	109.555	91.2051

A.5 Relation Between CFS Different Capacities Resulted From FEM.

Figures A.8 to A.12 illustrate the relationship between pure bending moment and compression capacities obtained from EEM and the capacities of the same identical members subjected to combined bending moment and compression forces. M_c represents the ultimate moment, and P_c is the ultimate compression capacities obtained from the FEM while the members are subjected to combined bending moment and compression forces. M_u represents the ultimate moment capacities obtained from the FEM while the members are subjected to pure bending moment. P_u is the ultimate compression capacities obtained from the FEM while the members are subjected to pure compression forces.

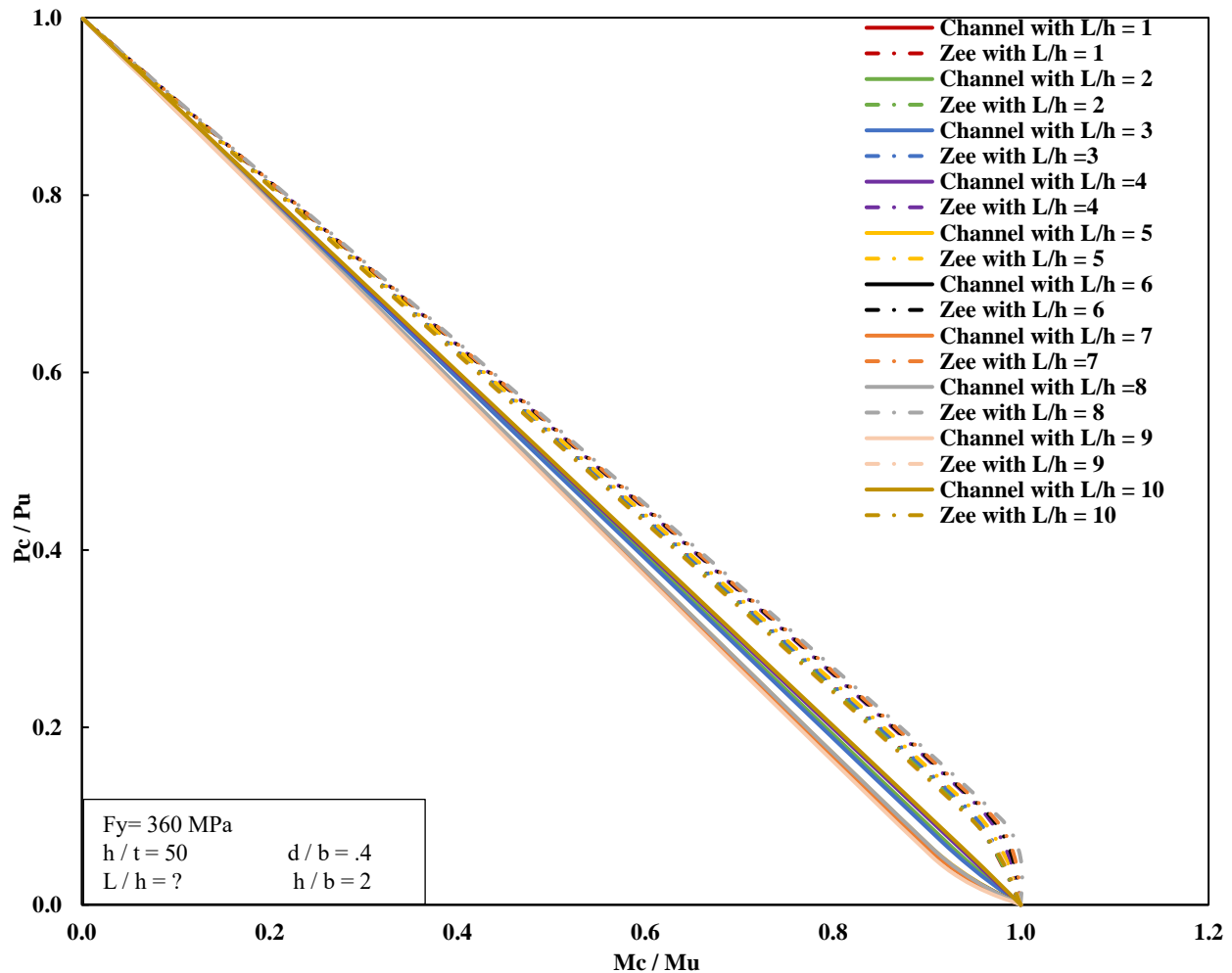


Figure A.8: - Relation between FEM different capacities of CFS members with different length-to-web plate depth ratios (L/h).

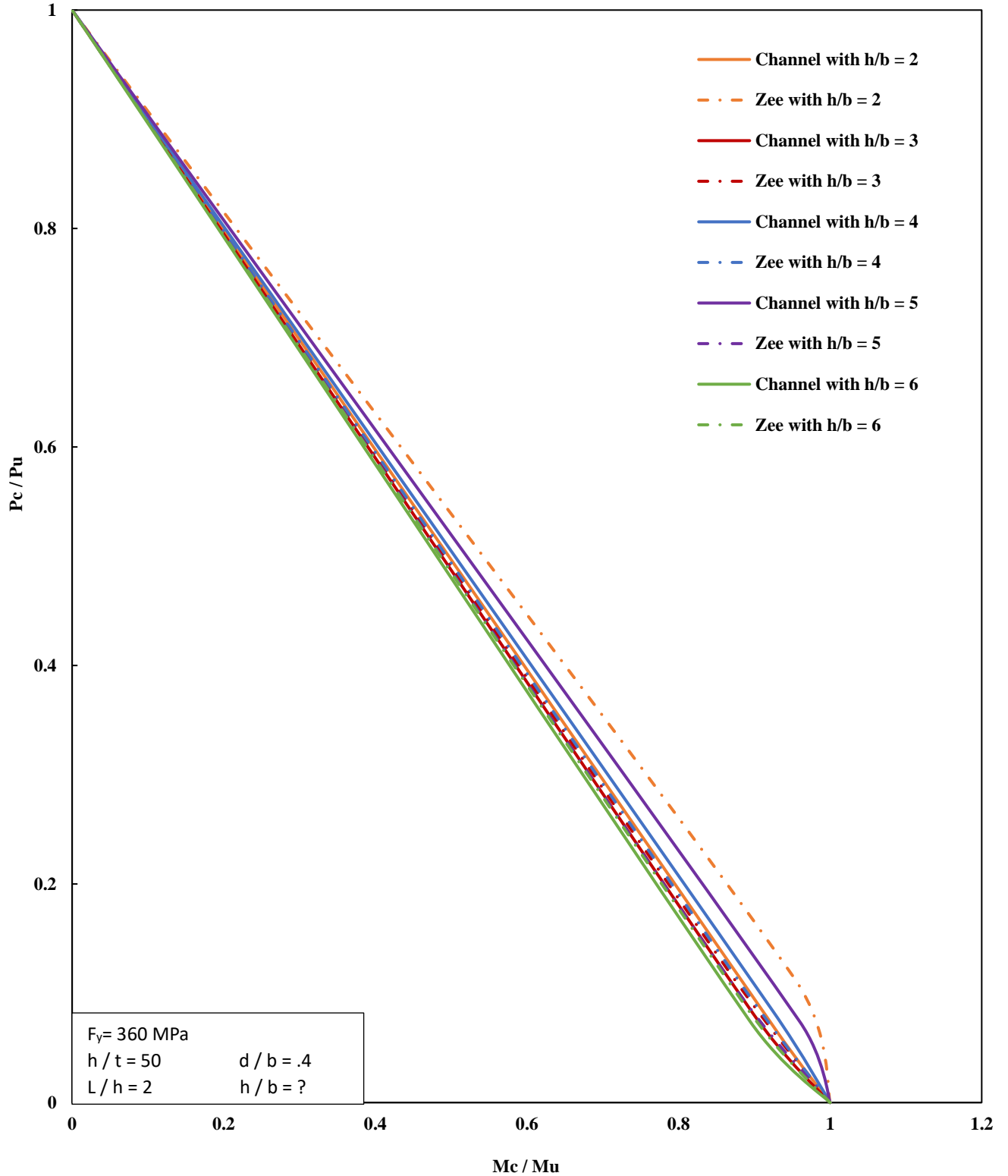


Figure A.9: - Relation between FEM different capacities of CFS members with different web-to-flange plate length ratios (h/b).

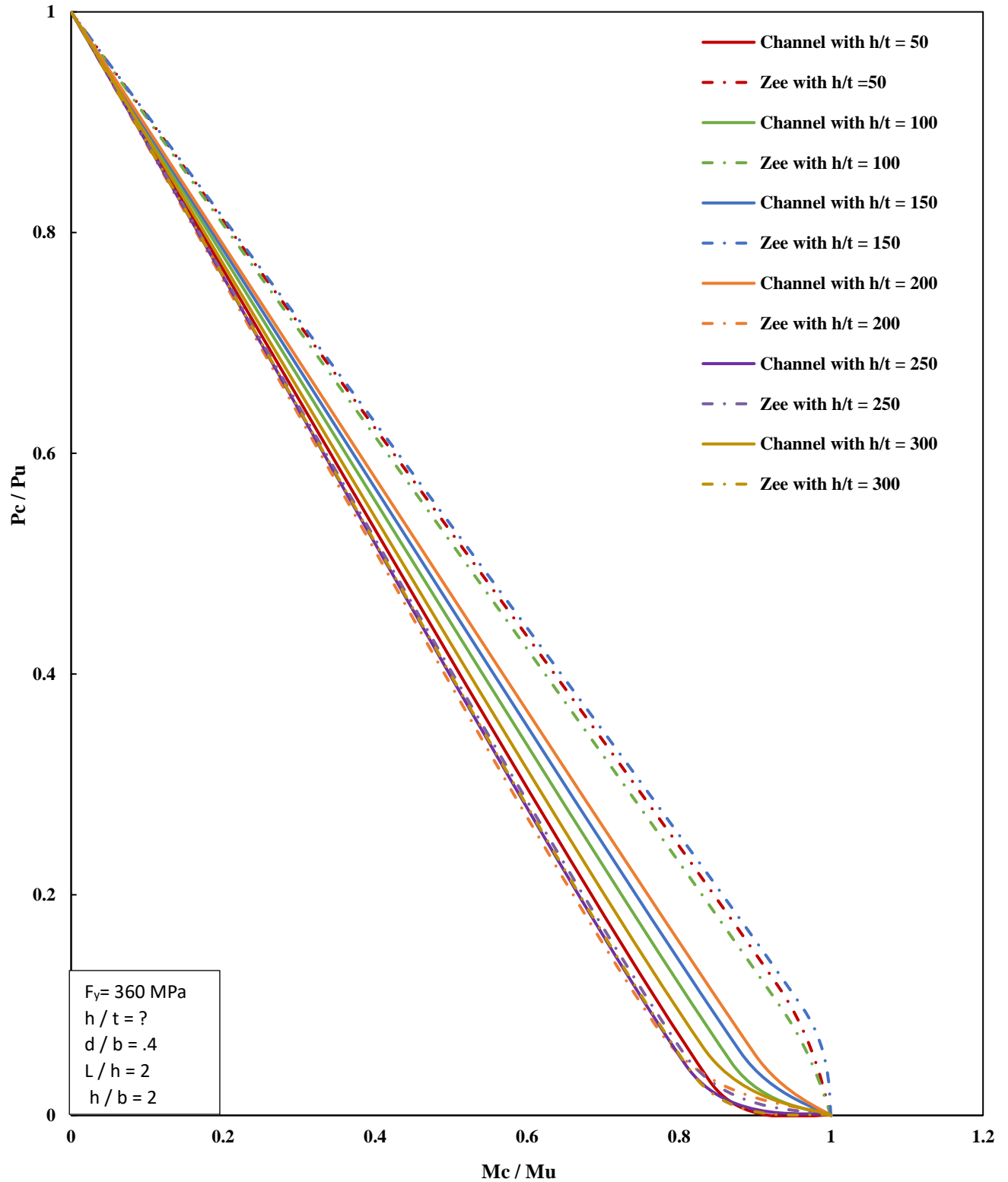


Figure A.10: - Relation between FEM different capacities of CFS members with different web plate slenderness ratio (h/t).

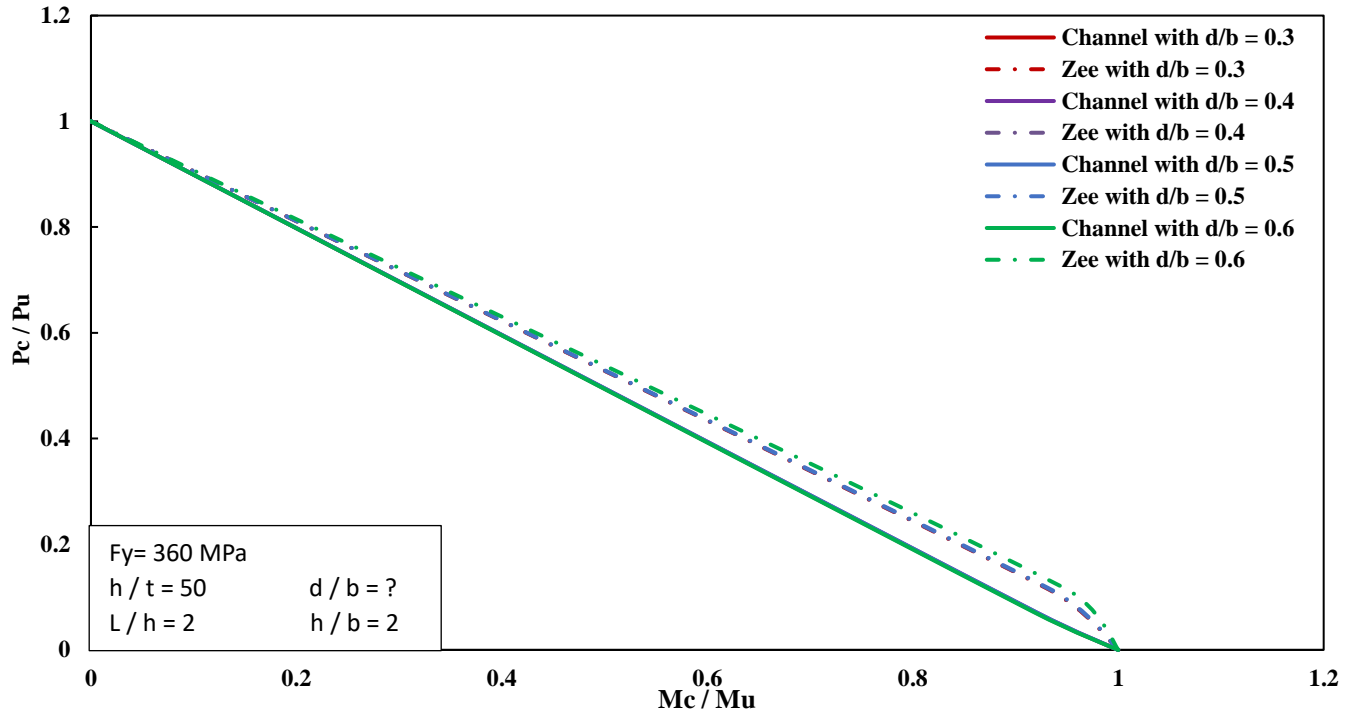


Figure A.11: - Relation between FEM different capacities of CFS members with different lip-to-flange plates length (d/b).

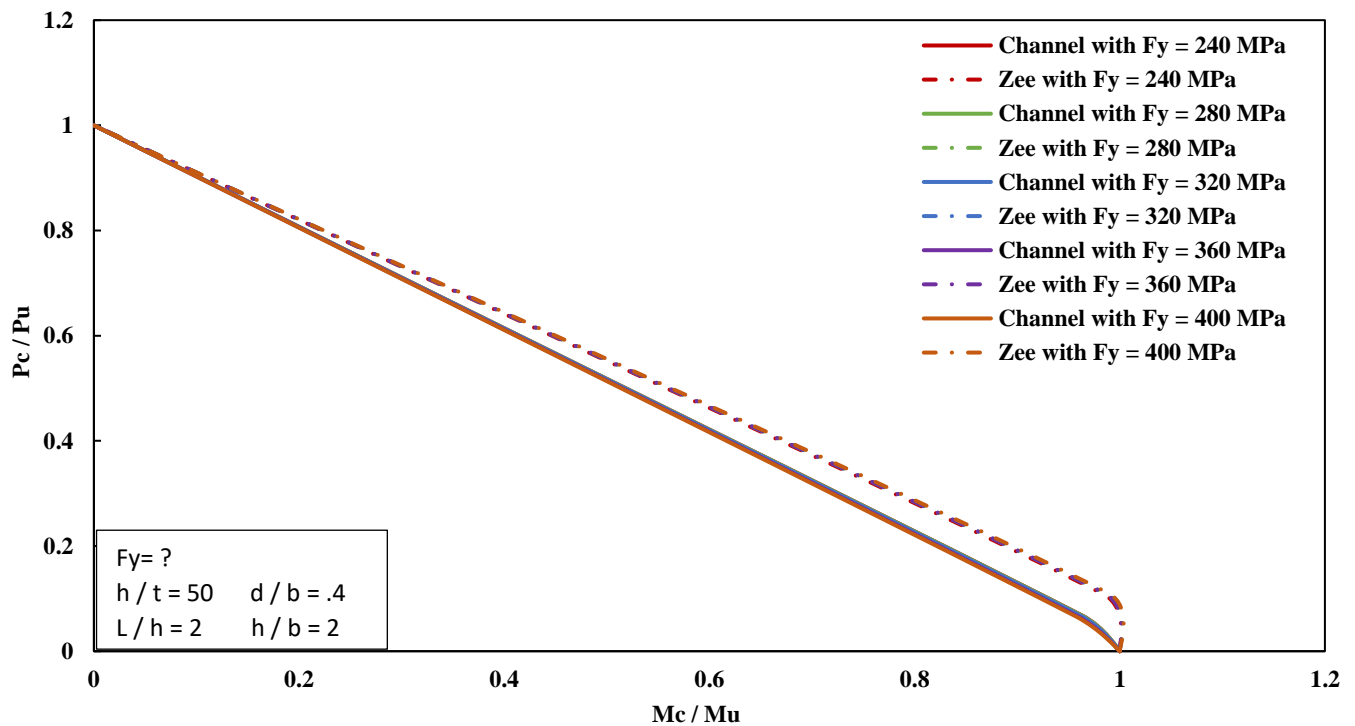


Figure A.12: - Relation between FEM different capacities of CFS members with different yielding steel strengths (F_y).

ARABIC SUMMARY

الملخص العربي

الخلاصة

تشمل هذه الرسالة على دراسة لقوة الضغط والانحناء للقطاعات الصلبة المشكّلة على البارد والتي يأخذ مقطعها شكل حرف C او Z. قامت الدراسة بتحليل شامل لـ 500 عضو من الصلب المشكل على البارد. تم إجراء تحليل عددي باستخدام نموذج العناصر المحدود (FEM) بناءً على برنامج ABAQUS ثم تم استخدام نتائج الاختبارات التجريبية المتاحة للتحقق من دقة النماذج العددية، وتم استخدامها بعد ذلك لتقييم تأثير مختلف العوامل على ساعات وقدرات هذه الأجزاء. هذه العوامل تتمثل في نسبة طول العضو إلى عمقه، نسبة عمق المقطع إلى عرضه، نسبة نحافة المقطع، نسبة عرض الشفة إلى الجناح، واجهاد الخضوع لمادة الحديد المكونة للقطاع. تمت مقارنة النتائج المستخلصة من النماذج العددية مع تلك المستمدة من طريقة العرض الفعّال (EWM)، كما هو مستخدم في جميع المعايير والأكواد التصميمية الحالية، وأيضًا مع طريقة القوة المباشرة (DSM) وهي طريقة متقدمة وحديثة لتصميم القطاعات الصلبة المشكّلة على البارد. تم استخدام المواصفات (الأكواد) الأمريكية، والأوروبية، والمصرية كأتمثلة لطريقة العرض الفعّال (EWM). تم استخدام الملحق 1 في المواصفة (الكود) الأمريكية كمثال لطريقة القوة المباشرة (EWM). من أجل تحسين العملية الحسابية، تم تطوير واجهة مستخدم رسومية (GUI) لبرمجة إجراءات حساب العرض الفعّال (EWM) و طريقة القوة

المباشرة (DSM) هذا التطور سهّل التحليل وأتاح إجراء تقييمات أكثر كفاءة ودقة لقدرات القطاعات الصلبة المشكّلة على البارد. تقدم هذه الدراسة رؤى حول أداء القطاعات الصلبة المشكّلة على البارد، مما يسهم في فهم أعمق لسعاتها الهيكلية ويوفر أساساً لتطبيقات محتملة في تصميم الهندسة الحديثة وممارسات البناء.

محتوي الرسالة

تحتوي الرسالة على سبعة أبواب:

- | | |
|---|----------------------------|
| <p>يحتوي على مقدمة عن محتوى الرسالة والهدف منها وأيضاً مقدمة سريعة عن القطاعات الصلبة المشكّلة على البارد.</p> | <p>الباب الأول</p> |
| <p>تم تقديم نبذة تاريخية عن القطاعات الصلبة المشكّلة على البارد وأنواعها ومكوناتها ثم عرض مختصر للأبحاث السابقة المختصة في القطاعات الصلبة المشكّلة على البارد.</p> | <p>الباب الثاني</p> |
| <p>تم تقديم شرح وافي عن المواصفات والاكواد المستخدمة في البحث الدراسة مثل المواصفات (الأكواد) الأمريكية، والاوربية، والمصرية.</p> | <p>الباب الثالث</p> |
| <p>يحتوي هذا الفصل على دليلا شاملا يغطي جميع جوانب البرنامج المطور بالكامل ويقدم للمستخدم نصائح حول كيفية استخدام البرنامج بنجاح أكبر. بالإضافة إلى التحقق من صحة ودقة نتائج البرنامج، فإنه يحتوي أيضاً على دراسة بارامترية تعتمد على المواصفات مختلفة.</p> | <p>الباب الرابع</p> |
| <p>يصف هذا الفصل النماذج العددية باستخدام العناصر المحدودة (FE) والتحقق من النتائج.</p> | <p>الباب الخامس</p> |
| <p>يشمل هذا الفصل المزيد من البيانات عن طريق إجراء دراسات حدودية حول قدرات القطاعات الصلبة المشكّلة على البارد باستخدام نموذج العناصر المحددة (FE) الذي تم التحقق منه. بالإضافة إلى ذلك، فهو يقدم تحليلاً مقارناً بين الرموز المختلفة ونموذج FE.</p> | <p>الباب السادس</p> |
| <p>يشتمل هذا الباب على أهم النتائج التي تم التوصل إليها من خلال الدراسة وكذلك توصيات للعمل المستقبلي.</p> | <p>الباب السابع</p> |



جامعة المنصورة
كلية الهندسة
قسم الهندسة الإنشائية



الإدارة العامة للمكتبات

ملخص الرسالة () بالمكتبة

الكلية :	الهندسة	قسم :	الهندسة الإنشائية	رقم :	
الاسم :	سمر السيد إبراهيم عبد القوي عطيه	الدرجة العلمية :	ماجستير العلوم في الهندسة	التاريخ :	
اسم الرسالة :	دراسة مقارنة بين الأكواد المختلفة في تصميم القطاعات المعدنية المشكّلة على البارد تحت تأثير الأحمال الإستاتيكية.				
الملخص					
<p>تشمل هذه الرسالة على دراسة لقوة الضغط والانحناء للقطاعات الصلبة المشكّلة على البارد والتي يأخذ مقطعها شكل حرف C او Z. قامت الدراسة بتحليل شامل لـ 500 عضو من الصلب المشكل على البارد. تم إجراء تحليل عددي باستخدام نموذج العناصر المحدود (FEM) بناءً على برنامج ABAQUS ثم تم استخدام نتائج الاختبارات التجريبية المتاحة للتحقق من دقة النماذج العددية، وتم استخدامها بعد ذلك لتقييم تأثير مختلف العوامل على ساعات وقدرات هذه الأعضاء. هذه العوامل تتمثل في نسبة طول العضو إلى عمقه، نسبة عمق المقطع إلى عرضه، نسبة نحافة المقطع، نسبة عرض الشفة إلى الجناح، واجهاد الخضوع لمادة الحديد المكونة للقطاع. تمت مقارنة النتائج المستخلصة من النماذج العددية مع تلك المستمدة من طريقة العرض الفعّال (EWM)، كما هو مستخدم في جميع المعايير والاكواد التصميمية الحالية، وأيضًا مع طريقة القوة المباشرة (DSM) وهي طريقة متقدمة وحديثة لتصميم القطاعات الصلبة المشكّلة على البارد. تم استخدام المواصفات (الأكواد) الأمريكية، والأوربية، والمصرية كأمثلة لطريقة العرض الفعّالة (EWM). تم استخدام الملحق 1 في المواصفة (الكود) الأمريكية كمثال لطريقة القوة المباشرة (DSM). من أجل تحسين العملية الحسابية، تم تطوير واجهة مستخدم رسومية (GUI) لبرمجة إجراءات حساب العرض الفعّال (EWM) و طريقة القوة المباشرة (DSM) هذا التطور سهّل التحليل وأتاح إجراء تقييمات أكثر كفاءة ودقة لقدرات القطاعات الصلبة المشكّلة على البارد. تقدم هذه الدراسة رؤى حول أداء القطاعات الصلبة المشكّلة على البارد، مما يسهم في فهم أعمق لساعاتها الهيكلية ويوفر أساسًا لتطبيقات محتملة في تصميم الهندسة الحديثة وممارسات البناء.</p> <p>تحتوي الرسالة على سبعة أبواب:</p>					



جامعة المنصورة
كلية الهندسة
قسم الهندسة الإنشائية



الباب الأول: يحتوي على مقدمة عن محتوى الرسالة والهدف منها وأيضاً مقدمة سريعة عن القطاعات الصلبة المشكّلة على البارد.

الباب الثاني: تم تقديم نبذة تاريخية عن القطاعات الصلبة المشكّلة على البارد وأنواعها ومكوناتها ثم عرض مختصر للأبحاث السابقة المختصة في القطاعات الصلبة المشكّلة على البارد.

الباب الثالث: تم تقديم شرح وافي عن المواصفات والاكواد المستخدمة في البحث الدراسة مثل المواصفات (الأكواد) الأمريكية، والاوربية، والمصرية.

الباب الرابع: يحتوي هذا الفصل على دليلاً شاملاً يغطي جميع جوانب البرنامج المطور بالكامل ويقدم للمستخدم نصائح حول كيفية استخدام البرنامج بنجاح أكبر. بالإضافة إلى التحقق من صحة ودقة نتائج البرنامج، فإنه يحتوي أيضاً على دراسة بارامترية تعتمد على المواصفات مختلفة.

الباب الخامس: يصف هذا الفصل النماذج العددية باستخدام العناصر المحدودة (FE) والتحقق من النتائج.

الباب السادس: يشمل هذا الفصل المزيد من البيانات عن طريق إجراء دراسات حدودية حول قدرات القطاعات الصلبة المشكّلة على البارد باستخدام نموذج العناصر المحددة (FE) الذي تم التحقق منه. بالإضافة إلى ذلك، فهو يقدم تحليلاً مقارناً بين الرموز المختلفة ونموذج FE.

الباب السابع: يشتمل هذا الباب على أهم النتائج التي تم التوصل إليها من خلال الدراسة وكذلك توصيات للعمل المستقبلي.

عناوين الموضوع

قطاعات الصلب المشكل على البارد؛ قدرة الضغط المحوري؛ قدرة الانبعاج؛ نموذج العناصر المحدودة؛ طريقة العرض الفعالة؛ طريقة القوة المباشرة؛ الأكواد المختلفة.



جامعة المنصورة
كلية الهندسة
قسم الهندسة الإنشائية



إقرار

يقر الباحث/ **سمر السيد ابراهيم عبد القوى عطية** بالالتزام بقوانين جامعة المنصورة وأنظمتها وتعليماتها وقراراتها السارية المفعول بها المتعلقة بإعداد رسائل الماجستير والدكتوراه عندما قامت بإعداد الرسالة العلمية تحت عنوان:

دراسة مقارنة بين الأكواد المختلفة في تصميم القطاعات المعدنية المشكلة على البارد تحت تأثير الأحمال الإستاتيكية

ولجنة الإشراف:

أ. د/ نبيل سيد محمود حسن.

أ.م. د/ فكري عبده سالم.

أ.م. د/ محمد محمد غنام.

كأحد متطلبات نيل درجة الماجستير في الهندسة تخصص الهندسة الإنشائية.

والإقرار بحدثة موضوع الدراسة البحثية وأنه لم يسبق تناول الموضوع والعنوان البحثي بصورته النهائية الكاملة أو نشره سابقاً في أي رسائل أو أطروحات أو كتب أو أبحاث أو أي منشورات علمية وذلك بما ينسجم مع الأمانة العلمية المتعارف عليها في كتابة الرسائل والأطروحات العلمية. وقبول عدد (1) بحث للنشر بعنوان: -

“Comparison between Different Codes in Design Cold-Formed Steel Lipped Channel Section Subjected to Axial Load or Bending Moment”

في مجله علميه محكمه ومتخصصه في مجال الهندسة، هي :

MANSOURA ENGINEERING JOURNAL, (MEJ), November 2023

وأن البحث المنشور مستخرج من الرسالة المذكورة أعلاه وأن أسماء جميع السادة المشرفين موجودة على البحث.

وهذا إقرار مني بذلك ،،،

المقر

م. سمر السيد ابراهيم عبد القوى عطية



جامعة المنصورة
كلية الهندسة
قسم الهندسة الإنشائية



أعضاء لجنة المناقشة والحكم

دراسة مقارنة بين الأكواد المختلفة فى تصميم القطاعات المعدنية
عنوان الرسالة : المشكلة على البارد تحت تأثير الأحمال الإستاتيكية.

اسم الباحث : **سمر السيد ابراهيم عبد القوى عطيه**
الدرجة العلمية : ماجستير العلوم في الهندسة (الهندسة الانشائية)

لجنة الإشراف

الاسم	الوظيفة	التوقيع
أ.د/ نبيل سيد محمود حسن	أستاذ متفرغ - قسم الهندسة الإنشائية كلية الهندسة - جامعة المنصورة	
أ.م.د/ فكري عبده سالم	أستاذ مساعد متفرغ - قسم الهندسة الإنشائية كلية الهندسة - جامعة المنصورة	
أ.م.د/ محمد محمد غنام	أستاذ مساعد - قسم الهندسة الإنشائية كلية الهندسة - جامعة المنصورة	

لجنة المناقشة والحكم

الاسم	الوظيفة	التوقيع
أ.د/ شريف أحمد مراد	أستاذ المنشآت المعدنية والكباري - قسم الهندسة الانشائية -كلية الهندسة - جامعة القاهرة	
أ.د/ نبيل سيد محمود حسن	أستاذ متفرغ - قسم الهندسة الانشائية -كلية الهندسة - جامعة المنصورة	
أ.د/ سعد الدين مصطفى محمد	أستاذ بقسم الهندسة الإنشائية كلية الهندسة - جامعة المنصورة	
أ.م.د/ فكري عبده محمود سالم	أستاذ مساعد متفرغ - قسم الهندسة الإنشائية كلية الهندسة - جامعة المنصورة	

القائم بعمل عميد الكلية

وكيل الكلية
لشئون الدراسات العليا والبحوث

رئيس مجلس القسم

أ.د/ شريف البدوي

أ.د/ شريف البدوي

أ.د/ محمد الزغبى



جامعة المنصورة
كلية الهندسة
قسم الهندسة الإنشائية



أعضاء لجنة المناقشة والحكم

دراسة مقارنة بين الأكواد المختلفة في تصميم القطاعات المعدنية

عنوان الرسالة : المشكلة على البار د تحت تأثير الأحمال الإستاتيكية.

اسم الباحث : عمر السيد ابراهيم عبد القوى عطيه
الدرجة العلمية : ماجستير العلوم في الهندسة (الهندسة الإنشائية)
لجنة الإشراف

التوقيع	الوظيفة	الاسم
	أستاذ متفرغ بقسم الهندسة الإنشائية كلية الهندسة - جامعة المنصورة	أ.د/ نبيل سيد محمود حسن
	أستاذ مساعد متفرغ بقسم الهندسة الإنشائية كلية الهندسة - جامعة المنصورة	أ.م.د/ فكري عهده سالم
	أستاذ مساعد بقسم الهندسة الإنشائية كلية الهندسة - جامعة المنصورة	أ.م.د/ محمد محمد عادل غنم

لجنة المناقشة والحكم

التوقيع	الوظيفة	الاسم
	أستاذ المنشآت المعدنية والكباري - قسم الهندسة الإنشائية - كلية الهندسة - جامعة القاهرة	أ.د/ شريف أحمد مراد
	أستاذ متفرغ بقسم الهندسة الإنشائية - كلية الهندسة - جامعة المنصورة	أ.د/ نبيل سيد محمود حسن
	أستاذ بقسم الهندسة الإنشائية كلية الهندسة - جامعة المنصورة	أ.د/ سعد الدين مصطفى محمد
	أستاذ مساعد متفرغ بقسم الهندسة الإنشائية كلية الهندسة - جامعة المنصورة	أ.م.د/ فكري عهده محمود سالم

وكيل الكلية لشئون الدراسات العليا والبحوث
أ.د/ شريف البدوي

رئيس مجلس القسم

أ.د/ محمد الزغبلي



جامعة المنصورة
كلية الهندسة
قسم الهندسة الإنشائية



لجنة الإشراف

عنوان الرسالة : دراسة مقارنة بين الأكواد المختلفة فى تصميم القطاعات المعدنية المشكلة على البارد تحت تأثير الأحمال الإستاتيكية.
اسم الباحث : سمر السيد ابراهيم عبد القوى عطيه
الدرجة العلمية : ماجستير العلوم فى الهندسة (الهندسة الإنشائية)

لجنة الإشراف

التوقيع	الوظيفة	الاسم
	أستاذ متفرغ - قسم الهندسة الإنشائية - كلية الهندسة - جامعة المنصورة	أ.د/ نبيل سيد محمود حسن
	أستاذ مساعد متفرغ - قسم الهندسة الإنشائية - كلية الهندسة - جامعة المنصورة	أ.م.د/ فكري عبده محمود سالم
	أستاذ مساعد - قسم الهندسة الإنشائية كلية الهندسة - جامعة المنصورة	أ.م.د/ محمد محمد عادل غنام

القائم بعمل عميد الكلية

أ.د/ شريف البدوي

وكيل الكلية
لشئون الدراسات العليا والبحوث

أ.د/ شريف البدوي

رئيس مجلس القسم

أ.د/ محمد الزغبى



جامعة المنصورة
كلية الهندسة
قسم الهندسة الإنشائية



لجنة الإشراف

عنوان الرسالة : دراسة مقارنة بين الأكواد المختلفة في تصميم القطاعات المعدنية المشكّلة على البارد تحت تأثير الأحمال الإستاتيكية.
اسم الباحث : سمر السيد ابراهيم عبد القوي عطيه
الدرجة العلمية : ماجستير العلوم في الهندسة (الهندسة الإنشائية)

لجنة الإشراف

التوقيع	الوظيفة	الاسم
	أستاذ متفرغ بقسم الهندسة الإنشائية .كلية الهندسة - جامعة المنصورة	أ.د/ نبيل سيد محمود حسن
	أستاذ مساعد متفرغ بقسم الهندسة الإنشائية - كلية الهندسة - جامعة المنصورة	أ.م.د/ فكري عبده محمود سالم
	أستاذ مساعد بقسم الهندسة الإنشائية كلية الهندسة - جامعة المنصورة	أ.م.د/ محمد محمد عادل غنم

رئيس مجلس القسم
أ.د/ محمد الزنجيد

وكيل الكلية
لشؤون الدراسات العليا والبحوث
أ.د/ شريف البدوي

العلم بعمل عميد الكلية
أ.د/ شريف البدوي

٢٠٢٠



Mansoura University
Faculty of Engineering
Structural Engineering Department



دراسة مقارنة بين الأكواد المختلفة في تصميم القطاعات المعدنية المشكلة على البارد تحت تأثير الأحمال الإستاتيكية

رسالة مقدمه من

المهندسة / سمر السيد ابراهيم عبد القوى عطيه

بكالوريوس الهندسة المدنية- كلية الهندسة-جامعة المنصورة ٢٠١٨

معيدة بقسم الهندسة الانشائية

كلية الهندسة – جامعة المنصورة

كجزء من متطلبات الحصول على

درجة الماجستير العلوم في هندسة الانشاءات

المشرفون

أ. د/ نبيل سيد محمود حسن

أستاذ بقسم الهندسة الإنشائية

كلية الهندسة – جامعة المنصورة

أ.م د/ محمد محمد غنام

أستاذ مساعد بقسم الهندسة الإنشائية

كلية الهندسة – جامعة المنصورة

أ.م د/ فكري عبده سالم

أستاذ مساعد بقسم الهندسة الإنشائية

كلية الهندسة – جامعة المنصورة